# Binding of phytochemicals derived from *Withania*somnifera to human serum albumin and its derivative peptides retard amyloid fibrillation

# Thesis Submitted for the Degree of Doctor of Philosophy

**Shreya Dubey** 



Department of Plant Sciences School of Life Sciences University of Hyderabad Hyderabad-500046

February 2021



# School of Life Sciences University of Hyderabad Hyderabad-500046

## **DECLARATION**

I, Shreya Dubey, hereby declare that this thesis entitled "Binding of phytochemicals derived from Withania somnifera to human serum albumin and its derivative peptides retard amyloid fibrillation" submitted by me under the guidance and supervision of Prof. S. Rajagopal is an original and independent research work. I also declare that it has not been submitted previously in part or in full to this University or any other University or Institution for the award of any degree or diploma.

Date: 01.02.21

Shreya Dubey

**14LPPH16** 



# School of Life Sciences University of Hyderabad Hyderabad-500046

#### CERTIFICATE

This is to certify that this thesis entitled "Binding of phytochemicals derived from Withania somnifera to human serum albumin and its derivative peptides retard amyloid fibrillation" is a record of bonafied work done by Shreya Dubey, a research scholar for Ph.D. in Plant Sciences, School of Life Sciences, University of Hyderabad under my guidance and supervision. This thesis has not been submitted previously in part or in full to this University or any other University or Institution for the award of any degree or diploma.

(Head of the Department) 2021

अध्यक्ष / HEAD

वनस्पति विज्ञान जिभाग / Dept. of Plant Sciences जैविक विज्ञान राकाय / School of Life Sciences हैदरावाद विश्वविद्यालय / University of Hyderabad हैदरावाद / Hyderabad-500 046, भारत / INDIA Prof. S. Rajagopal

Prof. S. RAJAGOPAL Dept. of Plant Sciences School of Life Sciences University of Hyderabad Hyderabad-500 046. (Dean of the School)

DEAN School of Life Sciences University of Hyderabad Hyderabad - 500 046.



# School of Life Sciences University of Hyderabad Hyderabad-500046

# Plagiarism Free Certificate

This is to certify that the similarity index of this thesis as checked by the Library of University of Hyderabad is 45%. Out of this 36% similarity has been found to be identified from the candidate's own publication which forms the major part of the thesis. The details of student's publication are as follows:

- 1. Unravelling the stability of plasma proteins upon interaction of synthesized uridine products: biophysical and molecular dynamics approach (Chapter 3).
- 2. Elucidating the active interaction mechanism of phytochemicals withanolide and withanoside derivatives with human serum albumin (Chapter 3).

About 9% similarity was identified from external sources in the present thesis which is according to the prescribed regulations of the University. All the publications related to this thesis have been appended at the end of the thesis. Hence, the present thesis should be considered plagiarism free.

Prof.S. Rajagopal

(Supervisor)

Prof. S. RAJAGOPAL Dept. of Plant Sciences School of Life Sciences University of Hyderabad Hyderabad-500 046.

## ACKNOWLEDGEMENT

I would like to express my heartful gratitude to my supervisor Prof. S. Rajagopal who has been a constant source of support and motivation. As a teacher and a guide, he made me believe in the value of integrity of effort and perseverance against all odds. I am grateful to him for encouraging my research and allowing me to grow as a research scientist. His advice on both research as well as on my career has been priceless.

My sincere thanks to the present and former Deans, Prof. S. Dayananda, Prof. K.Y.A. Ramaiah, and Prof. P. Reddenna, School of Life Sciences, to use school facilities.

I would like to express my thankfulness to present and former Heads, Prof. Attipalli R. Reddy and Prof. Ch. Venkata Ramana, Department of Plant Sciences for their support and encouragement during my research tenure allowing me to use department facilities.

I am incredibly indebted to my doctoral committee members Prof. Ch Venkatramana and Prof. Naresh Sepuri, for their constant support and valuable suggestions during my research period.

It would like to express my sincere thanks to all School of Life Sciences faculty members for their support and encouragement.

I thank the non-teaching and technical staff of the School of Life Sciences for their kind help and support.

I am very grateful to Prof. Naidu Subbarao, JNU who showed me a direction in my doctoral studies his students Lokesh Nigam and Waseem who helped me in executing the same.

I would also like to thank the central instrumentation laboratory, UOH, for allowing me to use CD spectroscopy. I thank CMSD and bioinformatics facility (SLS facility) for providing servers for molecular simulation studies. I would like to thank the School of Chemistry for allowing me to use AFM and Durga Prasad Sir who helped me with AFM and Department of Nanotechnology for TEM, FACS and Confocal microscopy.

I am grateful to my senior colleagues Dr. Mahesh and Dr. Mir Zahoor Gul, for their guidance and help acquire the technical skills and scientific insight.

My heartfelt thanks to my colleagues Saikiran, Elsinraju, Srilatha, Daniel, Aparna, Ranay, Nisha, Jai, Yusuf, Arijit, Vishnupriya, Saurabh, Roshan and lab assistant Ganesh for their cooperation and providing me with a peaceful atmosphere during my bench work.

I'm grateful to my friend and senior Dr. Monika, for her belief in me and being an exceptional part of this journey.

I extend my thanks to all friends at School of Life Sciences for maintaining a lively and amicable atmosphere.

I take this opportunity to sincerely acknowledge the funding agencies DST-FIST, DBT-CREBB and UGC-SAP for infrastructure. Also, I thank DST, DBT, CSIR and UPE-II for financial support to the lab. My sincere thanks to CSIR – JRF and SRF for providing fellowship.

I would like to take the privilege of thanking my family members without whose support and encouragement; I would not have been able to complete my doctorate research successfully. They have been eagerly looking forward to this personal milestone. My parents have been a true inspiration all along; they stood by me in every step I took and every decision I made. Their simplicity, revered advice, love and affection has helped me be to be what I am. Finally, and above all, I cannot begin to express my unfailing gratitude and love to my husband, Kartikeya Misra. Throughout this process, he had supported me and has continuously encouraged me when the tasks seemed arduous and insurmountable.

# **DEDICATION**

I gratefully dedicate this thesis to Gunnu and Kinshu....

-Shreya Dubey-

# **CONTENTS**

Chapter 1: Introduction	1-23
1.1 Serum Albumin	2
1.2 Human serum albumin	2
1.3 Structural features of HSA	3
1.4 Binding Studies of HSA	8
1.5 Herbal derivatives from plant Withania somnifera (Ashwagandha)	12
1.6 Role of Withania somnifera in Neurodegenerative Diseases	14
1.7 Alzheimer's Disease	15
1.8 Peptides based drugs for neurodegenerative diseases	21
1.9 β-Sheet breaker peptides used for our study	22
1.10 Objectives	23
Chapter 2: Materials and methods	24-41
2.1. Preparation of stock solutions	24
2.2. Room temperature fluorescence spectra	24
2.3. Molecular displacement studies	25
2.4. Circular dichroism measurements	25
2.5. Atomic force Microscopy	26
2.6. Transmission electron microscopy (TEM)	26
2.7. Thioflavin -T fluorescence assay	27
2.8. Cell Viability (MTT Assay)	28
2.9. Apoptosis assay by Annexin V	29
2.10. Tunel assay using confocal microscopy	30
2.11. ROS intracellular assay	30
2.12. Lactate dehydrogenase assay	31
2.13. Cellular mitochondrial membrane potential assay	31
2.14. Membrane potential assay with confocal microscopy	32
2.15. Molecular docking	33

2.16. Molecular dynamics simulations	33	
2.17. Generation and preparation of peptide libraries	35	
2.18. Protein preparation	35	
2.19. Receptor grid preparation and molecular screening and docking	36	
2.20. Post docking analysis	37	
2.21. Docking for HSA peptide generation	37	
2.22. Molecular mechanics poisson-boltzmann surface area (MMPBSA)	38	
2.23. Absorption, distribution, metabolism, excretion, and toxicity –	20	
structure-activity relationship database (ADMET SAR)	39	
Chapter 3: Deciphering the importance of phytochemicals of <i>Withania</i> somnifera to understand its therapeutic benefits in ameliorating Aβ <sub>1-42</sub> fibrillation and its binding studies with the cargo protein Human Serum Albumin	42-72	
3.1. Introduction	42	
3.2. Results and Discussion	43	
3.2.A. Interaction between HSA and phytochemicals of Withania	42	
somnifera	43	
3.2.A.1. Fluorescence spectroscopy	43	
3.2.A.2. Displacement studies	46	
3.2.A.3. Secondary structural analysis of HSA and its complexes	47	
3.2.A.4. Topological observations from AFM	49	
3.2.A.5. Transmission emission microscopy	51	
3.2.A.6. Molecular docking	52	
3.2.A.7. Results from molecular dynamics	53	
3.2.B. Interaction between Aβ and phytochemicals of <i>Withania</i> somnifera	56	
3.2.B.1. Thioflavin fluorescence assay	56	
3.2.B.2. MTT reduction assay	58	
3.2.B.3. Apoptosis annexin assay	60	

3.2.B.4. Tunel assay by confocal microscopy	61	
3.2.B.5. Intracellular ROS measurement	62	
3.2.B.6. Molecular docking by Autodock	64	
3.2.B.7. MD simulations of $A\beta_{1-42}$ and $A\beta_{1-42}$ withanolide and	65	
withanoside complexes	65	
3.3. Conclusion	71	
Chapter 4: Elucidating the inhibitory potential of HSA as well as		
synthesized peptides against amyloid fibrillation and amyloid associated neurotoxicity	73-103	
4.1. Introduction	73	
4.2. Results and Discussion	77	
4.2.1. Docking between HSA and $A\beta_{1-42}$	77	
4.2.2. Screening of BSBp by GLIDE module of Schrödinger	79	
4.2.3. Molecular Dynamics and simulations	85	
4.2.4. Free energy by MMPBSA	88	
4.2.5. Lipinski Rule of Five	89	
4.2.6. Thioflavin Assay	92	
4.2.7. Morphological changes	94	
4.2.8. Cell Viability Assay	96	
4.2.9. Lactate Dehydrogenase Assay	98	
4.2.10. Reactive Oxygen Species (ROS)	99	
4.2.11. Cellular MMP assay	100	
4.2.12. Cellular Mitochondrial Membrane Potential by laser scanning	101	
confocal microscopy	101	
4.3. Conclusion	102	
Chapter 5: Summary	104-107	
Bibliography	108-128	
List of Publications		

# **List of Figures**

- Fig. 1.1. Modular domain organization of HSA.
- Fig. 1.2. Schematic drawing of secondary structural elements and disulphide bridges of HSA.
- Fig. 1.3. Drug binding sites of HSA
- Fig. 1.4. The binding site of IIA domain of HSA
- Fig. 1.5. Based on crystallographic studies till date HSA binding with various ligands and fatty acids
- Fig. 1.6. The structure of withanolide A, withanolide B, withanoside IV and withanoside V
- Fig. 1.7. Pathway showing the  $A\beta_{1-42}$  accumulation
- Fig. 1.8. The action of peptides on the fibrils
- Fig. 1.9. Schematic representation of the  $A\beta_{1-42}$  hypothesis for the progression of AD
- Fig. 3.1. Fluorescence spectroscopic studies of HSA with Withanolide and Withanoside molecules
- Fig. 3.2. Site displacement studies using site-specific markers
- Fig. 3.3. Circular Dichroism studies of the free HSA and HSA-drug complexes
- Fig. 3.4. AFM studies to visualize alteration in HSA molecule topology in the presence of Withanolide and Withanoside derivatives
- Fig. 3.5. TEM studies to visualize alteration in HSA molecule topology in the presence of Withanolide and Withanoside derivatives
- Fig. 3.6. Molecular docking studies between HSA and Withanolide A, Withanolide B, Withanoside IV and Withanoside V
- Fig. 3.7. MD simulation of unliganded HSA and HSA- Withanolide (A, B) and Withanoside (IV, V) complexes (Rg, RMSD and RMSF) for 10 ns
- Fig. 3.8. Detection of  $A\beta_{1-42}$  aggregates using ThT assay for fluorescence
- Fig. 3.9. Inhibitory effect of *Withania somnifera* derivatives on the growth of SK-N-SH cells by MTT assay
- Fig. 3.10. Apoptosis studies by FACS
- Fig. 3.11. TUNEL nuclear staining on SK-N-SH neuroblastoma cells
- Fig. 3.12. Intracellular ROS generation in SK-N-SH cells after treatment with *Withania* somnifera derivatives

- Fig. 3.13. Molecular docking of  $A\beta_{1-42}$  with Withanolide A, Withanolide B, Withanoside IV, and Withanoside V
- Fig. 3.14. The molecular dynamics simulations of the  $A\beta_{1-42}$  with Withanolide (A, B) and Withanoside (IV, V) for 100 ns
- Fig. 3.15. The conformers of  $A\beta_{1-42}$  phytocompounds at different nanoseconds
- Fig. 4.1. A) Selected peptides derived from HSA through Haddock and Patchdock
   B) B) Pymol showing the amino acids interacting with Aβ<sub>1-42</sub> through hydrogen bonds
- Fig. 4.2. Docking images of the HSA derived peptides with  $A\beta_{1-42}$
- Fig. 4.3. Docking images of the BSBp with  $A\beta_{1-42}$
- Fig. 4.4. Time evolution of the Rg during 200 ns of MD simulation of unliganded  $A\beta_{1-42}$  and  $A\beta_{1-42} BSBp$  complexes
- Fig. 4.5. Detection of  $A\beta_{1-42}$  aggregates using ThT assay for fluorescence measurement
- Fig. 4.6. Cell morphology observed from inverted microscope
- Fig. 4.7. Treatment with the peptide increases the cell viability of SK-N-SH cells *in vitro*
- Fig. 4.8. LDH leakage values of BSBp in SK-N-SH cells
- Fig. 4.9. Intracellular ROS generation in SK-N-SH cells after treatment with BSBp derivatives
- Fig. 4.10. MMP of BSBp in SK-N-SH cells
- Fig. 4.11. Confocal images of Only cells, and cells with HSA-peptides, Tetra-peptides and Tripeptides: FGER, TESL, PERN, LQKF, CHGD  $A\beta_{1-42}$ , STR, KTW, HRQH, PHQW, THS, VRY, PHDW and NWHH after treatment with Rho13.

## **List of Tables**

Table 3.1 Percentage change in the secondary structure upon addition of different concentration of withanolide and withanoside molecules Table 3.2 Percentage of cells in each quadrant without addition of the drug and in the presence of withanolide and withanoside derivatives Table 4.1 Docking scores and X scores for tri and tetrapeptides against  $A\beta_{1-42}$ Table 4.2 Docking scores and X scores for HSA peptides and a positive control KLVEF with  $A\beta_{1-42}$ Free energy values evaluated by MMPBSA Table 4.3 Lipinski Rule of Five to see drug-likeness properties by analysing the five Table 4.4 physiochemical properties Table 4.5 Prediction of drug ability based on the ADMET properties Table 4.6 Tββhe IC<sub>50</sub> vβlues of the peptides in SK-N-SH cells

## **Abbreviations**

A $\beta_{1-42}$  Amyloid-Beta (1-42)

ADMET-SAR Absorption, Distribution, Metabolism, Excretion and

Toxicity – Structure-Activity Relationship

AFM Atomic force microscopy

AMBAR Alzheimer management by albumin replacement

BBB Blood-brain barrier

BSBp  $\beta$ -sheet breaker peptide

CADD Computer-aided drug design

CD Circular dichroism

CDD Clinical development design
DCFH Dichlorodihydrofluorescein

F Fluorescence intensity in presence quencher

Fcor Corrected fluorescence intensity

FDA Federal drug administration

Fo Fluorescence intensity in the absence of quencher

Fobs Observed fluorescence
HSA Human serum albumin

HTS High throughput screening

IC<sub>50</sub> Half maximal inhibitory concentration

K Binding constant

KD Stern-Volmer quenching constant

Kq Bimolecular quenching rate constant

LDH Lactate dehydrogenase assay

MD Molecular dynamics

MTT 3-(4,5-Dimethylthiazol-2-Y1)-2,5-Diphenyltetrazolium

MMP Mitochondrial membrane potential

MMPBSA Molecular mechanics Poisson-Boltzmann surface area

PDB Protein data bank

PPI Protein-protein interactions

Rg Radius of gyration

Rho123 Rhodamine

RMSD Root mean square deviation

RMSF Root mean square fluctuation

ROS Reactive oxygen Species

TEM Transmission electron microscopy

ThT Thioflavin - T

SK-N-SH Human neuroblastoma cells

 $\Delta G$  Free energy

 $\lambda_{em}$  Emission wavelength

 $\lambda_{ex}$  Excitation wavelength

# **List of Amino Acids**

Amino Acid	One letter code
Alanine	A
Arginine	R
Aspartic Acid	D
Asparagine	N
Cysteine	C
Glutamic Acid	E
Glutamine	Q
Glycine	G
Histidine	Н
Isoleucine	I
Leucine	L
Lysine	K
Methionine	M
Phenylalanine	F
Proline	P
Serine	S
Threonine	T
Tryptophan	W
Tyrosine	Y
Valine	V

**Chapter – 1 Introduction** 

## Introduction

Blood, the crucial constituent of the circulatory system is mostly liquid with various cells and serum proteins suspended in it. It is a specialized body fluid that supplies essential substances around the body, such as sugars, oxygen, and hormones. It also removes waste from the cells in the body. There are four basic components that comprise human blood: plasma, red blood cells, white blood cells and platelets. Most of the liquid content in the blood is the plasma and the main component of the plasma is serum, the plasma devoid of clotting factors/proteins but contain albumins and immunoglobulins. The total serum protein in blood is 7g/dL which accounts for 7% of total blood volume (Anderson & Anderson, 1977). Serum albumins are the most abundant soluble circulatory proteins in the blood and are made in parenchymal cells of the liver and finally enter the blood stream as non-glycosylated form of the proteins (Fanali et al., 2012). They serve various different functions, including transport of hormones, lipids, vitamins and minerals in activity and help in functioning of the immune system. Other blood proteins act as enzymes, complement components, kinin precursors. Against the popular belief, haemoglobin is not a blood protein, as it is carried within red blood cells, rather than in the blood serum. Serum albumin accounts for around 55% of blood proteins, it is a major contributing factor for maintaining the oncotic pressure of plasma and assists, as a carrier, in the transport of lipids and steroid hormones. Globulins are around 38% of blood proteins and, hormones, transport ions and lipids assisting in immune function. Fibrinogen comprises 7% of blood proteins; conversion of fibrinogen to insoluble fibrin is vital for blood clotting. The remainder of the plasma proteins which is 1% of the regulatory proteins, such as proenzymes, enzymes and hormones. All blood proteins are synthesized in the liver except for the gamma globulin.

#### 1.1 Serum Albumin

Serum albumin, also referred to simply as blood albumin, is an albumin (a type of globular protein) present in the vertebrate blood. Human serum albumin (HSA) is encoded by the serum albumin (ALB) gene. The albumin gene family is based on structural similarity and similar ancestral gene, comprises of the genes encoding serum albumin (ALB), α-fetoprotein (AFP), α-albumin (ALF) and vitamin D-binding protein (DBP) (Gibbs & Dugaiczyk, 1987). They have a similar structure revealed by their amino acid sequence. In addition to amino acid sequence parity, members of the albumin gene family also share a particular pattern of several S-S- cross-linked loops in their polypeptide chain, ensuing in a protein structure comprising of three domains. At the gene level, the exon/intron splitting pattern of the human AFP, ALB and DBP genes are likewise, besides for loss of two exons in DBP gene structure. In human, the genes for ALB, AFP, ALF, and DBP are located in the sub-centromeric region of chromosome 4q, and they are tandemly linked in the order 5'-ALB-5'-AFP-5'-ALF-5'-DBP-centromere. The four genes are expressed in liver, but the differential expression of these genes is developmentally regulated (He & Carter, 1992; Efimov, 1997).

#### 1.2. Human serum albumin

The word albumin derives from the latin albus, white. Serum albumin is the principal protein component of plasma and it binds a variety of molecules. HSA is the serum albumin present in human blood. It is the most prominent protein in human blood plasma; it comprises about half of serum protein. Albumin is synthesized in the liver as preproalbumin, which has an N-terminal peptide that is removed before the nascent protein is released from the rough endoplasmic reticulum. The product, proalbumin, is in turn

cleaved in the Golgi vesicles to produce the secreted albumin. It is water soluble and monomeric. HSA is carrier for all exogenous as well as endogenous substances like fatty acids, hormones and other compounds, buffers pH, and is major contributing factor for maintaining oncotic pressure (Sugio et al., 1999).

Hydrophobic substrate molecules are transported in human plasma and extravascular fluids via carrier proteins, and HSA is the most abundant protein present in the circulatory system. HSA comprises approximately 60% of the plasma protein and the versatile binding properties of HSA make it a major contributor in maintaining the oncotic pressure of the blood. The range for albumin concentration in serum is approximately 35–50 g/L (3.5–5.0 g/dL). It has a serum half-life of approximately 20 days. HSA is the rare plasma protein which cross blood brain barrier. The gene for albumin is present on 4<sup>th</sup> chromosome in mutations in this gene can result in anomalous proteins. The human albumin gene comprises of 16,961 nucleotides long from the putative 'cap' site to the first poly(A) addition site. It is divided into 15 exons that are symmetrically positioned within the 3 domains thought to have arisen by triplication of a single primordial domain.

#### 1.3. Structural features of HSA

Of the 609 amino acids in this sequence, encoded by the ALB gene and translated to form the precursor protein, only 585 amino acids are observed in the final product present in the blood; the first 24 amino acids, including the signal peptide (1–18) and propeptide portions are cleaved after translation. HSA consists of a single chain, 585 amino acids in length and the molecular mass of 66.5 kDa. The HSA protein incorporates three homologous domains (I, II, and III), the domain I consists of residues 5-197, domain II includes residues 198-382, and domain III is formed from residues 383-569. Each domain is comprised of two

sub-domains termed A and B (IA; residues 5-107, IB; residues 108-197, IIA; residues 198-296, IIB; residues 297-382, IIIA; residues 383-494, IIIB; residues 495-569) (Kragh-Hansen et al., 2013) (Fig. 1.1).

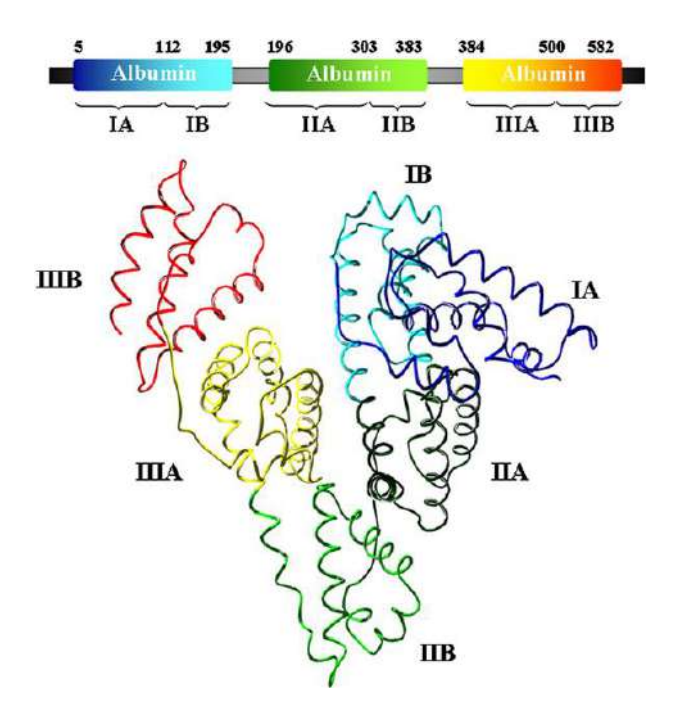


**Fig. 1.1.** Modular domain organization of HSA. The upper panel shows the architecture of the SA sequence, with three repeated conserved domains, as assigned by the NCBI CDD entry cd00015. The lower panel shows the three-dimensional structure of HSA with the subdomains rendered with different colors (domain IA, in blue; domain IB, in cyan; domain IIA, in dark green; domain IIB, in light green; domain IIIA, in yellow; domain IIIB, in red). Atomic coordinates were taken from the PDB entry 1AO6. Ribbon representation of HSA was drawn with the Swiss-PDB viewer (Privalov, 1979; Guex and Peitsch, 1997; Sugio et al., 1999).

HSA is widely studied protein because its primary structure is well known, and its tertiary structure has been determined by X-ray crystallography and now the structure is known at a resolution of 2.3 Å. It is a globular, single chain protein with 585 amino acids. Structurally, it is a non-glycosylated protein. In its biologically active state, HSA is an extremely versatile monomer with flexible structural organization. Although predominantly  $\alpha$ -helical, other secondary structures include 28  $\beta$ -turns, 2  $\gamma$ -turns, and 17

disulphide bridges involving 35 cysteine residues, except one (Cys 34) (Ghuman et al., 2005) (Fig. 1.2). The chain is characterized by having no carbohydrate moiety, a scarcity of tryptophan and methionine residues, an abundance of acidic (98 Glu<sup>+</sup> Asp) and basic (83 Lys<sup>+</sup> Arg) residues which make it highly soluble in aqueous media. It is a radical protein with 67 %  $\alpha$ -helix but no  $\beta$ -sheet that assemble to form a heart-shaped molecule (80 x 30 x 30 Å) (Meloun et al., 1975; Privalov & Gill., 1988; Bhattacharya et al., 2000).

Allosteric modulation and cooperativity characterize the binding sites of HSA and allow HSA to functionally mimic the activity of a multimeric enzyme. Localized defects in protein packing often culminate in closed cavities, which can potentially reduce the stability of a protein's structure. Beyond their classification as "packing defects," however, closed cavities are also credited as facilitators of conformational changes within the protein's monomeric structure. There are 19 total closed cavities inherent in the HSA structure (Chuang & Otagiri, 2006). Albumin the major non-glycosylated protein, has two crucial drug binding sites known as Sudlow's site II and I which are domain IIIA, IIA and also domain IB noticed as one of drug binding site, and it is also coupled with the Sudlow's site (Zsila, 2013).

Problems with adsorption, distribution, metabolism, and elimination must be considered and addressed throughout the development of any new drug. Thus, the biological function of HSA is of great interest to pharmaceutical companies, because HSA is an instrumental protein in dictating the active concentrations of administered drugs. HSA have two drug-binding sites; those are studded with basic side chains, thus conferring an affinity for anionic, lipophilic drugs. These two pockets are found within the core of subdomains IIA and IIIA. Non-esterified fatty acids are the primary physiological ligands of HSA, and the predominantly a polar nature of HSA's binding pockets promotes van der

Waals interactions between HSA and the associated fatty acid substrate (Carter et al.,1989). The half-life of circulatory albumin is extraordinarily long, and it is being utilized by conjugation, association or fusion therapy to extend the half-life of therapeutic molecules (Sleep et al., 2013).

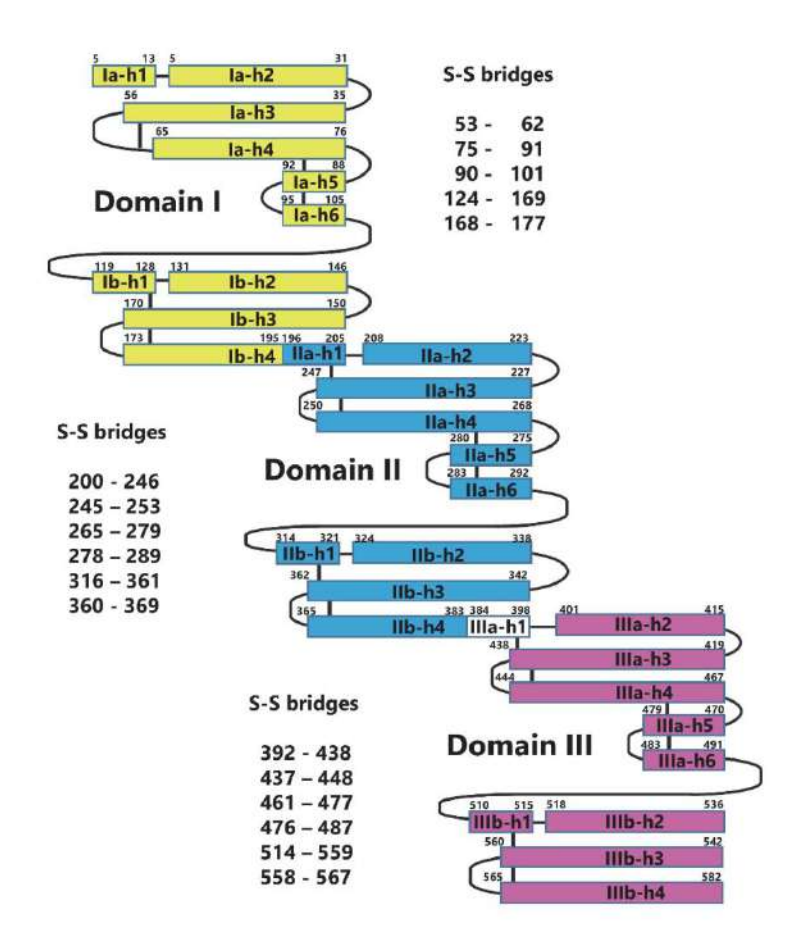


**Fig. 1.2.** Schematic drawing of secondary structural elements and Disulphide bridges of HSA. Helices are represented by rectangles and loops and turns by thin lines. Disulphide bridges are drawn with thick lines (Adapted from Sugio et al., 1999).

HSA achieves substrate selectivity via a small class of basic residues that are positioned both posteriorly (W-150, H-242, R-257) and around the periphery of drug binding site 1 (K-195, K-199, R-218, R-222). Through these residues, HSA effectively

anchors the substrate to the binding site via hydrogen bond interactions. Experimental data suggests that the majority of HSA drug site 1/substrate interactions involve K-199, R-222, and H-242. The existence of basic, positively charged residues and the absence of glutamate and aspartate residues is a distinctive structural feature of subdomain IIA that imparts specificity of function demonstrated by this binding site. Subdomain IIA also known as Sudlow's Site I is important in interaction of this protein with any molecule. Molecules binding on site 1 are mostly anionic or electronegative species that are inherently attracted to the positively charged residues positioned within the pocket of subdomain IIA. Although electrostatic interactions between the drug substrate and HSA account for a large portion of the substrate's affinity for the albumin IIA binding site, hydrogen bond interactions and Van der Waals forces also contribute to the overall attraction. Every compound that complexes with drug binding site 1 in subdomain IIA orients itself to generate a hydrogen bond interaction with W-150, making this residue essential for proper enzymatic function and drug transportation. If W-150 is occupied in a hydrogen bond with the carboxylate moiety of a fatty-acid, then the IIA site is no longer capable of the drug-binding interaction that is observed with defatted HSA. Although the interaction with W-150 is sacrificed upon fatty acid-binding, the interaction with H-242 is retained (Curry et al., 1999).

Drug site 2, located in subdomain IIIA, is topologically similar to site 1. Site 2 mimics site 1 in its hydrophobic nature and its polarity; it is composed of a large hydrophobic cavity with polar features mostly contributed by basic residues. Site II differs from site 1 in its size and accessibility. Site 2 is smaller, with an entrance that is less sterically hindered and more exposed to the surrounding environment (See Fig. 1.3). In contrast to site 1, site 2 bears only a single polar patch that is constricted to one side of the pocket and centred on W-411, R410, K-414, and S-489.

Sudlow's site II involves the hydroxyl group of W-411 as the main interaction amino acid for ligand binding. The discrepancies that exist between the HSA drug-binding sites are sufficient for sites 1 and 2 to be distinguishable from one another in terms of polarity, size, and shape. These differences illustrate the unique binding specificities and substrate selectivity of each site of HSA (Petitpas et al., 2001; Fasano et al., 2005). This negatively acute phase protein exerts pharmacological property because of its long half-life of 19 days, and its ability to bind with several exogenous as well as endogenous compounds (Lopukhin et al., 2000). The interaction between the drugs and plasma protein influences the absorption, bio-distribution, metabolism and excretion of the drug. Albumin, the major non-glycosylated protein, has two important drug binding sites known as Sudlow's site II and I which are domain IIIA, IIA and also domain IB noticed as one of ligand binding site and known as the third important binding site of has (Zsila, 2013; Zunszain et al., 2008).

## 1.4. Binding studies of HSA

After binding of ligand molecules to HSA, it controls the active concentration of the drug, for a long duration of action, and ultimately affects ligand ADMET (absorption, distribution, metabolism, excretion and toxicity) properties (Bertucci & Domenici, 2002). The clinical consequences of ligand-albumin interactions are now well understood. HSA has a number of binding sites for endogenous and exogenous ligands, may require dosages to be closely monitored. Such information is valuable to exploit the carrier properties of HSA in the development of novel therapeutic reagents for drug targeting particularly for analysing the pharmacokinetics and pharmacodynamics of the ligand molecule (Otagiri, 2005; Hosainzadeh et al., 2012).

HSA is known to have strong negative charge, but it is known to bind to both cations and anions reversibly and weakly. It is a plasma protein which has the capacity of binding to large variety of ligands and fatty acids with high affinity. It is the major transport protein in the blood also known as the cargo in the blood (Varshney et al., 2010). It also is known to possess an enzymatic property which is used to convert prodrugs to active therapeutics.

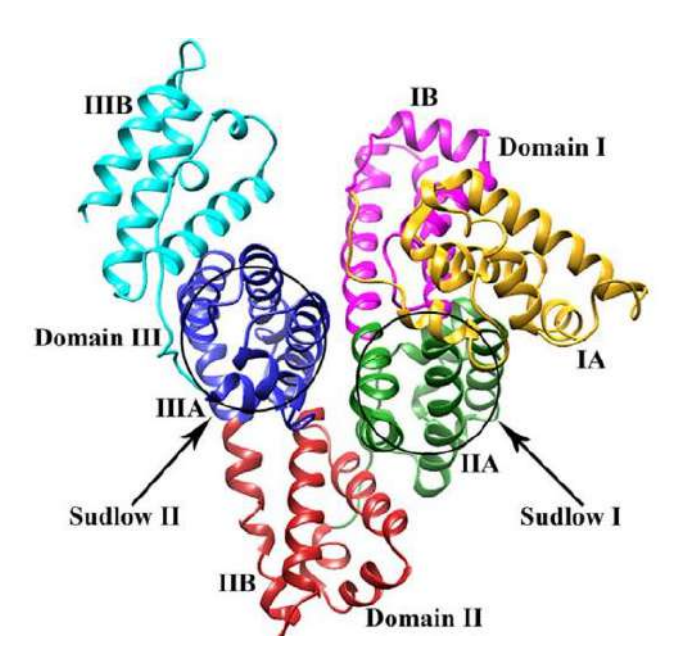


Fig. 1.3. Drug binding sites of HSA (adapted from Moumitha et al., 2017).

Phytochemicals are bioactive compounds that assist and promote health and ensure at the convergence of food and pharmaceutical industries. Such compounds may range from dietary supplements, isolated nutrients, and specific diets to genetically engineered designer foods, herbal products, beverages and processed foods (Surh, 1999; Kalra, 2003). There are several major groups of phytochemicals like flavonoids, terpenoids, carotenoids, limonoids, phytoestrogens phytosterols, glucosinolates, phytosterols, polyphenols, isoflavonoids anthocyanidins, phytoestrogens and anthocyanidins. These phytochemicals, either alone and/or in combination, have significant therapeutic potential for healing

various ailments (Pistollato & Sachana, 2016; Santini et al., 2017; Di Sotto et al., 2020). They play specific pharmacological effects in human health as anti-inflammatory, antibacterial, anti-allergic, antioxidants, antifungal, antispasmodic, chemo preventive, hypolipidemic, hepato-protective, antiaging, neuroprotective, hypotensive, induce apoptosis, diuretic, analgesic, CNS stimulant, protects from UVB-induced carcinogenesis, and as immuno-modulator.

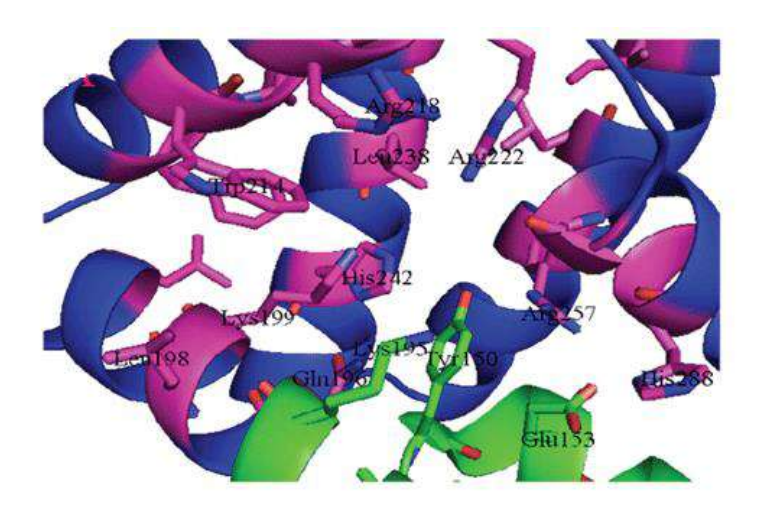
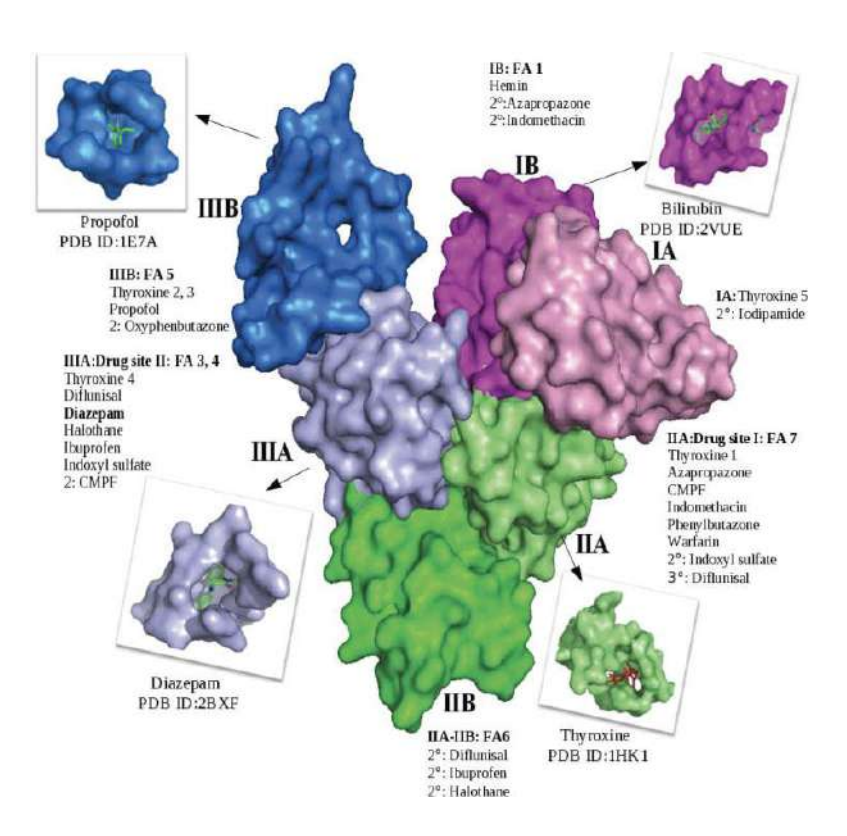


Fig. 1.4. The binding site of IIA domain of HSA (adapted from Zeyad Yasseen et al., 2016)

The binding association of ligands binding to HSA mostly occurs in site I of HSA. Site I is a hydrophobic cavity which has the property to hold multiple ligands at the same time (Simard et al., 2006; Yang et al., 2013) (Fig. 1.4.). It is a preformed pocket in the core of subdomain IIA, which consists of and a loop-helix feature and six helices of the subdomain. The interior of the pocket is hydrophobic, predominantly delimited by residues Trp214, Leu219, Phe223, Leu238, His242, Leu260, Ile264, Ser287, Ile290, and Ala291 (Fig. 1.4.). This subdomain also has two arrays of polar residues, an inner array of amino acids toward the bottom of the pocket (Tyr150, His242, Arg257) and an outer array at the pocket entrance composed of Lys195, Lys199, Arg218, and Arg222 (Fig. 1.4).

In our previous studies reported extensive binding mechanism of HSA with many drug molecules like  $\beta$ -sitosterol (Sudhamalla et al., 2010); coumarin derivatives (Garg et al., 2013); chitosan oligomers, asiatic acid; (Gokara et al., 2013). Many other phytochemicals were investigated like piperine, embelin, corilagin, andrographolide (Yeggoni et al., 2014a; 2016a; 2016b; 2017a). Even synthesized molecules like lupeol derivatives, androstenedione and its derivatives etc. have shown good binding and effective binding energy with HSA (Kallubai et al., 2015; Nerusu et al., 2017). Also, it is known protein for binding several drug molecules and that was proved using several experimental studies (Varshney et al., 2010) (see Fig. 1.5). The interaction studies of various ligands to the plasma protein may be of significant clinical importance.



**Fig. 1.5.** Based on crystallographic studies till date HSA binding with various ligands and fatty acids (adapated from Varshney et al., 2010).

## 1.5. Herbal derivatives from plant *Withania somnifera* (Ashwagandha)

Withania somnifera (Ashwagandha) is a medicinal plant used in Ayurvedic medicine as a remedy for various ailments since past 3,000 years. It is a major constituent for polyherbal preparation. It is being used as a rasayana to promote physical as well as mental health. The active components of the plant are known to have nootropic activities withanolides and withanosides are secondary metabolites; structurally comprising of a steroid backbone bound to a lactone or one of its derivatives generated by oxidation of steroids (Glotter, 1991). Various parts of these medicinal plants are known to have healthpromoting effects, particularly they are known to increase the immunity and are used as herbal supplement for various neurological disorders. These compounds can be isolated from Withania somnifera (Indian Ginseng; family:Solanaceae) also known as Ashwagandha; it is found to be loaded with numerous medicinal properties and useful in counteracting various illness like dehydration, muscle tension, memory loss and also restoring general health and vitality.

This plant is known to be found globally, with more occurrences in xeric and drier regions of tropical and subtropical areas (Mirjalili et al., 2009; Dar et al., 2015). The crude extract will give positive results, but we cannot say which molecules are effective in curing the diseases. Pure compounds always give the accurate action on the disease. *Withania somnifera* is rich in more than 35 different chemical constituents, including alkaloids, steroidal lactones, flavonoids, steroids and nitrogen-containing compounds. More than 40 structures of withanolide and withanosides were reported, which represent a collection of naturally occurring C-28 steroidal lactone triterpenoids assembled on integral or reorganized ergostane structure in which C-22 and C-26 are oxidized to form a six-membered lactone ring, whereas withanosides differ with an extra hydroxyl on C-20 and

C-27 atom. In which particular interest and importance are a group of C28 steroidal lactones called withanolides. We have selected four derivatives of this plant, which are withanolide A (C<sub>28</sub>H<sub>38</sub>O<sub>6</sub>- 470.6Da), with an olide B (C<sub>28</sub>H<sub>38</sub>O<sub>5</sub>- 454.6Da), with an oside IV (C<sub>40</sub>H<sub>62</sub>O<sub>15</sub>-782.9Da) and with anoside V ( $C_{40}H_{62}O_{14}$ - 766.9Da) for our study (Fig. 1.6). The withanolides and withanosides are distinctive with their C-28 and C-40 steroidal lactones, with six-membered lactone ring formed by oxidization of the C-22 and C-28 on ergostane backbone. Although structurally similar, with anolide A differs from with anolide B with the presence of an extra hydroxyl group on C-20 atom, whereas withanoside IV differs from with anoside V with the presence of an extra hydroxyl group on C-27 atom. The derivatives of Withania somnifera have been used since time immemorial in Ayurveda and ancient system of medicine for its pharmacological activities like chemopreventive, antiinflammatory, anti-arthritic, and angiogenesis activity and they are being used as a rasayana to promote immunity, health and longevity which acts as an adaptogen and immunomodulatory (Nair et al., 2019). These compounds are also known to exhibit nootropic effect and are effective against several neurodegenerative diseases including Alzheimer's and Parkinson's disease; - hence Ashwagandha derivatives have become very popular oral supplement globally because of its strong remedial properties. Owing to the remedial properties of withanolides and withanosides, their affinity to bind with HSA was carried out, which might play crucial role in its pharmacokinetics and pharmacodynamics (Halim et al., 2020; Zahiruddin et al., 2020).

**Fig. 1.6.** The structure of with anolide A ( $C_{28}H_{38}O_{6}$ -470.6Da), with anolide B ( $C_{28}H_{38}O_{5}$ -454.6Da), with anoside IV ( $C_{40}H_{62}O_{15}$ -782.9Da) and with anoside V ( $C_{40}H_{62}O_{14}$ -766.9Da).

Since, Indian Ginseng is having several kinds of biological importance; we presume that the other four derivatives of Withanolide A, Withanolide B, Withanoside IV and Withanoside V may also have an excellent therapeutic role. So far, these molecules role in biological samples, including in vitro or in vivo, has not been explored. In our current study, I have tried to decipher the binding mechanism, stability and conformation of these compounds with HSA.

## 1.6. Role of Withania somnifera in Neurodegenerative Diseases

Ashwagandha is used as an apoptogenic, nervine tonic for the treatment of general debility, nervous exhaustion, insomnia, anti-stress and memory dysfunctions. It has been suggested as a natural drug for neurological disorders like brain tumors, traumatic brain injuries and neurodegenerative pathologies (Kulkarni and Dhir, 2008; Kumar & Kumar, 2009;

Kuboyama et al., 2014; Pratte et al., 2014; Dar & Muzamil Ahmad, 2020). Ashwagandha root extracts also showed the neurodegenerative property in Amyloid  $\beta_{1-42}$  (A $\beta_{1-42}$ ) induced *in vitro* and a mouse model for AD (Kuboyama et al., 2006; Singh & Ramassamy, 2017). Derivatives of *Withania somnifera* are of immense use in pharmacological importance and are known to be effective for various Central nervous system disorders like stress, insomnia, memory loss, Parkinson's etc.

Hence, in our study focused on four steroidal derivatives of *Withania somnifera* which are Withanolide A, Withanolide B, Withanoside IV and Withanoside V; and further our interest was inclined towards brain pathology. The major hindrance for various potential drugs was found to be the limitation of crossing the blood-brain-barrier (BBB). Thus, our experimental results showed that the *Withania somnifera* derivatives of interest could inhibit the aggregation of  $A\beta_{1-42}$  peptides with time.

#### 1.7. Alzheimer's Disease

Dementia is a disease where people suffer from memory loss, and Alzheimer's is the most prevalent type of dementia with gradual loss of brain cells responsible for memory and other functions start to die. 60 to 80% of the people suffering from dementia are suffering from Alzheimer's (Hippius, 2003). It is an insidious, chronic and persistent disease. AD was discovered by a German psychiatrist and neuropathologist Dr. Alois Alzheimer in 1906 who reported "A peculiar severe disease process of the cerebral cortex" by studying histopathology of the brain of a 50-year-old female patient named Auguste D.

AD is a neurodegenerative disease which has impacted around 10% of the population of age 65 and older and around 40% of the population of age 85 and older. According to World Health Organization, 50 million people across the globe have dementia

and it is projected that the number is going to rise to 82 million by 2030 and 152 million by 2050 (Prince et al., 2013). It is a disease where the symptoms are seen years after the degeneration happens in the neurons. It is slow a progressive and irreversible disease. Around 90% of the population suffering from the AD are suffering from Sporadic form of Alzheimer's which is commonly known as LOAD form (Late-onset Alzheimer's Disease), and 3 % of people suffer from Familial form of Alzheimer's (FAD). FAD has been shown to be associated with the mutations in either of the three genes the  $A\beta_{1-42}$  precursor protein (APP) gene located on chromosome 21, Presenilin1 gene located on chromosome 14 or Presenilin2 gene located on Chromosome 1 (Genetics of familial and sporadic AD) (Rachakonda et al., 2004; DeTure & Dickson, 2019).

AD is a pathologically characterized by extracellular senile plaques and intracellular neurofibrillary tangles. There are two kind of lesions formed in the brain of Alzheimer's patients; they are neurofibrillary tangles (NFT) and senile plaques. Plaques are composed of insoluble aggregates of  $A\beta_{1-42}$  peptide which are generated by cleavage of APP by  $\alpha$ ,  $\beta$  and  $\gamma$  secretases (as shown in Fig 1.7). The nerve impulses are disrupted because of the degeneration happening in the neurons, which leads to memory loss. NFT develops first in the hippocampus which is the part of the brain responsible for memory and learning, and then the senile plaques are seen in the brain which is composed of the  $A\beta_{1-42}$  protein. The two lesions spread throughout the brain. NFT first develops in the hippocampus, which is essential for memory and learning. Aggregation of the  $A\beta_{1-42}$  is the main hallmark of the disease (Smith et al., 1995; Qui, 2020).

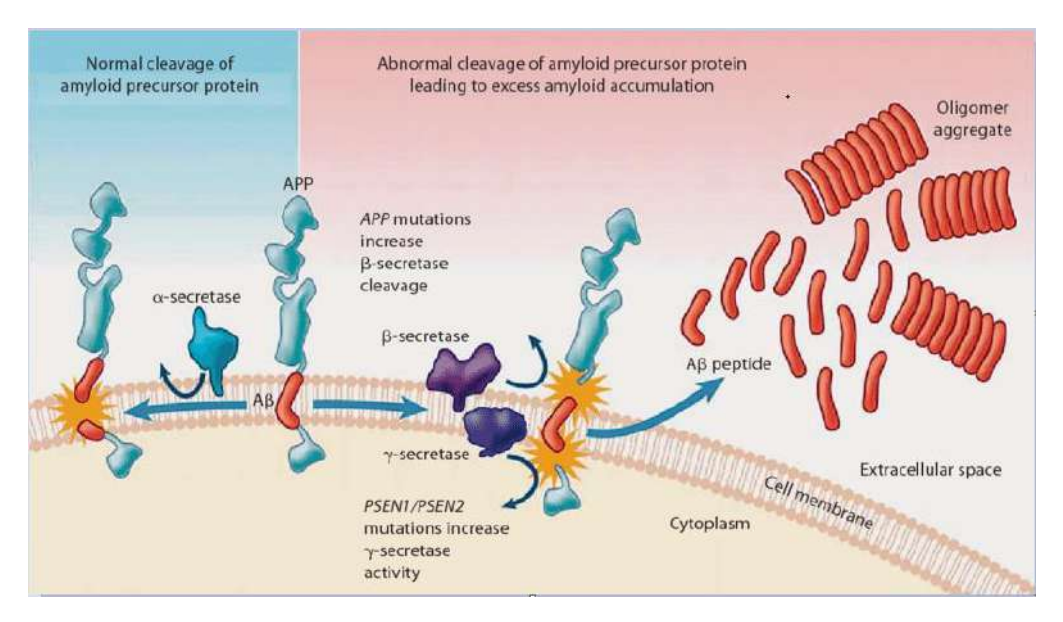


**Fig. 1.7.** Pathway showing the  $A\beta_{1-42}$  accumulation (adapted from Patterson et al., 2008).

 $A\beta_{1-42}$  is well known to be a central player in the pathogenesis of AD.  $A\beta_{1-42}$  is a monomeric in solution initially, but aggregate into low molecular weight structures, followed by higher molecular weight species like proto-fibrils, and eventually mature as  $A\beta_{1-42}$  fibrils. These fibrils are insoluble structures that are more than 1  $\mu$ m long, and 8-12 nm in diameter. The hippocampus region and cerebral cortex of the brain are the major parts affected by AD progression leading to their degeneration and plaque formation due to  $A\beta_{1-42}$  fibril deposition (Fig. 1.9) (Citron, 2010). In fact, the pre-fibrillar soluble oligomers have been found to be more cytotoxic than their fibrillar counterpart, even though they do not form insoluble aggregates (Roychaudhuri et al., 2008).

 $A\beta_{1-42}$  cascade hypothesis is the most accepted theory till now among the several theories which states that the primary neurologic damage is caused by the soluble and toxic oligomers, it states that the hallmark of the AD is the presence of  $A\beta_{1-42}$  fibrils (Hardy & Higgins, 1992).  $A\beta_{1-42}$  molecules are usually present in all human beings irrespective of their age or disease and they are cleared naturally and they are known to have neuroprotective properties at low concentrations if the  $A\beta_{1-42}$  protein is not cleared from

the brain then it accumulates as oligomers and eventually fibrils. Imbalance between the production and clearance of  $A\beta_{1-42}$  is known to be the major reason for the AD. Healthy individuals have the capacity to clear the  $A\beta_{1-42}$  from brain before it reaches the cytotoxic levels (Rachakonda et al., 2004).

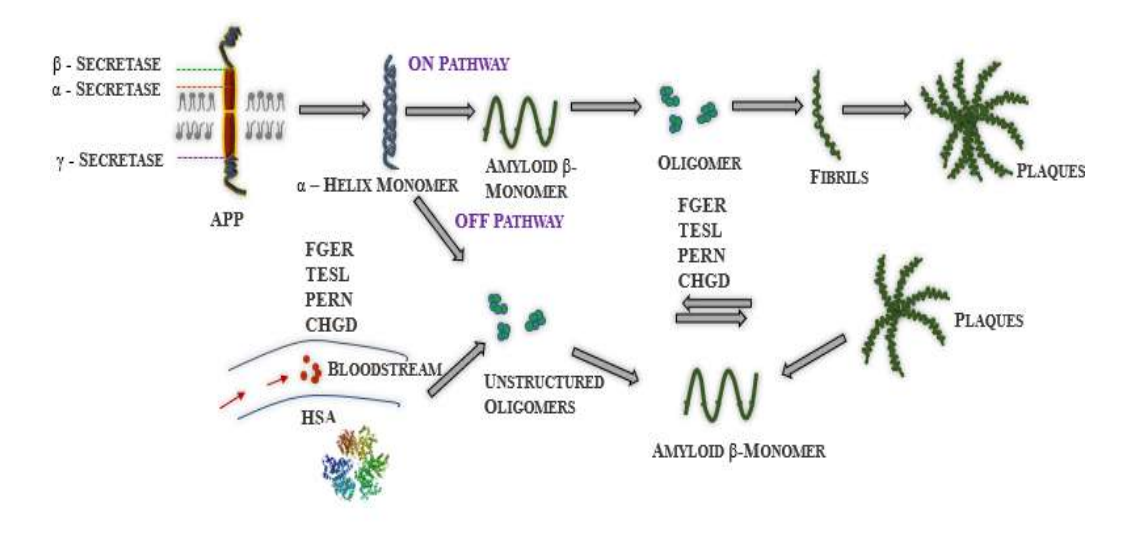


**Fig. 1.8.** The action of peptides on the fibrils.

 $A\beta_{1-42}$  aggregation proceeds through oligomerization, protofibrils and finally fibrils.  $A\beta_{1-40}$  and  $A\beta_{1-42}$  also seem to feature highly different conformational states, with the C-terminus of  $A\beta_{1-42}$  being more structured than that of the 1-40 fragment. The amino acid sequence of  $A\beta_{1-42}$  is as follows:

## DAEFRHDSGY EVHHQKLVFF AEDVGSNKGA IIGLMVGGVV IA

Amino acid 3 to 16 is region of  $\beta$ -turn and amino acid 17 to 21 is hydrophobic core while 22 to 42 is  $\beta$ -sheet. Hydrophobic core is made of aromatic amino acid 2 residues of phenylalanine. A $\beta_{1-42}$  has of a hydrophobic carboxyl terminus and a hydrophilic amino terminus. The carboxyl terminus of A $\beta_{1-42}$  comprises of  $\beta$ -sheets while the hydrophilic amino terminus comprises of  $\alpha$ -helixes and  $\beta$ -turns. Aggregation of monomeric A $\beta_{1-42}$  into

oligomers happens by the incorporation of the hydrophobic carboxyl terminus exposing the hydrophilic amino terminus. The carboxy terminus of  $A\beta_{1-42}$  is a requisite for  $A\beta_{1-42}$  formation. Inhibiting this hydrophobic core of  $A\beta_{1-42}$  by a probable drug molecule might mask the aggregation of  $A\beta_{1-42}$  (Giuffrida et al., 2009).

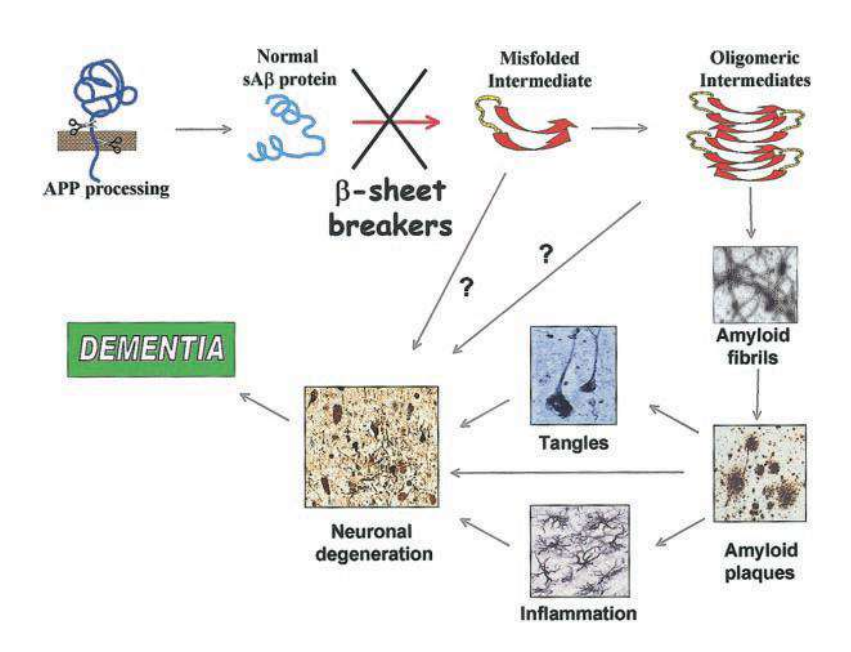


**Fig. 1.9.** Schematic representation of the  $A\beta_{1-42}$  hypothesis for the progression of AD adapted from Permanne et al., 2002.

As we can see,  $A\beta_{1-42}$  consists of a hydrophobic region KLVFF along with two hinge regions ED and SNK. The arrangement of the hinge brings both the hydrophobic regions close to each other, which is further stabilized by the production of a salt bridge between K28 and E22/D23. Electrostatic and hydrophobic interactions between these non-native side chains bring the peptides together, promoting the native backbone–backbone interactions to progress the assembly of  $\beta$ -sheets. The hydrophobic segments are the core of  $A\beta_{1-42}$  aggregates, and hydrophobic interactions are imperative for  $A\beta_{1-42}$  aggregation. It is suggested that the C-terminus of  $A\beta_{1-42}$  plays a crucial role in the process of oligomerization. HSA is a protein which is present in the human plasma at a concentration

of 640  $\mu$ M and in the brain at a concentration of 3  $\mu$ M and it was investigated that it binds to A $\beta_{1-42}$  when it is in oligomeric state and prevents another A $\beta_{1-42}$  to come and bind to it (Kim et al., 2020). As we know that HSA is a protein of 585 amino acids, and it has been studied that all the three individual domains of HSA are able to bind to the A $\beta_{1-42}$  in nanomolar concentration.

It becomes imperative to know which amino acids of HSA are interacting with the hydrophobic core of  $A\beta_{1-42}$  as HSA plays a very important role in clearance of the  $A\beta_{1-42}$  and the low concentrations of HSA is also one of the reasons for memory loss. HSA is known to be the key mediator for  $A\beta_{1-42}$  clearance. As the large majority of  $A\beta_{1-42}$  around 90% is bound to albumin, and very little is free, so plasma therapy by dialysis has come up as alternate treatment for early-stage Alzheimer's (Milojevic & Melacini, 2011; Algamal et al., 2013). AMBAR (Alzheimer's Management by Albumin Replacement) has already reached phase III of clinical trials, It is a very innovative approach for treating AD based on plasma exchange with albumin replacement as albumin is considered therapeutic in treating AD (Boada et al., 2019). My aim was to determine which amino acids of HSA interact with  $A\beta_{1-42}$  by employing molecular docking and on the basis of which amino acids are interacting taken fragments of HSA as tetrapeptides.

BSBp are short synthetic peptides that are able to bind to  $A\beta_{1-42}$  but not become a part of the  $\beta$ -sheet structure. They have a similar degree of hydrophobicity to the middle region of  $A\beta_{1-42}$  peptide but have a limited propensity to adopt  $\beta$ -sheet conformation, which is the characteristic for the fibrillization and the further neurotoxicity. Thus, these peptides have the ability to bind specifically with hydrophobic core of  $A\beta_{1-42}$  and block its aggregation. The first to be designed was the pentapeptide LPFFD and is the most extensively studied one (Soto et al., 1998). The hydrophobic core of the N-terminal domain

of A $\beta_{1-42}$  LVFFD corresponding to amino acids 17– 20 served as a template for designing of the pentapeptide LPFFD. It has been shown to prevent A $\beta_{1-42}$  fibrillization in rat models of AD. Soto *et al* (1998) was the first group to have postulated that fibrillization can be stopped by short peptides partially homologous to A $\beta_{1-42}$  which acts as  $\beta$ -sheet blockers by going and binding to the hydrophobic core of A $\beta_{1-42}$  which is KLVFF (amino acid number 17-21) thus inhibiting another strand of A $\beta_{1-42}$  to come and bind thus inhibiting aggregation, they called these peptides as  $\beta$ -sheet breaker peptides (BSBp) (Soto et al., 2002; Chacón et al., 2004; Laczkó et al., 2008; Viet et al., 2011; Camus, 2020).

#### 1.8. Peptides based drugs for neurodegenerative diseases

Peptides are now being considered as new generation of biologically active molecules because they are the key regulators in cellular and physiological responses, which has high potential for treatment various diseases. Although they have some limitations also like poor bioavailability, low stability in biological conditions and chances of getting cleaved by proteolytic enzymes. There are many strategies which are being implemented for making peptides more stable and which will create more opportunity for peptides being used as neurotherapeutic drugs. Peptide therapy is being used for various diseases, it is the most cutting-edge technology, use of medicinal peptides is giving very good results as they are very well tolerated, very safe and are highly specific and effective in their therapeutic action (Ahrens et al., 2012; Fosgerau & Hoffmann, 2015; Baig et al., 2018).

Peptides are now being used as drugs for various diseases as they are able to inhibit the protein-protein interaction (PPI) and also, they are easy and cheaper to synthesize in labs. PPI are foundation of essentially all cellular processes. Peptides synthesized by using D-enantiomers are to some extent resistant to proteolytic cleavages and the half-life of the

peptides is increased by interchanging L-isoforms by D-isoforms of amino acids. Crossing of the BBB and safe transportation of molecules into the brain is the major limitation for any drug to be effective. Use of peptides is further bolstered by their easy and cost-effective synthesis schemes in labs. More than 60 synthetic peptides are being used for treatment for various chronic diseases (Lee et al., 2019).

Peptides are known to have various benefits and are being used as drugs for various central nervous system diseases because of their capacity to inhibit protein-protein interactions. Particularly for Alzheimer's most of the  $A\beta_{1-42}$  inhibitors were synthesized based on the sequence of the  $A\beta_{1-42}$  and some were selected by random screening by using computational methods (Bruce et al., 2010). There are various issues when small molecular weight compounds are used as drugs that are circumvented by using peptides for the same purpose. The major limitation of the use of synthetic peptides as therapeutic agents is only their delivery in the brain and their bioavailability.

#### 1.9. β-sheet breaker peptides used for our study

Our main aim while designing the compounds is to have high CNS bioavailability and low immunogenicity and toxicity which is the major limitation for any drug designed for neurodegenerative diseases. Out of the 13 peptides under study, we have obtained very good results for a few peptides and would like to take them forward for this study. HSA peptides as well as other synthesized peptides are able to ameliorate the  $A\beta_{1-42}$  fibrillization in the *in vitro* experiments.

As it is said that "the future of medicine is within your molecules" and we know that HSA is a major player in the ameliorating  $A\beta_{1-42}$  fibrillization we wanted to identify the amino acids of HSA which are interacting with  $A\beta_{1-42}$ . So, we have taken five tetra

peptides fragments of HSA which were interacting with  $A\beta_{1-42}$ . Additionally, four tetrapeptides and tripeptides each were designed by CADD (computer-aided drug designing) for which we employed Schrodinger module from GLIDE for the same. According to the  $A\beta_{1-42}$  cascade hypothesis, we know that the  $A\beta_{1-42}$  fibrils are the major hallmark of the Alzheimer's disease, so our main focus was on analysing the fibrillization ameliorating properties of these peptides and see if have the capacity of acting as BSBp.

#### 1.10. Objectives:

Based on above findings, we have framed following objectives to prove our hypothesis.

- 1. Deciphering the importance of phytochemicals of *Withania somnifera* to understand its therapeutic benefits in ameliorating  $A\beta_{1-42}$  fibrillation and its binding studies with the cargo protein HSA.
  - a) Interaction between HSA and phytochemicals of Withania somnifera
  - b) Interaction between A $\beta_{1-42}$  and phytochemicals of Withania somnifera
- 2. Elucidating the inhibitory potential of HSA as well as synthesized peptides against  $A\beta_{1-42}$  fibrillation and  $A\beta_{1-42}$  associated neurotoxicity.

# Chapter – 2 Materials and Methods

#### Materials and methods

#### 2.1. Preparation of stock solutions

Fat free HSA was procured from Sigma Aldrich and working concentration of  $100\mu M$  was made by dissolving in 100mM PBS of pH 7.4 to maintain the physiological condition. Withanolides A, B and withanosides IV, V which are extracts of Indian Ginseng plant were procured from Natural Remedies Pvt. Ltd, Bengaluru, India with purity of ~99%. These compounds were first dissolved in dimethyl sulphoxide (DMSO) at 20 mM. This stock solution was further diluted to a concentration of  $100\mu M$  working stock in PBS (pH 7.4) similar to our previously reported studies (Gokara et al., 2016). The  $A\beta_{1-42}$  peptide used in this study was procured from GL Biochem (Shanghai, China) with a purity of 98%.  $A\beta_{1-42}$  was monomerised by dissolving in hexafluoro isopropanol at final concentration of 1mg mL<sup>-1</sup>, aliquoted and allowed to evaporate. It was then dissolved in DMSO to a concentration of 1mM and was further diluted to a working concentration of  $25 \mu M$  in PBS. Peptides under study were also procured from GL Biochem (Shanghai, China) with >95% purity and the stock concentration of 10 mM was made by dissolving in DMSO to maintain physiological conditions. All other chemicals used were of analytical grade from Sigma Aldrich.

#### 2.2. Room temperature fluorescence spectra

Fluorescence spectroscopy is an astounding technique used to study the interaction between protein and ligands, calculation of binding constant and free energy. Concentration of HSA was kept constant at  $1\mu M$  and withanolides A&B and withanosides IV&V were titrated in an increasing concentration from 1 to  $9\mu M$  in 0.1mM PBS of pH 7.4. Perkin Elmer LS55 fluorescence spectrometer was used to record the spectra and incubation time for all the

derivatives were kept constant for 5 min. Emission spectra was recorded in the range of 300-500nm, with parameters as per our previous studies (Gokara et al., 2010). Excitation wavelength of HSA was kept at 285 nm, and slit width was 5 nm for both excitation and emission spectra. Three independent experiments were carried out, and each time spectra recorded was almost identical (Yeggoni & Subramanyam, 2014b, Yeggoni et al., 2016b).

#### 2.3. Molecular displacement studies

For determining the exact binding site of the withanolides A&B and withanosides IV&V derivatives to HSA, we have studied the interaction of these derivatives with HSA in the presence of certain site-specific markers (Lidocaine for domain I, Phenylbutazone for domain II, and Ibuprofen for domain III) (Hein et al., 2010; Yeggoni et al., 2014a). The choices for the site-specific individual markers were based upon extensive earlier binding site studies of different ligands with HSA. The concentration of HSA and the markers were kept constant at 1 µM, and remaining all parameters were same as fluorescence spectroscopy. Experiments were done in triplicates and based upon the binding energy values; the binding sites were determined (Yamasaki et al., 2000; Subramanyam et al., 2009a, Sudhamalla et al., 2009b).

#### 2.4. Circular dichroism measurements

For exploring the conformational change of the protein upon addition of a ligand, circular dichroism (CD) is referred to as the 'Gold Standard' technique. Circular dichroism Spectropolarimeter, Jasco-815 was used for the study and the temperature was kept constant at 25 °C. Spectra were recorded in a quartz cell with path length of 0.02cm. Data was recorded from 190-260nm with a scan speed of 50 nm/sec (Min et al., 2004). The concentration of HSA was persistent at 1µM and the concentration of drugs 2, 4, 6 µM were added gradually

similar to the previous studies. CDNN 2.1 web-based software was used to calculate the change in percentage of  $\alpha$ -helix,  $\beta$ -sheet and random coils from its native conformation upon addition of withanolides and withanosides with increasing concentrations (Li et al., 2016, Yuan et al., 2017).

#### 2.5. Atomic force microscopy

Atomic Force Microscopy (AFM) was used to visually detect any change in the topography of the protein molecule surface upon addition of the ligand. AFM experiments were done by NT-MDT solver scanning probe microscopy in semi-contact mode using cantilever (0.3mm) with a force constant (5.5-22.5N/m), and the typical imaging resonance frequency was 140 kHz. 3.6x 1.6x0.4mm was the size of the gold-coated silicon probes used; tip height was 14-16 $\mu$ m and radius of curvature 10 nm. For sample preparation, 20  $\mu$ L of 2  $\mu$ M free HSA was spread on a glass slide and incubated for 10 min and then it was washed with 1mL de-ionized water to remove loosely bound molecules from the surface; and for HSA-ligand complexes, 20  $\mu$ L of a 10 $\mu$ M withanolides and withanosides were first incubated with HSA and similarly spread on a glass slide, washed and dried for 5 min. The dried samples were then imaged by AFM in non-contact mode.

#### 2.6. Transmission electron microscopy (TEM)

FE1 Tecnai  $G^2S$ -Twin-200kv instrument was used to observe the change in the morphology of the protein upon addition of the ligand, in high resolution.  $1\mu M$  HSA was used as the control and for HSA-ligand complexes,  $1\mu M$  HSA was incubated with  $2\mu M$  of withanolides (A and B) and withanosides (IV and V) individually. A drop of these samples was added on the carbon-coated copper grids and excess sample was removed by

absorption with filter paper. Before drying of the samples, 2% uranyl acetate negative stain was added, and final observation was made as described (Nagati et al., 2019).

#### 2.7. Thioflavin-T fluorescence assay

Thioflavin-T (ThT) is a fluorescent dye which can selectively bind to beta rich structures like  $A\beta_{1-42}$  fibrils. This assay is the most widely used 'gold standards' to selectively identify and analyze  $A\beta_{1-42}$  fibrillization, in both *in vitro* and *in vivo* systems. This contributes a great deal of insight into the morphology, development of the fibrils, and the effect of different inhibitory therapeutic molecules against the  $A\beta_{1-42}$  assembly.

Increase in the fluorescence intensity upon binding to fibrils is a defining and thoroughly studied characteristic of ThT, shows a dramatic shift of the excitation maximum (from 385 nm to 450 nm) and the emission maximum (from 445 nm to 482 nm) and that ThT fluorescence arises only from the dye bound to  $A\beta_{1-42}$  fibrils (Levine, 1993, Wang et al., 2002). The  $A\beta_{1-42}$  protein concentration was fixed at  $25\mu M$  and ligand concentrations were taken as  $100\mu M$ , in the ratio 1:4. An equal volume of both drug and peptides were taken and incubated at 37 °C. The first incubation period was kept for 6 hrs i.e., the lag phase period, in order to quantify  $A\beta_{1-42}$  oligomer formation and study its inhibition. The samples are then mixed with  $25\mu M$  ThT prepared in 50mM sodium phosphate buffer (pH  $\sim 7.2$ ) to make up the volume to  $100\mu L$ . The samples are then centrifuged at 15000xg for 10 min, and the supernatant was taken for analysis, since the oligomers are soluble.

A stock solution of 1 mM  $A\beta_{1-42}$  was prepared by dissolving 1 mg of lyophilized peptide in 220  $\mu$ L anhydrous DMSO. In a separate vial a stock solution of 10 mM BSBp was initially prepared and dissolving 2.3 mg of peptide in DMSO and then diluted 10 times by adding Phosphate Buffer Saline (PBS) to prepare a 1 mM solution. The final concentration of  $A\beta_{1-42}$  was fixed to 200  $\mu$ M and the peptide concentration was fixed at 50

 $\mu$ M. 80  $\mu$ L of 5  $\mu$ M ThT solution, prepared in PBS was added to the reaction mixture prepared in step III and further incubated for 5 min at room temperature. The excitation wavelength was fixed at 390 nm and the emission wavelength was set at 460 – 550 nm (Komatsu et al., 2019). A Horiba Fluoromax-3 fluorometer was used for carrying out the analysis, where the excitation and emission wavelengths were set at 450 nm and 482 nm respectively, and slit width kept as 4 nm, of 1cm quartz cuvette. The experiments were conducted at a constant temperature of 25 °C to prevent further aggregation during analysis. The samples were incubated again after oligomer analysis, and further kept for 48 hrs elongation phase period at 37 °C in order to quantify  $A\beta_{1-42}$  peptides in its fibrillar forms to determine the ameliorating effects of the drug molecules against  $A\beta_{1-42}$  oasis. All fluorescence experiments were done in triplicates.

#### 2.8. Cell Viability (MTT Assay)

SK cells were grown in a humidified incubator with 5% CO<sub>2</sub> and 95% air at 37 °C, in minimum essential medium supplemented with 10% fetal bovine serum, 200 IU/ penicillin, 200 g/mL streptomycin, and 1 mM sodium pyruvate. Every alternate day the medium was replaced, the cells were trypsinised, and sub-cultured after reaching around 80% confluency.

Cell viability was evaluated by using (3- (4, 5-dimethyl-thiazol-2-yl) -2, 5-Diphenyltetrazolium bromide)-MTT assay for 48 hrs, which indicates the importance of the molecules as a potential therapeutic agent determined from its IC<sub>50</sub> value. Cells were seeded in a 96 well plate at density of 10<sup>4</sup> cells per well. The cells were treated with the *Withania somnifera* derivatives at increasing concentrations of 10, 20, 40, 60, 80, 100μM and incubated for 48 hrs, after which 20 μL of MTT (5 g/mL in PBS) was added and incubated further for 4 hrs, whereas in control wells, the ligands were not added. To

dissolve the MTT crystals, 100  $\mu$ L of DMSO was added in each well. Finally, cell viability was measured at absorbance of 570 nm by using a Magellan plate reader. The experiment was carried out in triplicates, for each concentration of the withanolide and withanoside derivatives. Mean  $\pm$  SE was calculated and reported as the cell viability (%) vs concentration ( $\mu$ M). As the IC<sub>50</sub> value for A $\beta_{1-42}$  was found out to be 25 $\pm$ 1.33  $\mu$ M by dosedependent manner and the time required for A $\beta_{1-42}$  is around 6 hrs so we incubated the cells and once confluency was reached, we incubated it with 25  $\mu$ M of A $\beta_{1-42}$  for 6 hrs and then added half the concentration of IC<sub>50</sub> value and incubated for 24 hrs after which the protocol for MTT assay was followed.

#### 2.9. Apoptosis assay by Annexin V

Apoptotic cells have distinct morphological features like membrane blebbing, chromatin condensation, the formation of apoptotic bodies, but the hallmark of apoptotic cells is DNA fragmentation. Propidium iodide is used to stain the early apoptotic cells, and Annexin V binds to phosphatidylserine which is translocated to the outer membrane of the apoptotic cells, and Annexin V is linked to FITC which is a fluorochrome. Apoptosis was measured by the annexin V-FITC detection kit (Sigma cat. No. APOAF) on SK cells, after treatment with the withanolide and withanoside derivatives. The concentration of half the value of its IC50 value for 24 hrs was taken for the study. Following this, the cells were washed twice with phosphate-buffered saline and then resuspended in binding buffer. Finally, the cells were stained with annexin V-FITC for fifteen minutes and analyzed by flow cytometry. Annexin V conjugates with fluorescein isothiocyanate (FITC) which labels phosphatidylserine sites on the membrane surface and propidium iodide label the cellular DNA necrotic cells, where the cell membrane is almost disrupted. Cells were then collected

using a FACS Calibur flow cytometer (Becton Dickinson, USA) and Cell Quest Software (BD Bioscience, USA) was used for analysis (Kallubai et al., 2018).

#### 2.10. Tunel assay using confocal microscopy

Terminal deoxynucleotidyl transferase (tdt) d-UTP Nick-End Labeling (TUNEL) assay is used to analyze the apoptotic cells that undergo extensive DNA degradation during the late stages of apoptosis. The SK neuroblastoma cells were taken and seeded in 12 well plates at a density of  $10x10^4$  cells per well. The cells were incubated for 24 hrs, following which the derivatives were added at a concentration of half the IC<sub>50</sub> value. The cells were then once again incubated for 24 hrs. No drug was added in control well. Cell fixation was done by adding 4% formaldehyde and incubating at 4 °C for 30 minutes. Further, the protocol given in Takara MK 500 kit was followed and the cells were viewed under a confocal microscope ("Detection of Apoptosis by TUNEL Assay, Springer Nature Experiments", 2020).

#### 2.11. ROS intracellular assay

Intracellular reactive oxygen species (ROS) production was taken in fractions-treated and control cells by oxidation sensitive dye DCFH-DA. DCFDA dye after diffusing in the cell is deacetylated by cellular esterase's to a non-fluorescent compound, which is later oxidized by ROS into 2', 7'—dichlorofluorescein (DCF). DCF is a highly fluorescent compound which can be detected by fluorescence spectroscopy. Cells were grown in 96 well plates and exposed to fractions for 12 hrs. After incubation, the cells were washed thoroughly with PBS. The treated and control cells were re-suspended in 0.5 mL PBS containing 20 µM DCFHDA at 37 °C for 30 min in dark conditions. The incubated cells were again washed with PBS and fluorescence intensities were recorded in a spectrofluorometer (TECAN Infinite 200 PRO, Switzerland) at an excitation wavelength

of  $\lambda$  485 and an emission of  $\lambda$  535 nm. 25  $\mu$ M of  $A\beta_{1-42}$  was added to the confluent cells and incubated for 6 hrs which is the time required by  $A\beta_{1-42}$  to reach oligomeric state after which half the concentration of  $IC_{50}$  value of these phytocompounds were added and further incubated for 24 hrs. At each concentration of peptides, two different experiments were carried in duplicates. Mean  $\pm$  SE was calculated and reported as the cell viability (%) vs concentration ( $\mu$ M) (Chen et al., 2010).

#### 2.12. Lactate dehydrogenase assay

Cytotoxicity was measured by Lactate Dehydrogenase (LDH) Assay kit (Invitrogen Chemicals) in SK cells. Damaged cells upon treatment with LDH enzymes convert lactate into pyruvate with the release of NADH. This NADH is intensity is used to detect the cytotoxicity of drugs. Cells were seeded in a 96 well plate at density of  $10^4$  cells per well. The steps were carried as follows as given in the kit. Absorbance was measured at 450 nm using a Magellan plate reader. At each concentration of HSA derived peptides, two different experiments were carried in duplicates. Mean  $\pm$  SE was calculated and reported as the cell viability (%) vs concentration ( $\mu$ M) (Bhat et al., 2018).

#### 2.13. Cellular mitochondrial membrane potential assay

Mitochondrial Membrane Potential (MMP) measurement was carried using rhodamine123(Rho123) dye. Rhodamine fluorescence measure of membrane polarization in live cell assays within mitochondria. This use relies on the fact that rho 123 accumulates in membranes in a manner which is dependent on membrane polarization (Bhat et al., 2018). Cells were seeded in a 96 well plate at density of  $10^4$ cells per well. The cells were treated with  $A\beta_{1-42}$  after 8 hrs of seeding when the cells were distinguished and had 80% confluency and incubated. 12 hrs after the cells were treatment with  $A\beta_{1-42}$ , further the cells

were treated with the peptides and furthermore incubated for 24 hrs. The media was removed and washed with PBS after incubation.100  $\mu$ L of Rho123 was added (prepared by mixing 6  $\mu$ L of Rho123 and 5 mL of PBS) in each well plate and incubated for 45 min. The dye was removed and washed with PBS. The excitation and emission wavelength were set at 507 nm, and 529 nm, respectively and the reading was taken using a Magellan plate reader. At each concentration of HSA derived peptides, two different experiments were carried in duplicates. Mean  $\pm$  SE was calculated and reported as the cell viability (%) vs concentration ( $\mu$ M).

#### 2.14. Membrane potential assay with confocal microscopy

Mitochondrial membrane potential(MMP) measurement was carried using laser scanning confocal microscope and Rho 123 dye. Rhodamine fluorescence is important to see the presence of live neuroblastoma. Rho 123 accumulates in the membranes in a manner which is reliable for membrane polarization. Cells were seeded in a 12 well plate on coverslip placed inside the well plate at the density of  $10^4$  cells per well. The cells were treated with  $A\beta_{1-42}$  after 8 hrs of seeding when the cells were distinguished and had 80% confluency and incubated. 12 hrs after the cells were treatment with  $A\beta_{1-42}$ , the cells were treated with drugs and further incubated for 24 hrs. Rho123 solution and incubated for another 40 min. After the incubation the dye was removed and washed with the PBS buffer. 4% paraformaldehyde was added and incubated for 30 min. The coverslip was taken out from the well plate and placed on a glass slide with drop of 70% of glycerol and mounted for imaging. Imaging was done with Carl Zeiss LSM900 Confocal Laser Scanning Microscopes, and the excitation and emission wavelength was set at 507 nm and 529 nm, respectively.

#### 2.15. Molecular docking

An important tool to predict the binding mode of a ligand to the protein is the molecular docking tool. It will locate the conformer, which is geometrically and energetically stable. Autodock 4.2.3 is the latest user-friendly version to generate the 50 docked conformers of the protein-ligand complexes using a genetic Lamarckian algorithm (Malleda et al., 2011). From the protein data bank source, the crystal structure of HSA (PDB id:1AO6) and Aβ<sub>1</sub>-42 (PDB id:2BEG) structure was retrieved. 2D structures of withanolides and withanosides were built using Chemdraw and their geometry into three-dimensional structures, were optimized using Discovery studio 3.5 software. After preparation of ligand molecules, the receptors HSA Aβ<sub>1-42</sub> were prepared for docking. Water molecules in the protein were removed, Kolmann charges and hydrogen atomsat the polar were added. Both proteinligand were kept in the Grid within the size of  $126 \times 126 \times 126$  along X, Y and Z axis with 0.586 Å grid spacing to exhibit blind docking of withanolides and withanosides with HSA. The Final docking parameters were maximum number of energy evolutions: 250,000; GA population size: 150; and the number of GA runs; 50 (Sudhamalla et al., 2010; Yeggoni et al., 2017a). After 50 runs the docking analysis was done and the best conformer with lowest binding energy was selected out of all the 50 runs for further studies and the binding energy of the conformer also should correlate to the binding energy obtained with the experimental results by fluorescence spectroscopy. This conformer was further used to conduct docking simulations and to generate possible conformations of these derivatives binding to  $A\beta_{1-42}$ .

#### 2.16. Molecular dynamics simulations

The binding free energy obtained from fluorescence and the best conformer obtained from docking, which correlates with experimental results was used for the MD simulations. GROMACS V5.2 with force field GROMOS96 is the freely available software used to

conduct Molecular dynamics (MD) Simulations for 100 ns/200 ns. The parameters 300K and 1 bar pressure were set to energetically most stable conformer to perform simulations. Using Dundee PRODRG2.5 server (beta), the topology parameters of HSA were created, which is a starting file for the simulations. Then the prepared complex structure was immersed in a cubic box with extended simple point charge (SPC) water molecules; also, sodium counter ions were added to maintain electro-neutrality. Simulations were run on Linux cluster with 36 nodes (dual Xeon processor) and the trajectories containing frames at each 2 femtoseconds were saved for further conformational analysis.

PRODRG2.5 server (beta) was used to build the topology parameters of Ashwagandha derivatives (A, B, IV, V). The complexes were placed in a box of dimensions 80x80x80 Å of extended simple point charge (SPC) water molecules producing a system of 146 atoms of  $A\beta_{1-42}$  peptide. Sodium and chloride ions were added to maintain electroneutrality, energy minimization using steepest descent algorithm was performed in order to remove the local constraints occur due to bad vanderwal interactions. Once the system was converged, it was subjected to equilibration with NVT and NPT ensembles to attain the system temperature of 300K and 1 bar respectively. Finally, the system was subjected to MD simulation for 100 ns and the generated trajectory were analyzed using Xmgrace for root-mean-square deviations (RMSD), root-mean-square fluctuations (RMSF), and radius of gyration (Rg); and all the above simulations and analysis were performed on OSCAR Linux cluster with 12 nodes (dual xeon processor) at Bioinformatics facility, University of Hyderabad.

A 200 nanoseconds simulation was run using the software Gromacs v 5.2 package with force field GROMOS96 for A $\beta_{1-42}$  and peptide complexes. The topology parameters were created using Dundee PRODRG2.5 server (beta) (Mager et al., 2001). This is an *in-*

silico approach to determine the stability of the peptide-protein mixture in environment, whether they undergo any change in their torsional angle C-Cα-N and to understand the binding site of the drug on the protein. Rg, RMSD and RMSF are the respective outputs of the dynamic studies. Simulations and analysis were performed on the LINUX cluster at the Bioinformatics Facility, Jawaharlal Nehru University.

#### 2.17. Generation and preparation of peptide libraries

Peptide libraries of tri and tetra peptides were prepared *in silico* by parsing a python script to pymol molecular graphic system (Schrödinger, LLC, 2015). The build residue module of pymol was used for building all the possible combinations of 8000 tripeptides and 1,60,000 tetra-peptides. Prior to *in silico* screening and docking, the peptide libraries were subjected to Ligprep wizard of Glide docking (Friesner et al., 2004) module of Schrödinger suite. The Ligprep (Schrödinger, 2015) function of Glide, explicitly removes unwanted molecules, adds hydrogen, neutralizes charge groups, generates ionization states, tautomer's, stereoisomers, low-ring conformations and optimizes geometries of the ligand. Using Ligprep function, maximum of 32 tautomers of each peptide sequence was generated and their geometries and plausible ionization states were optimized at pH 7.0±2. Finally, 2,56,000 tripeptide and 51,20,000 tetrapeptide structures were generated (Friesner et al., 2004).

#### 2.18. Protein preparation

Solution structure for  $A\beta_{1-42}$  (1IYT) was downloaded from PDB database (www.rcsb.org). The solution structure, 1IYT comprised of 10 conformers resolved by NMR, thus, to scrutinize the final structure for *in silico* screening and docking protocols; ensemble structure, superimposition and morph conformations functions of chimera visualization

ensemble structures function of chimera. Conformers 8, 2, 4, 5, and 9 lied in one subfamily, while conformers 1 and 3, 6 and 10 comprised other sub families. Conformer 7 did not fit into any of the subfamilies and was considered independently. All the conformers in the sub families except conformer 7 were superimposed within the families, and a consensus single structure was extracted as a representative of each sub family. Further, all the representative structures and conformer 7 were superimposed and subjected to morph conformation function of chimera. The morphing of all the conformers was interpolated using corkscrew method with 1000 interpolation steps keeping default interpolation rate. The morph structure was then subjected to 1000 minimization steps and the final structure was used for *in silico* screening and docking. Prior to docking in Glide, the protein preparation wizard of Glide was used to assign bond orders and the addition of hydrogen. The Final, the structures were energy minimized using force field OPLS.

#### 2.19. Receptor grid preparation and molecular screening and docking

For docking of both tri and tetrapeptides, a common receptor grid with different sizes was prepared. A grid of 14 Å size for tripeptides and a grid of 18 Å size for tetra-peptides was used. The amino acids residues Leu-17, Val-18, Phe-19, Phe-20 and Ala-21 circumvented the grid. Post preparation of the grid, *in silico* screening of the tri and tetra peptides was carried out in three different steps. First high through put screening (HTVS) was performed to scrutinize peptides that can fit in the respective grids. The top 25% of both tri and tetrapeptides filtered by HTVS screening were then subjected to standard precision (SP) docking which computes protein-ligand interactions based on hydrophobicity, hydrophilicity and Vander wall, ionic and electrostatic forces and scrutinizes the ligand molecules on the basis of minimum energies with the target protein. The top 15% of each

peptide library resulting from SP computations were then subjected to extensive docking mode of Glide: the extra precision (XP) mode. The XP modes also compute the parameters described in SP mode. However, the computation time given for each ligand is more as compared to the SP mode. Based on XP docking, a consensus score defined as G score is computed, which is used to rank the top-scoring ligands based on minimum energies (Kcal/mol). Besides calculating Gscores, Glide also enlists Emodel value which is defined as the energy (Kcal/mol) of different binding poses of a ligand against the target protein (Friesner et al., 2004). Based on these Gscores and Emodel values, finally, top 3 tri and 4 tetrapeptides were selected for post docking analysis.

#### 2.20. Post docking analysis

Post docking analysis was performed using X score and Liginteraction programs. X score is a cumulative function comprising of three different scoring functions namely HPScore, HMScore and HSScore, which computes binding energies (Kcal/mol) of post docked protein-ligand complexes (Wang et al., 2002). The ligand-protein complex stability depends upon various intermolecular interaction forces including hydrogen bonds, hydrophobic and ionic interactions etc. To calculate these intermolecular forces, Liginteraction module of Glide, schrödinger suite was used. The Liginteaction modules calculate the number of intermolecular forces associated with the docked ligand-protein complexes and project them into a two-dimensional diagram.

#### 2.21. Docking for HSA peptide generation

Molecular docking is an important *in silico* tool to computationally analyze the interaction between any two molecules. Here, we have used HADDOCK (High ambiguity drove protein-protein docking) and PATCHDOCK for seeing the interaction between protein and

peptide (de Vries et al., 2010). The crystal structure of HSA (PDB ID: 1AO6) and  $A\beta_{1-42}$  (PDB id: 2BEG) structure was retrieved from RCSB protein data bank and docking was done using the online servers and then based on the scores the complexes were analyzed and based on the amino acids of HSA interacting with  $A\beta_{1-42}$  the tetra-fragments of HSA were taken and used as BSBp (Agrawal et al., 2019).

#### 2.22. Molecular mechanics poisson-boltzmann surface area (MMPBSA)

Free energy calculations are important to understand the protein-complex stability and the GMXPBSA 2.1 software is a convenient suite with Perl scripts and is adjustable also standardized depending upon the requirement (Paissoni et al., 2014). MMPBSA calculations on structural ensembles derived from GROMACS trajectories, can automatically calculate binding free energies for protein-protein or ligand-protein complexes (Bradshaw et al., 2011). Also, it compares the binding free energy of different complex trajectories, allowing to study the effects of non-alanine mutations, posttranslational modifications or unnatural amino acids on the binding free energy of the system under investigation (Paissoni et al., 2015). Eventually, it can perform relative affinity to the same receptor utilizing MD simulations of proteins in complex with different ligands and can be analyzed also ranked. In order to dissect the different MMPBSA energy including molecular mechanic (MM), electrostatic contributions, contribution to solvation (PB) and nonpolar contribution to solvation (SA), the tool combines two freely available programs: the MD simulations software GROMACS (Pronk et al., 2013) and the Poisson-Boltzmann equation solver APBS (Baker et al., 2001). All the calculations can be performed in single or distributed automated fashion on a cluster facility in order to increase the calculation by dividing frames across the available processors. Thus, we have calculated the binding energy by MM-PBSA to calculate the  $\Delta G$  bind of every selected ligand. Therefore, the final prioritization of the optimized lead compound was based on docking scores, ADMET studies and  $\Delta G$  bind (The PyMOL Molecular Graphics System, v 1.8 Schrödinger, LLC.)

## 2.23. Absorption, distribution, metabolism, excretion, and toxicity – structure-activity relationship database (ADMET-SAR)

ADMET data is being created since late 1990s, numerous pharmaceutical companies are now utilizing computational models that, in few cases, are replacing the "wet" screens (Hodgson, 2001). This paradigm shift has hence stimulated the making of various theoretical methods for the prediction of ADMET parameters. A host of these theoretical models have been implemented many of the software programs which are presently being utilized for drug discovery (OCHEM platform; Cruciani et al. 2000; Lhasa 2010; Schrödinger 2011), even though some of the predictions are often not totally satisfying (Tetko et al. 2006). The software tools usually used to predict the ADMET properties of potential drug candidates often utilize quantitative structure-activity relationships, QSAR (Hansch et al. 2004; Tetko et al. 2006) or knowledge-based methods (Greene et al. 1999; Cronin 2003; Button et al. 2003).

A set of ADMET-related properties were analysed by the QikProp program (Schrödinger 2011d) running in normal mode. QikProp generates physically relevant descriptors and uses them to perform ADMET predictions. An overall ADME-compliance score–drug-likeness parameter (indicated by #stars), was used to assess the pharmacokinetic profiles of the compounds within the StreptomeDB library (Onguéné et al., 2020). The #stars parameter indicates the number of property descriptors computed by QikProp that fall outside the optimum range of values for 95% of known drugs. The methods implemented were developed by Jorgensen and Duffy (Duffy and Jorgensen 2000;

Jorgensen and Duffy 2000; Jorgensen and Duffy 2002) and among the calculated descriptors are: the total solvent-accessible molecular surface,  $S_{mol}$  in Å (probe radius 1.4 Å) (range for 95% of drugs: 300–1000 Å); the hydrophobic portion of the solventaccessible molecular surface,  $S_{mol,hfob}$  in Å<sup>2</sup> (probe radius 1.4 Å) (range for 95% of drugs: 0–750 Å); the total volume of molecule enclosed by solvent-accessible molecular surface, V<sub>mol</sub> in Å (probe radius 1.4 Å) (range for 95% of drugs: 500–2000 Å); the logarithm of aqueous solubility, log Swat (range for 95% of drugs: -6.0 to 0.5) (Jorgensen and Duffy 2000; Jorgensen and Duffy 2002); the logarithm of predicted binding constant to HSA,  $\log K_{HSA}$  (range for 95% of drugs: -1.5 to 1.2) (Colmenarejo et al. 2001); the logarithm of predicted BBB partition coefficient, log B/B (range for 95% of drugs: -3.0 to 1.0) (Luco 1999; Ajay et al. 1999; Kelder et al. 1999) the predicted apparent Caco-2 cell membrane permeability (BIPcaco-2) in Boehringer-Ingelheim scale, in nm s<sup>-1</sup> (range for 95% of drugs: < 5 low, > 100 high) (Yazdanian et al. 1998; Irvine et al. 1999; Stenberg et al. 2001); the predicted apparent Madin-Darby canine kidney (MDCK) cell permeability in nm  ${
m s}^{\text{--}1}$  (< 25 poor, > 500 great) (Irvine et al., 1999) the index of cohesion interaction in solids, Indcoh, calculated from the number of hydrogen bond acceptors (HBA), donors (HBD) and the surface area accessible to the solvent, SASA ( $S_{mol}$ ) by the relation (0.00 to 0.05 for 95% of drugs) (Jorgensen and Duffy 2000); the globularity descriptor, Glob =  $(4\pi r^2)/S_{mol}$ , where r is the radius of the sphere whose volume is equal to the molecular volume (0.75)to 0.95 for 95% of drugs); the predicted polarizability,  $QP_{polrz}$  (13.0 to 70.0 for 95% of drugs); the predicted IC<sub>50</sub> value for blockage of HERG K<sup>+</sup> channels, log HERG (concern < -5) (De Ponti et al., 2001; Cavalli et al., 2002); the predicted skin permeability,  $\log K_p$  (-8.0 to -1.0 for 95% of drugs) (Potts

and Guy 1992; Potts and Guy 1995); and the number of likely metabolic reactions, #metab (range for 95% of drugs: 1–8).

Thus, to understand the drug-likeness properties of any compound ADMET-SAR gives us computational analysis for characterization of any molecule for being used as a drug. ADMET profiling of the BSBp was done by applying ADMET descriptors algorithm, toxicity prediction and ADMET-SAR database (freely available at http://www.admetexp.org) (Cheng et al., 2012).

### Chapter – 3

Deciphering the importance of phytochemicals of Withania somnifera to understand its therapeutic benefits in ameliorating  $A\beta_{1-42}$  fibrillation and its binding studies with the cargo protein HSA Deciphering the importance of phytochemicals of *Withania somnifera* to understand its therapeutic benefits in ameliorating  $A\beta_{1-42}$  fibrillation and its binding studies with the cargo protein Human Serum Albumin

#### 3.1. Introduction

Medicinal plants and their extracts have been used in traditional medicine as a remedy for various kinds of diseases since time immemorial. A plethora of therapeutic agents owe their origin to medicinal plants. Withania somnifera (Indian Ginseng; family: Solanaceae), also known as Ashwagandha, found to be loaded with numerous medicinal properties and useful in counteracting various illness like dehydration, muscle tension, memory loss and also restoring general health and vitality. Withanolides and Withanosides are secondary metabolites; structurally consists of a steroid backbone bound to a lactone or one of its derivatives generated from oxidation of steroids. The goal of this study was to elucidate the effect of interaction of phytocompounds, i.e., derivatives of Withania somnifera (Ashwagandha) namely withanolide A, withanolide B, withanoside IV and withanoside V, with carrier plasma protein HSA. Also, HSA is a major cargo protein known to transport all the exogenous and endogenous ligands. So, it is very imperative to study the binding of any compound to HSA to understand its pharmacokinetics. Through our current study, we would decipher the binding mechanism, stability and conformation of these compounds with HSA. Also, HSA is a rare protein which has the capacity to cross the BBB and also a key mediator in clearance of  $A\beta_{1-42}$ . The  $A\beta_{1-42}$  cascade hypothesis states that if  $A\beta_{1-42}$ protein is not cleared from the brain, it accumulates as oligomers and eventually forms fibrils, which is the hallmark of AD.

Also, we have performed extensive evaluation of these Ashwagandha derivatives in order to determine their inhibitory effects on  $A\beta_{1-42}$  oligomers as well as fibrils using

spectrophotometric methods and also *in vitro* cell culture assays. The cytotoxicity studies of plant derivatives against neuroblastoma cell lines were observed by apoptosis assays, which affirm their hypothesized therapeutic and pharmaceutical potential. Detailed knowledge of the active site of the peptide, and their interaction with the Ashwagandha derivatives were obtained by molecular docking studies. Furthermore, the stability of the ligand- $A\beta_{1-42}$  complexes were determined in 100ns timescale simulations. Our main aim was to understand first, the binding capacity of these phytocompounds with the plasma protein HSA and as it is the major carrier protein for all the endogenous as well as exogenous ligands. Also, it has the capacity to cross the BBB and the plant *Withania somnifera* is known to have neuroprotective properties so we wanted to further see if it can bind with  $A\beta_{1-42}$  and hence stop its aggregation which is the hallmark for Alzheimer's disease.

#### 3.2. Results and Discussion

#### 3.2.A. Interaction between HSA and phytochemicals of Withania somnifera

#### 3.2.A.1. Fluorescence spectroscopy

Since Ashwagandha is used as Ayurveda medicine, however, the active principles of these phytochemicals withanolide A, withanolide B, withanoside IV and withanoside V were not been understood well related to food supplements. Since HSA is an important protein to transport the small molecules to the target places; we have focused our study to understand the binding mechanism of these isolated molecules with HSA. The intrinsic fluorescence in HSA is imparted by a single tryptophan residue at the position 214, and also 18 tyrosine and 33 phenylalanine residues (Amdursky et al., 2015). By continuous titration of phytochemicals withanolide A, withanolide B, withanoside IV and withanoside V to HSA,

the fluorescence of the protein was quenched. These results stated that the intrinsic fluorescence of HSA is quenched gradually with increasing concentrations of withanolide and withanoside derivatives because of the change in microenvironment around Trp 214 residue. Its inner filter affect can be corrected by using the following equation,

$$F_{cor} = F_{obs10} (A_{exc} + A_{emi})/2$$

Where  $F_{cor}$  and  $F_{obs}$  are corrected and observed fluorescence intensity, respectively. A<sub>exc</sub> and A<sub>emi</sub> are absorbance at fluorescence excitation (285 nm) and emission (360 nm) wavelengths (Subramanyam et al., 2009a; Yadav et al., 2017). To validate whether the complex is undergoing dynamic or static quenching, bimolecular quenching constant was calculated from the slope of  $F_0/F$  vs Q and it was found to be linear, which indicates that it is undergoing static quenching. The fluorescence data was analyzed using the stern-volmer equation

$$F_0/F = 1 + K_0t_0 = 1 + KD[Q]$$

where  $F_0$  and F are fluorescence intensities, in the absence and presence of the quencher. Q is quencher concentration, and  $K_D$  is the stern-volmer quenching constant which can be written as  $K_D = Kqt_0$ ;  $t_0$  is the lifetime of the fluorophore for HSA (5.6ns). Since the interaction between withanolides and withanosides, and HSA is by static mode of binding, the modified stern-volmer regression curve is used to determine the binding constant (Ks) and the number of binding sites (n), where n is the slope and Ks is the binding constant.

$$\log[(F_0 - F) \div F] = \log K_s + n \times \log[Q]$$

The binding constants were calculated to be  $K_{Withanolide\ A} = 3.04 \pm 0.05\ X\ 10^4\ M^{-1}$ ,  $K_{Withanolide\ B} = 7.59 \pm 0.05\ X\ 10^4\ M^{-1}$ ,  $K_{Withanoside\ IV} = 6.74 \pm 0.03\ X\ 10^4\ M^{-1}$  and  $K_{Withanoside\ V} = 5.33 \pm 0.05\ X\ 10^4\ M^{-1}$  respectively as shown in (Fig.3.1A-D). This data indicates that withanolide and withanoside derivatives are strongly binding to the HSA. Hence, our

results are in agreement with previously published phytochemicals were strongly associated with HSA nav (Agudelo et al., 2012; Naveenraj & Anandan, 2013; Gokara et al., 2013). Also, the obtained binding constants are in concurrence with the food and drug administration (FDA) which indicates that phytochemicals used here withanolide A, withanolide B, withanoside IV and withanoside V could be potential therapeutic molecules.

The standard free energy change is calculated by using the following equation.

$$\Delta G^{\circ} = -RT \ln K_s$$

Where  $\Delta G$  is the free energy change, R is the gas constant at room temp and  $K_s$  is binding constant calculated from fluorescence data. The free energy changes upon binding of withanolides and withanosides with HSA was -5.61 Kcal M<sup>-1</sup>, -6.63 Kcal M<sup>-1</sup>, -6.56 Kcal M<sup>-1</sup> and -6.36 Kcal M<sup>-1</sup> respectively at 25 °C. This indicates that the interaction between the drugs with serum albumin is mainly hydrophobic interactions. The computationally derived free energy change was found to be totally in sync with the experimental data.

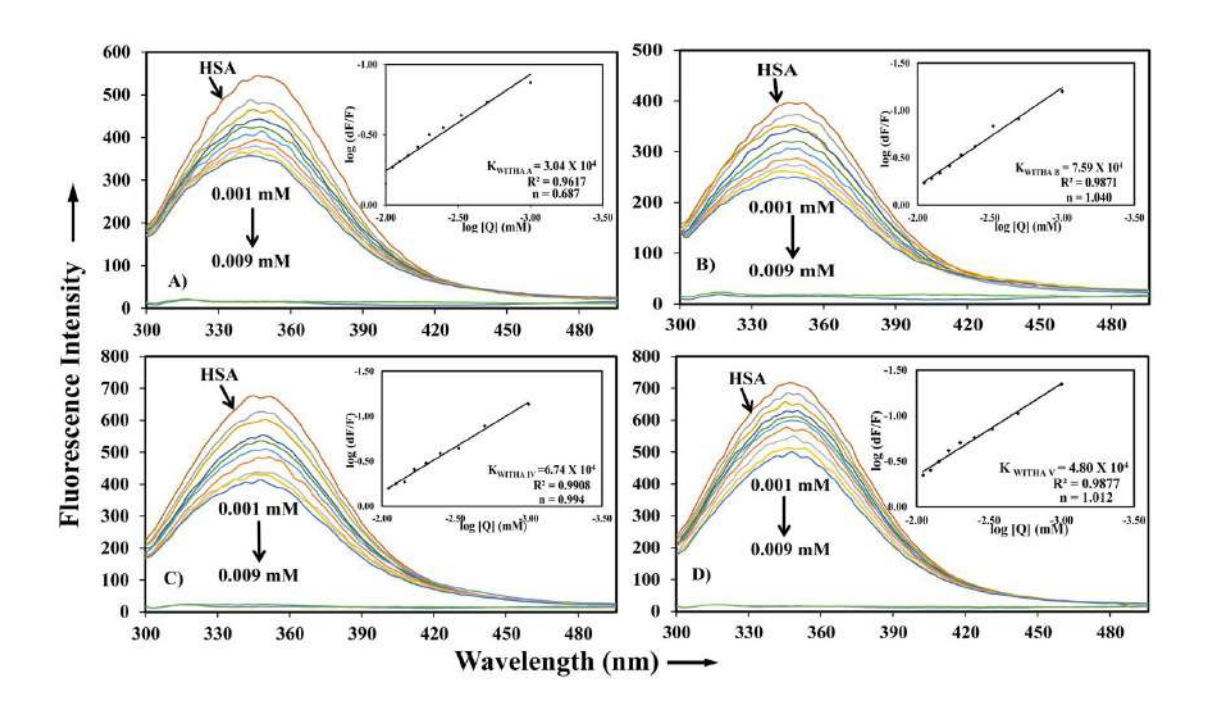


**Fig. 3.1.** Fluorescence spectroscopic studies of HSA with withanolide and withanoside molecules, indicating the interaction of the drug with plasma protein. The association constant ( $K_S$ ) and free energy change along with stern-volmer plots showing fluorescence quenching constant (kq) and plot of Fo/F against [Q] at  $\lambda_{ex} = 285$  nm and  $\lambda_{em} = 360$  nm for (A) withanolide A, (B) withanolide B, (C) withanoside IV and (D) withanoside V.

#### 3.2.A.2. Displacement studies

Using site specific markers, we can understand the exact binding of ligand molecules to the specific domains of HSA. Hence, there are different site specific markers like lidocaine for domain I, phenylbutazone for domain II and ibuprofen for domain III (Ghuman et al., 2005) and using these markers the fluorescence was performed to analyze the specific binding domain of HSA on interaction with withanoside and withanolide derivatives (Yeggoni et al., 2017). Because of the structural and molecular similarity of four derivatives, all of them showed fluorescence emission quenching by displacing phenylbutazone, i.e. they are binding on domain II of HSA with a binding constant were  $K_{Withanolide A+pb} = 2.57\pm0.05 \text{ X}$  $10^4 \, \text{M}^{-1}$ , Kwithanolide B+pb =  $6.84 \pm 0.05 \, \text{X} 10^4 \, \text{M}^{-1}$ , Kwithanoside IV+pb =  $1.89 \pm 0.05 \, \text{X} \, 10^4 \, \text{M}^{-1}$  and Kwithanoside V+pb= 4.80±0.03 X 10<sup>4</sup> M<sup>-1</sup>. The free energy changes for different were -6.09 Kcal  $M^{-1}$ , -6.56 Kcal  $M^{-1}$ , -7.17 Kcal  $M^{-1}$  and -6.42 Kcal  $M^{-1}$ , respectively (Fig 3.2 A-D). We also performed with other site specific markers (i.e lidocaine, ibuprofen), however, they were not displaced by the withnolide compounds. These results indicate that the drug molecules are specifically binding to Sudlow's drug binding site I. Our experimental results are in congruence with the computational data as also illustrated in our previous reports (Nerusu et al., 2017).

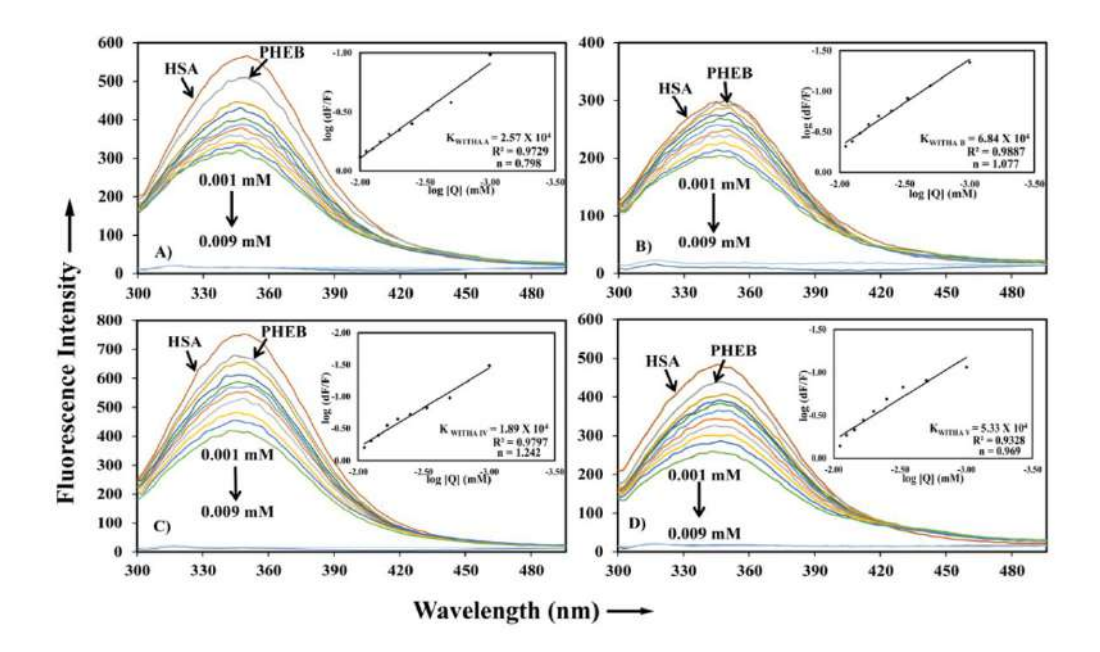


**Fig. 3.2.** Site displacement studies using site-specific markers; Phenylbutazone was used as a marker for HSA domain IIA (Sudlow's site I). Fluorescence spectroscopic studies performed using HSA and Phenylbutazone at equal concentrations (1 $\mu$ M) and ligand with increasing concentrations (1 $\mu$ M  $\sim$  9 $\mu$ M) (A) withanolide A, (B) withanolide B, (C) withanoside IV, (D) withanoside V.

#### 3.2.A.3. Secondary structural analysis of HSA and its complexes

Circular dichroism is a fundamental technique to study any secondary structural change upon interaction of protein and ligand. HSA showed a dip at 208 and 222nm in the far UV region which are mainly originated from helical structure (Subramanyam et al., 2009a). The secondary structure of HSA comprises of 58%  $\alpha$ -helix, 20%  $\beta$ -sheet (parallel and antiparallel) and 22% random coils, but upon titration with withanolide and withanoside compounds, there was partial unfolding of HSA protein and change in the dip in 208 and 222nm as shown in (Fig. 3.3 A-D). Conformational analysis was done using CDNN software, shows the percentage of  $\alpha$ -helix increasing up to 69.30±2.5, 70.54±2.5, 66.8±2.5 and 61.5±2.3 upon binding with withanolide A, withanolide B, withanoside IV and withanoside V respectively, and simultaneously there is decrease in the percentage of  $\beta$ -

sheet and random coil, the values were given in (Table 3.1). In general, most of the ligand molecules binding to HSA (Subramanyam et al., 2009b; Yuan et al., 2017). Similar studies were done for various molecules and revealed that upon binding of ligands, there is change in the secondary structure of HSA (Neelam et al., 2010).

**Table 3.1.** This table shows percentage change in the secondary structure upon addition of different concentration of withanolide and withanoside drugs.

Secondary Structures (%)	α-Helix	β-Turn	Random Coil
HSA	58.40±2.5	13.1±0.62	16.30±0.82
HSA + withanolide A (2μM)	66.40±2.5	12.0±0.65	13.20±0.82
HSA + withanolide A (4μM)	67.50±2.43	11.8±0.62	12.30±0.90
HSA + withanolide A (6μM)	69.30±2.5	11.7±0.66	11.2±0.83
HSA + withanolide B (2μM)	66.91±2.63	12.0±0.62	13.2±0.82
HSA + withanolide B (4μM)	68.31±2.53	11.7±0.71	12.1±0.86
HSA + withanolide B (6μM)	70.54±2.5	10.3±0.62	11.8±0.80
HSA + withanoside IV(2μM)	57.8±2.47	13.3±0.64	16.3±0.90
HSA + withanoside IV(4μM)	64.9±2.56	13.1±0.63	16.7±0.87
HSA + withanoside IV(6μM)	66.8±2.5	12.8±0.62	17.8±0.83
HSA + withanoside V(2μM)	58.8±2.3	13±0.62	15.3±0.84
HSA + withanoside V(4μM)	60.7±2.4	12.8±0.71	16.7±0.85
HSA + withanoside V(6μM)	61.5±2.3	12.9±0.63	18.3±0.87

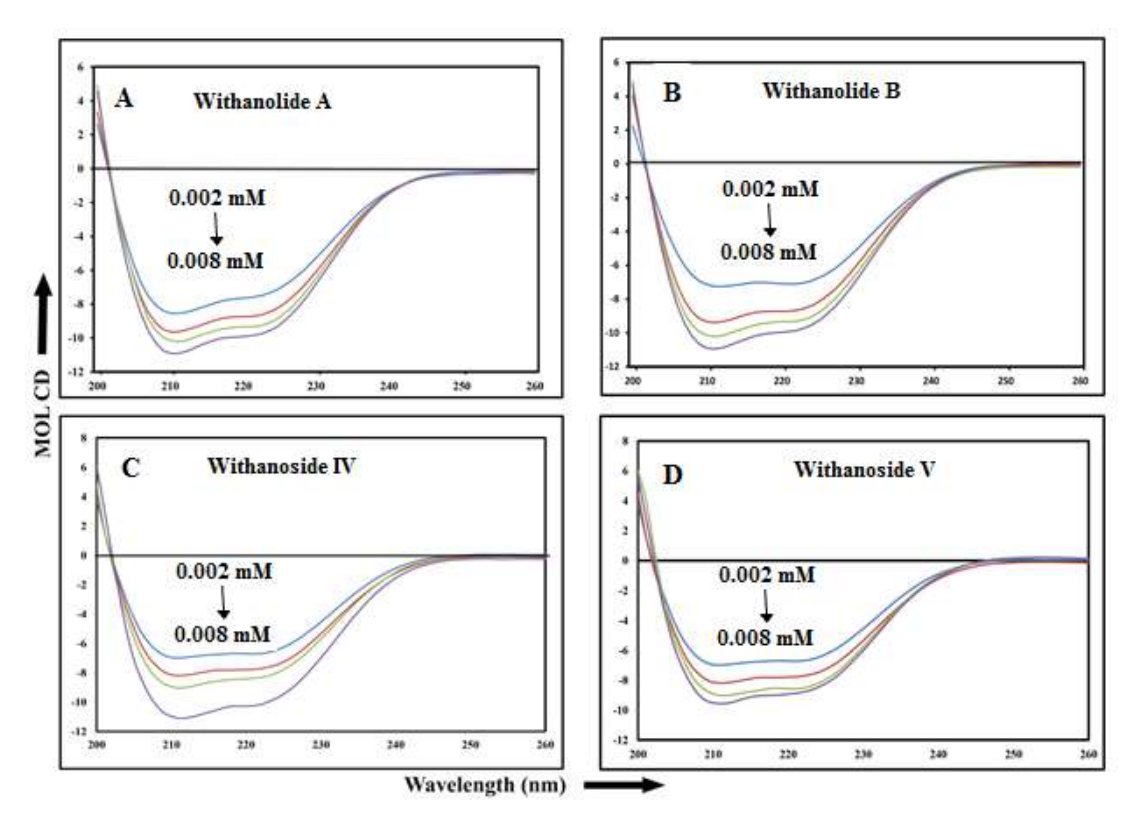


**Fig. 3.3.** Circular Dichroism studies of the free HSA and HSA–drug complexes. The free HSA and HSA–drug complexes in aqueous solution with a protein concentration fixed at  $1\mu M$  and increasing drug concentrations at 2,4, and 6  $\mu M$ . A) Withanolide A, B) Withanolide B, C)Withanoside IV, and D)Withanoside V.

#### 3.2.A.4. Topological observations from AFM

To corroborate topological changes in the surface of free HSA and HSA upon addition of drug derivatives, AFM was used. The results explain that upon incubation with drug molecules, there is a significant increase in the size of the complex, as shown in (Fig 3.4. A-J). But as the molecular weight of withanoside IV and withanoside V is larger than that of withanolide A and withanolide B, the complex formed by interaction with withanoside IV and withanoside V are larger. The unliganded HSA is showing a small size comparatively with bound HSA with withanolides, and the results corroborate with the previous studies (Kallubai et al., 2018). The complex in the presence of withanolide (A, B), and withanoside (IV, V) were showing remarkable increase in size i.e., growing around

to become 70, 130, 190 and 300 nm. These results indicate that the above molecules are formed complexes with HSA. Our results deciphered that it could be the hydrophobic contacts play a major role while binding of withanolides and withanosides compounds with HSA complexation (Chanphai et al., 2017) which is in an agreement with the free energy calculations. These experiments were performed in triplicates and similar results were reproduced always.

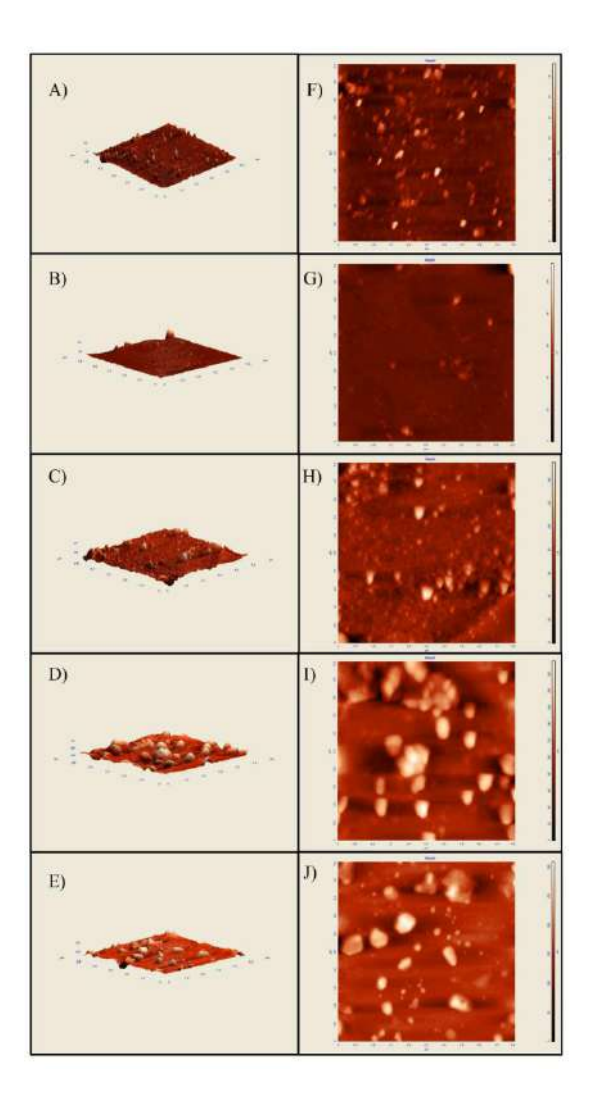


**Fig. 3.4.** AFM studies to visualize alteration in HSA molecule topology in presence of withanolide and withanoside derivatives at 10  $\mu$ M resolution. (A) ONLY HSA, (B) HSA+withanolide A, (C) HSA+withanolide B, (D) HSA+withanoside IV, (E) HSA+withanoside V. (F,G,H,I,J) represent the three-dimensional figures of only HSA and the complexes of HSA with the Withanolides and Withanosides.

#### 3.2.A.5. Transmission emission microscopy

TEM was used to visualize the structural and topographical change in HSA and ligated HSA upon incubation with various drug derivatives (Huang et al., 2010). At resolution of  $0.2\mu M$  the size of unligated HSA molecule were found to be of size  $0.04\pm10\mu M$ , whereas in the presence of withanolide A and B, and withanoside IV and V, it increased to  $0.06\pm10\mu M$ ,  $0.06\pm10\mu M$ , and  $0.07\pm10\mu M$ ,  $0.08\pm10\mu M$  respectively (Fig 3.5 A-E), which can interprets the complexes formed by the interaction of HSA with these derivatives. Thus, it can be derived that interaction among the protein and withanolide A, withanolide B, withanoside IV and withanoside V are taking place and these results are in harmony with the results obtained from other techniques (Nagati et al., 2018).

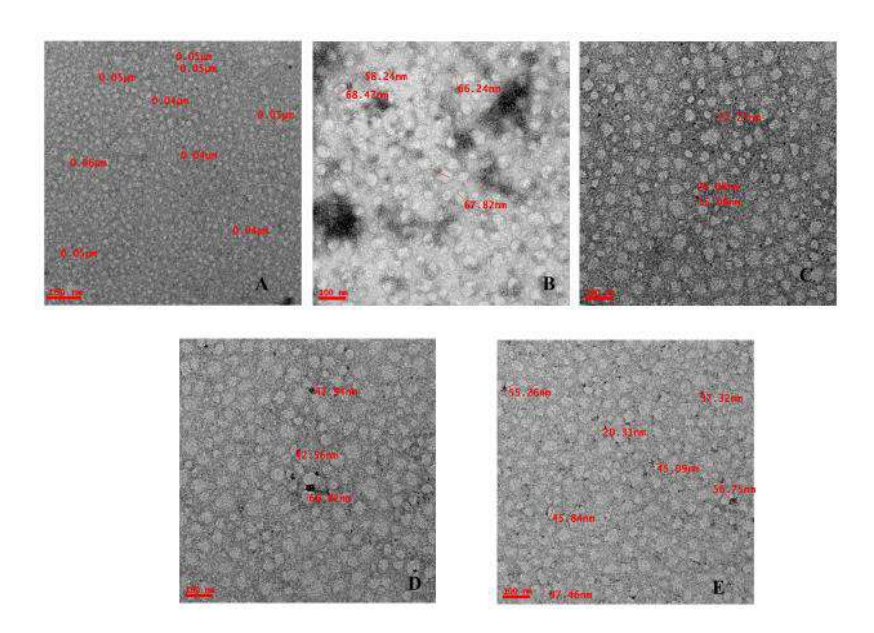


**Fig. 3.5.** Transmission Electron Microscopic (TEM) studies to visualize alteration in HSA molecule topology in presence of withanolide and withanoside derivatives at 200 nM resolution. A) Only HSA, B) HSA+withanolide A, C) HSA+withanolide B, D) HSA+withanoside IV and E) HSA+withanoside V.

#### 3.2.A.6. Molecular docking

The displacement studies by the use of site-specific markers indicated that the withanolide and withanoside derivatives were binding at Sudlow's drug binding site I of HSA. Autodock 4.2.4 software was used further to confirm the precise binding site and residues on HSA upon binding of these derivatives. Since the binding location of the protein is of utmost importance to study the biological activity of the drug and it also plays a major role in pharmacokinetics and pharmacodynamics of the drug. Crystal structure of HSA was procured from Protein Data Bank (PDB Code: 1AO6).

Withanolide A is binding to HSA by hydrogen bond formation by interacting with Glu208 in the hydrophobic cavity of subdomain IIA, and withanolide B is interacting with His338, withanoside IV is forming a hydrogen bond at Arg197 and Lys205, and withanoside V is interacting with residues of Tyr341 and Tyr334 and Leu305; with binding constants of Kwithanolide A = 4.93 X 10<sup>4</sup> M<sup>-1</sup>, Kwithanolide B = 7.42 X 10<sup>4</sup> M<sup>-1</sup>, Kwithanoside IV = 2.50 X 10<sup>4</sup> M<sup>-1</sup> and Kwithanoside V = 2.49 X 10<sup>4</sup> M<sup>-1</sup> and free energy were be -6.40 Kcal M<sup>-1</sup>, -6.64 Kcal M<sup>-1</sup>, -3.27 Kcal M<sup>-1</sup> and -3.26 Kcal M<sup>-1</sup> respectively at 25 °C respectively. The results were shown in (Fig. 3.6. A-L), and are generated by using the Pymol software, and Ligplot is used to illustrate the two-dimensional interaction by hydrogen bond formation and hydrophobic interactions. The Binding constant values calculated computationally were in accordance with the values obtained experimentally (Li et al., 2016).

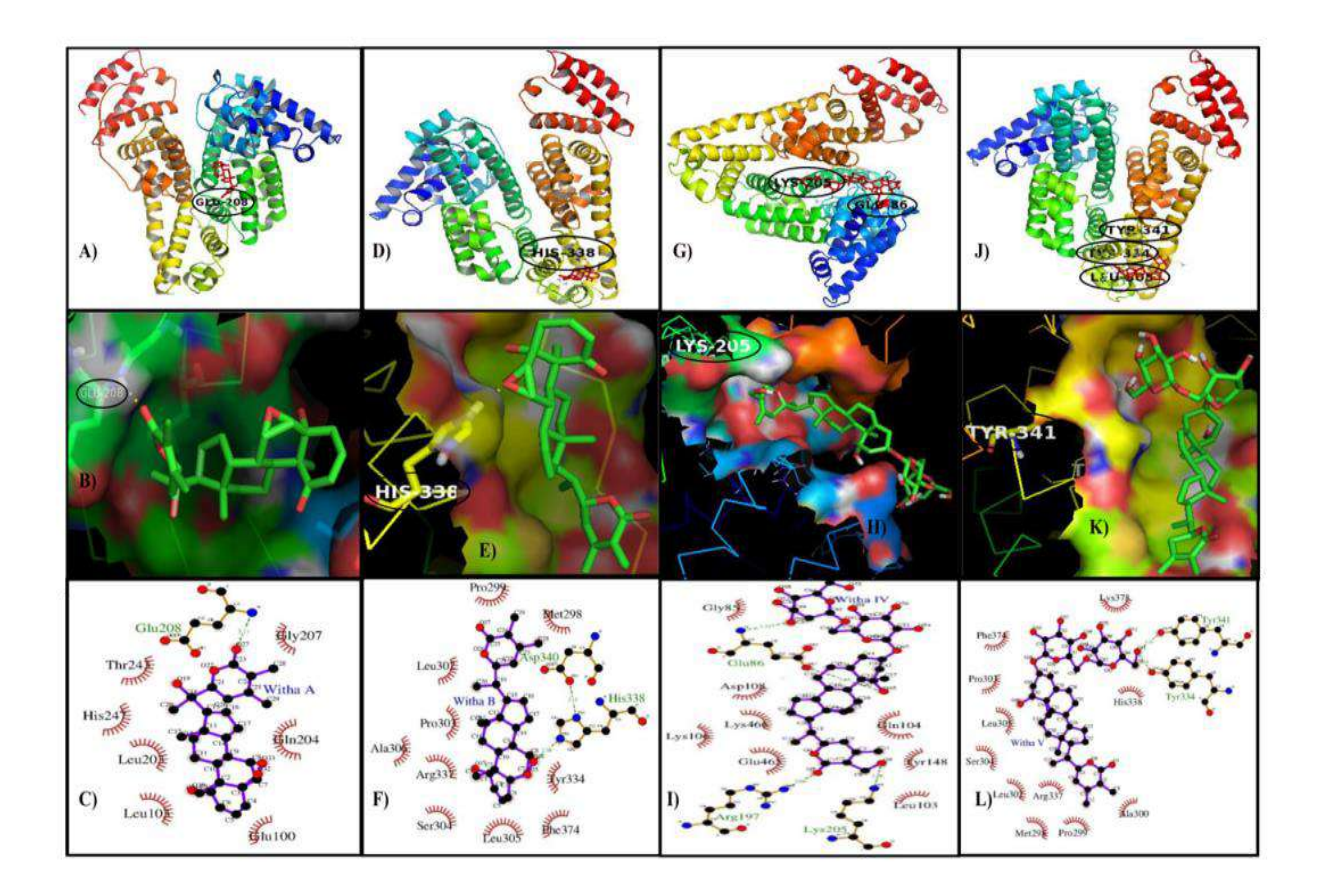


**Fig. 3.6.** Molecular docking studies between HSA and withanolide A, withanolide B, withanoside IV and withanoside V showed that the minimum binding energy conformer is very close to the experimentally determined values. (A,D,G,J). Overview of cartoon model of withanolide A, withanolide B, withanoside IV and withanoside V binding to HSA. Different views of the derivatives docked in the binding pocket HSA using Autodock 4.2.4. (B,E,H,K) Pymol is used to generate the images. The cavity of hydrophobic and hydrophilic amino acid residues surrounding the probe. (C,F,I,L). Ligplot is used to show the hydrophobic interactions of HSA with withanolide derivatives.

#### 3.2.A.7. Results from molecular dynamics

Molecular simulation studies compute the behavior of a system as a function of time. It has emerged as a powerful tool for understanding the interaction between protein and ligands to predict how conformational changes occur to achieve the lowest free energy conformer. Usually, RMSD, RMSF and Rg are used to know the change in the microenvironment, atomic fluctuation, rigidity and stability of the HSA-ligand complexes in comparison to

HSA alone (Rapaport, 1996; Radibratovic et al., 2016). Hence, in our study we have measured the same parameters for HSA with withanolide and withanoside complexes to understand the interaction mechanism.

Energetically the most stable complex of docking was taken, and dynamics was studied for 10ns. Generally, Rg is used for measuring the compactness of structure, hence Rg of withanolides and withanosides complexes showed stability throughout the 10ns after initial rigidity at 2ns. The Rg value of unliganded HSA is, 2.65±0.35nm, the complex HSAwithanolide A, HSA-withanolide B, HSA-withanoside IV and HSA-withanoside V showed fluctuations in between 2.63±0.05nm, 2.61±0.02nm, 2.65±0.03nm, and 2.65±0.02nm, respectively showing the stability of the complexes. These results indicate the conformational and stability changes in the secondary structure of HSA, which is totally in congruence with the results obtained from circular dichroism. To access the stability of the system RMSD of the complex atoms was analyzed as a function of time for MD trajectory. The RMSD values of atoms of protein backbone (C-Cα-N) were calculated for only HSA and HSA-ligand complex. RMSD of HSA-withanolide A, HSA-withanolide B, HSAwithanoside IV, and HSA-withanoside V showed stability at 3ns and remained constant throughout 10ns. From 0-10ns trajectory data the RMSD value of unliganded HSA is 0.4±0.03nm while for HSA-ligand complexes fluctuations were in between 0.3±0.03nm, while withanolide B had initial fluctuations which later stabilized at 6.5 ns from 0.35±0.03nm as shown in (Fig 3.7A-L). It can be concluded that the complexes remain stable with no major change from the initial docked conformer owing to the stability of the ligated HSA. Rigidity of peptide structure and thermal vibrations were measured by RMSF values.

Local protein mobility was seen by analysing the time-averaged RMSF values of only HSA and the HSA-drug complexes. As these derivates of withanolide A, withanolide B, withanoside IV and withanoside V binds to HSA, there is increased rigidity and flexibility in different sub domains of HSA which is plotted against the residue number. The micro-environment around the binding site showed strong overlapping of binding region of the HSA-withanolide A, HSA-withanolide B, HSA-withanoside IV and HSA-withanoside V and are in between 200-250 residues which are a part of hydrophobic cavity of HSA and there is more rigidity around those amino acids indicating strong interaction at binding site 1. Hence, MD data is an indication that the withanolide A, withanolide B, withanoside IV and withanoside V derivatives are binding with HSA with stable conformations and hence this study can be extended to study the therapeutic role in biological samples.

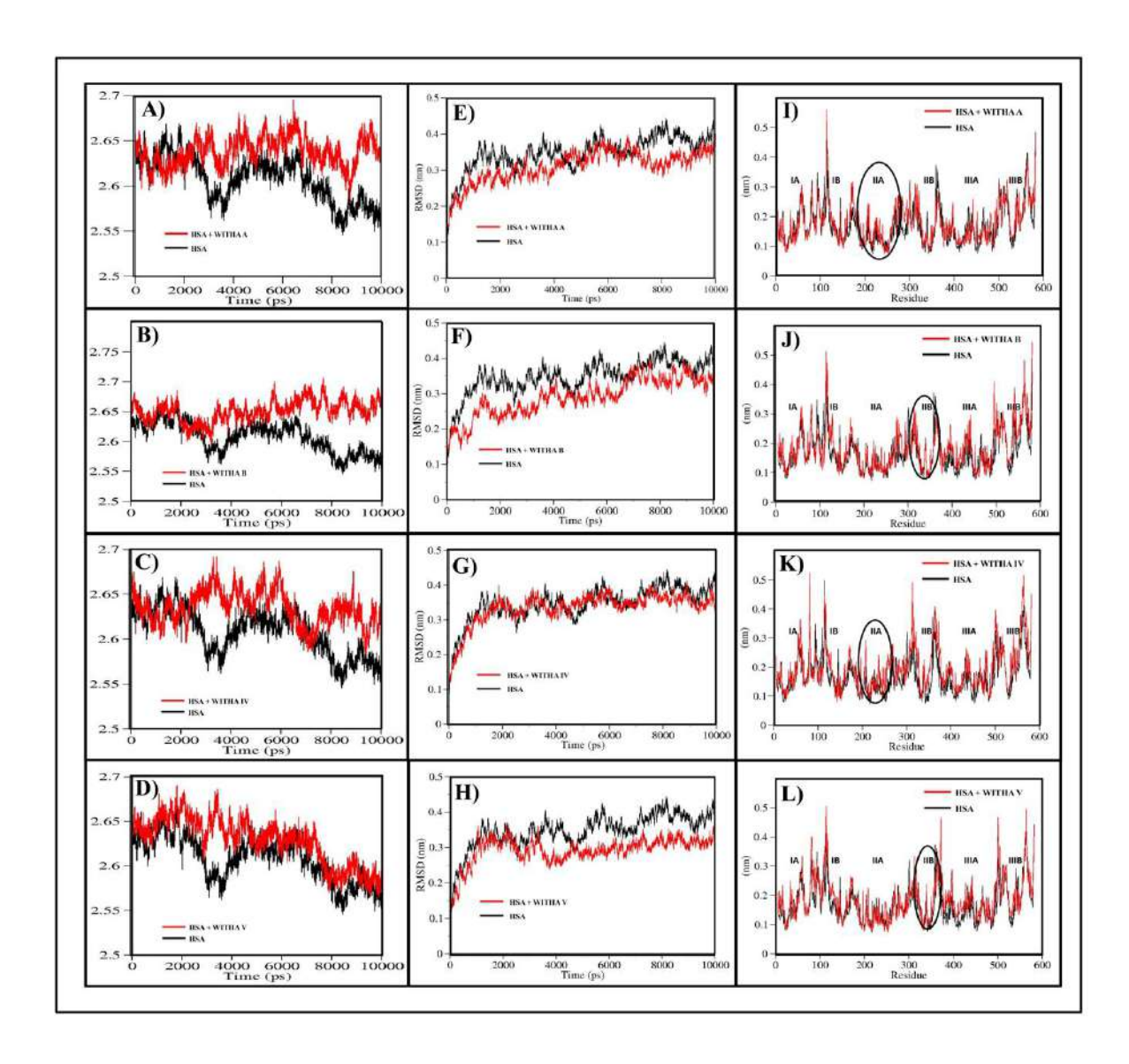


**Fig. 3.7.** A, B, C, D- Time evolution of the radius of gyration (Rg) during 10 ns of MD simulation of unliganded HSA and HSA–drug derivatives complexes. E, F, G, H- Plot of RMSD values for unliganded HSA and HSA–drug derivatives complexes. I, J, K, L - Comparison of the RMSF of Calcium atoms along the sequence derived from the 10 ns simulations

### 3.2.B. Interaction between AB and phytochemicals of Withania somnifera

# 3.2.B.1. Thioflavin fluorescence assay

Tht, although almost non-fluorescent alone gives significant fluorescence on binding to  $A\beta_{1-42}$  fibrils thus quantifying the fibrillar composition in the sample (McKoy et al., 2012).

Free  $A\beta_{1-42}$ , on account of its increased hydrophobicity (Stine et al., 2002) while the  $A\beta_{1-42}$  samples treated with ligands in the ratio 1:4, and quiescently incubated for 6 hrs interval keeping other conditions constant, showed a considerable decrease in the intensity of fluorescence.

The control showed a good amount of steady rapid aggregation of  $A\beta_{1-42}$  oligomers in the sample contributing to the increased fluorescence intensity. This indicates the inhibitory effect of these plant-based phytochemicals against the aggregation of  $A\beta_{1-42}$  which otherwise would contribute to Alzheimer's disease in individuals. All four Ashwagandha derivatives (Withanolide A, Withanolide B, Withanoside IV and Withanoside V), owing to their similar nature show good inhibitory property against peptide oligomeric assembly. The drugs do not self-aggregate, negating any chance of artifacts during the assay. To study the effect of these phytochemicals even on  $A\beta_{1-42}$  fibrils, the samples were again co-incubated for 48 hrs to further determine their activity against fibrillization.

The results show although the control peptides kept on aggregating in its log phase, the co-incubated samples showed a drastic reduction in the aggregation. To further consolidate the results, a time point study was done along with the control and treated samples, to observe near real-time view of the aggregation trend. The control showed a steady increase in its aggregation phenomena till it reaches stability at around 72 hrs (Fig. 3.8 C). The treated samples on the other hand, similar to the previous independent experiments showed generous containment of the  $A\beta_{1-42}$  oasis to its oligomeric state with increasing time period till 72 hrs, thus validating the applicability of the studied phytochemical derivatives.

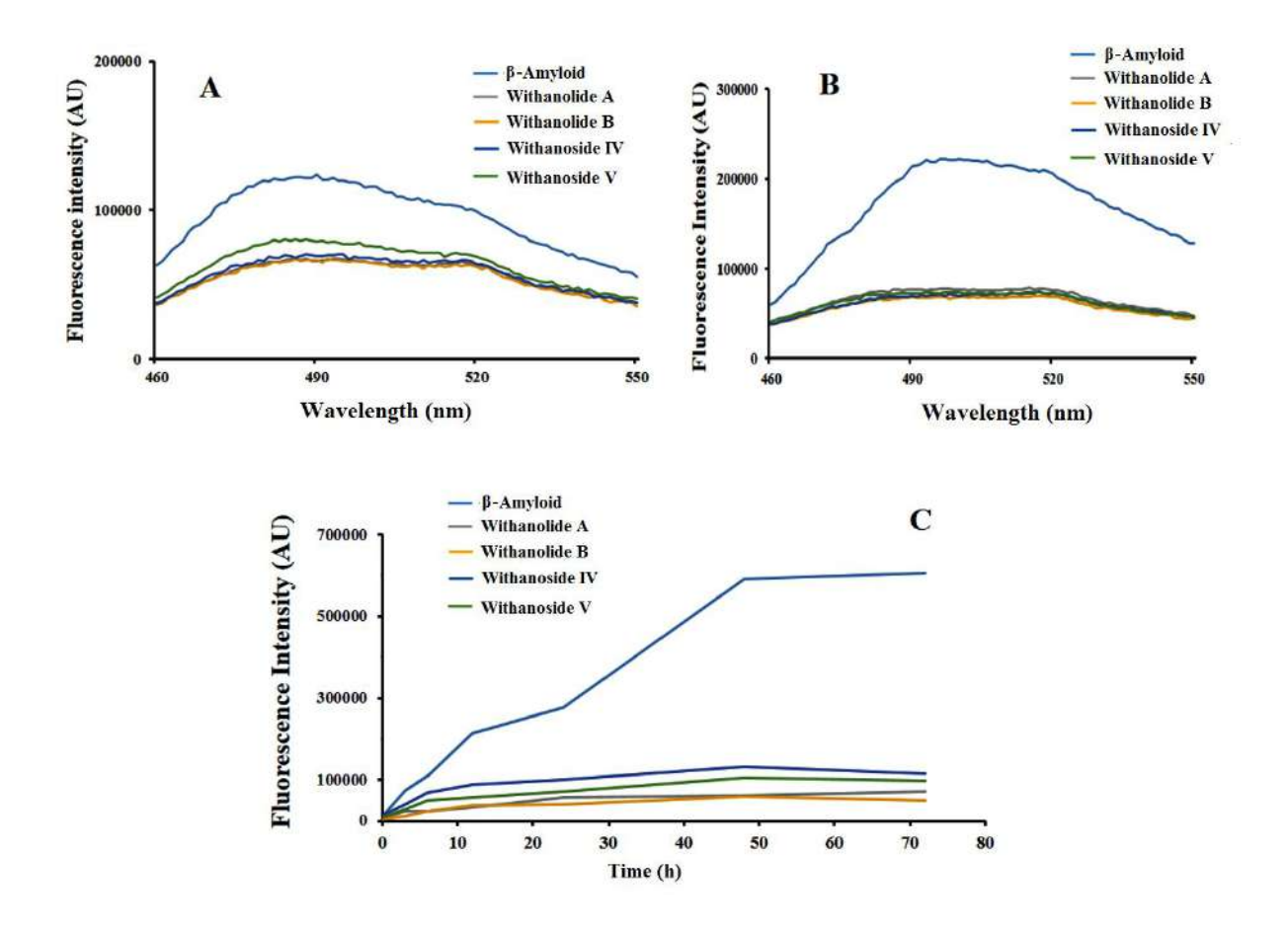


**Fig. 3.8.** Detection of  $A\beta_{1-42}$  aggregates using Tht assay; measurement of fluorescence enhancement spectra ( $\lambda_{ex}$ = 450nm,  $\lambda_{em}$ = 482nm) of 5 $\mu$ M Tht solution (in 50mM sodium phosphate buffer) mixed in 25 $\mu$ M  $A\beta_{1-42}$  with different drugs witha a, witha b, witha IV and witha IV at ratio 1:4, in their A) Oligomeric (6 h incubation) state, and B) Fibrillar (after 24 hrs of incubation) state, C) Fluorescence was measured at different time points upto 72 hrs to study the aggregation.

### 3.2.B.2. MTT reduction assay

Neuronal toxicity is the ultimate outcome of  $A\beta_{1-42}$  aggregation. Thus, the Withanolide A, Withanolide B, Withanoside IV and Withanoside V were further used to investigate its preventive effect on neuronal toxicity. In our study we have checked the dose-dependent effect of the Withanolides A, B and Withanosides IV, V on SK-N-SH cell line for 48 hrs and the IC<sub>50</sub> value found to be  $28.61\pm2.91$ ,  $14.84\pm1.45$ ,  $18.76\pm0.76$  and  $30.14\pm2.59$   $\mu$ M

respectively (Fig. 3.9). Neuronal cell viability visibly increased and subsequently diminished the toxicity of fibrillar  $A\beta_{1-42}$  aggregation. These results indicate that these derivatives have significant therapeutic potential against  $A\beta_{1-42}$  aggregation induced cell toxicity, which was further confirmed by apoptosis assay (Kurapati et al., 2014).

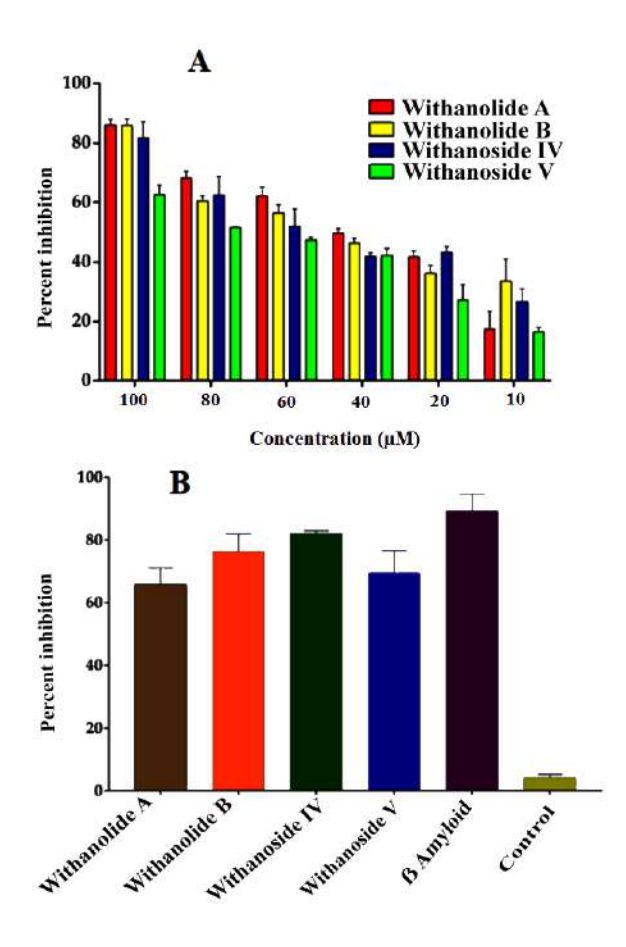


**Fig. 3.9.** A) Inhibitory effect of *Withania somnifera* derivatives on the growth of SK-N-SH cells by MTT assay. The cells were incubated with different concentrations of these treatments for 48 hrs. Data was represented as the mean  $\pm$  S.D (n = 3). B) After treatment with 25 μM of Aβ the cells were treated with half the conc of IC<sub>50</sub> value and incubated with of these treatments for 48 hrs.

### 3.2.B.3. Apoptosis annexin assay

Here, we induced apoptosis in SK-N-SH cell line at half of the inhibition constant concentration by addition of the Withanolides and Withanosides derivatives. It was observed that in control, the Q<sub>4</sub> quadrant that represents the viable cells, has a greater number of viable cells compared to the cells treated with Withanolides and Withanosides. In the treated sample, it was seen that the number of cells in the Q<sub>3</sub>, Q<sub>2</sub>, Q<sub>1</sub> quadrants that represents the early apoptosis, late apoptosis and dead cells have increased when compared to the control sample. The results are depicted as dot-plot representation (FITC-A on x-axis and PE-A on y-axis) in quadrants and histogram (Fig. 3.10 and Table 3.2). This indicates that these phytocompounds are showing cytotoxicity against SK-N-SH cells and have pharmaceutical potential, which should be further explored (Cohen et al., 1992).

**Table 3.2.** Percentage of cells in each quadrant without addition of the drug and in the presence of withanolide and withanoside derivatives (calculated from Fig. 3.10).

	% Live Cells	% Dead Cells	%Early Apoptosis	% Late Apoptosis
Control	96.1	1.3	2.2	0.4
Withanolide A	87.9	0.6	10.8	0.7
Withanolide B	93.7	1.1	4.7	0.5
Withanoside IV	94.9	1.1	3.4	0.6
Withanoside V	93.2	0.9	5.2	0.7

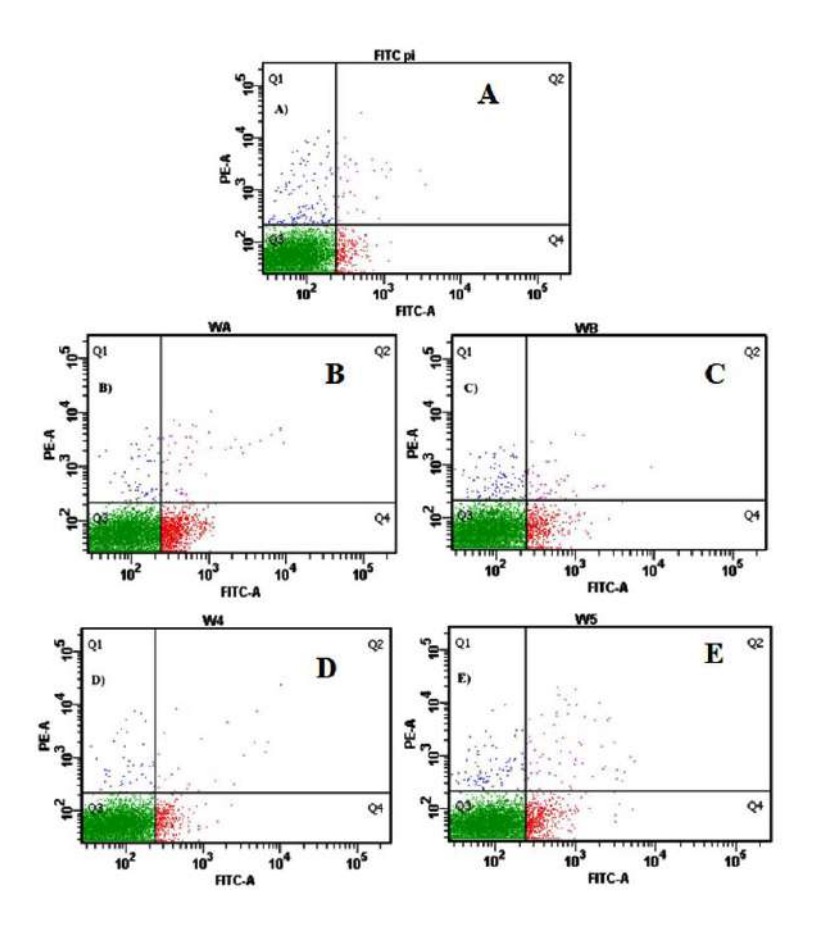


**Fig. 3.10.** Apoptosis studies by Flow cytometry by using after treatment with half concentration of  $IC_{50}$  value for 24hrs A) only cells B, C, D, E) after addition Withanolide A, Withanolide B, Withanoside IV and Withanoside V.

# 3.2.B.4. Tunel assay by confocal microscopy

The cleavage or fragmentation of nuclear DNA into nucleosome sized fragments is a hallmark of apoptosis. Cleaved DNA has a 3 'hydroxyl group which becomes the substrate for binding of fluorescein - isothiocyanate TUNEL Assay. After the treatment of the cells with half the concentration of IC<sub>50</sub> value, there was a remarkable reduction in the number of apoptotic cells (positively tunnel stained cells) thereby indicating the DNA damage (Fig. 3.11).

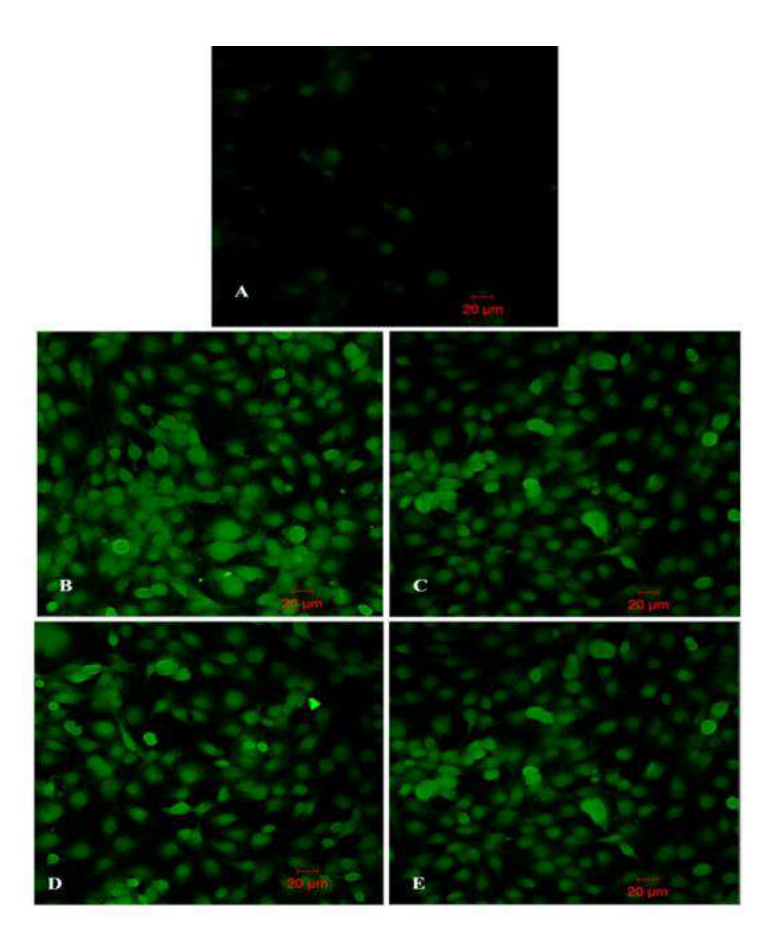


**Fig. 3.11.** TUNEL nuclear staining on SK-N-SH neuroblastoma cells. Cells in control are untreated and remaining cells are treated with half the conc of IC<sub>50</sub> value. Cells were collected, washed in phosphate-buffer saline, fixed and permeabilised and subjected to TUNEL nuclear staining, mounted and viewed by fluorescence microscopy with A) Only cells B,C,D,E) Withanolide A, Withanolide B, Withanoside IV and Withanoside V.

### 3.2.B.5. Intracellular ROS measurement

To investigate whether the derivatives of *Withania somnifera* protect the cells from excessive intracellular ROS, we evaluated the ROS production with the help of a fluorescent dye DCFH-DA. Cells treated with  $A\beta_{1-42}$  displayed an increase in ROS production. We can clearly see that there is a significant reduction in the ROS production when the cells were treated with the Withanolide A, Withanolide B, Withanoside IV and Withanoside V (Fig. 3.12). In which withanolide A and withanolide B are significantly reduced the ROS production which indicates their molecules can project much better than

withanoside IV and withanoside V. The difference with the withanolides and withanosides are C-28 and C-40 steroidal lactones, with six-membered lactone ring formed by oxidization of the C-22 and C-28 on ergostane backbone. Thus, this may be the reason the withanolide A and withanolide B can reduce ROS. Accumulation of ROS disturbs the integrity of plasma membrane and causes DNA damage because of oxidative stress. These derivatives are successful in rescuing cell death induced by the toxicity of  $A\beta_{1-42}$ , which ultimately leads to neuronal dysfuction. Earlier reports showed that withanolide A attenuated ROS generation in neuroblatoma cells and decreased the ROS levels in hypobaric hypoxia. Thus, we can infer our results that all the four derivatives withanolide A, withanolide B, withanoside IV and withanoside V reduced ROS production (Dar et al., 2017).

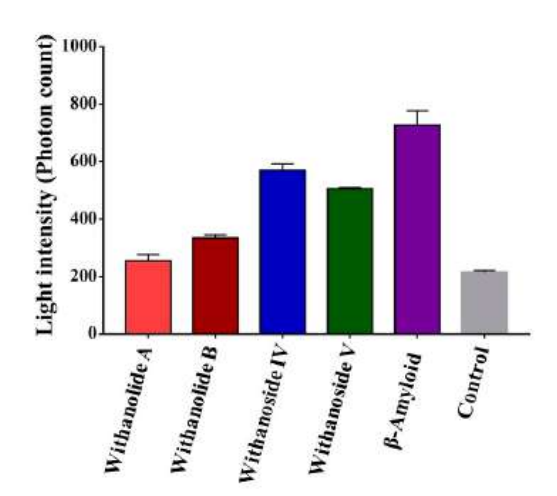


**Fig. 3.12.** Intracellular ROS generation in SK-N-SH cells after treatment with *Withania somnifera* derivatives. After treatment for 12 hrs, cells were stained with 20  $\mu$ M DCFH-DA for 30 minutes at 37°C in the dark. Data are expressed as mean  $\pm$  SD (n =3).

# 3.2.B.6. Molecular docking by Autodock

In our present study, we used Autodock tool to evaluate the molecular interaction between different Ashwagandha molecules (withanolide A, withanolide B, withanoside IV and with anoside V) and A $\beta_{1-42}$ . For our study, the crystal structure of A $\beta_{1-42}$  peptide with PDB id: 2BEG is used to understand the interaction between Ashwagandha derivatives and Aβ<sub>1</sub>-42 peptide, which is important in treatment of Alzheimer's disease. As these withanolide molecules can act as potential inhibitors, to prevent the oligomerization and aggregation of Aβ<sub>1-42</sub> peptides (Necula et al., 2007). Thioflavin-based small molecules were designed recently (Rodriguez-Rodriguez et al., 2015), which served as molecular probes in the detection of peptide A\(\beta\_{1-42}\) fibrils in the treatment of Alzheimer's disease. According to literature the most common view of  $A\beta_{1-42}$  is having 1-42 amino acids, among these 42 amino acids, the most flexible regions of this peptide in a fibril formation are the first 10 amino acids of the N-terminus and last few amino acids of the C-terminus (residues 39-42), and in between the residues Asp23 and Lys28 parallel β-sheet with a β-turn. Our present study finds an active site where the withanolide A interacted with Leu17 and Phe19, withanolide B with residues Phe19 and Phe20, whereas withanoside IV interacted with Asp23, Val24 and Ser26 and withanoside V like withanolide A and B molecules it is bound in the same site interacting with residues Leu17 and Leu19 (Fig 3.13 A, B, C and D). The results show that with anoside IV is in the  $\beta$ -turn region of the A $\beta_{1-42}$  peptide and is efficient with binding energy of -7.4 Kcal/mol compared to the withanolide A, B and withanoside V molecules with binding energy -6.4, -6.8 and -6.3 kcal/mol, respectively. Also, the cell viability test with SK-N-SH cell line showed better result with withanoside IV (Fig. 3.9).

Thus, molecular docking provided a detailed knowledge of small molecules binding to the active site of peptide, which further helps to design new molecules with low toxicity

and high specificity in peptide-based therapy in preventing  $A\beta_{1-42}$  aggregation. BSBp (BSB) are being used for therapy for neuroprotection as they usually are known to target the hydrophobic core region (HCR) of 17-21 residue of 42 residues of  $A\beta_{1-42}$  peptide (Basha et al., 2018). This HCR region is known to be mainly responsible for another  $A\beta_{1-42}$  peptide to come and bind to it but here we can see that these derivatives are blocking the HCR thus inhibiting fibrillization.

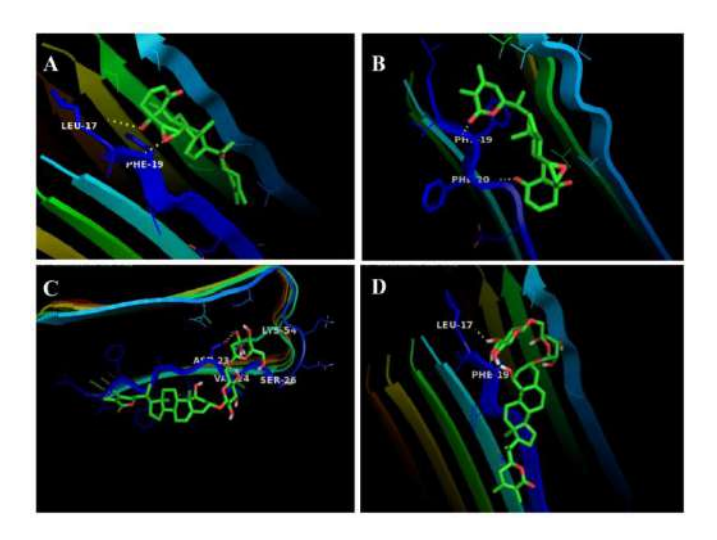


**Fig. 3.13**. Molecular docking of  $A\beta_{1-42}$  with- A) Withanolide A, B) Withanolide B, C) Withanoside IV and D) Withanoside V. Autodock 4.2.4 software was used for the docking studies.

# 3.2.B.7. MD simulations of A $\beta_{1-42}$ and A $\beta_{1-42}$ -withanolide and withanoside complexes

Filamentous  $A\beta_{1-42}$  aggregates are the main cause for the pathological condition of Alzheimer's disease. Previous reports explained that the normal  $A\beta_{1-42}$  peptides with  $\alpha$ -helical conformations were being nontoxic, but the neurotoxicity was observed with an increase in the origination of  $\beta$ -sheet structure (May et al., 1992; Behl, 1997). However, the exact mechanism of  $A\beta_{1-42}$  aggregation is still not clear. The most common view of  $A\beta_{1-42}$  is in fibrillar parallel  $\beta$ -sheets with a  $\beta$ -turn between residues Asp-23 and Lys-28.

According to literature an energetically favoured hydrophobic cleft on chain A comprising the residues LVFFA (17-21 region) seems to be a good binding site in terms of energetic point of view with respect to Chain E for binding inhibitors more effectively. In our study, all the four phytocompounds, withanolide A, withanolide B, withanoside IV, and withanoside V when docked with  $A\beta_{1-42}$  showed interactions with LVFFA regions among 50 runs. It is interesting to observe that withanolide A, withanolide B, withanoside IV and withanoside V bind in the LVFFA region, which is known to be the preferred region for many small molecule inhibitors of  $A\beta_{1-42}$  aggregation. The lowest binding energy conformer among 50 conformations was selected for MD simulations with explicit solvent and force fields to probe the structural stability and the conformational dynamics of  $A\beta_{1-42}$  fibril structures. All the 100ns simulations showed that the conformations of the  $A\beta_{1-42}$ -Ashwagandha derivatives (A, B, IV, and V) were stable after 20 ns.

The stability of the complexes was analysed and shown in the form of Rg and RMSD of the complexes. Rg of only  $A\beta_{1-42}$  oscillates for few nm  $\pm$  around 1.2 to 1.4 nm throughout 100 ns simulations, whereas the fluctuations were reduced after 20 ns simulations for all the Ashwagandha molecules (Fig. 3.14 A, C, E and G). The RMSD was used to evaluate structural stability of only  $A\beta_{1-42}$  as well as  $A\beta_{1-42}$ -Ashwagandha derivatives complexes (Fig. 3.14 B, D, F, H). For only  $A\beta_{1-42}$ , RMSD fluctuate to higher value (~1.2 nm) till the end of simulation Filamentous  $A\beta_{1-42}$  aggregates are the main cause for the pathological condition of AD. Previous reports explained that the normal  $A\beta_{1-42}$  peptides with  $\alpha$ -helical conformations were being nontoxic, but the neurotoxicity observed with an increase in the formation of  $\beta$ -sheet structure. However, the exact mechanism of  $A\beta_{1-42}$  aggregation is still not clear. The most common view of  $A\beta_{1-42}$  is in fibrillar parallel  $\beta$ -sheets with a  $\beta$ -turn between residues Asp-23 and Lys-28. According to literature an

energetically favoured hydrophobic cleft on chain A comprising the residues LVFFA (17-21 region) seems to be a good binding site in terms of energetic point of view with respect to Chain E for binding inhibitors more effectively. In our study all the four phytocompounds, withanolide A, withanolide B, withanoside IV and withanoside V when docked with  $A\beta_{1-42}$  showed interactions with LVFFA regions among 50 runs. It is interesting to observe that withanolide A, withanolide B, withanoside IV and withanoside V bind in the LVFFA region, which is known to be the preferred region for many small molecule inhibitors of  $A\beta_{1-42}$  aggregation. The lowest binding energy conformer among 50 conformations was selected for molecular dynamics (MD) simulations with explicit solvent and force fields to probe the structural stability and the conformational dynamics of  $A\beta_{1-42}$  fibril structures. All the 100ns simulations showed that the conformations of the  $A\beta_{1-42}$ -Ashwagandha derivatives (A, B, IV, and V) were stable after 20 ns. The stability of the complexes was analyzed and shown in the form of Rg and RMSD of the complexes.

Rg of only  $A\beta_{1-42}$  oscillates for few nm  $\pm$  around 1.2 to 1.4 nm throughout 100 ns simulations, whereas the fluctuations were reduced after 20 ns simulations for all the Ashwagandha molecules (Fig. 3.14 A, C, E and G). The RMSD was used to evaluate structural stability of only  $A\beta_{1-42}$  as well as  $A\beta_{1-42}$ -Ashwagandha derivatives complexes (Fig. 3.14 B, D, F, H). For only  $A\beta_{1-42}$ , RMSD fluctuate to higher value (~1.2 nm) till the end of simulation (Shuaib & Goyal, 2017), while for  $A\beta_{1-42}$ -withanolide A complex, RMSD shows less fluctuations till 50 ns and after that, there is an increase in fluctuation around  $\pm 0.3$  nm from initial, but in case of  $A\beta_{1-42}$ -withanolide B complex, the RMSD values remains stable till the end of simulation (Fig. 7D). Thus, a decrease in the RMSD value may cause enhanced structural stability of  $A\beta_{1-42}$ -withanolide B complex as compared to  $A\beta_{1-42}$  alone. While  $A\beta_{1-42}$ -withanoside IV complex and  $A\beta_{1-42}$ -withanoside V complex

showed an increase in the RMSD value of ~1.5 and 1.3 nm, which explains that these molecules were in interaction with the hydrophobic site for a stable period of the trajectory as shown in Fig. 3.14.

To illustrate interactions between binding residues of Aβ<sub>1-42</sub> with Ashwagandha derivatives, time frames were analysed at different nanoseconds (10, 30, 50, 70 and 100 ns). Recently, Zhao and co-workers investigated  $\pi$ - $\pi$  interactions between aromatic rings of curcumin and aromatic residues of  $A\beta_{1-42}$  by utilizing computational studies (Zhao et al., 2012). The authors highlighted that  $\pi$ - $\pi$  interactions contribute indirectly to a decline in  $\beta$ sheet content in  $A\beta_{1-42}$ . Similar results were observed with  $A\beta_{1-42}$ -withanolide A complex, the withanolide A showed hydrogen bond interaction with aromatic rings of Phe19, Phe20, and later in further increase in MD simulations above 50 ns there is a conformational change and decline in the structure of A $\beta_{1-42}$ , which is also confirmed through RMSD fluctuations (Fig. 3.14). The visual inspection of conformations of Aβ<sub>1-42</sub>-withanolide B complex during MD showed interactions in the central helix region (13-26 residues) indicates the presence of hydrophobic interactions between Withanolide B and residues of  $A\beta_{1-42}$  as this region is the prime hydrophobic core. The interactions with this region indicate stabilization of central helix of Aβ<sub>1-42</sub> by hydrophobic interactions. The visualization of snapshots from MD trajectory for the complexes Aβ<sub>1-42</sub>-withanoside IV and  $A\beta_{1-42}$ -withanoside V showed interaction of withanosides at the second core of  $A\beta_{1-42}$ at the end residues (Lys28 to Va140). This core has a β-sheet structure, is able to form noncovalent forces with other  $\beta$ -sheets of  $A\beta_{1-42}$  peptides (Mager et al., 2001), thus the with anolide B, with anoside IV and V binding in the hydrophobic regions may prevent fibrillation.

While for  $A\beta_{1-42}$ -withanolide A complex, RMSD shows less fluctuations till 50 ns and after that, there is an increase in fluctuation around  $\pm 0.3$  nm from initial, but in case of  $A\beta_{1-42}$ -withanolide B complex, the RMSD values remains stable till the end of simulation. Thus, a decrease in the RMSD value may cause enhanced structural stability of  $A\beta_{1-42}$ -withanolide B complex as compared to  $A\beta_{1-42}$  alone. While  $A\beta_{1-42}$ -withanoside IV complex and  $A\beta_{1-42}$ -withanoside V complex showed an increase in the RMSD value of  $\sim 1.5$  and 1.3 nm, which explains that these molecules were in interaction with the hydrophobic site for a stable period of the trajectory.

To illustrate interactions between binding residues of Aβ<sub>1-42</sub> with Ashwagandha derivatives, time frames were analysed at different nanoseconds (10, 30, 50, 70 and 100 ns). Recently, Zhao and co-workers investigated  $\pi$ - $\pi$  interactions between aromatic rings of curcumin and aromatic residues of A $\beta_{1-42}$  by utilizing computational studies. The authors highlighted that  $\pi$ - $\pi$  interactions contribute indirectly to a decline in  $\beta$ -sheet content in A $\beta_1$ -42. Similar results were observed with  $A\beta_{1-42}$ -withanolide A complex, the withanolide A showed hydrogen bond interaction with aromatic rings of Phe19, Phe20, and later in further increase in MD simulations above 50 ns there is a conformational change and decline in the structure of  $A\beta_{1-42}$ , which is also confirmed through RMSD fluctuations (Fig. 3.15). The visual inspection of conformations of Aβ<sub>1-42</sub>-withanolide B complex during MD showed interactions in the central helix region (13-26 residues) indicates the presence of hydrophobic interactions between Withanolide B and residues of Aβ<sub>1-42</sub> as this region is the prime hydrophobic core. The interactions with this region indicate stabilization of central helix of Aβ<sub>1-42</sub> by hydrophobic interactions. The visualization of snapshots from MD trajectory for the complexes  $A\beta_{1-42}$ -withanoside IV and  $A\beta_{1-42}$ -withanoside V showed interaction of withanosides at the second core of  $A\beta_{1-42}$  at the end residues (Lys28 to

Va140). This core has a  $\beta$ -sheet structure, is able to form non-covalent forces with other  $\beta$ -sheets of  $A\beta_{1-42}$  peptides; thus the withanolide A, B, withanoside IV and V binding in the hydrophobic regions may prevent fibrillation.

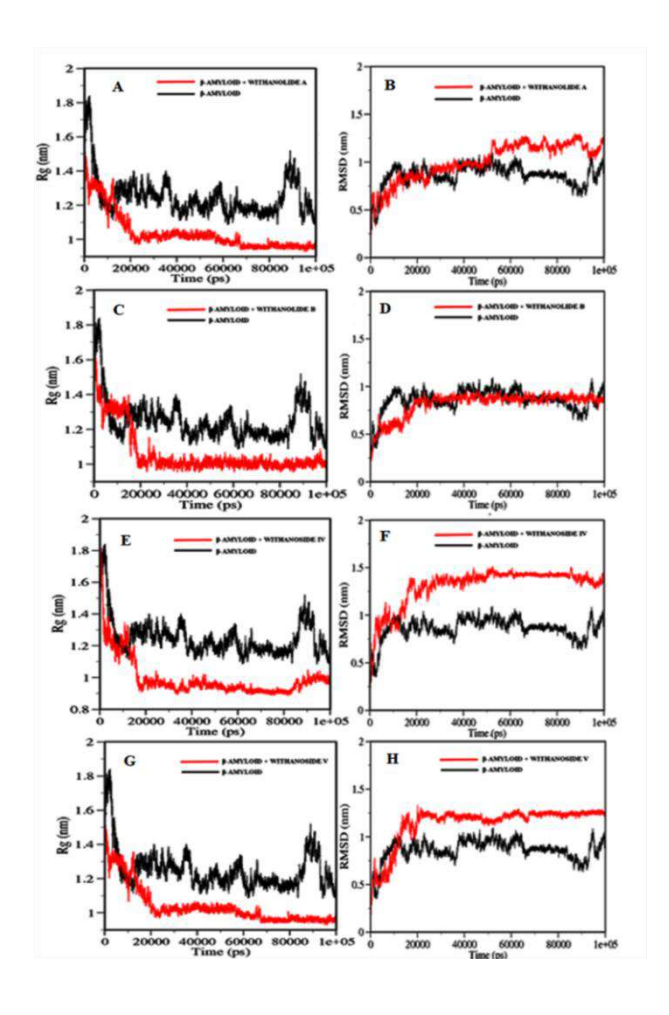


**Fig. 3.14**. The molecular dynamics simulations of  $A\beta_{1-42}$ -withanolide (A, B,) and withanoside IV, V for 100 ns. A, C, E, G- Plot of RMSD values for unliganded  $A\beta_{1-42}$  and  $A\beta_{1-42}$ — Ashwagandha derivatives complexes. B, D, F, H- Comparison of the RMSF of Calcium atoms along the sequence derived from the 10 ns simulations

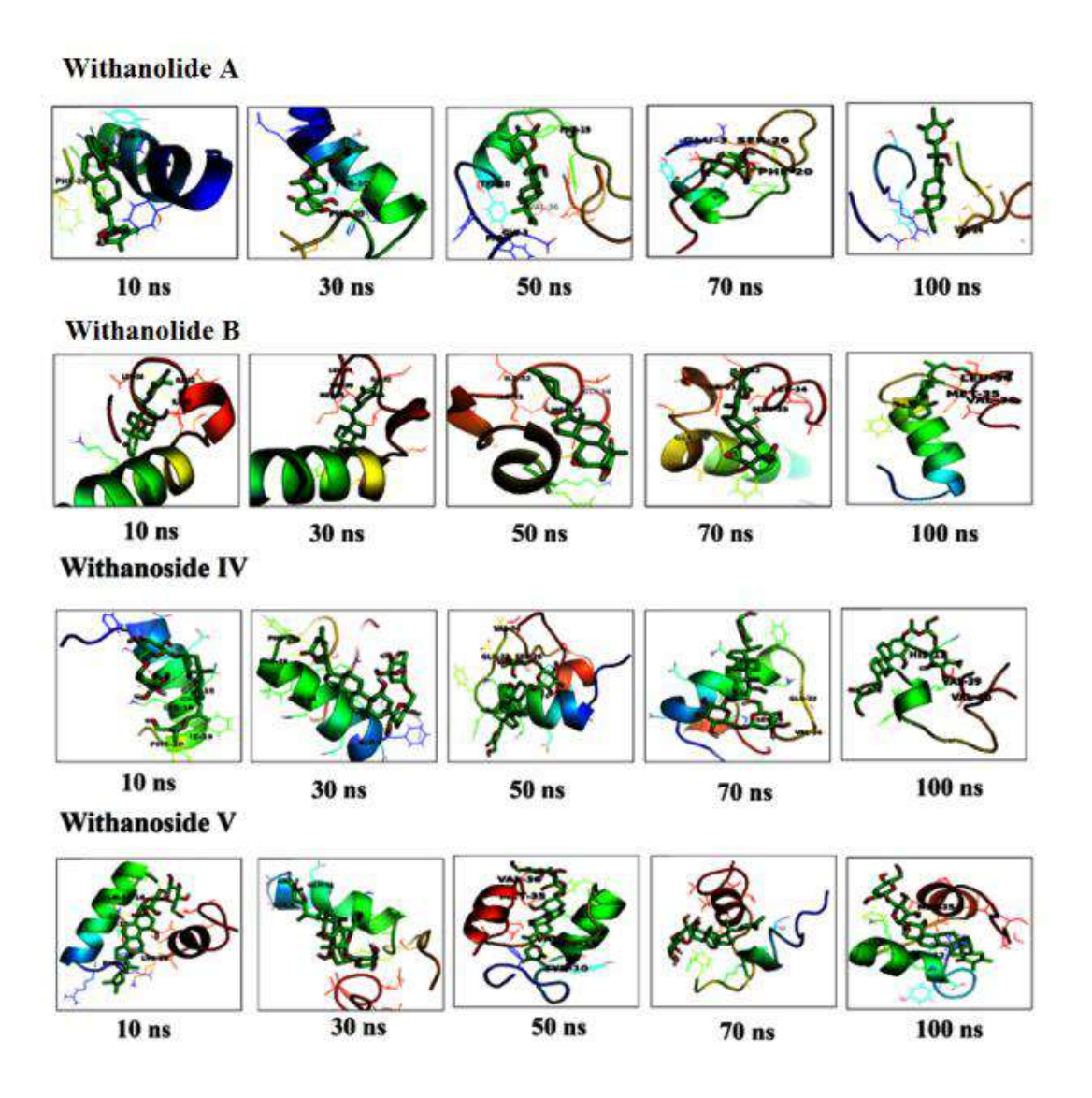


**Fig. 3.15.** The conformers of  $A\beta_{1-42}$ - phytocompounds at different nano seconds.

# 3.3. Conclusion

The main aim of this work was to analyze the interaction of phytocompounds, i.e., derivatives of *Withania somnifera* (Ashwagandha) namely withanolide A, withanolide B, withanoside IV and withanoside V, with HSA. Quenching of fluorescence emission of HSA showed the formation of HSA-ligand complex formation with binding constant of  $K_{Withanolide\ A} = 3.04\pm0.05\ X\ 10^4\ M^{-1}$ ,  $K_{Withanolide\ B} = 7.59\pm0.05\ X\ 10^4\ M^{-1}$ ,  $K_{Withanoside\ IV} = 6.74\pm0.03\ X\ 10^4\ M^{-1}$  and  $K_{Withanoside\ V} = 5.33\pm0.05\ X\ 10^4\ M^{-1}$ . These binding constants fall

under the range of  $10^3 - 10^6 \,\mathrm{M}^{-1}$ , which is in the range of known FDA approved drugs. Circular Dichroism also shows partial unfolding of the protein upon interaction of these molecules with HSA and further it was confirmed by AFM and TEM on basis of morphological and topological changes in the protein-ligand complexes. Our experimental results illustrated strong binding between these derivatives with HSA and are in corroboration with the *in-silico* data of molecular docking and MD simulations. Owing to similar molecular and structural formula all the derivatives of *Withania somnifera*, were seen to displace phenylbutazone and bind on Sudlow's site I. Using MD simulation, the stability of only HSA and HSA–drug complexes were qualitatively compared for 10 ns. The study undertaken in our lab will be helpful in further understanding the pharmacokinetics and pharmacodynamics of these compounds and it provides a base to further exploit the far-reaching pharmaceutical potential of these steroidal derivatives.

Our research exploits the far-reaching potential of the derivatives of *Withania Somnifera* derivatives against AD. The results depicted here indicate the ability of these derivatives to inhibit fibrillization, as indicated by the ThT assay. Moreover, the cell culture assays also indicate the ability of the derivatives to reduce the cytotoxic effects of  $A\beta_{1-42}$  fibrillation. Molecular Docking results indicate that the derivatives were interacting with the hydrophobic core (17-21) residues region of  $A\beta_{1-42}$  thus discouraging another peptide of  $A\beta_{1-42}$  to come and bind and hence inhibiting the process of fibrillization. Our 100 ns simulations suggest that the Withanolide B and withanoside V complexes were stable in the hydrophobic core of  $A\beta_{1-42}$ . We can infer that these derivatives of Ashwagandha have the potential for further study for neuroprotection.

# Chapter – 4

Elucidating the inhibitory potential of HSA as well as synthesized peptides against amyloid fibrillation and amyloid associated neurotoxicity

# Elucidating the inhibitory potential of HSA as well as synthesized peptides against amyloid fibrillation and amyloid associated neurotoxicity

#### 4.1. Introduction

Dementia is a condition where people suffer from memory loss, and AD is the most common type of senile dementia (Wang et al., 2017). Alzheimer's is a 110-year-old disease that is insidious, progressive, and degenerative in nature. According to the World Health Organization, 50 million people across the globe are suffering from dementia and it is projected that the number may rise to 82 million by 2030 and 152 million by 2050. AD is pathologically characterized by extracellular senile plaques and intracellular neurofibrillary tangles. The hippocampus region and cerebral cortex of the brain are the major parts affected by AD's progression leading to their degeneration and plaque formation due to amyloid fibril deposition. The amyloid cascade hypothesis was the most accepted theory till now among the several theories which states that the primary neurologic damage is caused by the soluble and toxic oligomers. Its further states that the hallmark of the AD's is the presence of amyloid fibrils (Hardy, 2002).  $A\beta_{1-42}$  molecule is usually present in all human beings irrespective of their age or disease and they are cleared naturally, and they are known to have neuroprotective properties at low concentrations. However, if the amyloid  $\beta$  protein is not cleared from the brain, it accumulates as oligomers and eventually fibrils. The imbalance between the production and clearance of  $A\beta_{1-42}$  is known to be the major reason for AD. Healthy individuals possess the capacity to clear the amyloid from the brain before it reaches the cytotoxic levels.

 $A\beta_{1-42}$  is a polypeptide present in the extracellular region in the brain and is produced by sequential cleavage by  $\gamma$  and  $\beta$ -secretase of amyloid precursor protein. Persistent failures have led investigators to develop new strategies for AD aiming at lowering the  $A\beta_{1-42}$  self-assembly. AMBAR is an effective treatment which has reached phase III of clinical trials (Boada et al., 2016). As the large majority of  $A\beta_{1-42}$  around 90% is bound to HSA and very limited is free (Biere et al., 1996). So, plasma therapy by dialysis has come up as an alternate treatment for early stage of Alzheimer's.

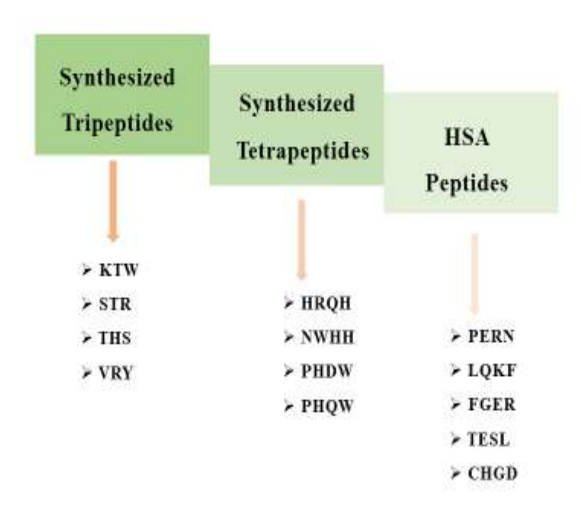
As HSA, the cargo plasma protein is known to have anti-amyloid properties along with its individual domains that inhibit  $A\beta_{1-42}$  fibrillization with almost same affinity. I aimed to determine which fragments of HSA interact with  $A\beta_{1-42}$ . I have employed molecular docking and taken fragments of HSA as tetrapeptides. HSA is a protein which is present in the human plasma at a concentration of 640  $\mu$ M and in the brain at a concentration of 3  $\mu$ M. The studies show that HSA binds to  $A\beta_{1-42}$  when it is in oligomeric state and prevents another  $A\beta_{1-42}$  to come and bind to it thus ameliorating fibrillization process. The affinity between the domains of HSA and  $A\beta_{1-42}$  is known to be in nanomolar concentration, but it was not known that which amino acids of HSA are interacting with the  $A\beta_{1-42}$  and inhibiting its self-aggregation.

The main aim of this study was to find out exactly which amino acids of HSA are actually interacting with  $A\beta_{1-42}$  polypeptide to retard its self-aggregation and also to analyze the binding is mainly by what kind of interactions, i.e. hydrophobic interaction, hydrogen bond formation, hydrophilic, Vander-walls interactions etc., Hydrophobicity is the major driving force for self-assembly of  $A\beta_{1-42}$ , so it was imperative to check if these peptides act as efficient drug candidates by competing with  $A\beta_{1-42}$  monomers.

So, for this study, I have designed five tetra-peptides fragments of HSA which were interacting with  $A\beta_{1-42}$ . The BSBp were designed are fragments of the protein HSA, as HSA itself has the ability to inhibit  $A\beta_{1-42}$  fibrillation (Choi et al., 2017). HSA molecules has three domains: Domain I, Domain II and Domain III and all the three domains of HSA are known to inhibit the aggregation process (Milojevic et al., 2007) but it was not well understood which part of HSA actually interacts with the hydrophobic core of  $A\beta_{1-42}$  for stopping the aggregation process. Based on molecular docking studies, five peptides were synthesized which were interacting with hydrophobic core of  $A\beta_{1-42}$ . The peptides designed were as follows:

- PERN: Amino acid sequence 120-123, Domain I
- LQKF: Amino acid sequence 227-230, Domain II
- FGER: Amino acid sequence 230-233, Domain II
- CHGD: Amino acid sequence 270-273, Domain II
- TESL: Amino acid sequence 552-555, Domain III

β sheet breaker peptides desighned to study β amyloid interaction



I have also used Glide module of Schrödinger to first computationally synthesize some peptides which can be used as BSBp and inhibit the fibrillization process of the protein  $A\beta_{1-42}$ . It was first in the rat brain (Soto et al., 1998), that BSBp significantly reduced  $A\beta_{1-42}$  fibrillization in rat model, since then studies have been going on for utilizing peptides for treatment of AD. These peptides are actually known to target the hydrophobic core of  $A\beta_{1-42}$ , which is the motif from amino acid number 17-21 of the polypeptide (Poduslo et al., 1999).

Peptides are known to have various benefits and are being used as drugs for various central nervous system diseases because of their capacity to inhibit protein-protein interactions. There are various issues when small molecular weight compounds are used as drugs that are circumvented by using peptides for the same purpose. Further, *in silico* generated peptides by High Throughput Screening (HTS) which are made by keeping in mind that peptides are being used for the treatment of various CNS diseases. The peptides larger than tri-tetra peptides do not seem to cross the BBB; thus, I have designed some potentially therapeutic peptides (Witt et al., 2001, Adessi and Soto, 2002).

Although, some studies have revealed that peptides have some limitation like short half-life and cleavage by peptidases, but these limitations can be overcome by using D-enantiomers of peptides and by specific chemical modifications. Hence, for these studies I have designed five tetrapeptides fragments of HSA which were interacting with  $A\beta_{1-42}$  and also four tetra-peptides and four tripeptides were designed by computer-aided drug designing (CADD). Various strategies have been applied to inhibit the amyloid formation and BSBp of structure as well as sequence based have been made, but for any molecule to be effective, it is imperative that it acts at the

hydrophobic core of  $A\beta_{1-42}$  so another molecule of the peptide cannot come and bind thus inhibiting the aggregation process (Mitra & Sarkar, 2020).

### 4.2. Results and Discussion

### 4.2.1. Docking between HSA and Aβ<sub>1-42</sub>

Molecular Docking is a way of studying the interaction between two compounds. There are many computational software's by which one can perform such studies. Here, for this study, Haddock and Patchdock software were used to dock  $A\beta_{1-42}$  with HSA, and the PDB structures of both 2BEG.pdb, 1AO6.pdb were downloaded from www.RCSB.org and docking was performed as HSA is known to bind to  $A\beta_{1-42}$  in oligomeric state. HSA has 585 amino acids divided into three domains and has multiple ligand binding sites (Sudlow et al., 1976; Varshney et al., 2010). I observed from the results that few amino acids of HSA were interacting with  $A\beta_{1-42}$  by forming hydrogen bonds (shown in Fig. 4.1). Those amino acids were taken as fragments/tetra-peptides to dock again, using Glide module of Schrödinger with  $A\beta_{1-42}$  to see the interaction between these peptides. Post-docking, I also performed molecular simulations for 200 ns for all the docked complexes to assess their stability.

Through these studies, I tried to explain the binding affinities of HSA, based on the docking scores, the more negative energy, the better binding affinity. The binding score of HSA tetra peptides computed was obtained around  $\pm 4$  to 5. Also, these peptides are bound with the hydrophobic core of A $\beta_{1-42}$ , i.e. amino acids 17-21, which is the main site in blocking the aggregation. Further, the pentapeptide KLVFF was used as a positive control to see the interaction of this peptide with A $\beta_{1-42}$  for the molecular docking, molecular simulations and free energy analysis (Austen et al., 2008). KLVFF is actually

the hydrophobic fragment of the  $A\beta_{1-42}$  residues (16 – 20 of  $A\beta_{1-42}$ ). From these results, I could see that the BSBp generated were also showing similar binding with  $A\beta_{1-42}$ . Peptides derived from HSA based on the docking results were as follows:

- PERN: Amino acid sequence 120-123, Domain I
- LQKF: Amino acid sequence 227-230, Domain II
- FGER: Amino acid sequence 230-233, Domain II
- CHGD: Amino acid sequence 270-273, Domain II
- TESL: Amino acid sequence 552-555, Domain I

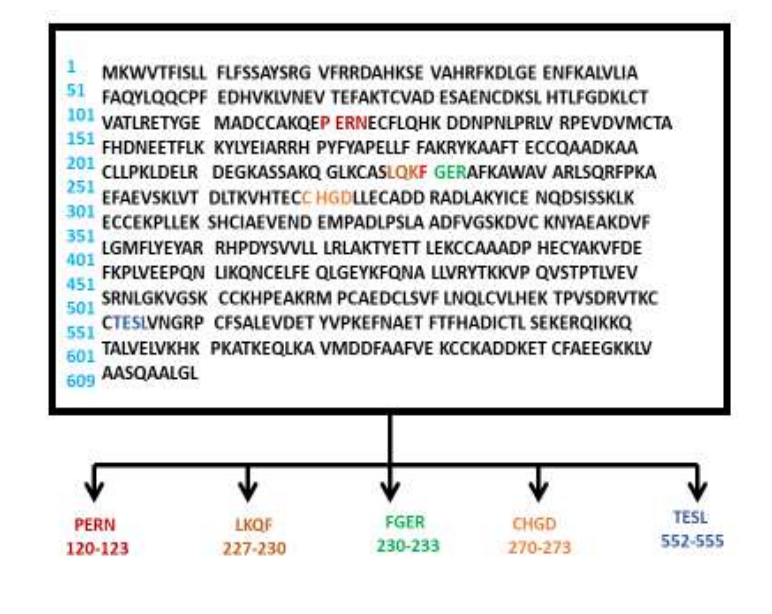




**Fig. 4.1.** A) Selected peptides derived from HSA through Haddock and Patchdock B) Pymol showing the amino acids interacting with  $A\beta_{1-42}$  through hydrogen bonds.

### 4.2.2. Screening of BSBp by GLIDE module of Schrödinger

*In silico* screening is a process by which many compounds/ligands can be filtered against a target protein, and one can predict that whether the ligand can bind strongly or weakly with the target protein in order to affect its function/activity. There are many computational software's by which one can perform the task. Software has its own algorithm and prescribed methodology to perform the task. I used GLIDE module from Schrödinger software for this *in silico* screening and docking studies of tri and tetra-peptide library against Aβ<sub>1-42</sub> as target. Once I have prepared the GRID, I performed screening of the ligands. This screening is done using HTVS function of GLIDE, which virtually screen the ligands against the target GRID. The ligands which can easily enter the GRID get better HTVS score (for example say -6.87) in comparison to the ligands which sparsly fit into the GRID (for example say -3.76). So based on this HTVS scores, I selected a range of score (say for example, I will select only the ligands within the HTVS scores of -6.87 to -5.5). So in my HTVS list, the top ligand will have HTVS score of -6.87, and the least one would have HTVS score of -5.5. I proceeded with another function of GLIDE called as SP docking (from here actual docking starts).

The standard precision (SP) function of GLIDE computes the various interacting forces like hydrogen bond, electrostatic interaction, between the ligand and the GRID gives a score called as SP score which is again as per described earlier may lie from -6 or -7 etc (Sliwoski et al., 2013). So again I have selected a range of top scored ligands and these ligands were further selected by the user for XP docking. The extra presicion (XP) docking function of GLIDE also calculates all the molecular interactions between the ligand and the GRID just like SP. The only difference is XP gives more time for such calculations. After geting the XP scores, it can be inferred that the top listed ligand with highest XP score

should be the most probable inhibitor with strongest binding among all of the ligands of a particular ligand library. After getting the list of say top 10 molecules, I compared their E-model values. E-model values are nothing but different poses of the corresponding ligand by which it fits into the GRID. I prefer the molecule with highest XP score and E-model values for further experimental validation. Here I must say that many times E-model value of second or third top ranked molecule can be more than the top molecule. In that case, I see what is the differences in their XP score, suppose XP score of top molecule is -7.35 but its E-model value is -50.23 while the second ranked molecule has XP score of -7.0 but its E-model value id -70.40, then in such case I prefer the second ranked molecule as the difference in its XP score with the top molecule is less but their E-model values differ a lot, so a molecule with competitive XP score and highest E-model value can be a much better inhibitor as compared to a molecule with just highest XP score. X-score is a program which calculates the probable binding affinity between the docked ligand against the target protein. The X-score program itself is made up of three independent scoring functions, namely HP-score, HM-score and HS-score. The X-score is an outcome of cumulative results from these three scoring functions.

### Docking between the designed BSBp and the Aβ<sub>1-42</sub>

So as explained in 4.2.1 and 4.2.2 there were two different approaches while designing the peptides. The first set of the peptides are fragments of the serum protein HSA, and they are CHGD, FGER, LQKF, PERN and TESL. The second group of peptides were screened by GLIDE module of Schrödinger. I have selected four most energetically stable tetrapeptides as well as four most energetically stable tripeptides and they are HRQH, PHDW, PHQW and NWHH and the tripeptides are STR, KTW, THS and VRY. And computational studies

were also done for the positive control peptide KLVFF, which is a BSBp (Tjernberg et al., 1996).

To see the binding interaction of these novel desighned BSBp, we have done molecular docking, molecular simulations and free energy calculations. The docking score for Tri-peptides were in the range from -5 to -6. The tripeptides VRY and KTW showed energetically more stable binding energy than THS and STR, whereas all the tetra-peptides showed approximately similar binding energy described as Glide score. The hydrogen-bonding interactions of Tri-peptides, Tetra-peptides and HSA peptides were within the residual range 11-27 of  $A\beta_{1-42}$ . Thus computational studies showed that all the peptides have an excellent binding affinity with the hydrophobic core of the  $A\beta_{1-42}$ .

The hydrogen bonds and hydrophobic interaction of all these peptides with  $A\beta_{1-42}$  was given in the Table 4.1 and Table 4.2. These results shows that peptides were binding strongly to the  $A\beta_{1-42}$  Fig. 4.2 add Fig. 4.3. The binding of these peptide to the  $A\beta_{1-42}$  indicates that the aggregation of  $A\beta_{1-42}$  may reduce, which is further discussed in later sections.

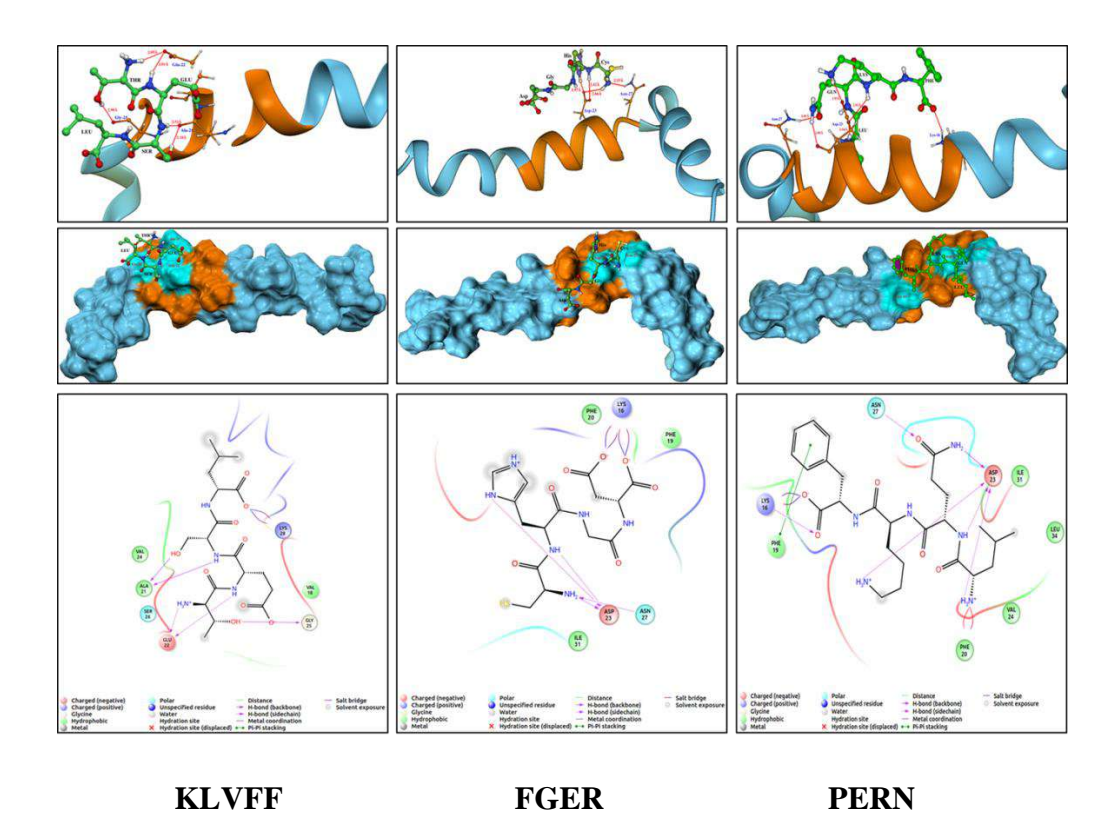
**Table 4.1.** Docking scores and X scores for tri and tetra peptides against  $A\beta_{1-42}$ .

	Glide Score (Kcal/mol)	Xscore (Kcal/mol)	Hydrogen Bonds	Hydrophobic Interaction	Number of Non- bounded Interactions
нкон	-6.58	-7.46	Gin-15, Glu-22	Phe-19, Asp- 23, Ser-26, Asn- 27	7
PHDW	-6.62	-8.01	Glu-22, Ser-26, Lys- 28	Phe-20, Ala- 21, Val-24, Gly- 25	6

PHQW	-6.65	-8.31	Ala-21, Glu-22, Lys- 28	Phe-20, Val- 24, Gly-25, Ser- 26	6
NWHH	-6.76	-7.02	Glu-22 (2), Asp-23 (2)	Gln-15, Phe- 19, Ser-26	5
STR	-5.74	-7.02	Glu-22(4), Val-18, Ser- 26(2)	Ala-21, Gly- 25	5
KTW	-6.60	-7.82	His-14	Glu-11, His- 13, GLn-15, Leu- 17, Val-18	5
THS	-5.35	-7.00	Glu-22 (3), Val-18, Ser-2	Ala-21, Gly- 25	5
VRY	-6.51	-7.32	Glu-11, Gln-15, Glu- 22	His-14, Val- 18	5

Table 4.2 Docking scores and X scores for HSA peptides and a positive control KLVEF with A $\beta_{1\text{--}42}$ .

Peptide	Glide Score (Kcal/mol)	X Score (Kcal/mol)
CHGD	-5.261	-4.89
FGER	-4.917	-4.36
LQKF	-5.160	-5.89
KLVEF	-4.932	-5.42
PERN	-5.021	-6.89
TESL	-4.554	-5.39



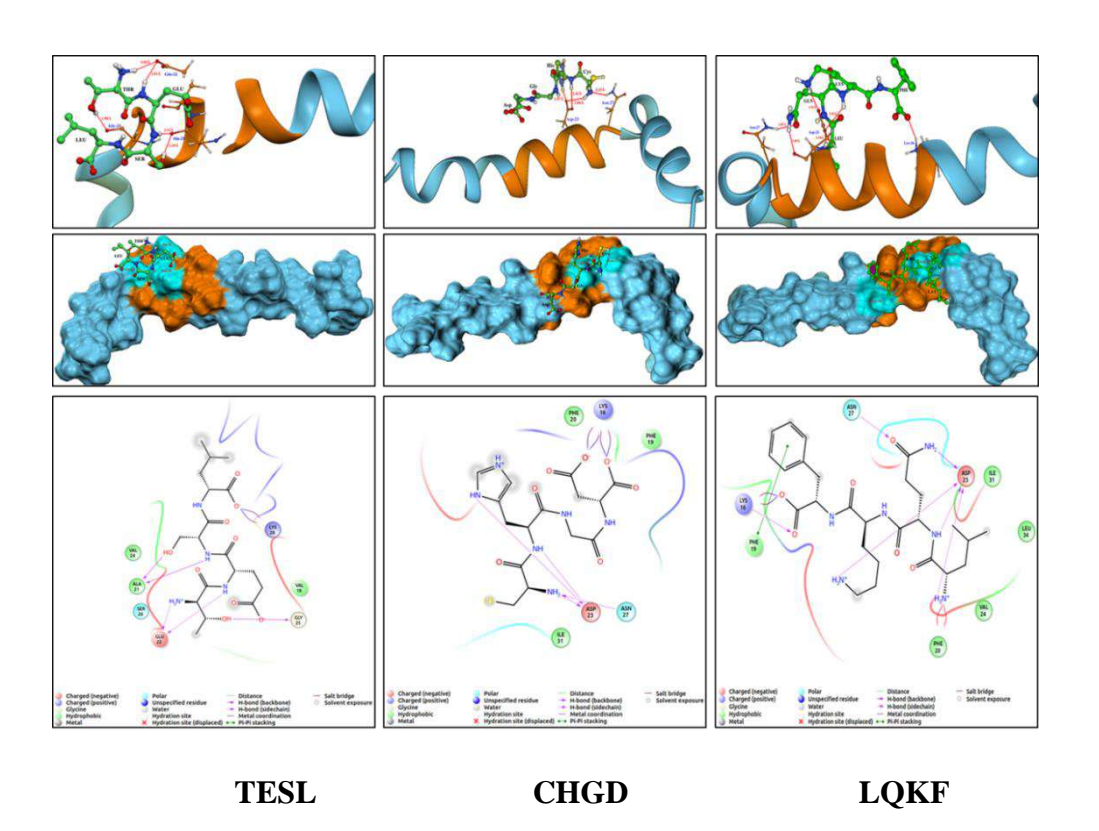


**Fig. 4.2.** Docking images of the HSA derived peptides with  $A\beta_{1-42}$ . Pictures were generated by pymol, the first row shows the secondary structure figures, second row gives the surface figures and the third row is the lighlot images showing which amino acids were interacting.

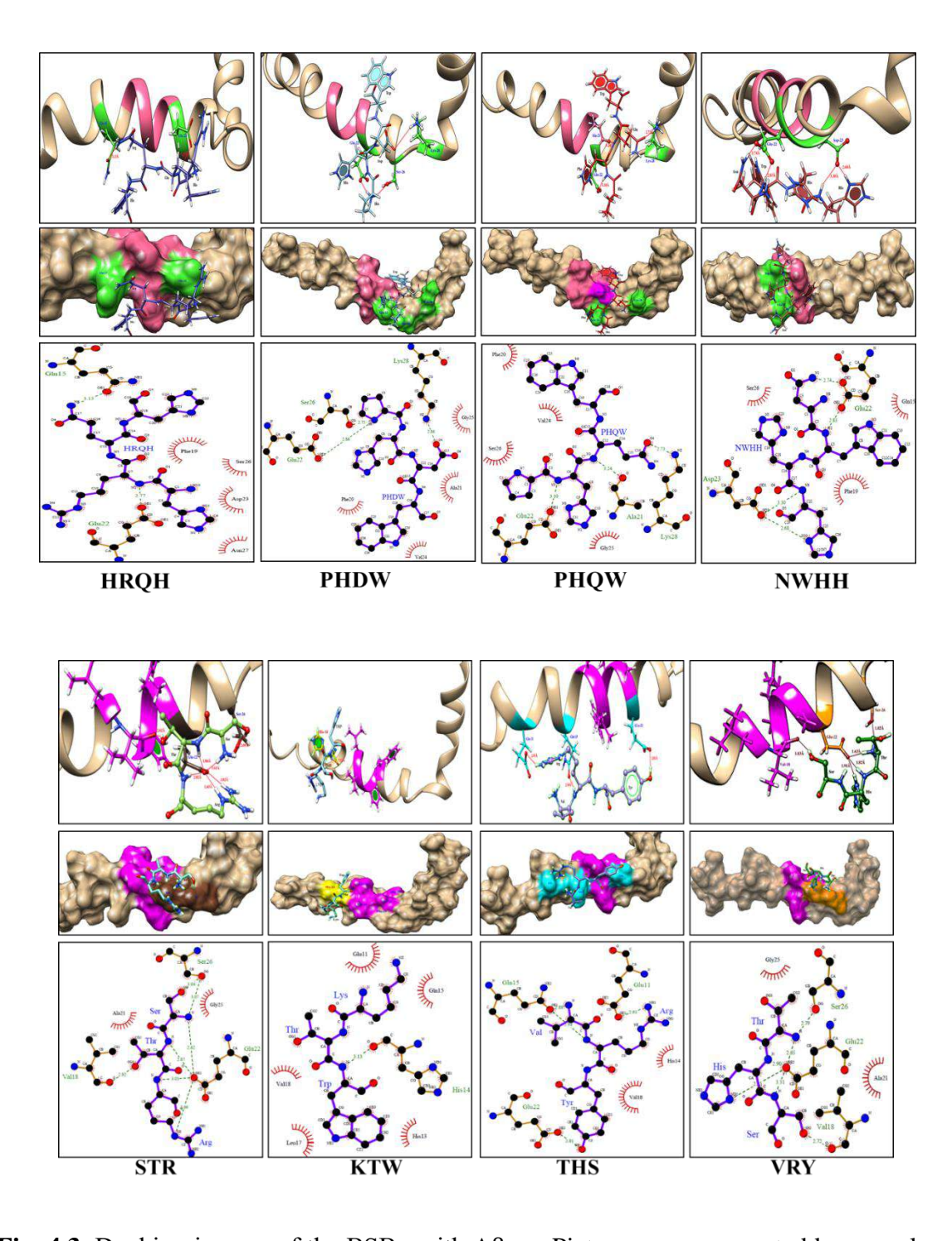


**Fig. 4.3.** Docking images of the BSBp with  $A\beta_{1-42}$ . Pictures were generated by pymol, the first row shows the secondary structure figures second row gives the surface figures and the third row is the ligplot images showing which amino acids were interacting.

### 4.2.3. Molecular dynamics and simulations

To investigate the stability and molecular interactions between the protein-ligand, molecular dynamics simulations is a crucial and useful technique. From the docking results, the best docking conformation which correlates with the experimental results, such complex was chosen as the starting point for 200 ns simulations (Eskici & Gur, 2013). The trajectories of complex structures are the result of 200 ns of only  $A\beta_{1-42}$  and  $A\beta_{1-42}$ -peptides followed by the equilibration protocol described above. In this study Rg, RMSD and RMSF, were determined to know the rigidity of the protein, and stability of the HSA derived peptides complex with  $A\beta_{1-42}$ . The RMSD values for tri, tetra-peptides and HSA peptides were  $\pm 1.2$  nm, the control selected for the comparison is KLVFF peptide (red color) which is around 0.5 nm and the only  $A\beta_{1-42}$  (black color) is around 1.5 nm. These values illustrate the stability of the complex over the certain period of the simulation during which the RMSD values were consistent for the last 50 ns. Prolongation of the integrity of the hydrophobic core of the protofibril explains the observed structures. From Fig. 4.4, it can be derived that the  $A\beta_{1-42}$ -peptides did not deviate remarkably compared to the only  $A\beta_{1-42}$ .

The Rg of all the peptides explains whether they are compact with  $A\beta_{1-42}$  throughout the 200 ns compared to the positive control KLVFF. The Fig. 4.4 shows that the only  $A\beta_{1-42}$  is around 1.0 nm whereas the positive control KLVFF is highly fluctuating around 2.0 nm at 100 ns simulation, for further simulations, the control showed equilibration. However, the tri, tetra, and HSA peptides showed compact structures throughout the 200 ns simulations which explain that the selected peptides were stable in complex with the

 $A\beta_{1-42}$ . This also indicate that these complexes were conformationally stable, which further indicates that the selected peptides bind to the right active cite.

Binding free energies were analysed by MM/PBSA method, based on the MD trajectories (Table 4.3). After taking a stable pose, for control KLVFF with the free energy of –92.008 kj/mol; the other tripeptides, tetra-peptides and HSA peptides were analysed and they have energies from 47.702 to –288.63 Kj/mol, respectively. The individual energy calculations for each peptide were given in Table 4.3. For all the peptide complexes, energetically favourable complex exhibits a strong intermolecular electrostatic stabilization and counters the destabilizing effect with the charged interacting groups. In addition to hydrophobic interactions, even the charged interactions provide an extra stabilization when it binds to the β-sheet surface. These interactions are purely hydrophobic to other binding sites on the fibril. Thus, I can suggest that these structures may be thermodynamically stable.

The trajectories after a series of 200 ns MD simulations, they were analysed for complete details of protein-ligand interactions in terms of different conformations and their stability. Also, to cross-check our results from docking (HSA) derived peptides to hydrophobic core of  $A\beta_{1-42}$  which prevents development of the  $A\beta_{1-42}$  fibrillation, cytotoxicity thus progression of AD. *In silico* interaction studies showed the good stability of peptides with  $A\beta_{1-42}$ . RMSF of FGER, PERN, STR, KTW and THS showed less fluctuation after binding with amyloid indicates that these peptides formed rigid structure with  $A\beta_{1-42}$ . Also, they have good hydrogen bond interaction throughout the simulation which explains that the  $A\beta_{1-42}$  is stabilized upon binding of these peptides.

The stability of tri, tetra, HSA peptides after complex formation with  $A\beta_{1-42}$  were observed by Rg and RMSD values. The complexes were stable from initial ns to 200 ns

simulations. The rigidity of residues where the peptides bind to the  $A\beta_{1-42}$  was showed through RMSF. Thus, altogether our *in-silico* studies explain that tri, tetra and HSA peptides were interacting with the  $A\beta_{1-42}$  in the hydrophobic core through hydrogen bonding and were stable after interaction.

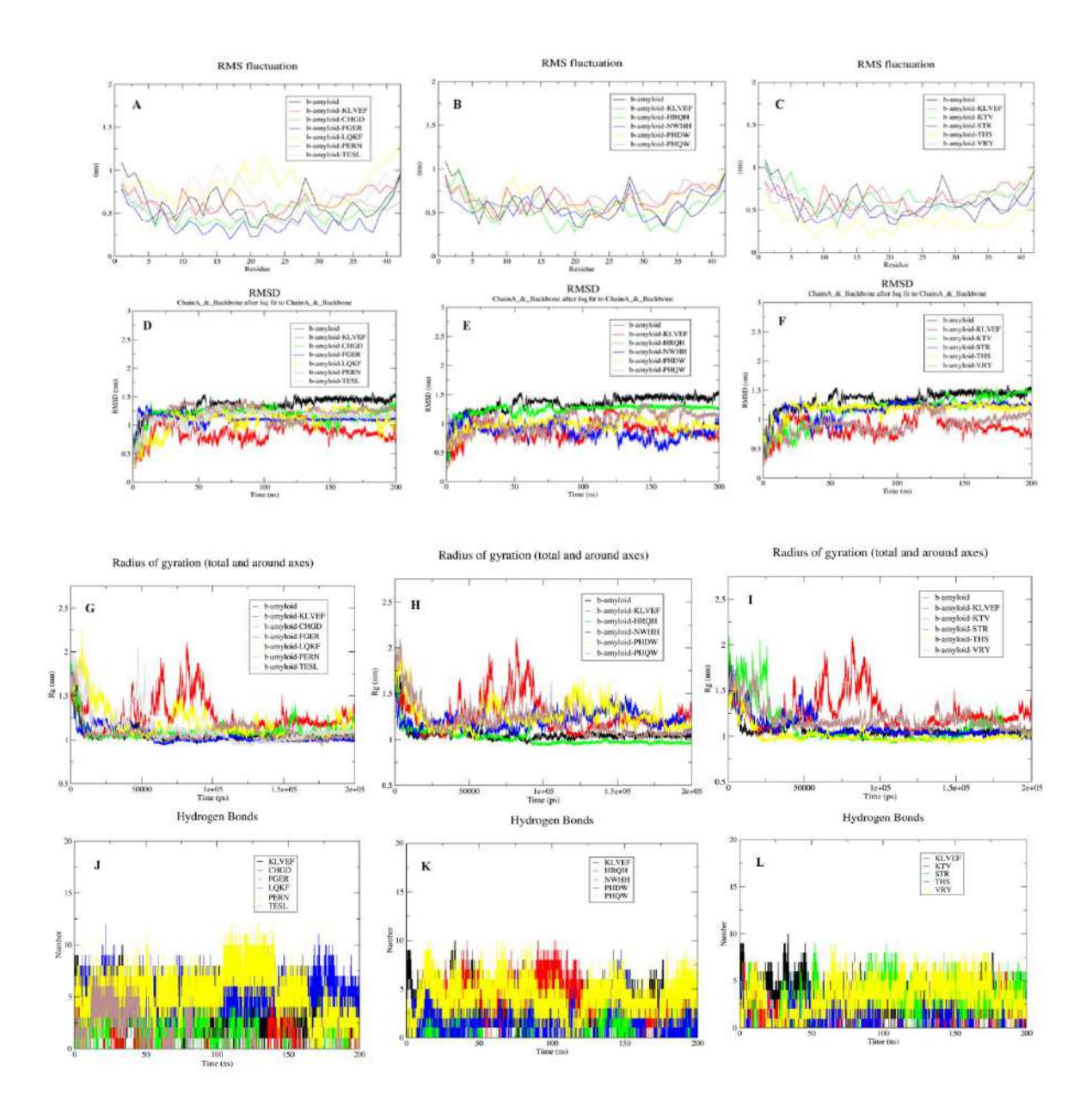


**Fig. 4.4.** Time evolution of Rg (G-I) during 200 ns of MD simulation of unliganded  $A\beta_{1-42}$  and HSA, Tetra, Tri peptide- $A\beta_{1-42}$  complexes. (D-F)-Plot of RMSD values for unliganded  $A\beta_{1-42}$  and HSA, Tetra, Tri peptide- $A\beta_{1-42}$  complexes. (A-C) Comparison of the RMSF of unliganded  $A\beta_{1-42}$  and HSA, Tetra, Tri peptide- $A\beta_{1-42}$  complexes along the sequence derived from the 200 ns simulations and its (J-L) hydrogen bonds of with  $A\beta_{1-42}$ 

# 4.2.4. Free energy by MMPBSA

For a better understanding on strength of these interactions, binding free energies between  $A\beta_{1-42}$  monomer and the peptides were calculated using the MM/PBSA approach (Genheden & Ryde, 2015). This method has been proved to be an effective tool which can be used to estimate the relative binding free energy as well as provide a decomposition of the residue contribution to binding. In our study, coordinates were saved every 20 ps from 100-200 ns frames and binding free energy analysis and its related components were obtained from the MM/PBSA calculation based on the saved frames in the trajectories (Table 4.3). Here, the value of KTW, VRY and PHQW peptide are looking very energetically stable.

**Table 4.3.** Free energy values evaluated by MMPBSA

STR	-129.312 +/- 70.898 kj/mol
KTW	-288.464 +/- 160.611 kj/mol
THS	-13.481 +/- 25.935 kj/mol
VRY	-352.664 +/- 288.633 kj/mol
HRQH	-231.169 +/- 121.555 kj/mol
PHQW	-208.431 +/- 170.814 kj/mol
PHDW	6.972 +/- 143.813 kj/mol
NWHH	-85.576 +/- 41.468 kj/mol
FGER	-166.646 +/- 98.444 kj/mol
TESL	15.145 +/- 91.509 kj/mol

PERN	-168.147 +/- 165.005 kj/mol
CHGD	134.317 +/- 47.702 kj/mol
LQKF	-185.769 +/- 258.816 kj/mol
KLVFF	-348.624 +/- 92.008 kj/mol

### 4.2.5. Lipinski rule of five

Before going into the *in vitro* studies, it was imperative for us to see the drug likeness properties of these derived peptides. In the field of drug designing for understanding the dug likeness properties and to study the pharmacokinetics of the same, this rule of five gives us a clear picture about a molecule for being suitable to use as an oral drug. The molecules which conform to this rule usually have a lower attrition rate, and their chances of being a suitable drug molecule is higher (Lipinski et al., 1997). The drug-likeness of the peptides under study was estimated by Lipinski Rule of Five using the server given in the web link (Lipinski, 2004; Jayaram et al., 2012; Husain et al., 2016) and I saw that the values obtained were in the range of this rule particularly the tri-peptides were totally in the range and were following this rule as given in the Table 4.4. The famous rule of 5 is based on the study and analysis of structural parameters and molecular structures and the concerned molecules were evaluated based on the following parameters.

- (I) the molecular mass should be below 500.
- (II) The octanol /H2O partition coefficient (Log P) should be below 5.
- (III) The molecule possesses lesser than 5 H bond donors (OH and NH groups).
- (IV) The molecule possesses fewer than 10 H bond acceptors (specifically N and O).
- (V) Molar Refractivity should be between 40-130.

**Table 4.4.** Lipinski rule of five to see drug likeness properties by analysing the five physiochemical properties.

	Molecul	Hydrogen	Hydro	LogP	Molar				
	ar Mass	bond donors	gen bond						
	(Da)	bolia dollors	acceptors	(Lipophicity)	Refractivity				
Permissi	< 500		.10		40, 120				
ble values	Dalton	<5	<10	<5	40-130				
<u> </u>		HSA de	rived peptide	es					
CHGD	312	5	6	-0.05	77.14				
FGER	489	5	13	-4.44	107.61				
LQKF	517	4	11	-3.29	119.31				
PERN	496	4	15	-5.64	105.23				
TESL	429	5	12	-5.97	90.67				
		Tetr	a-peptides						
HRQH	312	5	6	-0.05	77.14				
NWHH	574	4	15	-4.54	130.68				
PHDW	534	3	13	-4.24	120.89				
PHQW	548	3	13	-3.50	126.81				
	Tripeptides								
KTW	419	6	8	-4.06	96.95				
STR	348	8	10	-4.75	75.66				
THS	329	7	9	-4.42	72.81				
VRY	422	8	9	-3.79	96.55				

# 4.2.13. Analysis of absorption, metabolism and toxicity prediction by ADMET-SAR

## **Software**

1. #starts -Molecule having a smaller number of stars is less drug like molecule

(Range 0-5)

2. #rtvfg - Toxicity (Range 0-2)

3. CNS - CNS activity of molecules (Range-2 (inactive) to +2(active))

4. Mol MW - (Range < 500)

5. Donorhb - Hydrogen bond donor (Range < 5)

6. Accepthb - Hydrogen bond acceptor (Range <10)

7. Qplogpo/w - Partition coefficient (Range -2.0 to -6.0)

8. Qplogbzb - Blood brain partition coefficient (Range -3.0 to -1.2)

9. Rule of Five - Number of violations of Lipinski rule of 5 (Range max 4)

**Table 4.5** Prediction of drug ability based on the ADMET properties

Title	#stars	#rtvFG	CNS	molMW	donorHB	QPlogPo/W	QPlogBB	Rule
								of Five
STR	9	0	-2	349.386	6.5	-5.032	-3.241	2
THS	4	0	-2	329.355	4.5	-3.477	-2.201	1
VRY	6	0	-2	436.51	8.5	-2.492	-3.937	2
KTW	0	0	-2	374.482	4.25	1.695	-1.315	1
CHGD	9	1	-2	432.451	6.5	-4.837	-3.22	2
FGER	9	0	-2	507.545	8.75	-3.124	-3.789	3
LQKF	10	0	-2	534.654	7.75	-3.41	-3.335	3
PERN	11	0	-2	514.537	9.5	-5.738	-6.526	3

Chapter 4 | Elucidating the inhibitory potential of HSA as well as synthesized peptides

HRQH	3	0	-2	215.208	0.75	-2.27	-1.803	0
KLVEF	9	0	-2	634.771	7	-1.561	-3.973	3
LPFFD	4	0	-2	637.731	4.5	0.361	-2.005	3
NWHH	12	0	-2	580.645	8.75	-4.535	-4.45	3
PHDW	3	0	1	131.177	1	2.599	0.34	0
PHQW	10	0	-2	542.594	8.75	-4.813	-3.939	3

For any molecule for becoming a suitable drug candidate, evaluating its ADMET properties becomes very important in modern drug discovery for advancement and suitable candidate selection is a prediction of its pharmacokinetics and pharmacodynamics. In present times, ADMET characterization is usually being adopted as essential part of the modern drug discovery method as it is a very expeditious way to analyse molecule exhibiting desired drug like capability. Molecules with poor pharmacokinetics and toxicity can be ignored and incompatible molecules can be segregated (Cao et al., 2012, Cheng et al., 2012; Malik et al., 2017). Here, I could see that the values are in the desired range particularly for the tripeptides as shown in Table 4.5.

#### 4.2.6. Thioflavin assay

In order to compare the computational studies with experimental, I have carried out the experiments, i.e., thioflavin, a fluorescent dye can selectively stain and quantify formation and inhibition of protein aggregates. ThT assay is also referred as the "gold standard" experiment, because of its widespread use in the study of fluorescence emission upon rapid association with the fibrils of  $A\beta_{1-42}$ . This contributes a great deal of insight into the morphology, development of the fibrils, and also the effect of different inhibitory therapeutic molecules against the amyloid assembly. The increase in fluorescence upon

binding to amyloid has been ascribed to the rotational immobilization of the central C-C, which connects the benzothiazole and aniline rings (Pate et al., 2018). It is understood that ThT binds to the side chain along the long axis of the amyloid fibrils. In my study, I have checked the free A\(\beta\_{1-42}\) because of its increased hydrophobicity aggregated rapidly in 6 hrs forming oligomers, contributing to the increased fluorescence intensity (Fig. 4.5) and also been observed similar results (Levine, 1993). While the amyloid samples treated with drugs in the ratio 1:4 and incubated for 24 hrs of interval keeping other conditions constant showed a considerable reduction in the fluorescence intensity. The control showed good amount of aggregation in the sample. This indicates the inhibitory effect of these HSA derived peptides (drugs) against the aggregation of A\(\beta\_{1-42}\), which otherwise would lead to AD in individuals. Interestingly, all the five peptides derived from HSA, owing to their similar nature show good ameliorative property against peptide oligomeric assembly. Tubulin was used as a negative control. From previous studies I know that there are different kinds of BSBp being made and they are also being used to treat AD but at the same time one major limitation is, capacity to cross the BBB and it the lesser is the size, the better are its chances to cross the BBB (Di Natale et al., 2018; Tanaka et al., 2020).

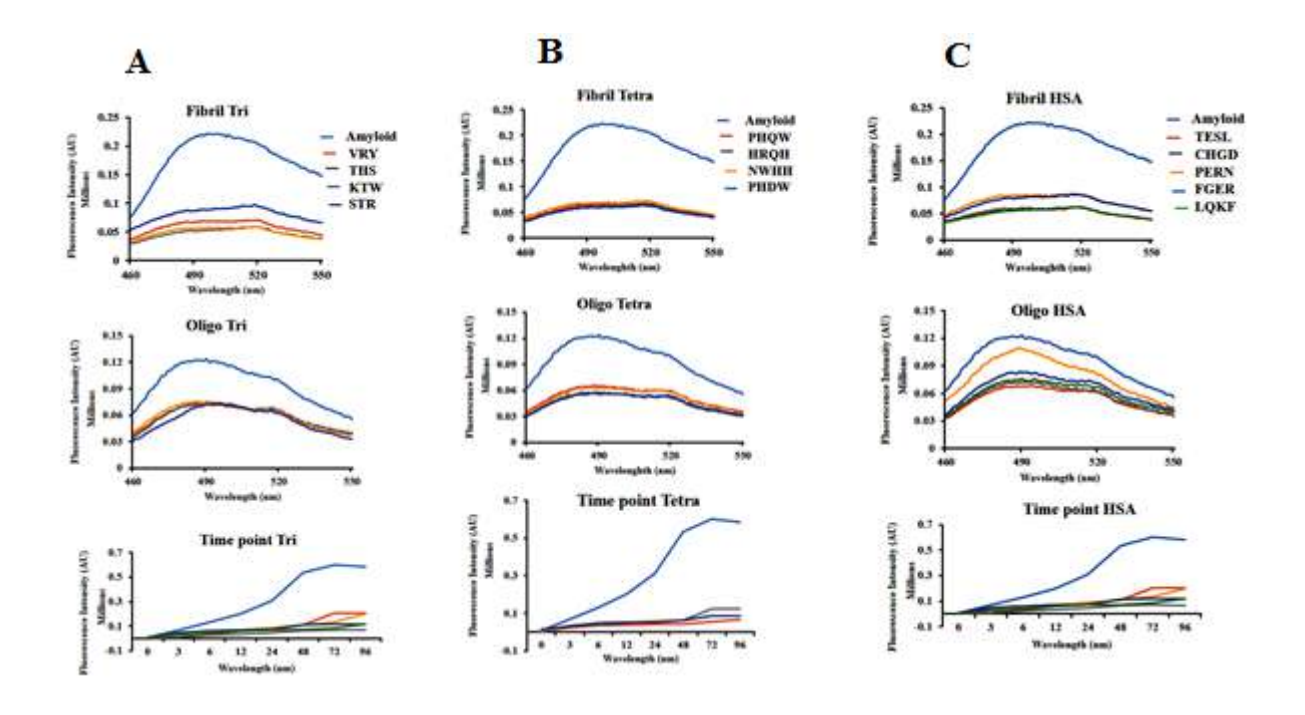


**Fig. 4.5.** Detection of  $Aβ_{1-42}$  aggregates using Tht assay; measurement of fluorescence enhancement spectra ( $λ_{ex}$ = 450nm,  $λ_{em}$ = 482nm) of 5μm Tht solution (in 50mm sodium phosphate buffer) mixed in 25μm  $Aβ_{1-42}$  with different bsbp at ratio 1:4, in their A) Tripeptides ,B) Tetrapeptides, C) HSA peptides showing fibrillar (after 24 hrs of incubation) state, Oligomeric (6 hrs incubation) state, and Fluorescence was measured at different time points upto 72 hrs to study the aggregation.

#### 4.2.7. Morphological changes

These images were photographed by using a light fluorescence inverted microscope and it can be seen that cell morphology can be drastically changed after addition of the  $A\beta_{1-42}$  and similar report was observed in previous report (Datki et al., 2004). The morphology of the cells after the addition of  $A\beta_{1-42}$ , as it is known to induce stress in the cells. As I can see in the images of the cells can observe that once  $A\beta_{1-42}$  is added, then the morphology of the cells is changing and after 6 hrs. Previous studies showed with increase in the concentration of  $A\beta_{1-42}$  there is increase in the neurotoxicity and decrease in the cell viability (Green et al., 1996). When the peptides are added then there is protection imparted by these peptides

to the cells, so after incubating for around 24 hrs the cells are healthy like in normal cells but they are able to maintain their morphology and are almost round in shape. The oligomeric species of this  $A\beta_{1-42}$  is much more toxic than the fibrillar structure of the same protein. The oligomeric structure is formed in time period of around 6-8 hrs and it is supposed to reach the fibrillar state in around 48 hrs (Barr et al., 2015; Barale et al., 2019).

The morphological changes of the cells were seen by using light fluorescence inverted microscope. The cells pretreated with peptides for 12 hrs and then treated with the  $A\beta_{1-42}$  for 6 hrs showed remarkable differences when compared to treatments with the  $A\beta_{1-42}$  alone (Fig. 4.6). Most of these cells has usual morphological characteristics like an easily differentiated nucleus, flattened cells and continuity of the monolayer. The oligomeric species of this  $A\beta_{1-42}$  is much more toxic than the fibrillar structure of the same protein. The oligomeric structure is formed in time period of around 6-8 hrs and it is supposed to reach the fibrillar state in around 48 hrs (Barr et al., 2015). For any molecule to be used for therapy against AD, it is very important that the molecule itself should not be cytotoxic so it should have the capacity to reduce the neurotoxicity created by the aggregation of  $A\beta_{1-42}$  which is the underlying cause for AD (Jang et al., 2018).

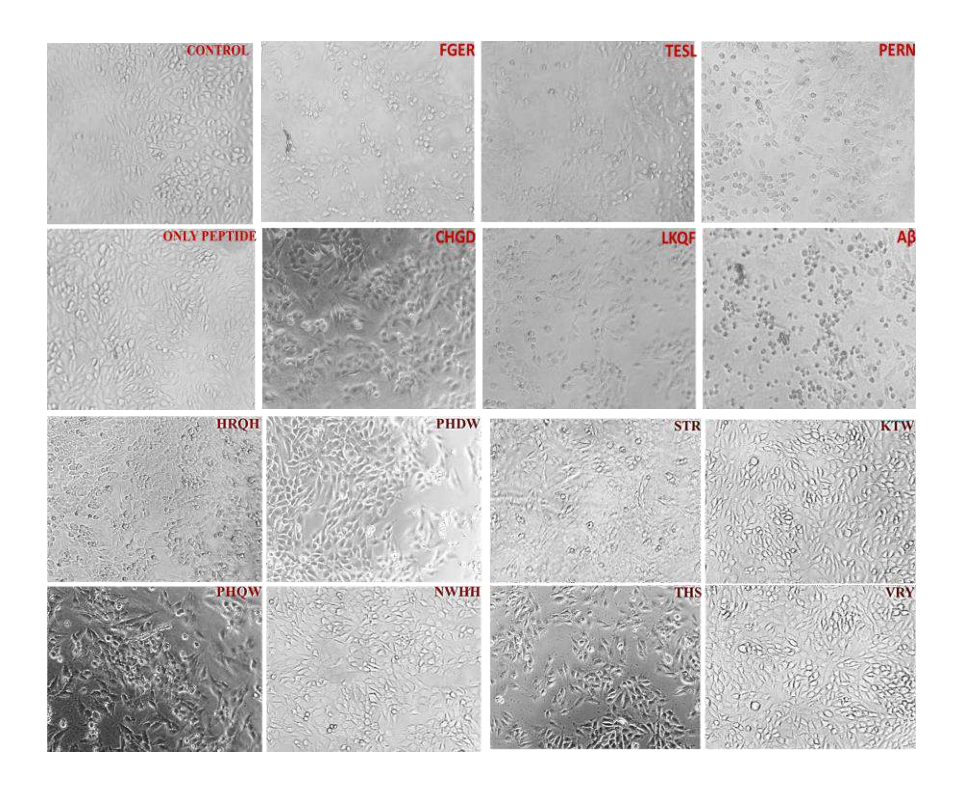
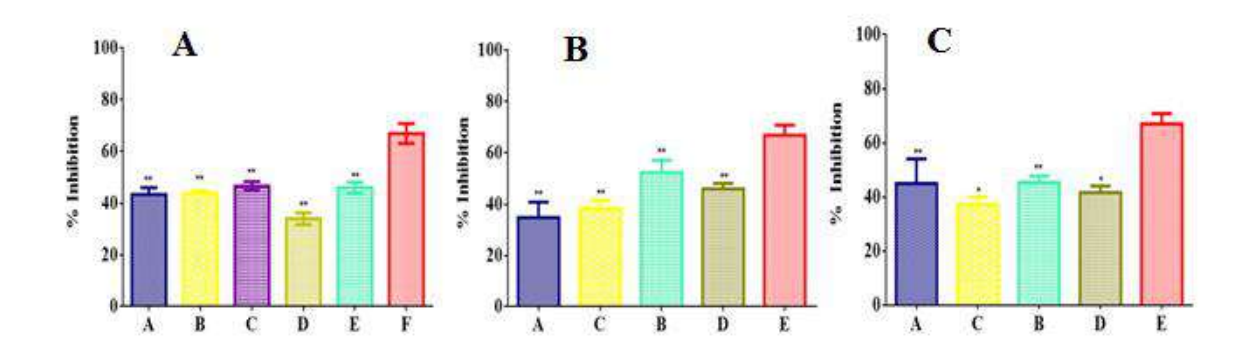


Fig. 4.6. Cell morphology observed from inverted microscope.

## 4.2.8. Cell viability assay

Here, I have used SK-N-SH cells as *in vitro* cellular model since this model is convenient for the primary screening of peptides specifically in AD. In this study I explored the effects of the BSBp on the cell viability of SK-N-SH cells *in vitro*. The cells were exposed to various concentrations of the peptides for 48 hrs and cell viability was determined using MTT assay. As depicted in Fig. 4.7, the cell viability of SK-N-SH cells exposed to the peptides was significantly increased compared with the control (cells treated  $A\beta_{1-42}$ ) (Table 4.6). It is difficult to interpret which peptide has better neuroprotective activity as they demonstrated near about same cell viability. These results are of interest, as it indicates that these peptides could protect the SK-N-SH cells against  $A\beta_{1-42}$ -induced cytotoxicity ( $A\beta_{1-42}$ 

fibrillation) and these results are in accordance of earlier studies, which demonstrated the protective effects of HSA peptides (Jha et al., 2018).



**Fig. 4.7.** Treatment with the peptide increases the cell viability of SK-N-SH cells *in vitro*. Data was represented as the mean  $\pm$  S.D(n = 3). In the Fig. (A) A- FGER, B-TESL, C- PERN, D-LQKF, E-CHGD, F  $-A\beta_{1-42}$ . (B) A-HRQH, B- PHDW, C-PHQW, D-NWHH, E- $A\beta_{1-42}$ . (C) A-STR, B-THS, C-KTW, D-VRY, E- $A\beta_{1-42}$ .

**Table 4.6.** This table shows the  $IC_{50}$  values of the peptides in SK-N-SH cells.

Only Amyloid	74.66 +/- 9.44
FGER	115.26 +/- 14.81
TESL	114.02 +/- 16.91
PERN	107.22 +/- 8.98
CHGD	108.61 +/- 11.23
LQKF	147 +/- 12.22
HRQH	143.57 +/- 12.56
PHQW	130.33 +/- 8.98
PHDW	95.98 +/- 11.32

Chapter 4 | Elucidating the inhibitory potential of HSA as well as synthesized peptides

NWHH	108.61+/- 14.23
STR	111.21 +/-15.68
KTW	134.50 +/- 17.85
THS	110.03 +/- 87.54
VRY	120.19 +/- 19.32

### 4.2.9. Lactate dehydrogenase assay

Cell membrane rupturing or cell expiry can be analyzed by leakage of LDH enzyme into the cell's growth medium. LDH is a soluble enzyme present in virtually present in all the living cells but is discharged into extracellular space by the rupturing of the cell membrane. LDH assay is based upon the principle of NADH generation by damaged cells. More the damaged cell, more is the pyruvate released with conversion of NAD to NADH (Konjević et al., 1997). In this study, I further investigated LDH release in the evaluation of the cellular toxicity in SK-N-SH cells. The LDH assay confirmed that the cytotoxicity was significantly decreased when the SK-N-SH cells were treated with the peptides (Fig. 4.8). The peptide LQKF and HRQH showed least cytotoxicity among all peptides. In the present study, I observed that the pattern of the cell leakage is decreased by the addition of these peptides in the cells suggesting that these compounds are exhibiting some neuroprotection. So, it can be inferred that these BSBp significantly prevent  $A\beta_{1-42}$  induced membrane damage. This indicates that these peptide molecules are protecting cells from  $A\beta_{1-42}$  fibrillation and have pharmaceutical potential which need to be further explored.

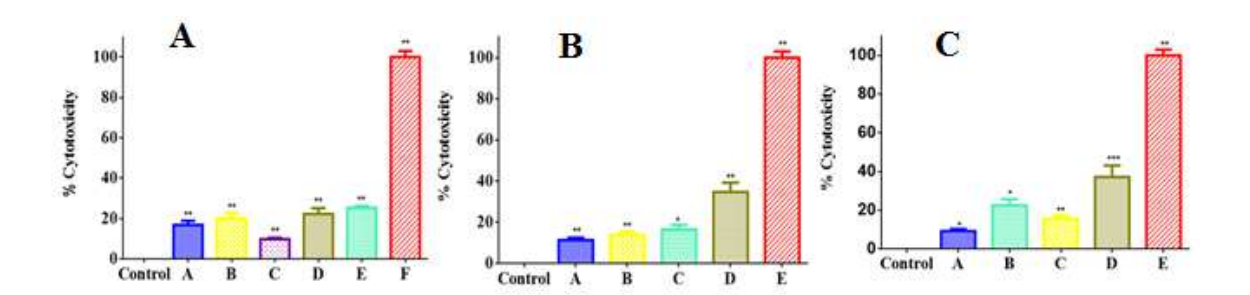


**Fig. 4.8.** LDH leakage values can be seen in the above graph (A) A- FGER, B- TESL, C-PERN, D-LQKF, E-CHGD,  $F-A\beta_{1-42}$ . (B) A-HRQH, B- PHDW, C-PHQW, D-NWHH, E- $A\beta_{1-42}$ . (C) A-STR, B-THS, C-KTW, D-VRY, E- $A\beta_{1-42}$ .

## 4.2.10. Reactive oxygen species (ROS)

Oxidative stress is the crucial underlying mechanism for  $A\beta_{1-42}$  mediated neurotoxicity in AD. ROS is generation of oxidative species in the cells which are a product of cells experiencing biochemical toxic assault or stressful milieu (Kumar et al., 2016; Oparka et al., 2016). Intracellular ROS production was measured in peptide-treated and control cells using DCFH-DA. The result showed high intensity for the  $A\beta_{1-42}$ , while the intensity was significantly low for the peptide treated sample. Peptide CHGD and PERN showed almost same intensity for ROS compared to  $A\beta_{1-42}$ . These results show that the oxidative stress is generated by A $\beta_{1-42}$  fibrillation have reduced in presence of BSBp as shown in Fig. 4.9. The cell culture assays further increased in cell viability and MMP while decrease in ROS generation and cytotoxicity observed. In the pathogenesis of AD, it is known that ROS production is increased (Kadowaki et al., 2004). Therefore, for any molecule to potentially treat the symptoms of AD should also be capable of decreasing the ROS generation as it is known that ROS is involved in involved in regulation of mitochondrial cascade and activation of apoptotic proteins (Kumar et al., 2016). The increased concentration of LDH leakage and ROS production in the presence of  $A\beta_{1-42}$  show that there is neurotoxicity, some extent is being countered by these BSBp (Qu et al., 2011; Barale et al., 2019).

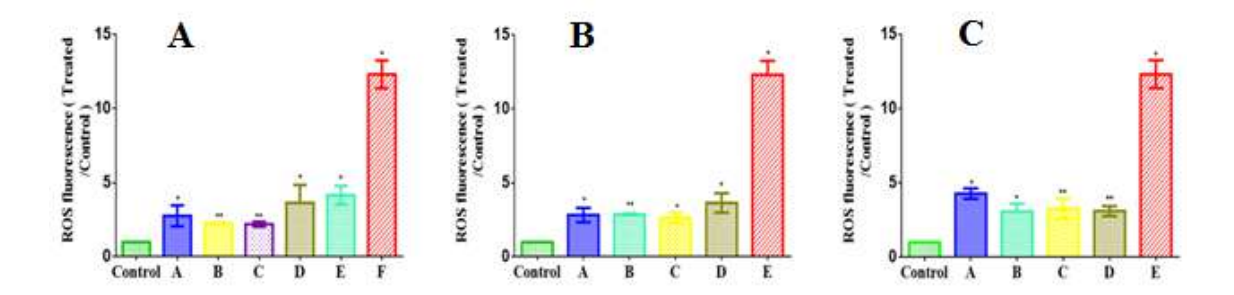


**Fig. 4.9.** Intracellular ROS generation in SK-N-SH cells after treatment with bsbpderivatives. After treatment for 12 h, cells were stained with 20 μM DCFH-DA for 30 min at 37 °C in the dark. Data are expressed as mean  $\pm$  SD (n =3). (A) A- FGER, B- TESL, C- PERN, D-LQKF, E-CHGD, F -A $\beta_{1-42}$ . (B) A-HRQH, B- PHDW, C-PHQW, D-NWHH, E-A $\beta_{1-42}$ . (C) A-STR, B-THS, C-KTW, D-VRY, E-A $\beta_{1-42}$ .

#### 4.2.11. Cellular MMP assay

Since, high ROS production either intrinsically or by any external substance can lead to disturbance in mitochondrial membrane which in turn can lead to lack of membrane depolarization or mitochondrial trans membrane potential (Tajeddine, 2016). Rho123 dye used to measure the MMP of the cells. Rho123 fluorescence is directly proportional to the number of live cells and its mitochondrial content (Li et al., 2017). The MMP assay gives the significant results that in  $A\beta_{1.42}$  treated sample the fluorescence was quite low indicating few mitochondrial presences while in drug treated samples the fluorescence was enhanced as shown in Fig. 4.10. Peptide TESL showed highest intensity for MMP followed by CHGD, indicates that these peptides control the ROS production.

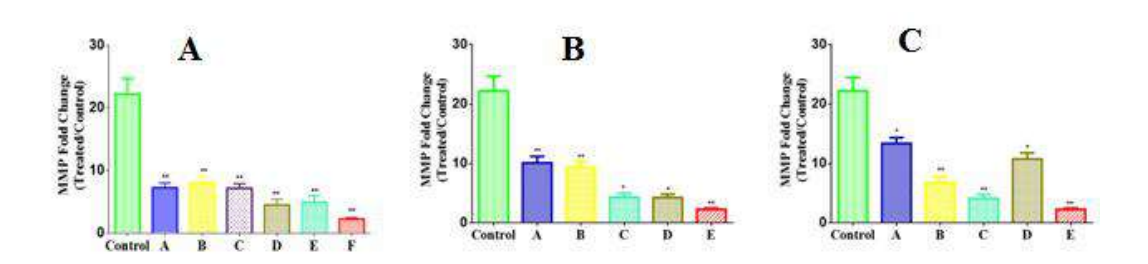


**Fig. 4.10.** MMP assay of (A) A- FGER, B- TESL, C- PERN, D-LQKF, E-CHGD, F  $-A\beta_{1-42}$ . (B) A-HRQH, B- PHDW, C-PHQW, D-NWHH, E- $A\beta_{1-42}$ . (C) A-STR, B-THS, C-KTW, D-VRY, E- $A\beta_{1-42}$ .

# 4.2.12. Cellular mitochondrial membrane potential by laser scanning confocal microscopy

Since, high ROS production can be either responsible for disturbance in the mitochondrial membrane which in turn can lead to lack of membrane depolarization or lack of mitochondrial trans membrane potential.

The neuroblastoma cell localization was performed using the dye Rho123 (Tajeddine, 2016). The untreated sample had high cell confluency while the very few cells were localized in  $A\beta_{1-42}$  treated sample. The cellular confluency increased in presence of peptides under study but was low compared to untreated sample. The cellular confluency showed significant resemblance to microscopic images taken after 48 hrs. Though it seems most of cells were away when compared to light microscope images as shown in Fig. 4.11. These results show that the drugs are quite effective increasing cell viability and reducing  $A\beta_{1-42}$  fibrillation.

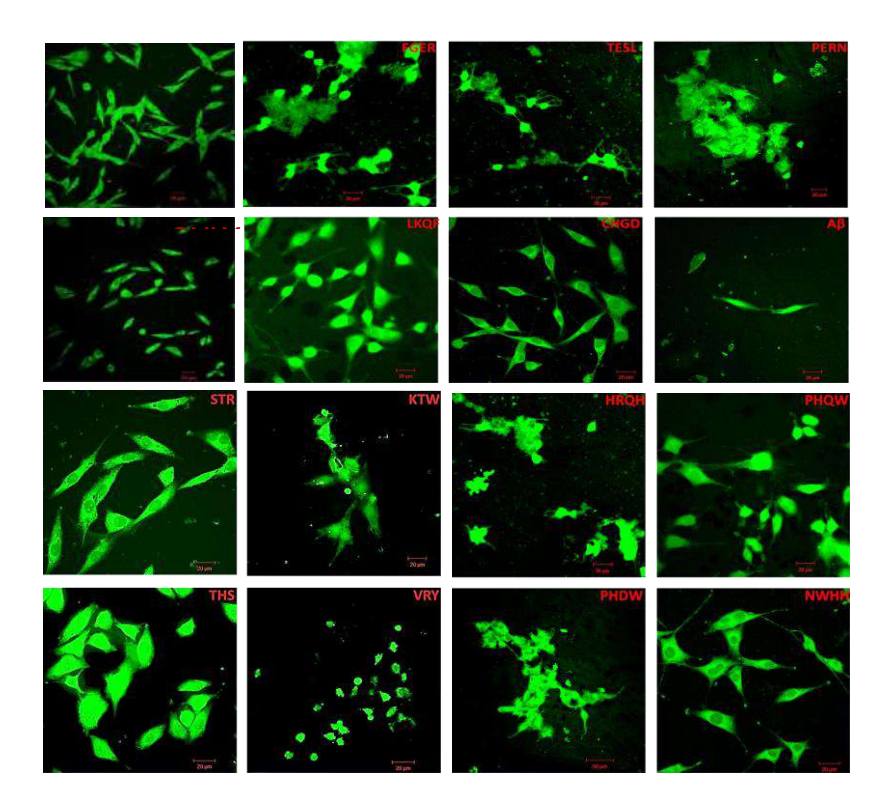


**Fig. 4.11.** Confocal images of Only cells, and cells with HAS peptides, Tetrapeptides and tripeptides: FGER, TESL, PERN, LQKF, CHGD  $A\beta_{1-42}$ , STR, KTW, HRQH, PHQW, THS, VRY, PHDW and NWHH after treatment with Rho13.

#### 4.3. Conclusion

 $A\beta_{1-42}$  protein aggregates are formed through oligomerization, protofibril formation and finally amyloid fibrils.  $A\beta_{1-42}$  fibril accumulation is responsible for cytotoxicity in AD. The interaction studies between these BSBp to hydrophobic core of  $A\beta_{1-42}$  prevents development of the  $A\beta_{1-42}$  fibrillation, and cytotoxicity thus progression of AD. *In-silico* interaction studies showed the stability of peptides with  $A\beta_{1-42}$ . The cell culture assays further increased in cell viability and MMP, while decrease in ROS generation and cytotoxicity observed. It is difficult to conclude that which peptides among these are more effective as  $A\beta_{1-42}$  fibrillation is inhibited by various experiments by different assays.

These studies show that this tri, tetra as well as HSA derived peptides should be used for further study as an effective molecule for treating AD. Based on the obtained results it can be inferred that the HSA derived peptides as well as the tri-peptides are more effective in ameliorating the aggregation. These peptides are very effective for combating the  $A\beta_{1-42}$  neurotoxicity but it is still difficult to say that which among these 13 peptides are better to treat the symptoms of AD as one crucial point is that these peptides should be able to cross the BBB. Thus, further studies such as BBB crossing capability of these peptides and animal model studies can be performed.

Chapter – 5 Summary

# Summary

HSA is a plasma protein of utmost importance in the blood. It is the carrier protein known to transport all the exogenous as well as endogenous ligands. In this study, the binding of four derivatives of Withania somnifera (Withanolide A, Withanolide B, Withanoside IV and Withanoside V) with the carrier protein HSA was carried out. Ashwagandha plant is being used for the treatment of various chronic diseases particularly central nervous system diseases in Ayurvedic and Chinese medicine. It has multiple remedial properties and is also being used as a geriatric tonic for memory loss or stress. Hence, understanding the pharmacodynamics and pharmacokinetics of any molecule by binding to the cargo protein HSA is very important. In the first part of the chapter 3, I have explained about interaction of these phytocompounds with HSA by using various biophysical techniques, molecular docking and dynamics were carried out to see the stability for 10ns. Both the data obtained by biophysical as well as the *in silico* data was in congruence and due to the similar structure of these four steroidal derivatives of Ashwagandha, I observed that all these molecules were displacing phenylbutazone and were binding in the Site I i.e. domain II of HSA. Based on this study one can think of designing new inspired therapeutic compounds to curing the life-threatening diseases especially neurological diseases.

Various phytocompounds of the plant in the Indian Ayurvedic as well as Chinese system of medicine is already being used for various illnesses. Particularly they are known to slow down the process of aging and are known to be imparting various neuroprotective properties. Hence, in our study we wanted to analyse the effectiveness of these molecules to treat dementia by ameliorating the fibrils formed by  $A\beta_{1-42}$ . For this analysis we have employed various techniques to understand the interaction between these four phytocompounds independently with the protein. In Chapter 3 we have illustrated the

ability of these derivatives to inhibit fibrillization, as indicated by the ThT assay. When these phytocompounds were incubated with  $A\beta_{1-42}$  we saw the decrease in the fluorescence for up to 72 hrs. Moreover, the cell culture assays also indicate the ability of the derivatives to reduce the cytotoxic effects of  $A\beta_{1-42}$  fibrillation. Neuronal cell viability increased visibly and subsequently diminished the toxicity because fibrillar  $A\beta_{1-42}$  aggregation. Further molecular docking results indicate that the derivatives were interacting with the hydrophobic core (17-21) residues region of  $A\beta_{1-42}$  thus discouraging another peptide of  $A\beta_{1-42}$  to come and bind and hence inhibiting the process of fibrillization.

Furthermore, 100 ns simulations suggest that the withanolide B and withanoside V complexes were stable in the hydrophobic core of  $A\beta_{1-42}$ . Hence, our experimental results illustrated strong binding between these derivatives with the plasma protein HSA as well as the protein  $A\beta_{1-42}$ . Also, neuronal cell viability was increased and the toxicity of the fibrillar  $A\beta_{1-42}$  was diminished in the presence of these phytocompounds. This study has given an important message that these phytochemicals, withanolide A, withanolide B, withanoside IV and withanoside V acting against the amyloid  $\beta$ -peptide fibril thus it is our hope that these results would provide an insight role of these phytochemicals in the drug design against Alzheimer's disease.

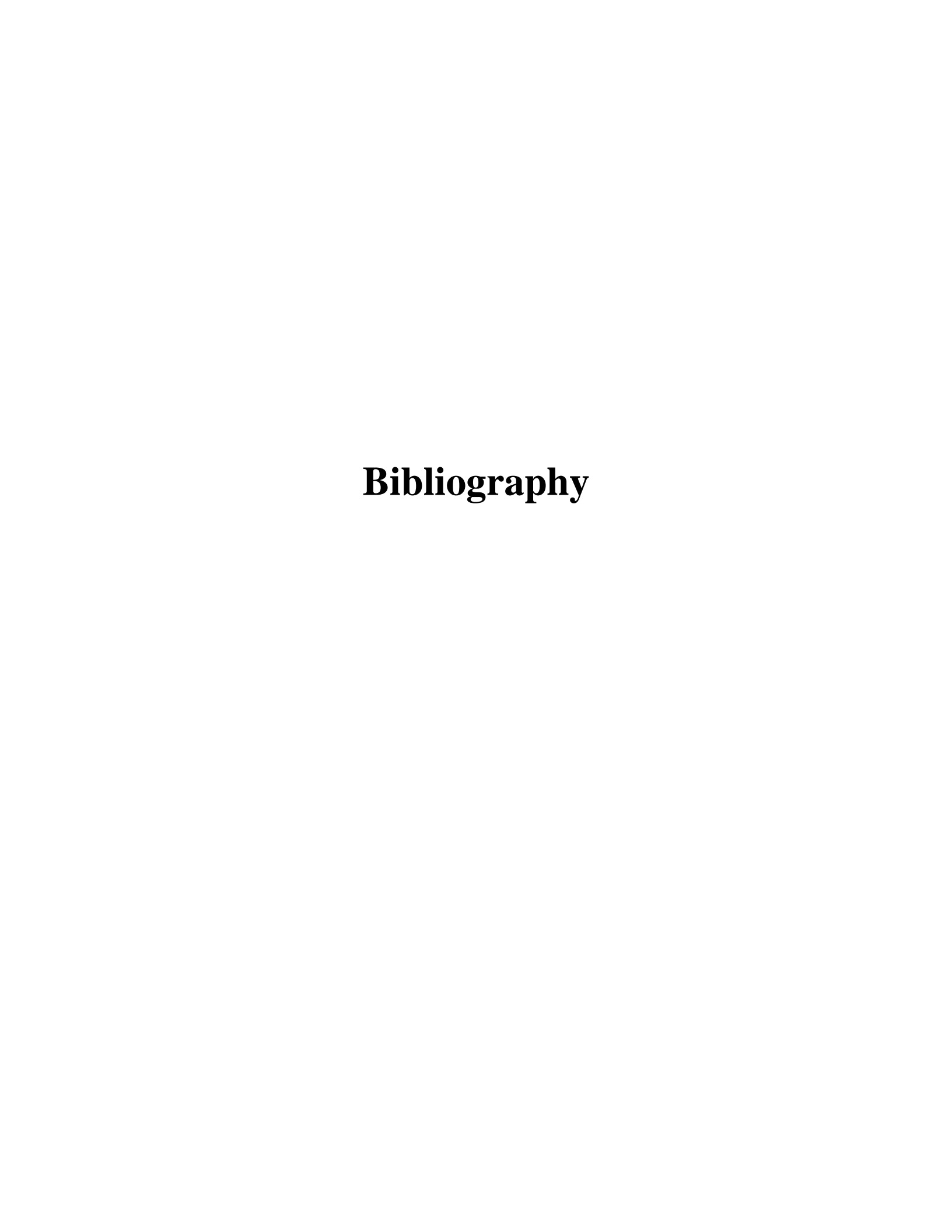
As HSA has the capacity of crossing the BBB and it is also known that the individual domains of HSA can inhibit the  $A\beta_{1-42}$  fibrillization with the binding in micromolar range. HSA, the plasma protein is known for clearing the  $A\beta_{1-42}$  aggregates which are known to cause neuronal dysfunction and are the hallmark of AD. Through this study I have tried to unravel the fragments of HSA responsible for interacting with  $A\beta_{1-42}$ . The interaction studies between HSA derived peptides to hydrophobic core of  $A\beta_{1-42}$  prevents development of the  $A\beta_{1-42}$  fibrillation, cytotoxicity thus progression of AD. These

studies show that HSA peptides are the potential candidate for becoming therapeutic drug molecule for treatment of neurodegenerative diseases. As in the field of Alzheimer's there is an urgent need for a breakthrough drug as most of the molecules are failing in the clinical trials.

Further, peptides discovered from chemical libraries are being used as drugs for various diseases as they can inhibit the PPI (protein-protein interaction) which are a foundation of essentially all cellular processes. Use of peptides is further bolstered by their easy and cost-effective synthesis schemes in labs. More than 60 synthetic peptides are being used for treatment for various chronic diseases. As there is a need of breakthrough drug for AD we wanted to see if the HSA derived peptides and other synthesized peptides have the capacity of acting as BSBp and help in diminishing fibrillization of  $A\beta_{1-42}$  which is the root cause for Alzheimer's.

In Chapter 4 we have analysed the BSBp of four as well as three amino acids using D amino acids and also HSA derived fragments and studied the interaction between those synthesized peptides to hydrophobic core of  $A\beta_{1-42}$  preventing formation of the  $A\beta_{1-42}$  fibrillation.  $A\beta_{1-42}$  protein aggregates are formed through oligomerization, protofibril formation and finally amyloid fibrils.  $A\beta_{1-42}$  fibril accumulation is responsible for cytotoxicity in AD. The interaction studies between derived peptides to hydrophobic core of  $A\beta_{1-42}$  prevents development of the  $A\beta_{1-42}$  fibrillation, cytotoxicity thus progression of AD. Molecular Docking of these designed BSBp showed that these molecules are binding to the hydrophobic core of  $A\beta_{1-42}$  and Molecular simulation trajectory was stable for 200ns. The interaction studies showed the stability of BSBp with  $A\beta_{1-42}$ . The cell culture assays further demonstrate the increase in cell viability and MMP while decrease in ROS generation and cytotoxicity was observed.

Hence, it can be inferred that the novel BSBp are showing neuroprotection against toxicity because of  $A\beta_{1-42}$  in SK-N-SH cells. Our inference was that these peptides are showing amelioration of  $A\beta_{1-42}$  fibrils in *in vitro*, *in silico* as well as in cell culture experiments. So, they should be further exploited for study as anti-dementia drug molecules. In view of the evidence presented, it is imperative to assign a greater role of HSA peptides and BSBp are reducing the  $A\beta_{1-42}$  fibrillation. It is our hope that the results presented here may provide new grounds for further investigations of the pharmaceutical potential of these peptides and will be useful for monitoring its biological functions *in vivo*.



# **Bibliography**

Agrawal, P., Singh, H., Srivastava, H., Singh, S., Kishore, G., & Raghava, G. (2019). Benchmarking of different molecular docking methods for protein-peptide docking. *BMC Bioinformatics*, 19.

Agudelo, D., Bourassa, P., Bruneau, J., Bérubé, G., Asselin, É., & Tajmir-Riahi, H. (2012). Probing the Binding Sites of Antibiotic Drugs Doxorubicin and N-(trifluoroacetyl) Doxorubicin with Human and Bovine Serum Albumins. *PLoS One*, 7(8), e43814.

Ahrens, V., Bellmann-Sickert, K., & Beck-Sickinger, A. (2012). Peptides and peptide conjugates: therapeutics on the upward path. *Future Medicinal Chemistry*, 4(12), 1567-1586.

Ajay, Bemis, G., & Murcko, M. (1999). Designing Libraries with CNS Activity. *Journal of Medicinal Chemistry*, 42(24), 4942-4951.

Algamal, M., Milojevic, J., Jafari, N., Zhang, W., & Melacini, G. (2013). Mapping the Interactions between the Alzheimer's Aβ-Peptide and Human Serum Albumin beyond Domain Resolution. *Biophysical Journal*, *105*(7), 1700-1709.

Amdursky, N., Kundu, P., Ahrens, J., Huppert, D., & Klajn, R. (2015). Noncovalent Interactions with Proteins Modify the Physicochemical Properties of a Molecular Switch. *Chempluschem*, 81(1), 44-48.

Anderson, L., & Anderson, N. (1977). High resolution two-dimensional electrophoresis of Human Plasma Proteins. *Proceedings of the National Academy of Sciences*, 74(12), 5421-5425.

Austen, B., Paleologou, K., Ali, S., Qureshi, M., Allsop, D., & El-Agnaf, O. (2008). Designing Peptide Inhibitors for Oligomerization and Toxicity of Alzheimer's β-Amyloid Peptide. *Biochemistry*, 47(7), 1984-1992.

Autiero, I., Langella, E., & Saviano, M. (2013). Insights into the mechanism of interaction between trehalose-conjugated beta-sheet breaker peptides and  $A\beta(1-42)$  fibrils by molecular dynamics simulations. *Molecular Biosystems*, 9(11), 2835.

Baig, M., Ahmad, K., Saeed, M., Alharbi, A., Barreto, G., Ashraf, G., & Choi, I. (2018). Peptide based therapeutics and their use for the treatment of neurodegenerative and other diseases. *Biomedicine & Pharmacotherapy*, *103*, 574-581.

Baker, N., Sept, D., Joseph, S., Holst, M., & McCammon, J. (2001). Electrostatics of nanosystems: Application to microtubules and the ribosome. *Proceedings of the National Academy of Sciences*, 98(18), 10037-10041.

Barale, S., Parulekar, R., Fandilolu, P., Dhanavade, M., & Sonawane, K. (2019). Molecular Insights into Destabilization of Alzheimer's Aβ Protofibril by Arginine Containing Short Peptides: A Molecular Modeling Approach. *ACS Omega*, *4*(1), 892-903.

Barr, R., Verdile, G., Wijaya, L., Morici, M., Taddei, K., & Gupta, V. et al. (2015). Validation and Characterization of a Novel Peptide That Binds Monomeric and Aggregated β-Amyloid and Inhibits the Formation of Neurotoxic Oligomers. *Journal of Biological Chemistry*, 291(2), 547-559.

Basha, S., Mohan, P., Yeggoni, D., Babu, Z., Kumar, P., & Rao, A. et al. (2018). New Flavone-Cyanoacetamide Hybrids with a Combination of Cholinergic, Antioxidant, Modulation of β-Amyloid Aggregation, and Neuroprotection Properties as Innovative Multifunctional Therapeutic Candidates for Alzheimer's Disease and Unraveling Their Mechanism of Action with Acetylcholinesterase. *Molecular Pharmaceutics*, *15*(6), 2206-2223.

Behl, C. (1997). Amyloid  $\beta$ -protein toxicity and oxidative stress in Alzheimer's disease. *Cell and Tissue Research*, 290(3), 471-480.

Bertucci, C., & Domenici, E. (2002). Reversible and Covalent Binding of Drugs to Human Serum Albumin: Methodological Approaches and Physiological Relevance. *Current Medicinal Chemistry*, *9*(15), 1463-1481.

Bhat, M., Gul, M., Maurya, R., Khan, N., Qureshi, I., & Ghazi, I. (2018). Growth Inhibition and Apoptosis Inducing Effects of Artemisia absinthium L. Fractions on Chronic Myeloid Leukemia (K562) Cells. *Journal of Biologically Active Products from Nature*, 8(2), 70-89.

Bhattacharya, A., Grüne, T., & Curry, S. (2000). Crystallographic analysis reveals common modes of binding of medium and long-chain fatty acids to human serum albumin. *Journal of Molecular Biology*, 303(5), 721-732.

Biere, A., Ostaszewski, B., Stimson, E., Hyman, B., Maggio, J., & Selkoe, D. (1996). Amyloid β-Peptide Is Transported on Lipoproteins and Albumin in Human Plasma. *Journal of Biological Chemistry*, 271(51), 32916-32922.

Boada, M., López, O., Núñez, L., Szczepiorkowski, Z., Torres, M., Grifols, C., & Páez, A. (2019). Plasma exchange for Alzheimer's disease Management by Albumin Replacement (AMBAR) trial: Study design and progress. *Alzheimer's & Dementia: Translational Research & Clinical Interventions*, 5(1), 61-69.

Boada, M., Ramos-Fernández, E., Guivernau, B., Muñoz, F., Costa, M., & Ortiz, A. et al. (2016). Treatment of Alzheimer disease using combination therapy with plasma exchange and haemapheresis with albumin and intravenous immunoglobulin: Rationale and treatment approach of the AMBAR (Alzheimer Management by Albumin Replacement) study. *Neurología* (*English Edition*), 31(7), 473-481.

Bradshaw, R., Patel, B., Tate, E., Leatherbarrow, R., & Gould, I. (2010). Comparing experimental and computational alanine scanning techniques for probing a prototypical protein–protein interaction. *Protein Engineering, Design and Selection*, 24(1-2), 197-207.

Bruce, N., Chen, D., Dastidar, S., Marks, G., Schein, C., & Bryce, R. (2010). Molecular dynamics simulations of A $\beta$  fibril interactions with  $\beta$ -sheet breaker peptides. *Peptides*, 31(11), 2100-2108.

Bruzzoni-Giovanelli, H., Alezra, V., Wolff, N., Dong, C., Tuffery, P., & Rebollo, A. (2018). Interfering peptides targeting protein–protein interactions: the next generation of drugs? *Drug Discovery Today*, 23(2), 272-285.

Cao, D., Wang, J., Zhou, R., Li, Y., Yu, H., & Hou, T. (2012). ADMET Evaluation in Drug Discovery. 11. PharmacoKinetics Knowledge Base (PKKB): A Comprehensive Database of Pharmacokinetic and Toxic Properties for Drugs. *Journal of Chemical Information and Modeling*, 52(5), 1132-1137.

Carter, D., He, X., Munson, S., Twigg, P., Gernert, K., Broom, M., & Miller, T. (1989). Three-dimensional structure of human serum albumin. *Science*, *244*(4909), 1195-1198.

Cavalli, A., Poluzzi, E., De Ponti, F., & Recanatini, M. (2002). Toward a Pharmacophore for Drugs Inducing the Long QT Syndrome: Insights from a CoMFA Study of HERG K+Channel Blockers. *Journal of Medicinal Chemistry*, *45*(18), 3844-3853.

Chacón, M., Barría, M., Soto, C., & Inestrosa, N. (2004). β-sheet breaker peptide prevents Aβ-induced spatial memory impairments with partial reduction of amyloid deposits. *Molecular Psychiatry*, *9*(10), 953-961.

Chanphai, P., Froehlich, E., Mandeville, J., & Tajmir-Riahi, H. (2017). Protein conjugation with PAMAM nanoparticles: Microscopic and thermodynamic analysis. *Colloids and Surfaces B: Biointerfaces*, *150*, 168-174.

Chen, X., Zhong, Z., Xu, Z., Chen, L., & Wang, Y. (2010). 2',7'-Dichlorodihydrofluorescein as a fluorescent probe for reactive oxygen species measurement: Forty years of application and controversy. *Free Radical Research*, 44(6), 587-604.

Cheng, F., Li, W., Zhou, Y., Shen, J., Wu, Z., & Liu, G. et al. (2012). admetSAR: A Comprehensive Source and Free Tool for Assessment of Chemical ADMET Properties. *Journal of Chemical Information and Modeling*, 52(11), 3099-3105.

Choi, T., Lee, H., Han, J., Lim, M., & Kim, H. (2017). Molecular Insights into Human Serum Albumin as a Receptor of Amyloid-β in the Extracellular Region. *Journal of The American Chemical Society*, *139*(43), 15437-15445.

Chuang, V., & Otagiri, M. (2006). Stereoselective binding of human serum albumin. *Chirality*, 18(3), 159-166.

Citron, M. (2010). Alzheimer's disease: strategies for disease modification. *Nature Reviews Drug Discovery*, *9*(5), 387-398.

Cohen, J., Duke, R., Fadok, V., & Sellins, K. (1992). Apoptosis and Programmed Cell Death in Immunity. *Annual Review of Immunology*, *10*(1), 267-293.

Colmenarejo, G., Alvarez-Pedraglio, A., & Lavandera, J. (2001). Cheminformatic Models to Predict Binding Affinities to Human Serum Albumin. *Journal of Medicinal Chemistry*, 44(25), 4370-4378.

Curry, S., Brick, P., & Franks, N. (1999). Fatty acid binding to human serum albumin: new insights from crystallographic studies. *Biochimica et Biophysica Acta (BBA) - Molecular and Cell Biology of Lipids*, *1441*(2-3), 131-140.

Dar, N., Hamid, A., & Ahmad, M. (2015). Pharmacologic overview of Withania somnifera, the Indian Ginseng. *Cellular and Molecular Life Sciences*, 72(23), 4445-4460.

Dar, N., & MuzamilAhmad. (2020). Neurodegenerative diseases and Withania somnifera (L.): An update. *Journal of Ethnopharmacology*, 256, 112769.

Dar, N., Satti, N., Dutt, P., Hamid, A., & Ahmad, M. (2017). Attenuation of Glutamate-Induced Excitotoxicity by Withanolide-A in Neuron-Like Cells: Role for PI3K/Akt/MAPK Signaling Pathway. *Molecular Neurobiology*, *55*(4), 2725-2739.

Dakti, Z., Papp, R., Zadori, D., Soos, K., Fulop, L., & Juhasz, A. et al. (2004). In vitro model of neurotoxicity of A? 1?42 and neuroprotection by a pentapeptide: irreversible events during the first hour. *Neurobiology of Disease*, 17(3), 507-515.

De Ponti, F., Poluzzi, E., & Montanaro, N. (2001). Organising evidence on QT prolongation and occurrence of Torsades de Pointes with non-antiarrhythmic drugs: a call for consensus. *European Journal of Clinical Pharmacology*, *57*(3), 185-209.

DeTure, M., & Dickson, D. (2019). The neuropathological diagnosis of Alzheimer's disease. *Molecular Neurodegeneration*, 14:1-32.

De Vries, S., van Dijk, M., & Bonvin, A. (2010). The HADDOCK web server for data-driven biomolecular docking. *Nature Protocols*, *5*(5), 883-897.

Dhar, N., Razdan, S., Rana, S., Bhat, W., Vishwakarma, R., & Lattoo, S. (2015). A Decade of Molecular Understanding of Withanolide Biosynthesis and In vitro Studies in Withania somnifera (L.) Dunal: Prospects and Perspectives for Pathway Engineering. *Frontiers in Plant Science*, 6.

Di Natale, G., Zimbone, S., Bellia, F., Tomasello, M., Giuffrida, M., Pappalardo, G., & Rizzarelli, E. (2018). Potential therapeutics of Alzheimer's diseases: New insights into the neuroprotective role of trehalose-conjugated beta sheet breaker peptides. *Peptide Science*, 110(5), e24083.

Di Sotto, A., Vitalone, A., & Di Giacomo, S. (2020). Plant-Derived Nutraceuticals and Immune System Modulation: An Evidence-Based Overview. *Vaccines*, 8(3), 468.

Efimov, A. (1997). Structural trees for protein superfamilies. *Proteins: Structure, Function, And Genetics*, 28(2), 241-260.

Eskici, G., & Gur, M. (2013). Computational Design of New Peptide Inhibitors for Amyloid Beta (Aβ) Aggregation in Alzheimer's Disease: Application of a Novel Methodology. *PLOS One*, 8(6), e66178.

Fanali, G., di Masi, A., Trezza, V., Marino, M., Fasano, M., & Ascenzi, P. (2012). Human serum albumin: From bench to bedside. *Molecular Aspects of Medicine*, *33*(3), 209-290.

Fasano, M., Curry, S., Terreno, E., Galliano, M., Fanali, G., & Narciso, P. et al. (2005). The extraordinary ligand binding properties of human serum albumin. *IUBMB Life* (*International Union of Biochemistry and Molecular Biology: Life*), 57(12), 787-796.

Fosgerau, K., & Hoffmann, T. (2015). Peptide therapeutics: current status and future directions. *Drug Discovery Today*, 20(1), 122-128.

Friesner, R., Banks, J., Murphy, R., Halgren, T., Klicic, J., & Mainz, D. et al. (2004). Glide: A New Approach for Rapid, Accurate Docking and Scoring. 1. Method and Assessment of Docking Accuracy. *Journal of Medicinal Chemistry*, 47(7), 1739-1749.

Garg, A., Mark Manidhar, D., Gokara, M., Malleda, C., Suresh Reddy, C., & Subramanyam, R. (2013). Elucidation of the Binding Mechanism of Coumarin Derivatives with Human Serum Albumin. *PLOS One*, 8(5), e63805.

Genheden, S., & Ryde, U. (2015). The MM/PBSA and MM/GBSA methods to estimate ligand-binding affinities. *Expert Opinion on Drug Discovery*, *10*(5), 449-461.

Ghuman, J., Zunszain, P., Petitpas, I., Bhattacharya, A., Otagiri, M., & Curry, S. (2005). Structural Basis of the Drug-binding Specificity of Human Serum Albumin. *Journal of Molecular Biology*, *353*(1), 38-52.

Gibbs, P., & Dugaiczyk, A. (1987). Origin of structural domains of the serum-albumin gene family and a predicted structure of the gene for vitamin D-binding protein. *Molecular Biology and Evolution*, 4(4), 364-379.

Giuffrida, M., Caraci, F., Pignataro, B., Cataldo, S., De Bona, P., & Bruno, V. et al. (2009). -Amyloid Monomers Are Neuroprotective. *Journal of Neuroscience*, 29(34), 10582-10587.

Glotter, E. (1991). Withanolides and related ergostane-type steroids. *Natural Product Reports*, 8(4), 415.

Gokara, M., Kimavath, G., Podile, A., & Subramanyam, R. (2013). Differential interactions and structural stability of chitosan oligomers with human serum albumin and  $\alpha$ -1-glycoprotein. *Journal of Biomolecular Structure and Dynamics*, 33(1), 196-210.

Gokara, M., Malavath, T., Kalangi, S., Reddana, P., & Subramanyam, R. (2013). Unraveling the binding mechanism of asiatic acid with human serum albumin and its biological implications. *Journal of Biomolecular Structure and Dynamics*, 32(8), 1290-1302.

Gokara, M., Narayana, V., Sadarangani, V., Chowdhury, S., Varkala, S., Ramachary, D., & Subramanyam, R. (2016). Unravelling the binding mechanism and protein stability of human serum albumin while interacting with nefopam analogues: a biophysical and insilico approach. *Journal of Biomolecular Structure and Dynamics*, *35*(10), 2280-2292.

Gokara, M., Sudhamalla, B., Amooru, D., & Subramanyam, R. (2010). Molecular Interaction Studies of Trimethoxy Flavone with Human Serum Albumin. *PLoS One*, *5*(1), e8834.

Green, P., Gridley, K., & Simpkins, J. (1996). Estradiol protects against β-amyloid (25–35)-induced toxicity in SK-N-SH human neuroblastoma cells. *Neuroscience Letters*, *218*(3), 165-168.

Guex, N., & Peitsch, M. (1997). SWISS-MODEL and the Swiss-Pdb Viewer: An environment for comparative protein modeling. *Electrophoresis*, *18*(15), 2714-2723.

Halim, M., Rosli, I., Jaafar, S., Ooi, H., Leong, P., & Shamsuddin, S. et al. (2020). Withania somnifera showed neuroprotective effect and increase longevity in Drosophila Alzheimer's disease model.

Hardy, J., & Higgins, G. (1992). Alzheimer's disease: the amyloid cascade hypothesis. *Science*, 256(5054), 184-185.

He, X., & Carter, D. (1992). Atomic structure and chemistry of human serum albumin. *Nature*, *358*(6383), 209-215.

Hein, K., Kragh-Hansen, U., Morth, J., Jeppesen, M., Otzen, D., Møller, J., & Nissen, P. (2010). Crystallographic analysis reveals a unique lidocaine binding site on human serum albumin. *Journal of Structural Biology*, 171(3), 353-360.

Hosainzadeh, A., Gharanfoli, M., Saberi, M., & Chamani, J. (2012). Probing the Interaction of Human Serum Albumin with Bilirubin in the Presence of Aspirin by Multi-Spectroscopic, Molecular Modeling and Zeta Potential Techniques: Insight on Binary and Ternary Systems. *Journal of Biomolecular Structure and Dynamics*, 29(5), 1013-1050.

Howell, B., McCune, S., & Schaffer, R. (1979). Lactate-to-pyruvate or pyruvate-to-lactate assay for lactate dehydrogenase: a re-examination. *Clinical Chemistry*, 25(2), 269-272.

Huang, J., Xie, J., Chen, K., Bu, L., Lee, S., & Cheng, Z. et al. (2010). HSA coated MnO nanoparticles with prominent MRI contrast for tumor imaging. *Chemical Communications*, 46(36), 6684.

Husain, A., Ahmad, A., Khan, S., Asif, M., Bhutani, R., & Al-Abbasi, F. (2016). Synthesis, molecular properties, toxicity and biological evaluation of some new substituted imidazolidine derivatives in search of potent anti-inflammatory agents. *Saudi Pharmaceutical Journal*, 24(1), 104-114.

Irvine, J., Takahashi, L., Lockhart, K., Cheong, J., Tolan, J., Selick, H., & Grove, J. (1999). MDCK (Madin-Darby Canine Kidney) Cells: A Tool for Membrane Permeability Screening. *Journal of Pharmaceutical Sciences*, 88(1), 28-33.

Jang, J., Rhim, H., & Kang, S. (2018). NABi, a novel β-sheet breaker, inhibits Aβ aggregation and neuronal toxicity: Therapeutic implications for Alzheimer's disease. *Biochimica et Biophysica Acta (BBA) - General Subjects*, 1862(1), 71-80.

Jayaram, B., Singh, T., Mukherjee, G., Mathur, A., Shekhar, S., & Shekhar, V. (2012). Sanjeevini: a freely accessible web-server for target directed lead molecule discovery. *BMC Bioinformatics*, *13*(S17).

Jha, A., Kumar, M., Gopi, H., & Paknikar, K. (2018). Inhibition of β-Amyloid Aggregation through a Designed β-Hairpin Peptide. *Langmuir*, *34*(4), 1591-1600.

Jorgensen, W., & Duffy, E. (2000). Prediction of drug solubility from Monte Carlo simulations. *Bioorganic & Medicinal Chemistry Letters*, *10*(11), 1155-1158.

Kadowaki, H., Nishitoh, H., Urano, F., Sadamitsu, C., Matsuzawa, A., & Takeda, K. et al. (2004). Amyloid β induces neuronal cell death through ROS-mediated ASK1 activation. *Cell Death & Differentiation*, *12*(1), 19-24.

Kallubai, M., Rachamallu, A., Yeggoni, D., & Subramanyam, R. (2015). Comparative binding mechanism of lupeol compounds with plasma proteins and its pharmacological importance. *Molecular Biosystems*, 11(4), 1172-1183.

Kallubai, M., Reddy, S., Dubey, S., Ramachary, D., & Subramanyam, R. (2018). Spectroscopic evaluation of synthesized  $5\beta$ -dihydrocortisol and  $5\beta$ -dihydrocortisol acetate binding mechanism with human serum albumin and their role in anticancer activity. *Journal of Biomolecular Structure and Dynamics*, 37(3), 623-640.

Kalra, E. (2003). Nutraceutical-definition and introduction. AAPS Pharmsci, 5(3), 27-28.

Kim, J., Byun, M., Lee, J., Yi, D., Jeon, S., & Sohn, B. et al. (2020). Serum albumin and beta-amyloid deposition in the human brain. *Neurology*, *95*(7), e815-e826.

Komatsu, H., Meurice, C., & Axelsen, P. (2019). Variable Binding of Thioflavin T to Amyloid Fibrils. *Biophysical Journal*, *116*(3).

Konjević, G., Jurišić, V., & Spužić, I. (1997). Corrections to the original lactate dehydrogenase (LDH) release assay for the evaluation of NK cell cytotoxicity. *Journal of Immunological Methods*, 200(1-2), 199-201.

Kragh-Hansen, U., Minchiotti, L., Galliano, M., & Peters, T. (2013). Human serum albumin isoforms: Genetic and molecular aspects and functional consequences. *Biochimica et Biophysica Acta (BBA) - General Subjects*, 1830(12), 5405-5417.

Kuboyama, T., Tohda, C., & Komatsu, K. (2006). Withanoside IV and its active metabolite, sominone, attenuate Aβ (25-35)-induced neurodegeneration. *European Journal of Neuroscience*, 23(6), 1417-1426.

Kuboyama, T., Tohda, C., & Komatsu, K. (2014). Effects of Ashwagandha (Roots of Withania somnifera) on Neurodegenerative Diseases. *Biological and Pharmaceutical Bulletin*, *37*(6), 892-897.

Kulkarni, S., & Dhir, A. (2008). Withania somnifera: An Indian ginseng. *Progress in Neuro-Psychopharmacology and Biological Psychiatry*, 32(5), 1093-1105.

Kumar, J., Namsechi, R., & Sim, V. (2015). Structure-Based Peptide Design to Modulate Amyloid Beta Aggregation and Reduce Cytotoxicity. *PLOS One*, *10*(6), e0129087.

Kumar, P., & Kumar, A. (2009). Possible Neuroprotective Effect of Withania somnifera Root Extract Against 3-Nitropropionic Acid-Induced Behavioral, Biochemical, and Mitochondrial Dysfunction in an Animal Model of Huntington's Disease. *Journal of Medicinal Food*, 12(3), 591-600.

Kumar, S., Paul, A., Kalita, S., Ghosh, A., Mandal, B., & Mondal, A. (2016). Protective effects of β-sheet breaker  $\alpha/\beta$ -hybrid peptide against amyloid β-induced neuronal apoptosis in vitro. *Chemical Biology & Drug Design*, 89(6), 888-900.

Kurapati, K., Samikkannu, T., Atluri, V., Kaftanovskaya, E., Yndart, A., & Nair, M. (2014). β-Amyloid1-42, HIV-1Ba-L (Clade B) Infection and Drugs of Abuse Induced Degeneration in Human Neuronal Cells and Protective Effects of Ashwagandha (Withania somnifera) and Its Constituent Withanolide A. *PLOS One*, *9*(11), e112818.

Kyrylkova, K., Kyryachenko, S., Leid, M., & Kioussi, C. (2012). Detection of Apoptosis by TUNEL Assay. *Methods in Molecular Biology*, 41-47.

Laczkó, I., Vass, E., Soós, K., Fülöp, L., Zarándi, M., & Penke, B. (2008). Aggregation of Aβ(1–42) in the presence of short peptides: conformational studies. *Journal of Peptide Science*, *14*(6), 731-741.

Lee, A., Harris, J., Khanna, K., & Hong, J. (2019). A Comprehensive Review on Current Advances in Peptide Drug Development and Design. *International Journal of Molecular Sciences*, 20(10), 2383.

Levine, H. (1993). Thioflavine T interaction with synthetic Alzheimer's disease  $\beta$ -amyloid peptides: Detection of amyloid aggregation in solution. *Protein Science*, 2(3), 404-410.

Li, J., Kwon, N., Jeong, Y., Lee, S., Kim, G., & Yoon, J. (2017). Aggregation-Induced Fluorescence Probe for Monitoring Membrane Potential Changes in Mitochondria. *ACS Applied Materials & Interfaces*, *10*(15), 12150-12154.

Li, S., He, J., Huang, Y., Wang, Q., Yang, H., Xu, K., & Li, H. (2016). Interactions of cucurbit urils with human serum albumin and their effects on zaltoprofen transportation. *RSC Advances*, 6(89), 85811-85819.

Lipinski, C., Lombardo, F., Dominy, B., & Feeney, P. (1997). Experimental and computational approaches to estimate solubility and permeability in drug discovery and development settings. *Advanced Drug Delivery Reviews*, 23(1-3), 3-25.

Lopukhin, Y., Dobretsov, G., & Gryzunov, Y. (2000). Conformational changes in albumin molecule: A new response to pathological process. *Bulletin of Experimental Biology and Medicine*, *130*(1), 615-619.

Luco, J. (1999). Prediction of the Brain-Blood Distribution of a Large Set of Drugs from Structurally Derived Descriptors Using Partial Least-Squares (PLS) Modeling. *Journal of Chemical Information and Computer Sciences*, 39(2), 396-404.

Mager, P., Reinhardt, R., & Fischer, K. (2001). Molecular Simulation to Aid in the Understanding of the A $\beta$ (1–42) Peptide of Alzheimer's Disease. *Molecular Simulation*, 26(6), 367-379.

Malik, N., Dhiman, P., & Khatkar, A. (2017). In-silico Design and ADMET Studies of Natural Compounds as Inhibitors of Xanthine Oxidase (XO) Enzyme. *Current Drug Metabolism*, 18(6), 577-593.

Malleda, C., Ahalawat, N., Gokara, M., & Subramanyam, R. (2011). Molecular dynamics simulation studies of betulinic acid with human serum albumin. *Journal of Molecular Modeling*, 18(6), 2589-2597.

May, P., Gitter, B., Waters, D., Simmons, L., Becker, G., Small, J., & Robison, P. (1992). β-amyloid peptide in vitro toxicity: Lot-to-lot variability. *Neurobiology of Aging*, *13*(5), 605-607.

McKoy, A., Chen, J., Schupbach, T., & Hecht, M. (2012). A Novel Inhibitor of Amyloid β (Aβ) Peptide Aggregation. *Journal of Biological Chemistry*, 287(46), 38992-39000.

Meloun, B., Morávek, L., & Kostka, V. (1975). Complete amino acid sequence of human serum albumin. *FEBS Letters*, *58*(1-2), 134-137.

Milojevic, J., & Melacini, G. (2011). Stoichiometry and Affinity of the Human Serum Albumin-Alzheimer's Aβ Peptide Interactions. *Biophysical Journal*, *100*(1), 183-192.

Min, J., Meng-Xia, X., Dong, Z., Yuan, L., Xiao-Yu, L., & Xing, C. (2004). Spectroscopic studies on the interaction of cinnamic acid and its hydroxyl derivatives with human serum albumin. *Journal of Molecular Structure*, 692(1-3), 71-80.

Milojevic, J., Esposito, V., Das, R., & Melacini, G. (2007). Understanding the Molecular Basis for the Inhibition of the Alzheimer's Aβ-Peptide Oligomerization by Human Serum Albumin Using Saturation Transfer Difference and Off-Resonance Relaxation NMR Spectroscopy. *Journal of the American Chemical Society*, *129*(14), 4282-4290.

Mirjalili, M., Moyano, E., Bonfill, M., Cusido, R., & Palazón, J. (2009). Steroidal Lactones from Withania somnifera, an Ancient Plant for Novel Medicine. *Molecules*, *14*(7), 2373-2393.

Mitra, A., & Sarkar, N. (2020). Sequence and structure-based peptides as potent amyloid inhibitors: A review. *Archives of Biochemistry and Biophysics*, 695, 108614.

Moumitha, M., Pragna, L., Ramadas, K., Natarajan, S. (2017). Molecular interaction between human serum albumin (HSA) and Phloroglucinol derivative that shows selective anti-proliferative potential. *Journal of Luminiscence*, 192: 990-998.

Nagati, V., Nakkka, S., Yeggoni, D., & Subramanyam, R. (2019). Forskolin-loaded human serum albumin nanoparticles and its biological importance. *Journal of Biomolecular Structure and Dynamics*, 38(5), 1539-1550.

Nagati, V., Kallubai, M., Chinthapalli, D., & Subramanyam, R. (2018). Exploration of binding studies of  $\beta$ -oxalyldiamino propionic acid ( $\beta$ -ODAP), a non-protein amino acid with human serum albumin-biophysical and computational approach. *Journal of Biomolecular Structure and Dynamics*, *37*(15), 3914-3922.

Nair, A., Chattopadhyay, D., & Saha, B. (2019). Plant-Derived Immunomodulators. *New Look to Phytomedicine*, 435-499.

Naveenraj, S., & Anandan, S. (2013). Binding of serum albumins with bioactive substances – Nanoparticles to drugs. *Journal of Photochemistry and Photobiology C: Photochemistry Reviews*, *14*, 53-71.

Necula, M., Kayed, R., Milton, S., & Glabe, C. (2007). Small Molecule Inhibitors of Aggregation Indicate That Amyloid β Oligomerization and Fibrillization Pathways Are Independent and Distinct. *Journal of Biological Chemistry*, 282(14), 10311-10324.

Neelam, S., Gokara, M., Sudhamalla, B., Amooru, D., & Subramanyam, R. (2010). Interaction Studies of Coumaroyltyramine with Human Serum Albumin and Its Biological Importance. *The Journal of Physical Chemistry B*, 114(8), 3005-3012.

Nerusu, A., Reddy, P., Ramachary, D., & Subramanyam, R. (2017). Unraveling the Stability of Plasma Proteins upon Interaction of Synthesized Androstenedione and Its Derivatives—A Biophysical and Computational Approach. *ACS Omega*, 2(10), 6514-6524.

Nevola, L., & Giralt, E. (2015). Modulating protein–protein interactions: the potential of peptides. *Chemical Communications*, *51*(16), 3302-3315.

Onguéné, P., Ntie-Kang, F., Mbah, J., Lifongo, L., Ndom, J., Sippl, W., & Mbaze, L. (2014). The potential of anti-malarial compounds derived from African medicinal plants, part III: an *in-silico* evaluation of drug metabolism and pharmacokinetics profiling. *Organic and Medicinal Chemistry Letters*, 4:6.

Oparka, M., Walczak, J., Malinska, D., van Oppen, L., Szczepanowska, J., Koopman, W., & Wieckowski, M. (2016). Quantifying ROS levels using CM-H 2 DCFDA and HyPer. *Methods*, 109, 3-11.

Otagiri, M. (2005). A Molecular Functional Study on the Interactions of Drugs with Plasma Proteins. *Drug Metabolism and Pharmacokinetics*, 20(5), 309-323.

Paissoni, C., Spiliotopoulos, D., Musco, G., & Spitaleri, A. (2014). GMXPBSA 2.0: A GROMACS tool to perform MM/PBSA and computational alanine scanning. *Computer Physics Communications*, 185(11), 2920-2929.

Paissoni, C., Spiliotopoulos, D., Musco, G., & Spitaleri, A. (2015). GMXPBSA 2.1: A GROMACS tool to perform MM/PBSA and computational alanine scanning. *Computer Physics Communications*, 186, 105-107.

Pate, K., Kim, B., Shusta, E., & Murphy, R. (2018). Transthyretin Mimetics as Anti-β-Amyloid Agents: A Comparison of Peptide and Protein Approaches. *Chemmedchem*, 13(9), 968-979.

Patterson, C., Feightner, J., Garcia, A., Hsiung, G., MacKnight, C., & Sadovnick, A. (2008). Diagnosis and treatment of dementia: 1. Risk assessment and primary prevention of Alzheimer disease. *Canadian Medical Association Journal*, 178(5), 548-556.

Peitsch, M., & Guex, N. (1997). Large-Scale Comparative Protein Modelling. *Proteome Research: New Frontiers in Functional Genomics*, 177-186.

Permanne, B., Adessi, C., Saborio, G., Fraga, S., Frossard, M., & Van Dorpe, J. et al. (2002). Reduction of amyloid load and cerebral damage in transgenic mouse model of Alzheimer's disease by treatment with a β-sheet breaker peptide. *The FASEB Journal*, *16*(8), 860-862.

Petitpas, I., Grüne, T., Bhattacharya, A., & Curry, S. (2001). Crystal structures of human serum albumin complexed with monounsaturated and polyunsaturated fatty acids. *Journal of Molecular Biology*, 314(5), 955-960.

Pistollato, F., & Sachana, M. (2016). Prevention of Neurodegenerative Disorders by Nutraceuticals. *Nutraceuticals*, 15-28.

Poduslo, J., Curran, G., Kumar, A., Frangione, B., & Soto, C. (1999). β-sheet breaker peptide inhibitor of Alzheimer's amyloidogenesis with increased blood-brain barrier permeability and resistance to proteolytic degradation in plasma. *Journal of Neurobiology*, 39(3), 371-382.

Potts, R., & Guy, R. (1992). Journal search results - Cite This For Me. *Pharmaceutical Research*, 09(5), 663-669.

Potts, R., & Guy, R. (1995). Journal search results - Cite This For Me. *Pharmaceutical Research*, *12*(11), 1628-1633.

Pratte, M., Nanavati, K., Young, V., & Morley, C. (2014). An Alternative Treatment for Anxiety: A Systematic Review of Human Trial Results Reported for the Ayurvedic Herb Ashwagandha (Withania somnifera). *The Journal of Alternative and Complementary Medicine*, 20(12), 901-908.

Prince, M., Bryce, R., Albanese, E., Wimo, A., Ribeiro, W., & Ferri, C. (2013). The global prevalence of dementia: A systematic review and metaanalysis. *Alzheimer's & Dementia*, 9(1), 63-75. e2.

Privalov, P. (1979). Stability of Proteins Small Globular Proteins. *Advances in Protein Chemistry Volume 33*, 167-241.

Privalov, P., & Gill, S. (1988). Stability of Protein Structure and Hydrophobic Interaction. *Advances In Protein Chemistry*, 191-234. -0

Pronk, S., Páll, S., Schulz, R., Larsson, P., Bjelkmar, P., & Apostolov, R. et al. (2013). GROMACS 4.5: a high-throughput and highly parallel open source molecular simulation toolkit. *Bioinformatics*, 29(7), 845-854.

Qu, M., Zhou, Z., Xu, S., Chen, C., Yu, Z., & Wang, D. (2011). Mortalin overexpression attenuates beta-amyloid-induced neurotoxicity in SH-SY5Y cells. *Brain Research*, *1368*, 336-345.

Rachakonda, V., Pan, T., & Le, W. (2004). Biomarkers of neurodegenerative disorders: How good are they? *Cell Research*, *14*(5), 349-358.

Radibratovic, M., Minic, S., Stanic-Vucinic, D., Nikolic, M., Milcic, M., & Cirkovic Velickovic, T. (2016). Stabilization of Human Serum Albumin by the Binding of Phycocyanobilin, a Bioactive Chromophore of Blue-Green Alga Spirulina: Molecular Dynamics and Experimental Study. *PLoS One*, *11*(12), e0167973.

Rajasekhar, K., Madhu, C., & Govindaraju, T. (2016). Natural Tripeptide-Based Inhibitor of Multifaceted Amyloid β Toxicity. *ACS Chemical Neuroscience*, 7(9), 1300-1310.

Rajput, R., G L, B., Srivastava, A., Wahi, D., Shrivastava, N., Kundu, B., & Grover, A. (2019). Specific keratinase derived designer peptides potently inhibit Aβ aggregation resulting in reduced neuronal toxicity and apoptosis. *Biochemical Journal*, 476(12), 1817-1841.

Rapaport, D., Blumberg, R., McKay, S., & Christian, W. (1996). The Art of Molecular Dynamics Simulation. *Computers in Physics*, 10(5), 456.

Rodríguez-Rodríguez, C., Telpoukhovskaia, M., Alí-Torres, J., Rodríguez-Santiago, L., Manso, Y., & Bailey, G. et al. (2015). Thioflavin-based molecular probes for application in Alzheimer's disease: from in silico to *in vitro* models. *Metallomics*, 7(1), 83-92.

Roychaudhuri, R., Yang, M., Hoshi, M., & Teplow, D. (2008). Amyloid β-Protein Assembly and Alzheimer Disease. *Journal of Biological Chemistry*, 284(8), 4749-4753.

Santini, A., Tenore, G., & Novellino, E. (2017). Nutraceuticals: A paradigm of proactive medicine. *European Journal of Pharmaceutical Sciences*, *96*, 53-61.

Schrodinger: QikProp, version3.4, Newyork, NY:LLC;2011d.

Shuaib, S., & Goyal, B. (2017). Scrutiny of the mechanism of small molecule inhibitor preventing conformational transition of amyloid-β42 monomer: insights from molecular dynamics simulations. *Journal of Biomolecular Structure and Dynamics*, 36(3), 663-678.

Simard, A., & Rivest, S. (2006). Neuroprotective properties of the innate immune system and bone marrow stem cells in Alzheimer's disease. *Molecular Psychiatry*, 11(4), 327-335.

Simard, J., Zunszain, P., Hamilton, J., & Curry, S. (2006). Location of High and Low Affinity Fatty Acid Binding Sites on Human Serum Albumin Revealed by NMR Drug-competition Analysis. *Journal of Molecular Biology*, *361*(2), 336-351.

Singh, M., & Ramassamy, C. (2017). In vitro screening of neuroprotective activity of Indian medicinal plant Withania somnifera. *Journal of Nutritional Science*, 6.

Sleep, D., Cameron, J., & Evans, L. (2013). Albumin as a versatile platform for drug half-life extension. *Biochimica et Biophysica Acta (BBA) - General Subjects*, 1830(12), 5526-5534.

Sliwoski, G., Kothiwale, S., Meiler, J., & Lowe, E. (2013). Computational Methods in Drug Discovery. *Pharmacological Reviews*, 66(1), 334-395.

Smith, M., Dewitt, D., Praprotnik, D., & Perry, G. (1995). Senile plaques and neurofibrillary tangles: The concurrent lesions of alzheimer's disease. *Neurobiology of Aging*, *16*(3), 343-344.

Soto, C., Brañes, M., Alvarez, J., & Inestrosa, N. (2002). Structural Determinants of the Alzheimer's Amyloid β-Peptide. *Journal of Neurochemistry*, *63*(4), 1191-1198.

Soto, C., Sigurdsson, E., Morelli, L., Asok Kumar, R., Castaño, E., & Frangione, B. (1998). BSBpinhibit fibrillogenesis in a rat brain model of amyloidosis: Implications for Alzheimer's therapy. *Nature Medicine*, *4*(7), 822-826.

Stine, W., Dahlgren, K., Krafft, G., & LaDu, M. (2002). In VitroCharacterization of Conditions for Amyloid-β Peptide Oligomerization and Fibrillogenesis. *Journal of Biological Chemistry*, 278(13), 11612-11622.

Subramanyam, R., Gollapudi, A., Bonigala, P., Chinnaboina, M., & Amooru, D. (2009a). Betulinic acid binding to human serum albumin: A study of protein conformation and binding affinity. *Journal of Photochemistry and Photobiology B: Biology*, *94*(1), 8-12.

Subramanyam, R., Goud, M., Sudhamalla, B., Reddeem, E., Gollapudi, A., & Nellaepalli, S. et al. (2009b). Novel binding studies of human serum albumin with trans-feruloyl maslinic acid. *Journal of Photochemistry and Photobiology B: Biology*, 95(2), 81-88.

Sudhamalla, B., Gokara, M., Ahalawat, N., Amooru, D., & Subramanyam, R. (2010). Molecular Dynamics Simulation and Binding Studies of  $\beta$ -Sitosterol with Human Serum Albumin and Its Biological Relevance. *The Journal of Physical Chemistry B*, 114(27), 9054-9062.

Sugio, S., Kashima, A., Mochizuki, S., Noda, M., & Kobayashi, K. (1999). Crystal structure of human serum albumin at 2.5 Å resolution. *Protein Engineering, Design and Selection*, 12(6), 439-446.

Surh, Y. (1999). Molecular mechanisms of chemopreventive effects of selected dietary and medicinal phenolic substances. *Mutation Research/Fundamental and Molecular Mechanisms of Mutagenesis*, 428(1-2), 305-327.

Tajeddine, N. (2016). How do reactive oxygen species and calcium trigger mitochondrial membrane permeabilisation? *Biochimica et Biophysica Acta (BBA) - General Subjects*, 1860(6), 1079-1088.

Tanaka, F., Shibata, K., Monobe, Y., Akagi, K., & Masuda, Y. (2020). Design and synthesis of β-strand-fixed peptides inhibiting aggregation of amyloid β-protein. *Bioorganic & Medicinal Chemistry*, 28(18), 115676.

Tjernberg, L., Näslund, J., Lindqvist, F., Johansson, J., Karlström, A., & Thyberg, J. et al. (1996). Arrest of -Amyloid Fibril Formation by a Pentapeptide Ligand. *Journal of Biological Chemistry*, 271(15), 8545-8548.

Varshney, A., Sen, P., Ahmad, E., Rehan, M., Subbarao, N., & Khan, R. (2010). Ligand binding strategies of human serum albumin: How can the cargo be utilized? *Chirality*, 22(1), 77-87.

Viet, M., Ngo, S., Lam, N., & Li, M. (2011). Inhibition of Aggregation of Amyloid Peptides by Beta-Sheet Breaker Peptides and Their Binding Affinity. *The Journal of Physical Chemistry B*, 115(22), 7433-7446.

Wang, J., Gu, B., Masters, C., & Wang, Y. (2017). A systemic view of Alzheimer disease-insights from amyloid-β metabolism beyond the brain. *Nature Reviews Neurology*, *13*(10), 612-623.

Wang, R., Lai, L., & Wang, S. (2002). Further development and validation of empirical scoring functions for structure-based binding affinity prediction. *Journal of Computer-Aided Molecular Design*, 16(1), 11-26.

Yadav, S., Yeggoni, D., Devadasu, E., & Subramanyam, R. (2017). Molecular binding mechanism of 5-hydroxy-1-methylpiperidin-2-one with human serum albumin. *Journal of Biomolecular Structure and Dynamics*, *36*(3), 810-817.

Yamasaki, K., Rahman, M., Tsutsumi, Y., Maruyama, T., Ahmed, S., Kragh-Hansen, & Otagiri, M. (2000). 3ircular dichroism simulation shows a site-II-to-site-I displacement of human serum albumin-bound diclofenac by ibuprofen. *AAPS Pharm sci tech*, *1*(2), 45-54.

Yang, X., Ye, Z., Yuan, Y., Zheng, Z., Shi, J., Ying, Y., & Huang, P. (2013). Insights into the binding of paclitaxel to human serum albumin: multi spectroscopic studies. *Luminescence*, 28(3), 427-434.

Yasseen, Z., & El Ghossain, M. (2016). Studies on Binding of Widely used Drugs with Human Serum Albumin at Different Temperatures and PHs. *Journal of Biomedical Sciencies*, 5(3):19.

Yazdanian, M., Glynn, S., Wright, J., & Hawi, A. (1998). Journal search results - Cite This For Me. *Pharmaceutical Research*, *15*(9), 1490-1494.

Yeggoni, D., Rachamallu, A., Kallubai, M., & Subramanyam, R. (2014a). Cytotoxicity and comparative binding mechanism of piperine with human serum albumin and  $\alpha$ -1-acid glycoprotein. *Journal of Biomolecular Structure and Dynamics*, 33(6), 1336-1351.

Yeggoni, D., & Subramanyam, R. (2014b). Binding studies of 1-3,4-dihydroxyphenylalanine with human serum albumin. *Mol. Biosyst.*, *10*(12), 3101-3110.

Yeggoni, D., Rachamallu, A., & Subramanyam, R. (2016a). Protein stability, conformational change and binding mechanism of human serum albumin upon binding of embelin and its role in disease control. *Journal of Photochemistry and Photobiology B: Biology*, *160*, 248-259.

Yeggoni, D., Rachamallu, A., & Subramanyam, R. (2016b). A comparative binding mechanism between human serum albumin and  $\alpha$ -1-acid glycoprotein with corilagin: biophysical and computational approach. *RSC Advances*, 6(46), 40225-40237.

Yeggoni, D., Manidhar, D., Suresh Reddy, C., & Subramanyam, R. (2016c). Investigation of binding mechanism of novel 8-substituted coumarin derivatives with human serum albumin and α-1-glycoprotein. *Journal of Biomolecular Structure and Dynamics*, *34*(9), 2023-2036.

Yeggoni, D., Kuehne, C., Rachamallu, A., & Subramanyam, R. (2017a). Elucidating the binding interaction of andrographolide with the plasma proteins: biophysical and computational approach. *RSC Advances*, 7(9), 5002-5012.

Yeggoni, D., Rachamallu, A., Dubey, S., Mitra, A., & Subramanyam, R. (2017b). Probing the interaction mechanism of menthol with blood plasma proteins and its cytotoxicity activities. *Journal of Biomolecular Structure and Dynamics*, *36*(2), 465-474.

Yuan, L., Liu, M., Liu, G., Li, D., Wang, Z., & Wang, B. et al. (2017). Competitive binding of (–)-epigallocatechin-3-gallate and 5-fluorouracil to human serum albumin: A fluorescence and circular dichroism study. *Spectrochimica Acta Part A: Molecular and Biomolecular Spectroscopy*, 173, 584-592.

Zahiruddin, S., Basist, P., Parveen, A., Parveen, R., Khan, W., Gaurav, & Ahmad, S. (2020). Ashwagandha in brain disorders: A review of recent developments. *Journal of Ethnopharmacology*, 257, 112876.

Zhao, L., Chiu, S., Benoit, J., Chew, L., & Mu, Y. (2012). The Effect of Curcumin on the Stability of Aβ Dimers. *The Journal of Physical Chemistry B*, 116(25), 7428-7435.

Zsila, F. (2013). Subdomain IB Is the Third Major Drug Binding Region of Human Serum Albumin: Toward the Three-Sites Model. *Molecular Pharmaceutics*, *10*(5), 1668-1682.

Zunszain, P., Ghuman, J., McDonagh, A., & Curry, S. (2008). Crystallographic Analysis of Human Serum Albumin Complexed with 4Z,15E-Bilirubin-IXα. *Journal of Molecular Biology*, *381*(2), 394-406.

## **List of Publications**

- 1. **Dubey, S.**, Kallubai, M., & Subramanyam, R. (2021). Improving the inhibition of β-amyloid aggregation by withanolide and withanoside derivatives. *International Journal of Biological Macromolecules*, 173:56-65
- 2. **Dubey, S.**, Kallubai, M., & Subramanyam, R. (2020). Comparative binding of Swertiamarin with human serum albumin and α-1 glycoprotein and its cytotoxicity against neuroblastoma cells. *Journal of Biomolecular Strucutre and dynamics*, 38(5):1539-1550.
- 3. **Dubey, S.**, Madana, S., Kallubai, M., Sarkar, A., & Subramanyam, R. (2019). Unraveling the stability of plasma proteins upon interaction of synthesized uridine products: biophysical and molecular dynamics approach. *Journal of Biomolecular Structure and Dynamics*, 38(7), 1927-1937.
- 4. **Dubey, S.**, Kallubai, M., Sakar, A., & Subramanyam, R. (2018). Elucidating the active interaction mechanism of phytochemicals withanolide and withanoside derivatives with human serum albumin. *PLoS One*, 13(11), e0200053.
- 5. Kallubai, M., Reddy, S., **Dubey, S.**, Ramachary, D., & Subramanyam, R. (2018). Spectroscopic evaluation of synthesized 5β-dihydrocortisol and 5β-dihydrocortisol acetate binding mechanism with human serum albumin and their role in anticancer activity. *Journal of Biomolecular Structure and Dynamics*, 37(3), 623-640.
- 6. Yeggoni, D., Rachamallu, A., **Dubey, S.**, Mitra, A., & Subramanyam, R. (2017). Probing the interaction mechanism of menthol with blood plasma proteins and its cytotoxicity activities. *Journal of Biomolecular Structure and Dynamics*, 36(2), 465-474.



Contents lists available at ScienceDirect

### International Journal of Biological Macromolecules

journal homepage: http://www.elsevier.com/locate/ijbiomac



## Improving the inhibition of $\beta$ -amyloid aggregation by with anolide and withanoside derivatives



Shreya Dubey, Monika Kallubai, Rajagopal Subramanyam \*

Department of Plant Sciences, School of Life Sciences, University of Hyderabad, Gachibowli, Telangana 500046, India

#### ARTICLE INFO

Article history:
Received 29 October 2020
Received in revised form 11 December 2020
Accepted 14 January 2021
Available online 16 January 2021

Keywords: Amyloid  $\beta_{1-42}$  Withania somnifera Thioflavin-T fluorescence assay Cell viability assay Molecular docking Molecular dynamics

### ABSTRACT

Here, we have studied the ameliorative effects of *Withania somnifera* derivatives (Withanolide A, Withanolide B, Withanoside IV, and Withanoside V) on the fibril formation of amyloid- $\beta_{42}$  for Alzheimer's disease. We analyzed reduction in the aggregation of  $\beta$  amyloid protein with these Ashwagandha derivatives by Thioflavin T assay in the oligomeric and fibrillar state. We have tested the cytotoxic activity of these compounds against human SK-N-SH cell line for 48 h, and the IC  $_{50}$  value found to be  $28.61\pm2.91$ ,  $14.84\pm1.45$ ,  $18.76\pm0.76$  and  $30.14\pm2.59\,\mu\text{M}$ , respectively. After the treatment of the cells with half the concentration of IC  $_{50}$  value, there was a remarkable decrease in the number of apoptotic cells stained by TUNEL assay indicating the DNA damage and also observed significant decrease of reactive oxygen species. Also, the binding and molecular stability of these derivatives with amyloid  $\beta$  was also studied using bioinformatics tools where these molecules were interacted at LVFFA region which is inhibition site of amyloid- $\beta 1$   $_{42}$ . These studies revealed that the Withanolides and Withanosides interact with the hydrophobic core of amyloid- $\beta 1$   $_{42}$ . In the oligomeric stage, preventing further interaction with the monomers and diminishing aggregation.

© 2021 Elsevier B.V. All rights reserved.

### 1. Introduction

Amyloid  $\beta$  (A $\beta$ ) is well known to be a central player in the pathogenesis of Alzheimer's disease. Amyloid  $\beta$  is monomeric in solution initially, but aggregate into low molecular weight structures, followed by higher molecular weight species like proto-fibrils, and eventually mature as amyloid fibrils. These fibrils are insoluble structures that are more than 1  $\mu$ m long, and 8–12 nm in diameter. The hippocampus region and cerebral cortex of the brain are the major parts affected by Alzheimer's disease progression leading to their degeneration and plaque formation due to amyloid fibril deposition [1,2]. In fact, the pre-fibrillar soluble oligomers are more cytotoxic than their fibrillar counterpart, even though they do not form insoluble aggregates [3].

Withania somnifera (Indian Ginseng) is a plant used in Ayurveda and Chinese medicine since ancient times because of its remedial properties against several ailments. They are of immense use in pharmacological importance. They are used to treat cancer, rheumatoid arthritis, decrease stress, and show anti-inflammatory activity, and are known to treat various central nervous system (CNS) disorders [4,5]. More than 40 structures of withanolide and withanosides were reported, which represent a collection of naturally occurring C-28 steroidal lactone triterpenoids assembled on integral or reorganized ergostane structure in which C-22 and C-26 are oxidized to form a six-membered lactone ring [6]. In contrast,

\* Corresponding author. E-mail address: srgsl@uohyd.ernet.in (R. Subramanyam). withanosides differ with an extra hydroxyl on C-20 and C-27 atoms. As our study was inclined towards brain pathology, and the major hindrance for various potential drugs was found to be the limitation of crossing the blood-brain-barrier (BBB), and our previous study has analyzed that these phytocompounds can be easily transported across BBB owing to its binding capacity with Human Serum Albumin (HSA) [7]. Hence, our current study focused on four steroidal derivatives of this plant which are Withanolide A ( $C_{28}H_{38}O_{6}$ ), Withanolide B ( $C_{28}H_{38}O_{5}$ ), Withanoside IV ( $C_{40}H_{62}O_{14}$ ). These compounds are also known to exhibit several neurodegenerative diseases including Alzheimer's and Parkinson's disease [8]. Additionally, due to its natural plant derived origin, it has become very popular oral supplement globally because of its strong remedial properties [7].

So far, the purified derivatives of withanolide and withanosides are not been evaluated the protective role of fibril formation of amyloid-  $\beta_{42}$  which is a very important for Alzheimer's. Thus, our experimental results showed that the Withania somnifera derivatives of interest can inhibit the aggregation of amyloid peptides with time. We performed extensive evaluation of the derivatives in order to determine their inhibitory effects on amyloid oligomers as well as fibrils using spectrophotometric methods and also in vitro cell culture assays. The cytotoxicity studies of phytochemical derivatives against neuroblastoma cell lines were observed by apoptosis assays, which affirms their hypothesized therapeutic and pharmaceutical potential. Detailed knowledge of the active site of peptide, and their interaction with the Ashwagandha derivatives were obtained by molecular docking studies. Furthermore,

the stability of the ligand-amyloid complexes were determined in 100 ns time scale simulations.

### 2. Materials and methods

### 2.1. Preparation of stock solutions

Withanolide A, withanolide B, withanoside IV and withanoside V were procured from Natural Remedies Pvt. Ltd., Bengaluru, India with purity of 99%. These compounds were first dissolved in dimethyl sulphoxide (DMSO) with the concentration of 20 mM. This stock solution was further diluted to a concentration of 100  $\mu$ M working stock in PBS (pH 7.4), similar to our previously reported studies [7]. All other chemicals used were of analytical grade from Sigma Aldrich. The amyloid- $\beta(1-42)$  peptide used in this study was procured from GL Biochem (Shanghai, China) with a purity of 98%. A $\beta_{1-42}$  was monomerized by dissolving in hexafluoroisopropanol at final concentration of 1 mg mL $^{-1}$ , aliquoted, and allowed to evaporate. It was then dissolved in DMSO to a concentration of 1 mM and was further diluted to a working concentration of 25  $\mu$ M in PBS.

### 2.2. Thioflavin-T fluorescence assay

Thioflavin-T is a fluorescent dye which can selectively bind to beta rich structures like amyloid fibrils. This assay is the most widely used 'gold standards' to selectively identify and analyze amyloid  $\beta$  fibrillogenesis, in both *in vitro* and *in vivo* systems [9,10]. This contributes a great deal of insight into the morphology, development of the fibrils, and also the effect of different inhibitory therapeutic molecules against the amyloid assembly.

Fluorescence enhancement upon binding to fibrils is the most defining and thoroughly studied property of ThT, displays a dramatic shift of the excitation maximum (from 385 nm to 450 nm) and the emission maximum (from 445 nm to 482 nm) and that ThT fluorescence originates only from the dye bound to amyloid fibrils [11,12]. The amyloid protein concentration was fixed at 25 µM and ligand concentrations were taken as 100 µM, in the ratio 1:4. Equal volume of both photochemicals and peptides were taken and incubated at 37 °C. The first incubation period was kept for 6 h, i.e., the lag phase period, in order to quantify amyloid oligomer formation and study its inhibition. The samples are then mixed with 25 µM ThT prepared in 50 mM sodium phosphate buffer  $(pH \sim 7.2)$  to make up the volume to 100 µL. The samples are then centrifuged at 15,000 ×g for 10 min, and the supernatant was taken for analysis, since the oligomers are soluble. A Horiba Fluoromax-3 fluorometer was used for carrying out the analysis, where the excitation and emission wavelengths were set at 450 nm and 482 nm respectively, and slit width kept as 4 nm, of 1 cm quartz cuvette. The experiments were conducted at constant temperature of 25 °C to prevent further aggregation during analysis. The samples were incubated again after oligomer analysis, and further kept for 48 h elongation phase period at 37 °C in order to quantify amyloid peptides in their fibrillar forms to determine the ameliorating effects of the phytochemicals against amyloidosis. All fluorescence experiments were done in triplicates.

### 2.3. Cell viability (MTT assay)

SK cells were grown in a humidified incubator with 5% CO<sub>2</sub> and 95% air at 37 °C, in minimum essential medium supplemented with 10% fetal bovine serum, 200 IU/ penicillin, 200 g/mL streptomycin, and 1 mM sodium pyruvate. Every alternate day the medium was replaced, the cells were trypsinised, and sub-cultured after reaching around 80% confluency.

Cell viability was evaluated by using (3-(4,5-dimethyl-thiazol-2-yl)-2,5-Diphenyltetrazolium bromide)-MTT assay for 48 h, which indicates the importance of the molecules as a potential therapeutic agent determined from its IC50 value [13,14]. Cells were seeded in a 96 well plate at density of  $10^4$  cells per well. The cells were treated with the *Withania* 

somnifera derivatives at increasing concentrations of 10, 20, 40, 60, 80, 100 µM and incubated for 48 h, after which 20 µL of MTT (5 g/mL in PBS) was added and incubated further for 4 h, whereas in control wells, the ligands were not added. To dissolve the MTT crystals, 100 µL of DMSO was added in each well. Finally, cell viability was measured at absorbance of 570 nm by using a Magellan plate reader. The experiment was carried out in triplicates, for each concentration of the withanolide and withanoside derivatives. Mean  $\pm$  SE was calculated and reported as the cell viability (%) vs. concentration (µM). As the IC50 value for A $\beta$  was found out to be 25  $\pm$  1.33 µM by dose dependent manner and the time required for A $\beta$  is around 6 h. Hence, we incubated the cells, and once confluency was reached, we incubated it with 25 µM of A $\beta$  for 6 h and then added half the concentration of IC50 value and incubated for 24 h, after which the protocol for MTT assay was followed.

### 2.4. Apoptosis assay by Annexin V

Apoptotic cells have distinct morphological features like membrane blebbing, chromatin condensation, the formation of apoptotic bodies, but the hallmark of apoptotic cells is DNA fragmentation. Propidium iodide is used to stain the early apoptotic cells, and Annexin V binds to phosphatidylserine, which is translocated to the outer membrane of the apoptotic cells, and Annexin V is linked to FITC which is a fluorochrome. Apoptosis was measured by the annexin V-FITC detection kit (Sigma cat. No. APOAF) on SK cells, after treatment with the withanolide and withanoside derivatives. The concentration of half the value of its IC<sub>50</sub> value for 24 h was taken for the study. Following this, the cells were washed twice with phosphate-buffered saline, and then resuspended in binding buffer. Finally, the cells were stained with annexin V-FITC for 15 min and analyzed by flow cytometry. Annexin V conjugates with fluorescein isothiocyanate (FITC) which labels phosphatidylserine sites on the membrane surface and propidium iodide labels the cellular DNA in necrotic cells, where the cell membrane is almost disrupted. Cells were then collected using a FACS Calibur flow cytometer (Becton Dickinson, USA), and Cell Quest Software (BD Bioscience, USA) was used for analysis.

### 2.5. Tunel assay using confocal microscopy

Terminal deoxynucleotidyl transferase (tdt) d-UTP Nick-End Labeling (TUNEL) assay is designed to detect the apoptotic cells that undergo extensive DNA degradation during the late stages of apoptosis. The SK neuroblastoma cells were taken and seeded in 12 well plates at a density of  $10\times10^4$  cells per well. The cells were incubated for 24 h, following which the derivatives were added at a concentration of half the IC50 value. The cells were then once again incubated for 24 h. No phytochemical was added to the control well. Cell fixation was done by adding 4% formaldehyde and incubating at 4 °C for 30 min. Further, the protocol given in Takara MK 500 kit was followed and the cells were viewed under a confocal microscope.

### 2.6. ROS intracellular assay

Intracellular reactive oxygen species (ROS) production was measured in fractions-treated and control cells using oxidation sensitive dye DCFH-DA. Cells were grown in 96 well plates and exposed to fractions for 12 h. After incubation, the cells were washed thoroughly with PBS. The treated and control cells were re-suspended in 0.5 mL PBS containing 20  $\mu$ M DCFHDA at 37 °C for 30 min in dark conditions. The incubated cells were again washed with PBS, and fluorescence intensities were recorded in spectrofluorometer (TECAN Infinite 200 PRO, Switzerland) at an excitation wavelength of  $\lambda$  485 and an emission of  $\lambda$  535 nm. 25  $\mu$ M of A $\beta$  was added to the confluent cells and incubated for 6 h, which is the time required by A $\beta$  to reach an oligomeric state after which half the concentration of IC50 value of these phytocompounds were added and further incubated for 24 h. The experiment was repeated in triplicates.

### 2.7. Molecular docking of β-amyloid and Withania somnifera derivatives

Molecular docking is a computational approach that specifies the site at which the ligand binds with the protein through many hydrogen bonds. Here, Autodock v.4.2.3 tool is used for molecular docking studies and internal conformational searches. Autodock uses a Genetic Algorithm (GA) and a Lamarckian Genetic Algorithm to generate suitable conformations. For in silico analyses, the structure of the  $\beta$ -amyloid (PDB id:2BEG) was retrieved from the RCSB protein data bank [15]. The ligand structures were created using Discovery Studio, optimization, and energy minimization was done using SYBYL software. The macromolecules were then opened with Autodock (v.4.2.3), where the water molecules were removed, following which the polar hydrogen groups and Kollman charges were added [7,16,17]. After optimizing ligand and protein, a grid-based procedure was used and saved as. PDBQT file. The grid box is then sketched and saved as .gpf files. The program Autogrid then generated ligand-centered maps with a spacing of 0.586 Å and dimensions of  $(126 \times 126 \times 126)$  points, and this was followed by blind docking. In the parameter position, they were set in their default settings. The output was then selected as Lamarckian GA (4.2), and the file was saved as .dpf. This dpf file was used to conduct docking simulations and to generate possible conformations of these derivatives binding to β-amyloid. The conformer with the lowest binding energy was chosen from the nearly 50 available conformations.

### 2.8. Molecular dynamics of $\beta$ -amyloid and Withania somnifera derivatives

Molecular simulation is one of the best methods to explain the peptide-ligand complex's stability and conformational changes at atomic levels. The lowest energy conformation obtained from the docking studies was selected for simulation studies using the GROMACS tool to analyze the interaction between peptide and the Ashwagandha molecules. This gives information regarding key residues in fibril formation. A 100 ns simulation was run using the software Gromacs v.5.0 package with force field GROMOS96, as illustrated in our previous studies [18,19]. PRODRG2.5 server (beta) was used to build the topology parameters of Ashwagandha derivatives (A, B, IV, V). The complexes were placed in a box of 80x80x80 Å of extended simple point charge (SPC) water molecules producing a system of 146 atoms of the β-amyloid peptide. Sodium and chloride counter ions were added to maintain electro-neutrality and releasing conflicting contacts. This was succeeded by energy minimization using the steepest descent algorithm to remove the local strain due to lousy van der Waal interactions. Once the system was converged, it was subjected to equilibration with NVT and NPT ensembles to attain the system temperature and pressure of 300 K and 1 bar, respectively. Finally, the system was subjected to MD simulation for 100 ns, and the generated trajectory was analyzed using Xmgrace for root-mean-square deviations (RMSD), root-mean-square fluctuations (RMSF), and radius of gyration (Rg); and the above simulations and analysis were performed on OSCAR Linux cluster with 12 nodes (dual xeon processor) at Bioinformatics facility, University of Hyderabad.

### 3. Results and discussion

### 3.1. Thioflavin fluorescence assay

Thioflavin (Tht) is a dye used for quantifying the amyloid fibrils/aggregation [20]. Free  $\beta$ -amyloid (1–42) can increase hydrophobicity [21]. The amyloid samples treated with ligands in the ratio 1:4 and

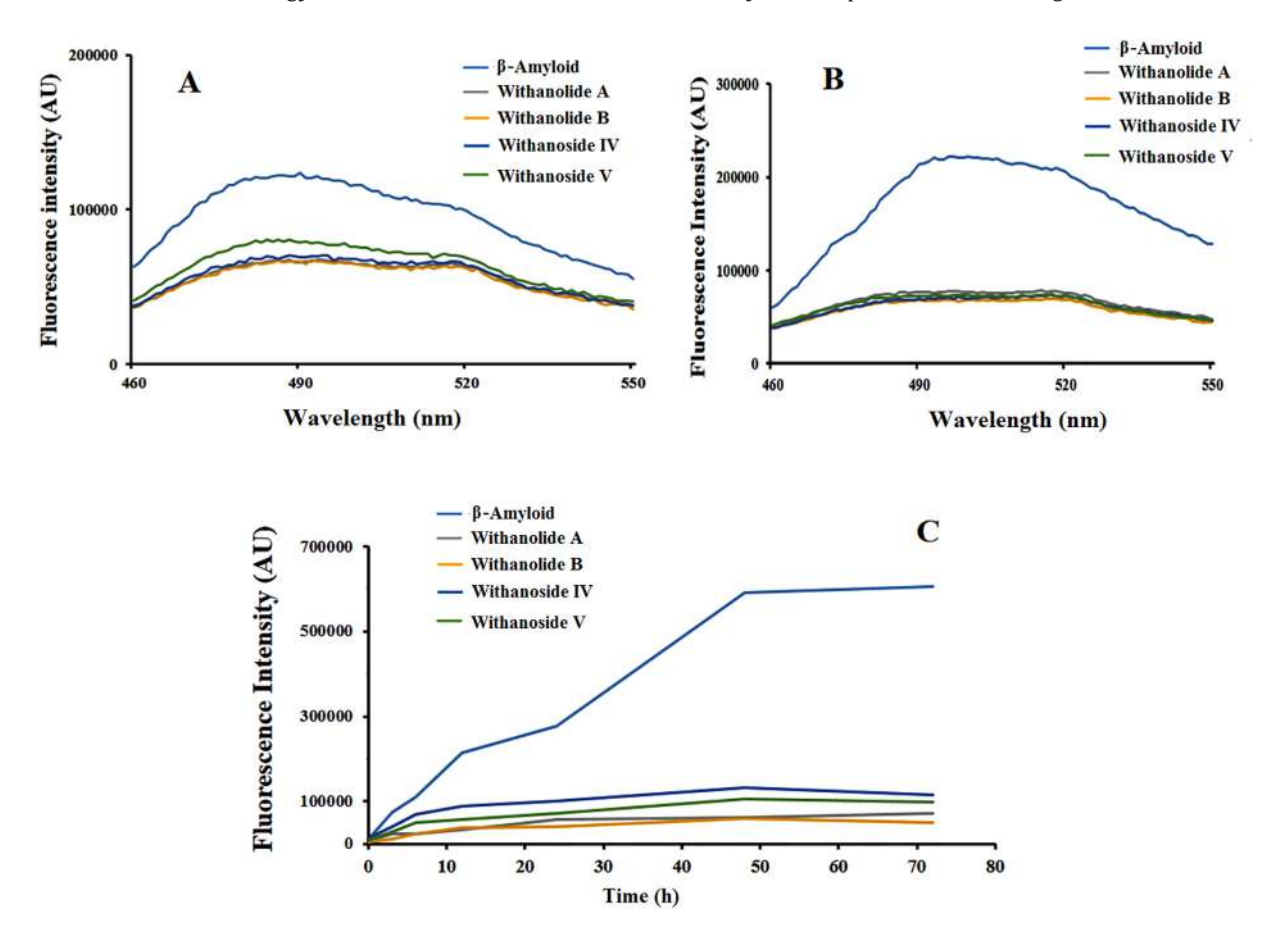


Fig. 1. Detection of A $\beta$  aggregates using Tht assay; measurement of fluorescence enhancement spectra ( $\lambda_{ex} = 450 \text{ nm}$ ,  $\lambda_{em} = 482 \text{ nm}$ ) of 5  $\mu$ M Tht solution (in 50 mM sodium phosphate buffer) mixed in 25  $\mu$ M A $\beta$ (1–42) with different phytochemicals Withanolide A, Withanolide B, Withanoside IV and Withanoside IV at ratio 1:4, in their A) Oligomeric (6 h incubation) state, and B) Fibrillar (after 24 h of incubation) state, C) Fluorescence was measured at different time points upto 72 h to study the aggregation.

quiescently incubated for 6-h intervals keeping other conditions constant, showed a considerable decrease in the fluorescence intensity. Recent studies on Human lysozyme with Entacapone also showed similar results: the decline in the fluorescence indicates a reduction of cross βsheet structures in the human lysozyme [22]. Even the β-amyloid-Ashwagandha complexes showed a reduced fluorescence signal. Thus, we can assume that there is a reduction in the  $\beta$ -sheet structures of amyloid. The control showed a fair amount of steady rapid aggregation of amyloid oligomers in the sample contributing to the increased fluorescence intensity. This indicates the inhibitory effect of these plantbased phytochemicals against the accumulation of β-amyloid, which otherwise would contribute to Alzheimer's disease. All four Ashwgandha derivatives (Withanolide A, Withanolide B, Withanoside IV, and Withanoside V), owing to their similar nature, show suitable inhibitory property against oligomeric peptide assembly. The drugs do not self-aggregate, negating any chance of artifacts during the assay. To study the effect of these phytochemicals even on amyloid fibrils, the samples were again co-incubated for 48 h to further determine their activity against fibrillization. The results show although the control peptides kept on aggregating in their log phase, the co-incubated samples showed a drastic reduction in the aggregation. To further consolidate the results, a time point study was done along with the control and treated samples to observe the aggregation trend's near real-time view. The control showed a steady increase in its aggregation phenomena till it reaches stability at around 72 h (Fig. 1C). On the other hand, the treated samples, similar to the previous independent experiments, showed generous containment of the amyloidosis to its oligomeric state with an increasing period until 72 h, thus validating the studied applicability of phytochemical derivatives. Recently, our collaborative work on new flavone-cyanoacetamide hybrids shows a significant reduction of aggregation of amyloid β fibrillization with similar conditions, as mentioned above [10].

### 3.2. MTT reduction assay

Neuronal toxicity is the outcome of AB aggregation. Thus, Withanolide A, Withanolide B, Withanoside IV, and Withanoside V were further used to investigate its preventive effect on neuronal toxicity. In our study, we have checked the dose-dependent result of the Withanolides A, B, and Withanosides IV, V on SK-N-SH cell line for 48 h, and the IC<sub>50</sub> value found to be 28.61  $\pm$  2.91, 14.84  $\pm$  1.45, 18.76  $\pm$  0.76, and 30.14  $\pm$  2.59  $\mu M$  respectively (Fig. 2A). Neuronal cell viability visibly increased and subsequently diminished the toxicity of fibrillar AB42 aggregation. In vitro studies of withanolide A were previously shown to accumulate β-amyloid in SH-APP cells (neuroblastoma cell lines expressing human APP751) [23]. In some other reviews, they have tested the neuroprotective effects of Withanolide A against β-amyloid induced toxicity, HIV-1(Ba-L) (clade B) infection, and the impact of drug-using a human neuronal SK-N-MC cell line and observed that  $\beta$ -amyloid induced cytotoxic effects in SK-N-MC cells. Still, Withanolide A, when added to AB, treated cells, the toxic effects were neutralized [24]. Our studies focused on four derivatives of Withania somnifera, and all the results indicate that the Withanolide A, Withanolide B, Withanoside IV, and Withanoside V have significant therapeutic potential against amyloid-\beta aggregation-induced cell toxicity, as the number of live cells was increasing when we are adding these compounds after the addition of A $\beta$  (Fig. 2B). So, we can deduce that these phytocompounds are showing neuroprotective activity against Aβ.

### 3.3. Apoptosis annexin assay

To detect the effects of withanolide and withanoside derivatives on early apoptosis and late apoptosis/necrosis induced by  $\beta$ -amyloid, human neuroblastoma (SK-N-SH) cells were stained with FITC-conjugated Annexin V and propidium iodide (PI). Since apoptotic

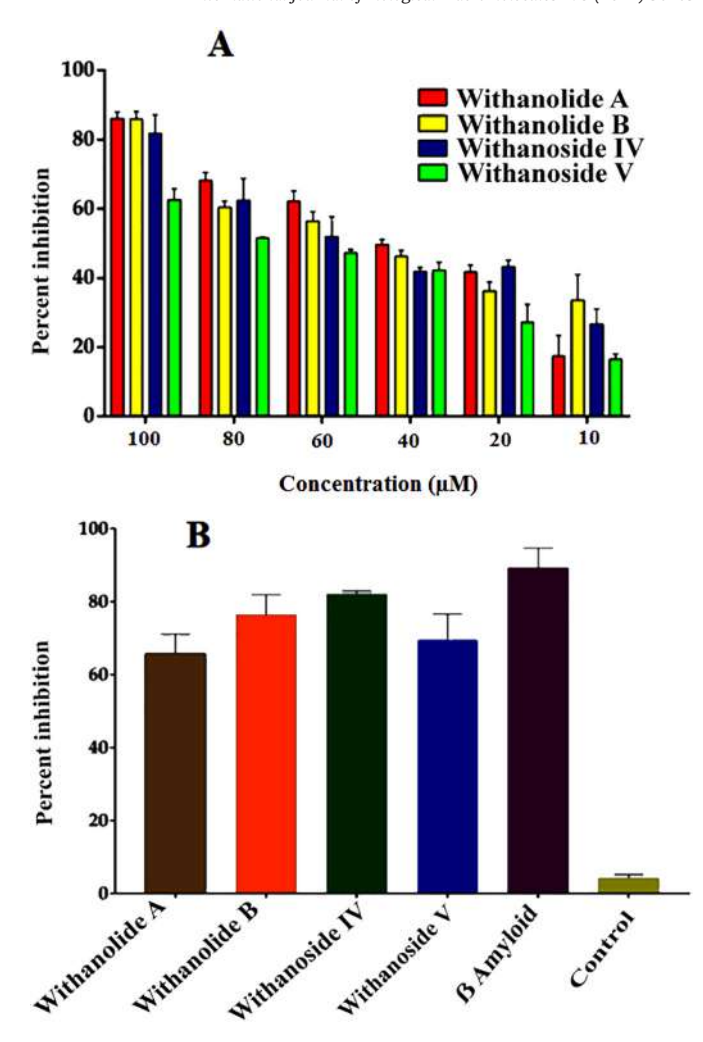


**Fig. 2.** A) Inhibitory effect of *Withania somnifera* derivatives on the growth of SK-N-SH cells by MTT assay by dose dependant. B) After treatment with 25  $\mu$ M of A $\beta$ , the cells were treated with half the concentration of IC50 value and incubated for 48 h. Data was represented as the mean + S·D(n=3).

lymphocytes lose membrane phospholipid asymmetry, resulting in exposure of phosphatidylserine (PS) on the outer leaflet of the plasma membrane, apoptotic-like cell death is often quantified by measuring PS externalization by binding of Annexin V. PI is a non-specific DNA intercalating agent, which is excluded by the plasma membrane of living cells, and thus can be used to distinguish necrotic cells from apoptotic and living cells by supravital staining without prior permeabilization [25,26]. Therefore, we induced apoptosis in the SK-N-SH cell line at half of the inhibition constant concentration by adding the withanolides and withanosides derivatives. It was observed that in control, the Q4 quadrant that represents the viable cells has a more significant number of viable cells compared to the cells treated with Withanolides and Withanosides (Fig.3 A-E). In the treated sample, it was seen that the number of cells in the Q<sub>3</sub>, Q<sub>2</sub>, Q<sub>1</sub> quadrants that represent the early apoptosis, late apoptosis, and dead cells have increased when compared to the control sample. The results are shown as dot-plot representation (FITC-A on the x-axis and PE-A on the y-axis) in quadrants and histograms (Fig. 3, Table 1). In the present study, our data show that Ashwagandha derivatives prevented this cellular degeneration. Some studies suggest that one pathway of β-amyloid induced cytotoxicity could be mediated by free radicals and oxidative stress [24]. This indicates that the Withanolide A, Withanolide B, Withanoside IV, and Withanoside V show cytotoxicity against SK-N-SH cells and have pharmaceutical potential.

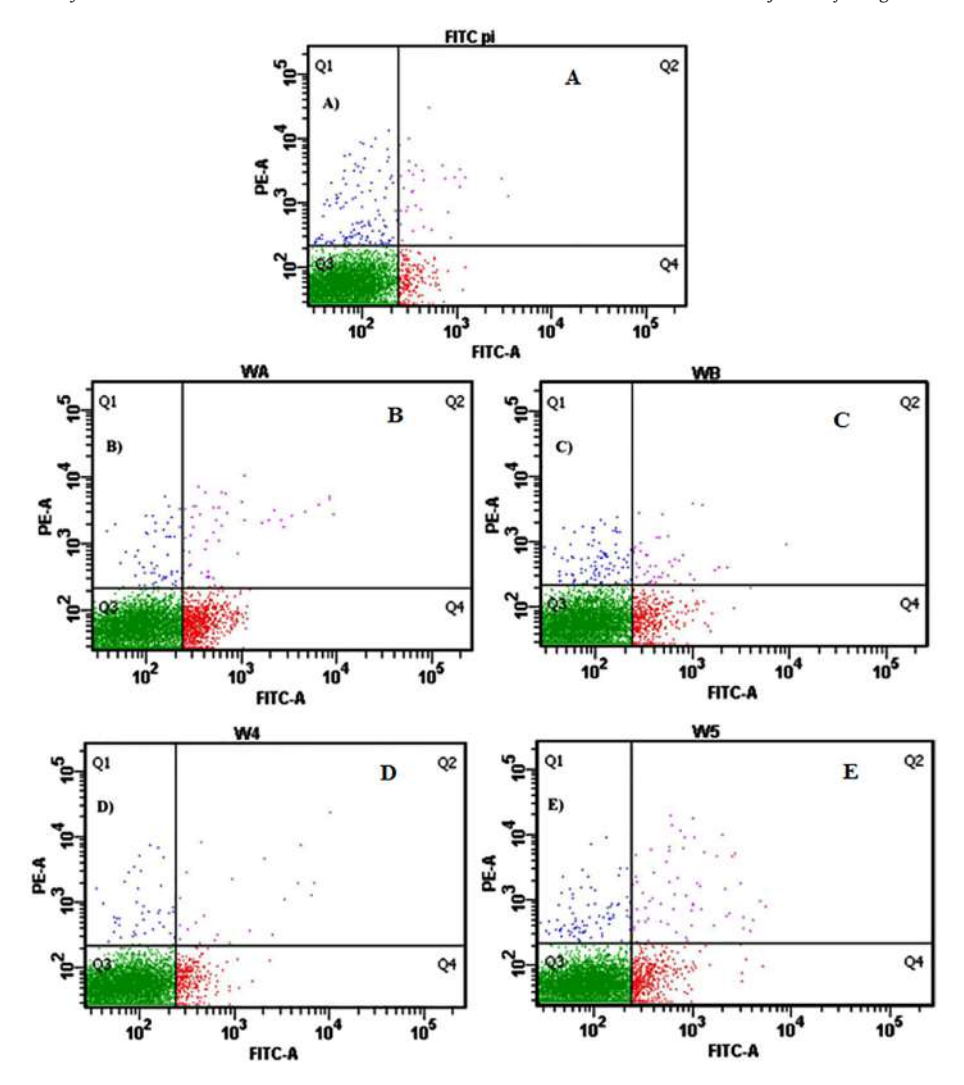


Fig. 3. Apoptosis studies by Flow cytometry by using after treatment with half concentration of IC<sub>50</sub> value for 24 h A) only cells B, C, D, E after addition of Withanolide A, Withanolide B, Withanoside IV, and Withanoside V.

### 3.4. Tunel assay by confocal microscopy

The cleavage or fragmentation of nuclear DNA into nucleosome-sized fragments is a hallmark of apoptosis. Cleaved DNA has a 3 'hydroxyl group, which becomes the substrate for binding of fluorescein – isothiocyanate TUNEL assay. After the cells' treatment with half the concentration of  $IC_{50}$  value, there was a remarkable decrease in the number of apoptotic cells (positively tunnel stained cells), thereby indicating the DNA damage (Fig. 4A-E).

### 3.5. Intracellular ROS measurement

To investigate whether the derivatives of Withania somnifera protect the cells from excessive intracellular ROS, we evaluated the ROS

**Table 1**Percentage of cells in each quadrant without addition of the drug and in the presence of withanolide and withanoside derivatives. All these values are in %.

	Live cells	Dead cells	Early apoptosis	Late apoptosis
Control	96.1	1.3	2.2	0.4
Withanolide A	87.9	0.6	10.8	0.7
Withanolide B	93.7	1.1	4.7	0.5
Withanoside IV	94.9	1.1	3.4	0.6
Withanoside V	93.2	0.9	5.2	0.7

production with a fluorescent dye DCFH-DA. Cells treated with amyloid β displayed an increase in ROS production. We can see a significant reduction in ROS production when the cells were treated with the Withanolide A, Withanolide B, Withanoside IV, and Withanoside V (Fig. 5). In which with anolide A and with anolide B are significantly reduced the ROS production, which indicates these molecules can project much better than withanoside IV and withanoside V. The difference between the withanolides and withanosides are C-28 and C-40 steroidal lactones, with six-membered lactone ring formed by oxidization of the C-22 and C-28 on ergostane backbone [7]. Thus, this may be the reason the withanolide A and withanolide B can reduce ROS. Accumulation of ROS disturbs the integrity of the plasma membrane and causes DNA damage because of oxidative stress. These derivatives are successful in rescuing cell death induced by the toxicity of AB, which ultimately leads to neuronal dysfunction. Earlier reports showed that withanolide A attenuated ROS generation in neuroblastoma cells and decreased the ROS levels in hypobaric hypoxia [27]. Thus, we can infer our results that all the four derivatives withanolide A, withanolide B, withanoside IV, and withanoside V reduced ROS production.

### 3.6. Molecular docking by Autodock

Our present study used the Autodock 4.2.3 tool to evaluate the molecular interaction between different Ashwagandha molecules (withanolide A, withanolide B, withanoside IV, and withanoside

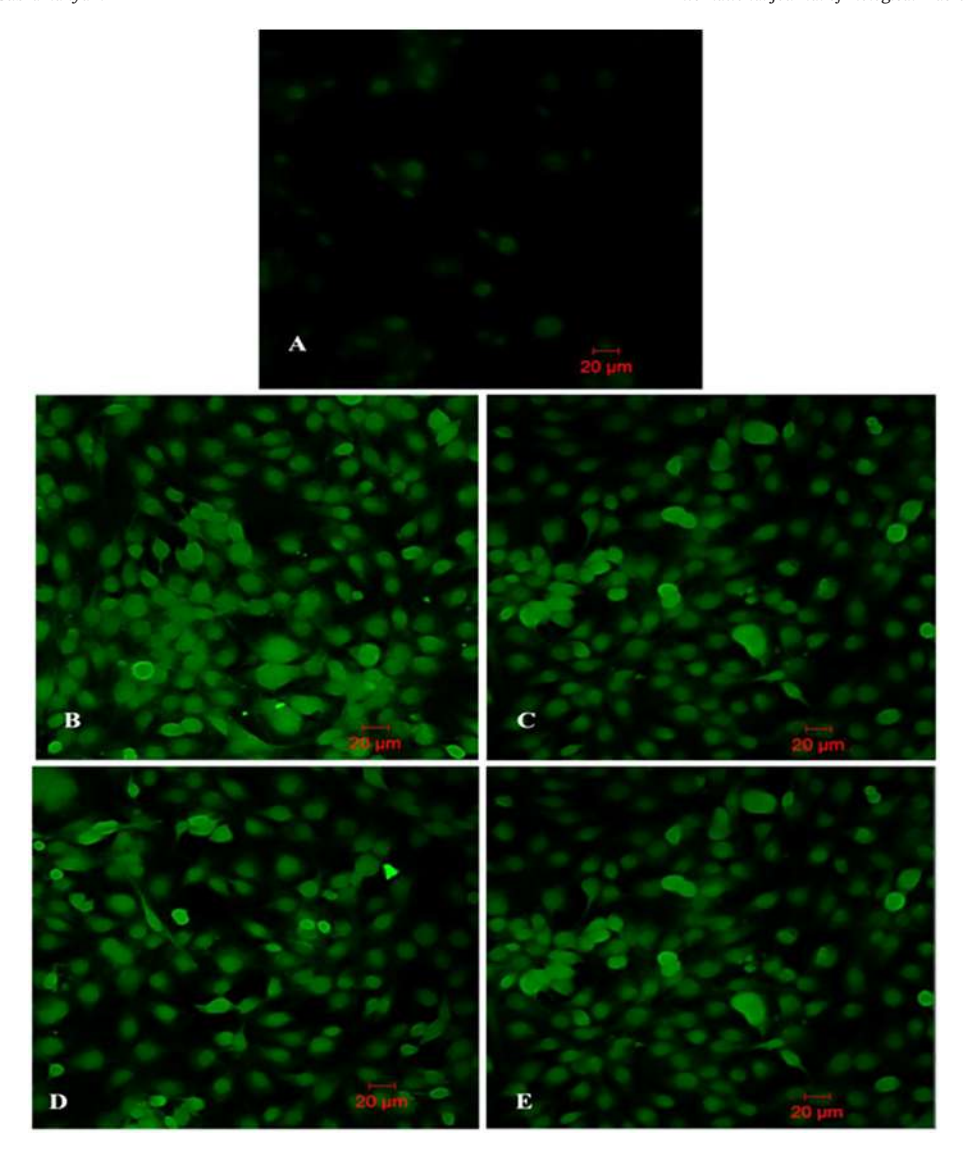
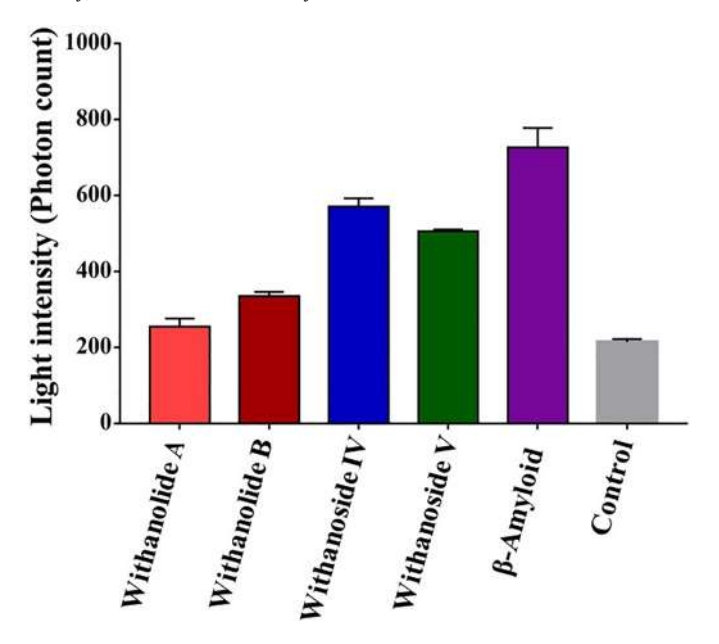


Fig. 4. TUNEL nuclear staining on SK-N-SH neuroblastoma cells.Cells in control are untreated, and remaining cells are treated with half the conc of IC<sub>50</sub> value. Cells were collected, washed in phosphate-buffer saline, fixed and permeablised and subjected to TUNEL nuclear staining, mounted and viewed by fluorescence microscopy. A) only cells B, C, D, E after addition of WithanolideA, Withanolide B, Withanoside IV, and Withanoside V.

V) and β-amyloid. The essential criteria to study molecular docking are understanding binding energy, interacting amino acid residues, and bonding distance between a protein with each ligand. Docking studies using the known NMR or PDB structures may not accurately picture ligand-protein interactions [28]. In contrast, they are an essential tool to predict potential ligand binding sites of AB aggregates [29,30]. Thus for this study, we retrieved the crystal structure of amyloid- $\beta$  peptide with PDB id: 2BEG to understand the interaction between Ashwagandha derivatives and amyloid-\beta peptide essential in the treatment of Alzheimer's disease [28]. These Ashwagandha molecules can act as potential inhibitors to prevent the oligomerization and aggregation of amyloid-\beta peptides [31]. According to literature, the most common view of AB is having 1-42 amino acids, among these 42 amino acids, the most flexible regions of this peptide in a fibril formation are the first 10 amino acids of the N-terminus and last few amino acids of the C-terminus (residues 39–42), and in between the residues Asp23 and Lys28 are in parallel  $\beta$ -sheet with a  $\beta$ -turn. Some previous studies explained that the peptide KLVFF (fragment A\beta16-20) and hydrophobic region of AB17-21 motif LVFFA showed significant binding of inhibitory molecules, preventing AB fibrillation [32,33]. This fragment is the Hydrophobic core of  $\beta$ -amyloid, which is most susceptible for another

monomer to come and bind. Our present study also finds an active site where the withanolide A interacted with Leu17 and Phe19, withanolide B with residues Phe19 and Phe20, whereas withanoside IV interacted with Asp23, Val24 and Ser26 and withanoside V like withanolide A and B molecules it is bound in the same site interacting with residues Leu17 and Leu19 (Fig. 6A, B, C and D). The results show that with anoside IV is in the  $\beta$ -turn region of the amyloid peptide and is efficient with the binding energy of -7.4 kcal/mol compared to the Withania somnifera A, B, and V molecules with binding energy -6.4, -6.8, and -6.3 kcal/mol, respectively. The cell viability test with the SK-N-SH cell line showed better withanoside IV (Fig. 2). Thus, molecular docking provided detailed knowledge of small molecules binding to the peptide's active site, especially in the hydrophobic region of amyloid motif (AB17-21), further designing new molecules with low toxicity and high specificity in peptide-based therapy in preventing β-amyloid aggregation. Thus aromatic residues of the hydrophobic region in βamyloid can act as hot spot regions or critical target areas for the development of amyloid agents [34]. Especially  $\beta$ -sheet breaker peptides (BSB) are being used for therapy for neuroprotection as they usually are known to target the hydrophobic core region (HCR) of 17-21 residue of 42 residues of β-amyloid peptide. This HCR region is known to



**Fig. 5.** Intracellular ROS generation in SK-N-SH cells after treatment with *Withania somnifera* derivatives. After treatment for 12 h, cells were stained with 20  $\mu$ M DCFH-DA for 30 min at 37 °C in the dark. Data are expressed as mean  $\pm$  SD (n = 3).

be mainly responsible for another  $\beta$ -amyloid peptide to come and bind to it but here we can see that these derivatives are blocking the HCR thus inhibiting fibrillization.

### 3.7. Molecular dynamics simulations of $\beta$ -amyloid-Ashwagandha complexes

Filamentous amyloid aggregates are the leading cause of the pathological condition of Alzheimer's disease. Previous reports explained that the standard A $\beta$  peptides with  $\alpha$ -helical conformations were nontoxic, but the neurotoxicity was observed with an increase in the formation of  $\beta$ -sheet structure [35–37]. However, the exact mechanism of A $\beta$  aggregation is still not precise. The most common view of A $\beta$  (1–42)

is fibrillar parallel  $\beta$ -sheets with a  $\beta$ -turn between residues Asp-23 and Lys-28. According to the literature, an energetically favored hydrophobic cleft on chain A comprising the residues LVFFA (17–21 region) seems to be an excellent binding site in terms of energetic point of view concerning Chain E for binding inhibitors more effectively [38]. In our study, all the four phytocompounds, withanolide A, withanolide B, withanoside IV and withanoside V, when docked with  $\beta$ -amyloid, showed interactions with LVFFA regions among 50 runs. It is interesting to observe that withanolide A, withanolide B, withanoside IV, and withanoside V bind in the LVFFA region, which is the preferred region for many small molecule inhibitors of AB142 aggregation. The lowest binding energy conformer among 50 conformations was selected for molecular dynamics (MD) simulations with explicit solvent and force fields to probe the structural stability and the conformational dynamics of  $\beta$ -amyloid fibril structures. All the 100 ns simulations showed that the β-amyloid-Ashwagandha derivatives' conformations (A, B, IV, and V) were stable after 20 ns. The complexes' stability was analyzed and shown in the Radius of Gyration and Root Mean Square Deviation of the complexes (Fig. 7). The radius of gyration of only β-amyloid oscillates for a few nm  $\pm$  around 1.2 to 1.4 nm throughout 100 ns simulations, whereas the fluctuations were reduced after 20 ns simulations Ashwagandha molecules (Fig. 7A, C, E and G). The Root mean square deviation (RMSD) was used to evaluate the structural stability of only βamyloid as well as β-amyloid-Ashwagandha derivatives complexes (Fig. 7B, D, F, H). For only β-amyloid, RMSD fluctuates to higher value (~1.2 nm) until the simulation [39]. Simultaneously, for β-amyloidwithanolide A complex, RMSD shows less fluctuations till 50 ns, and after that, there is an increase in fluctuation around  $\pm 0.3$  nm from initial. Still, in the case of β-amyloid-withanolide B complex, the RMSD values remain stable till the end of the simulation (Fig. 7D). Thus, a decrease in the RMSD value may cause the enhanced structural stability of  $\beta$ -amyloid-withanolide B complex compared to  $\beta$ -amyloid alone. While β-amyloid-withanoside IV complex and β-amyloid-withanoside V complex showed an increase in the RMSD value of ~1.5 and 1.3 nm, which explains that these molecules were in interaction with the hydrophobic site for a stable period of the trajectory as shown in Fig. 8.

To illustrate interactions between binding residues of  $\beta$ -amyloid with Ashwagandha derivatives, time frames were analyzed at different

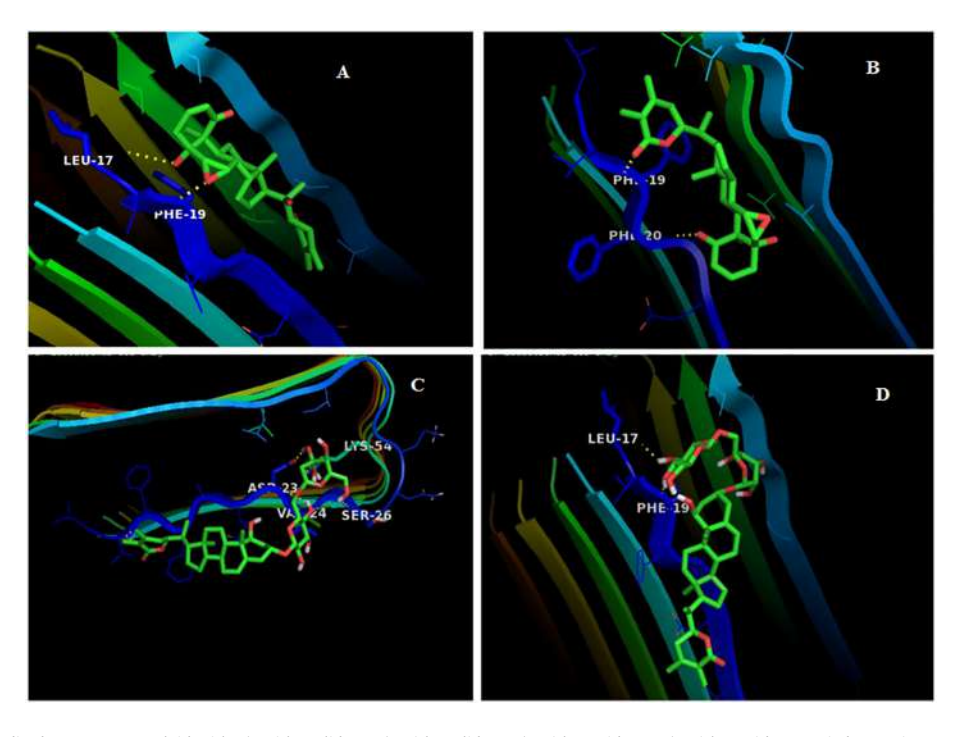


Fig. 6. Molecular docking studies between β-Amyloid with A) Withanolide A, B) Withanolide B, C) Withanoside IV, D) Withanoside V carried out using Autodock 4.2.4. Pymol is used to generate the images to represent hydrogen bond interactions between them.

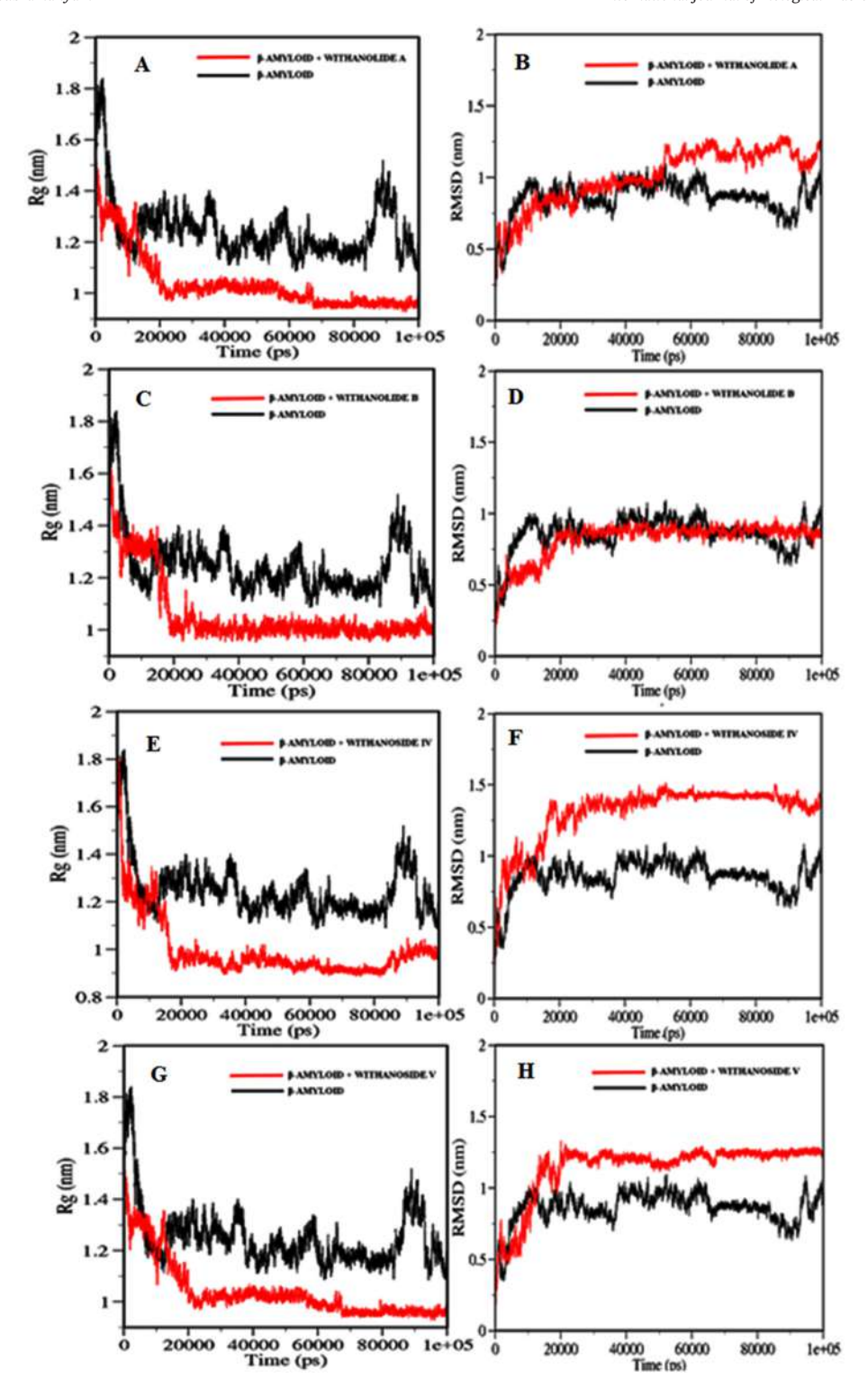
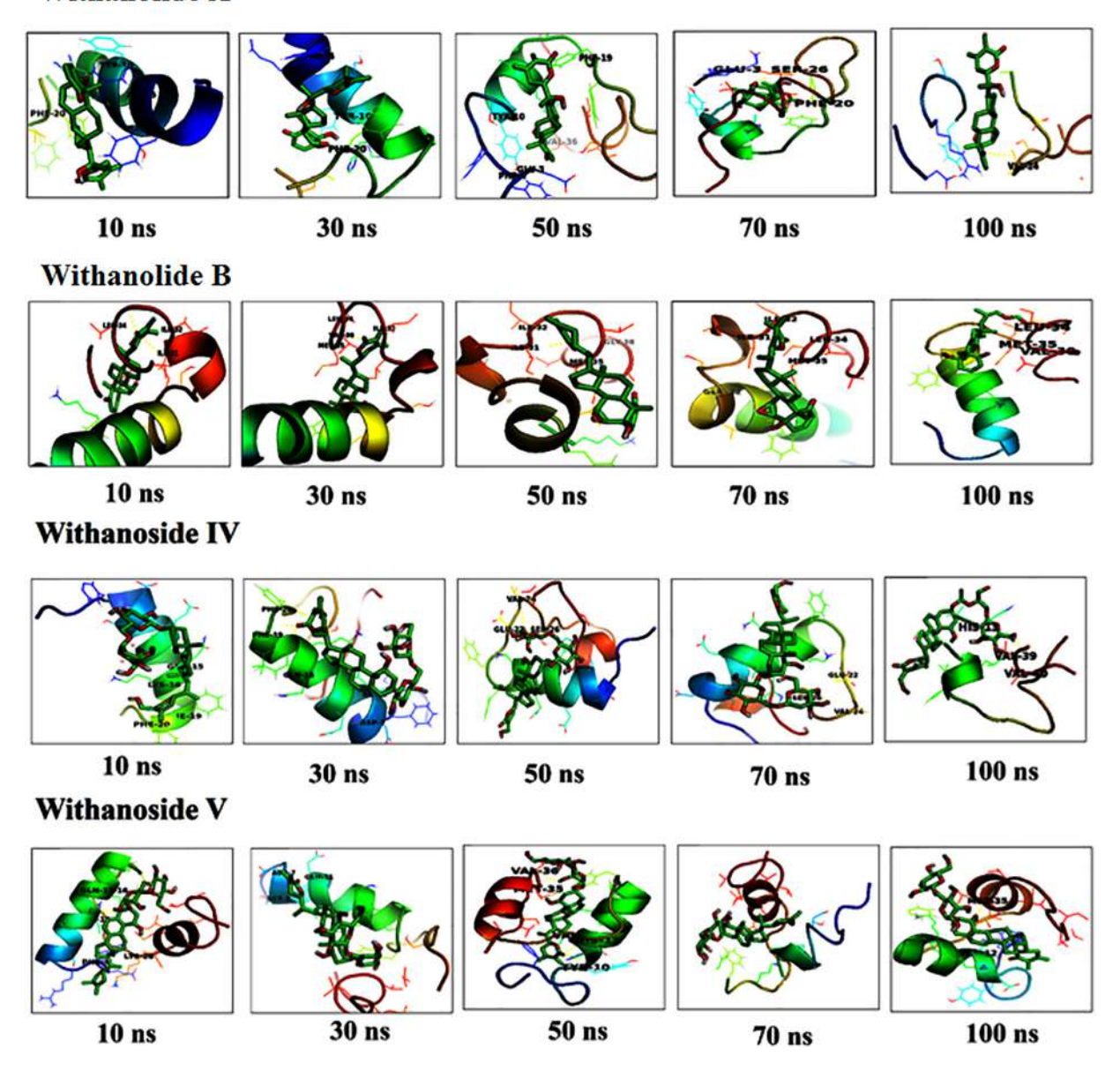


Fig. 7. The time evolution of the radius of gyration (Rg) (A,C,E,G) and Root mean square deviation (RMSD) (B,D,F,H) of only amyloid and  $\beta$ -amyloid-Ashwagandha derivatives complexes during 100 ns of simulations.

nanoseconds (10, 30, 50, 70, and 100 ns). Zhao and co-workers recently investigated  $\pi$ - $\pi$  interactions between aromatic rings of curcumin and aromatic residues of  $\beta$ -amyloid by utilizing computational studies [40]. The authors highlighted that  $\pi$ - $\pi$  interactions contribute indirectly to a decline in  $\beta$ -sheet content in A $\beta$ 42. Similar results were observed with  $\beta$ -amyloid-withanolide A complex, the withanolide A showed hydrogen bond interaction with aromatic rings of Phe19, Phe20, and later in further increase in MD simulations above 50 ns, there is a conformational change and decline in the structure of  $\beta$ -amyloid, which is also

confirmed through RMSD fluctuations (Fig. 7B). The visual inspection of conformations of  $\beta$ -amyloid-withanolide B complex during MD showed interactions in the central helix region (13–26 residues) indicates the presence of hydrophobic interactions between Withanolide B and residues of  $\beta$ -amyloid as this region is the prime hydrophobic core. The interactions with this region indicate stabilization of the central helix of  $\beta$ -amyloid by hydrophobic interactions. Previous reports on green tea constituents like gallic acid explained that it inhibits the conformation of  $\alpha$ -helix to  $\beta$ -sheet [41]. The visualization of snapshots

### Withanolide A



 $\textbf{Fig. 8.} \ \ \textbf{The conformers of } \beta \textbf{-amyloid-Ashwagandha derivatives at different nano seconds.}$ 

from MD trajectory for the complexes  $\beta$ -amyloid-withanoside IV and  $\beta$ -amyloid-withanoside V showed interaction of withanosides at the second core  $\beta$ -amyloid at the end residues (Lys28 to Va140) through hydrogen bonding and hydrophobic interactions. Even some of the studies on green tea constituent (—)-epigallocatechin gallate (EGCG), showed important mechanism of EGCG binding to amyloid aggregation of insulin through hydroxyl groups on the aromatic rings [42]. Our results also explain that the lactone ring-containing hydroxyl groups in the Ashwagandha derivatives stabilizes through hydrogen and hydrophobic bonding with  $\beta$ -amyloid in the hydrophobic core. This core has a  $\beta$ -sheet structure, is able to form noncovalent forces with other  $\beta$ -sheets of A $\beta$  peptides [43], thus the withanolide B, withanoside IV and V binding in the hydrophobic regions may prevent fibrillation.

### 4. Conclusion

Our research exploits the far potential of the derivatives of *Withania somnifera* derivatives against Alzheimer's disease. The results depicted here indicate the ability of these derivatives (withanolide A, withanolide B, withanoside IV and withanoside V) to inhibit fibrillization, as indicated

by the ThT assay. Moreover, the cell culture assays also indicate the ability of the derivatives to reduce the cytotoxic effects of amyloid  $\beta$  fibrillation. Further molecular docking results indicate that the derivatives were interacting with the hydrophobic core (17–21) residues region of  $\beta$ -amyloid thus discouraging another peptide of  $\beta$ -amyloid to come and bind and hence inhibiting the process of fibrillization. Furthermore, 100 ns simulations suggest that the Withanolide B and withanoside V complexes were stable in the hydrophobic core of  $\beta$ -amyloid. Our study is a novel biophysical, cellular and *in silico* study of phytochemicals, withanolide A, withanolide B, withanoside IV and withanoside V against the amyloid  $\beta$ -peptide fibril responsible for Alzheimer's disease, and we hope that these results would provide an insight role of these phytochemicals in the drug design against Alzheimer's disease.

### **Author statment**

RS and SD have designed the experiments; SD and MK conducted the experiments; SD and MK drafted the manuscript and SR corrected the manuscript; SR procured the financial support.

The authors does not have any conflict of the interest.

### Acknowledgement

This work was supported by Science and Engineering Research Board (SB/EMEQ-064/2014 dated 14-07-2015), India. DST-FIST, UGC-SAP, UPE-2 University of Hyderabad and DBT-CREBB, India supported infrastructure to the Department of Plant Sciences. We thank BIF, for Bioinformatics facilities and also acknowledge the AFM facility provided by School of Chemistry, University of Hyderabad. SD acknowledges CSIR for providing financial support.

### References

- M. Citron, Alzheimer's disease: strategies for disease modification, Nat. Rev. Drug Discov. 9 (5) (2010) 387.
- [2] A. Ghosh, N. Pradhan, S. Bera, A. Datta, J. Krishnamoorthy, N.R. Jana, A. Bhunia, Inhibition and degradation of amyloid beta (Af340) fibrillation by designed small peptide: a combined spectroscopy, microscopy, and cell toxicity study, ACS Chem. Neurosci. 8 (4) (2017) 718–722.
- [3] R. Roychaudhuri, M. Yang, M.M. Hoshi, D.B. Teplow, Amyloid β-protein assembly and Alzheimer disease, J. Biol. Chem. 284 (8) (2009) 4749–4753.
- [4] S. Mondal, S. Roy, S. Maity, R. Sangwan, S. Misra-Bhattacharya, Withanolide D, Carrying the baton of indian rasayana herb as a lead candidate of anti-leukemic agent in modern medicine. In: Biochem. Roles. Eukar. Cell. Surface. Macromol. Springer, Newyork, pp. 295–312.
- [5] S. Kumar, R.J. Harris, C.J. Seal, E.J. Okello, An aqueous extract of Withania somnifera root inhibits amyloid β fibril formation in vitro, Phytother. Res. 26 (1) (2012) 113–117.
- [6] E. Glotter, Withanolides and related ergostane-type steroids, Nat. Prod. Rep. 8 (4) (1991) 415–440.
- [7] S. Dubey, M. Kallubai, A. Sarkar, R. Subramanyam, Elucidating the active interaction mechanism of phytochemicals withanolide and withanoside derivatives with human serum albumin, PLoS One 13 (11) (2018), e0200053, .
- [8] L.-C. Mishra, B.B. Singh, S. Dagenais, Scientific basis for the therapeutic use of Withania somnifera (ashwagandha): a review, Altern. Med. Rev. 5 (4) (2000) 334–346.
- [9] S. Hashioka, A. Monji, T. Ueda, S. Kanba, H. Nakanishi, Amyloid-β fibril formation is not necessarily required for microglial activation by the peptides, Neurochem. Int. 47 (5) (2005) 369–376.
- [10] S.J. Basha, P. Mohan, D.P. Yeggoni, Z.R. Babu, P.B. Kumar, A.D. Rao, R. Subramanyam, A.G. Damu, New flavone-cyanoacetamide hybrids with a combination of cholinergic, antioxidant, modulation of β-amyloid aggregation, and neuroprotection properties as innovative multifunctional therapeutic candidates for Alzheimer's disease and unraveling their mechanism of action with acetylcholinesterase, Mol. Pharmacol. 15 (6) (2018) 2206–2223.
- [11] H. Levine III, Thioflavine T interaction with synthetic Alzheimer's disease  $\beta$ -amyloid peptides: detection of amyloid aggregation in solution, Protein Sci. 2 (3) (1993) 404–410.
- [12] M. Biancalana, S. Koide, Molecular mechanism of Thioflavin-T binding to amyloid fibrils, Biochim. Biophys. Acta Protein Proteomics 1804 (7) (2010) 1405–1412.
- [13] D.P. Yeggoni, A. Rachamallu, S. Dubey, A. Mitra, R. Subramanyam, Probing the interaction mechanism of menthol with blood plasma proteins and its cytotoxicity activities, J. Biomol. Struct. Dyn. 36 (2) (2018) 465–474.
- [14] D.P. Yeggoni, C. Kuehne, A. Rachamallu, R. Subramanyam, Elucidating the binding interaction of andrographolide with the plasma proteins: biophysical and computational approach, RSC Adv. 7 (9) (2017) 5002–5012.
- [15] T. Lührs, C. Ritter, M. Adrian, D. Riek-Loher, B. Bohrmann, H. Döbeli, D. Schubert, R. Riek, 3D structure of Alzheimer's amyloid-β (1–42) fibrils, Proc. Natl. Acad. Sci. 102 (48) (2005) 17342–17347.
- [16] M. Kallubai, S.P. Reddy, S. Dubey, D.B. Ramachary, R. Subramanyam, Spectroscopic evaluation of synthesized 5β-dihydrocortisol and 5β-dihydrocortisol acetate binding mechanism with human serum albumin and their role in anticancer activity, J. Biomol. Struct. Dyn. (2018) 1-46.
- [17] D.P. Yeggoni, A. Rachamallu, M. Kallubai, R. Subramanyam, Cytotoxicity and comparative binding mechanism of piperine with human serum albumin and  $\alpha$ -1-acid glycoprotein, J. Biomol. Struct. Dyn. 33 (6) (2015) 1336–1351.
- [18] B. Sudhamalla, M. Gokara, N. Ahalawat, D.G. Amooru, R. Subramanyam, Molecular dynamics simulation and binding studies of beta-sitosterol with human serum albumin and its biological relevance, J. Phys. Chem. B 114 (27) (2010) 9054–9062.
- [19] M. Kallubai, A. Rachamallu, D.P. Yeggoni, R. Subramanyam, Comparative binding mechanism of lupeol compounds with plasma proteins and its pharmacological importance, Mol. BioSyst. 11 (4) (2015) 1172–1183.

- [20] A.F. McKoy, J. Chen, T. Schupbach, M.H. Hecht, A novel inhibitor of amyloid  $\beta$  (A $\beta$ ) peptide aggregation from high throughput screening to efficacy in an animal model of alzheimer disease, J. Biol. Chem. 287 (46) (2012) 38992–39000.
- [21] W.B. Stine, K.N. Dahlgren, G.A. Krafft, M.J. LaDu, In vitro characterization of conditions for amyloid-β peptide oligomerization and fibrillogenesis, J. Biol. Chem. 278 (13) (2003) 11612–11622.
- [22] L. Jin, W. Gao, C. Liu, N. Zhang, S. Mukherjee, R. Zhang, H. Dong, A. Bhunia, Z. Bednarikova, Z. Gazova, Investigating the inhibitory effects of entacapone on amyloid fibril formation of human lysozyme, Int. J. Biol. Macromol. 161 (2020) 1393–1404.
- [23] S. Tiwari, V.S.R. Atluri, A. Yndart Arias, R.D. Jayant, A. Kaushik, J. Geiger, M.N. Nair, Withaferin a suppresses beta amyloid in APP expressing cells: studies for tat and cocaine associated neurological dysfunctions, Front. Aging Neurosci. 10 (2018) 291.
- [24] K.R.V. Kurapati, T. Samikkannu, V.S.R. Atluri, E. Kaftanovskaya, A. Yndart, M.P. Nair, β-Amyloid 1-42, hiv-1 ba-l (clade b) infection and drugs of abuse induced degeneration in human neuronal cells and protective effects of ashwagandha (Withania somnifera) and its constituent withanolide a, PLoS One 9 (11) (2014), e112818, .
- [25] J.J. Cohen, R.C. Duke, V.A. Fadok, K.S. Sellins, Apoptosis and programmed cell death in immunity, Annu. Rev. Immunol. 10 (1) (1992) 267–293.
- [26] L.C. Crowley, B.J. Marfell, A.P. Scott, N.J. Waterhouse, Quantitation of apoptosis and necrosis by annexin V binding, propidium iodide uptake, and flow cytometry, Cold Spring Harb Protoc 2016 (11) (2016) (pdb. prot087288).
- [27] N.J. Dar, N.K. Satti, P. Dutt, A. Hamid, M. Ahmad, Attenuation of glutamate-induced excitotoxicity by Withanolide-A in neuron-like cells: role for PI3K/Akt/MAPK signaling pathway, Mol. Neurobiol. 55 (4) (2018) 2725–2739.
- [28] T. Luhrs, C.A. Ritter M., D. Riek-Loher, B. Bohrmann, Proc. Natl. Acad. Sci. U. S. A. 102 (2005) 17342.
- [29] Q. Cheng, W. Qiang, Solid-state-nmr-structure-based inhibitor design to achieve selective inhibition of the parallel-in-register  $\beta$ -sheet versus antiparallel lowa mutant  $\beta$ -amyloid fibrils, J. Phys. Chem. B 121 (22) (2017) 5544–5552.
- [30] Y. Jin, Y. Sun, J. Lei, G. Wei, Dihydrochalcone molecules destabilize Alzheimer's amyloid-β protofibrils through binding to the protofibril cavity, Phys. Chem. Chem. Phys. 20 (25) (2018) 17208–17217.
- [31] M. Necula, R. Kayed, S. Milton, C.G. Glabe, Small molecule inhibitors of aggregation indicate that amyloid β oligomerization and fibrillization pathways are independent and distinct, J. Biol. Chem. 282 (14) (2007) 10311–10324.
- [32] L.O. Tjernberg, J. Näslund, F. Lindqvist, J. Johansson, A.R. Karlström, J. Thyberg, L. Terenius, C. Nordstedt, Arrest of-amyloid fibril formation by a pentapeptide ligand, J.Biol.Chem. 271 (15) (1996) 8545–8548.
- [33] C. Soto, M.S. Kindy, M. Baumann, B. Frangione, Inhibition of Alzheimer's amyloidosis by peptides that prevent  $\beta$ -sheet conformation, Biochem. Biophys. Res. Commun. 226 (3) (1996) 672–680.
- [34] R.K. Kar, Z. Gazova, Z. Bednarikova, K.H. Mroue, A. Ghosh, R. Zhang, K. Ulicna, H.-C. Siebert, N.E. Nifantiev, A. Bhunia, Evidence for inhibition of lysozyme amyloid fibrillization by peptide fragments from human lysozyme: a combined spectroscopy, microscopy, and docking study, Biomacromolecules 17 (6) (2016) 1998–2009
- [35] C. Behl, Amyloid  $\beta$  -protein toxicity and oxidative stress in Alzheimer's disease, Cell Tissue Res. 290 (3) (1997) 471–480.
- [36] P.C. May, B.D. Gitter, D.C. Waters, L.K. Simmons, G.W. Becker, J.S. Small, P.M. Robison, β-Amyloid peptide in vitro toxicity: lot-to-lot variability, Neurobiol. Aging 13 (5) (1992) 605–607.
- [37] L.K. Simmons, P.C. May, K.J. Tomaselli, R.E. Rydel, K.S. Fuson, E.F. Brigham, S. Wright, I. Lieberburg, G.W. Becker, D.N. Brems, Secondary structure of amyloid beta peptide correlates with neurotoxic activity in vitro, Mol. Pharmacol. 45 (3) (1994) 373–379.
- [38] I. Autiero, E. Langella, M. Saviano, Insights into the mechanism of interaction between trehalose-conjugated beta-sheet breaker peptides and A $\beta$  (1–42) fibrils by molecular dynamics simulations, Mol. BioSyst. 9 (11) (2013) 2835–2841.
- [39] S. Shuaib, B. Goyal, Scrutiny of the mechanism of small molecule inhibitor preventing conformational transition of amyloid-β42 monomer: insights from molecular dynamics simulations, J. Biomol. Struct. Dyn. 36 (3) (2018) 663–678.
- [40] L.N. Zhao, S.-W. Chiu, J.r.m. Benoit, L.Y. Chew, Y. Mu, The effect of curcumin on the stability of Aβ dimers, J. Phys. Chem. B 116 (25) (2012) 7428–7435.
- [41] J. Jayamani, G. Shanmugam, Gallic acid, one of the components in many plant tissues, is a potential inhibitor for insulin amyloid fibril formation, Eur. J. Med. Chem. 85 (2014) 352–358.
- [42] M. Gancar, E. Kurin, Z. Bednarikova, J. Marek, P. Mucaji, M. Nagy, Z. Gazova, Amyloid aggregation of insulin: an interaction study of green tea constituents, Sci. Rep. 10 (1) (2020) 1–12.
- [43] P.P. Mager, R. Reinhardt, K. Fischer, Molecular simulation to aid in the understanding of the  $A\beta$  (1–42) peptide of Alzheimer's disease, Mol. Simul. 26 (6) (2001) 367–379.



# Journal of Biomolecular Structure and Dynamics



ISSN: 0739-1102 (Print) 1538-0254 (Online) Journal homepage: https://www.tandfonline.com/loi/tbsd20

# Comparative binding of Swertiamarin with human serum albumin and $\alpha$ -1 glycoprotein and its cytotoxicity against neuroblastoma cells

Shreya Dubey, Monika Kallubai & Rajagopal Subramanyam

To cite this article: Shreya Dubey, Monika Kallubai & Rajagopal Subramanyam (2019): Comparative binding of Swertiamarin with human serum albumin and  $\alpha$ -1 glycoprotein and its cytotoxicity against neuroblastoma cells, Journal of Biomolecular Structure and Dynamics, DOI: 10.1080/07391102.2019.1695672

To link to this article: <a href="https://doi.org/10.1080/07391102.2019.1695672">https://doi.org/10.1080/07391102.2019.1695672</a>

	Accepted author version posted online: 22 Nov 2019. Published online: 04 Dec 2019.
Ø,	Submit your article to this journal 🗹
ılıl	Article views: 11
ď	View related articles 🗗
CrossMark	View Crossmark data 🗗



# Journal of Biomolecular Structure and Dynamics



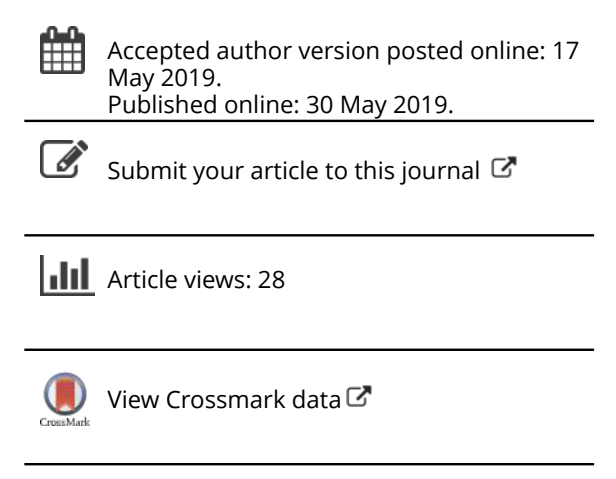
ISSN: 0739-1102 (Print) 1538-0254 (Online) Journal homepage: https://www.tandfonline.com/loi/tbsd20

# Unraveling the stability of plasma proteins upon interaction of synthesized uridine products: biophysical and molecular dynamics approach

Shreya Dubey, Suneel Kumar Madana, Monika Kallubai, Arijit Sarkar & Rajagopal Subramanyam

**To cite this article:** Shreya Dubey, Suneel Kumar Madana, Monika Kallubai, Arijit Sarkar & Rajagopal Subramanyam (2019): Unraveling the stability of plasma proteins upon interaction of synthesized uridine products: biophysical and molecular dynamics approach, Journal of Biomolecular Structure and Dynamics, DOI: <a href="https://doi.org/10.1080/07391102.2019.1620127">10.1080/07391102.2019.1620127</a>

To link to this article: <a href="https://doi.org/10.1080/07391102.2019.1620127">https://doi.org/10.1080/07391102.2019.1620127</a>









Citation: Dubey S, Kallubai M, Sarkar A, Subramanyam R (2018) Elucidating the active interaction mechanism of phytochemicals withanolide and withanoside derivatives with human serum albumin. PLoS ONE 13(11): e0200053. https://doi.org/10.1371/journal.pone.0200053

**Editor:** Durai Sundar, Indian Institute of Technology Delhi, INDIA

Received: June 12, 2018
Accepted: October 5, 2018
Published: November 7, 2018

Copyright: © 2018 Dubey et al. This is an open access article distributed under the terms of the Creative Commons Attribution License, which permits unrestricted use, distribution, and reproduction in any medium, provided the original author and source are credited.

**Data Availability Statement:** All relevant data are within the manuscript and its Supporting Information files.

**Funding:** This work was supported by Science and Engineering Research Board (SB/EMEQ-064/2014 dated 14-07-2015). SD and MK acknowledge CSIR and UGC-Kothari for fellowship.

**Competing interests:** The authors have declared that no competing interests exist.

RESEARCH ARTICLE

# Elucidating the active interaction mechanism of phytochemicals withanolide and withanoside derivatives with human serum albumin

Shreya Dubey, Monika Kallubai, Arijit Sarkar, Rajagopal Subramanyamo\*

Department of Plant Sciences, School of Life Sciences, University of Hyderabad, Gachibowli, Telangana, India

\* srgsl@uohyd.ernet.in

### **Abstract**

Withania somnifera (Ashwagandha) is an efficient medicinal plant known in Ayurveda and Chinese medicine since ancient times, whose extracts are consumed orally as food supplement or as a health tonic owing to its several restorative properties for various CNS disorders, inflammation, tumour, stress, rheumatism etc. In this study, we have analyzed the binding interaction of four derivatives of Withania somnifera (Withanolide A, Withanolide B, Withanoside IV and Withanoside V) with HSA because of their important pharmacological properties. To unravel the binding between derivatives of Withania somnifera and HSA, fluorescence spectroscopy was used. Binding studies were further studied by molecular docking and dynamics and results confirmed greater stability upon binding of derivatives with HSA. Circular dichroism data illustrated change in the secondary structure of protein upon interaction with these derivatives, particularly the helical structure was increased and βsheets and random coils were decreased. Furthermore, morphological and topological changes were observed using AFM and TEM upon binding of ligands with HSA indicating that HSA-withnoside/withanolide complexes were formed. All the results cumulatively demonstrate strong binding of withanosides and withanolides derivatives with serum albumin, which should further be explored to study the pharmacokinetics and pharmacodynamics of these derivatives.

### Introduction

Withanolide exits as secondary metabolites; structurally it consists of a steroidal backbone bound to a lactone or one of its derivatives generated from oxidation of steroids [1]. These compounds can be isolated from *Withania somnifera* (Indian Ginseng; family: *Solanacea*), also known as Ashwagandha, it is found to have numerous medicinal properties and useful in counteracting various illness like dehydration, muscle tension, memory loss and also restoring general health and vitality. This plant is known to be found globally, with more occurrences in



xeric and drier regions of tropical and subtropical areas [2,3]. We have selected four derivatives of this plant, which are withanolide A (C<sub>28</sub>H<sub>38</sub>O<sub>6</sub>-470.6Da), withanolide B (C<sub>28</sub>H<sub>38</sub>O<sub>5</sub>-454.6Da), with anoside IV ( $C_{40}H_{62}O_{15}$ -782.9Da) and with anoside V ( $C_{40}H_{62}O_{14}$ -766.9Da) for our study (Fig 1). The withanolides and withanosides are distinctive with their C-28 and C-40 steroidal lactones, with six-membered lactone ring formed by oxidization of the C-22 and C-28 on ergostane backbone. Although structurally similar, withanolide A differs from withanolide B with the presence of an extra hydroxyl group on C-20 atom, whereas withanoside IV differs from withanoside V with the presence of an extra hydroxyl group on C-27 atom. The derivatives of Withania somnifera have been used since time immemorial in Ayurveda and ancient system of medicine for its pharmacological activities like chemopreventive, antiinflammatory, anti-arthritic, and angiogenesis activity [4]. These compounds are also known to exhibit nootropic effect and are effective against several neurodegenerative diseases including Alzheimer's and Parkinson's disease [5], hence Ashwagandha derivatives have become very popular oral supplement globally because of its strong remedial properties. Owing to the remedial properties of withanolides and withanosides, their affinity to bind with human serum albumin (HSA) was carried out, which might play crucial role in its pharmacokinetics and pharmacodynamics.

Albumin is a major circulating protein in blood plasma, comprising approximately 60% of the blood proteins [6,7] is a non-glycosylated protein of 66.5KDa, and 585 amino acids having 67%  $\alpha$ - helix in its native conformation [8]. It has three domains I, II and III; each having two

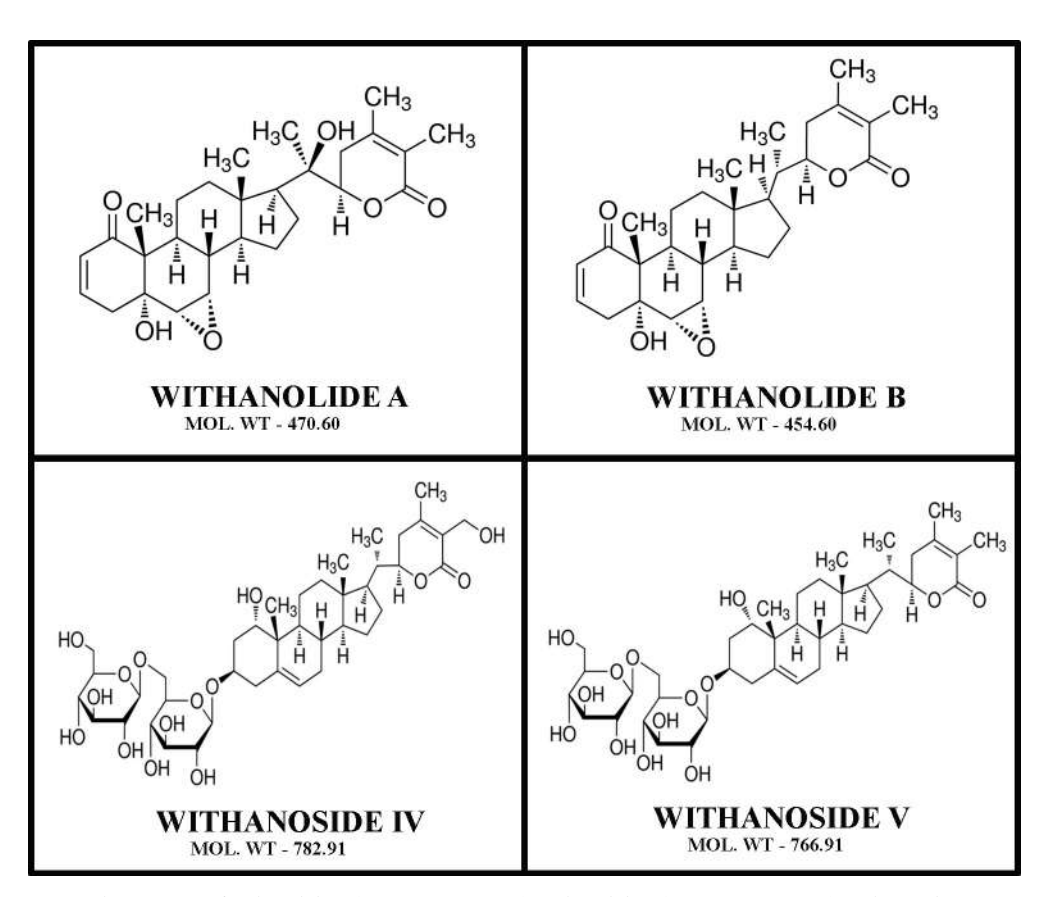


Fig 1. The structure of with anolide A ( $C_{28}H_{38}O_6$ -470.6Da), with anolide B ( $C_{28}H_{38}O_5$ -454.6Da), with anoside IV ( $C_{40}H_{62}O_{15}$ -782.9Da) and with anoside V ( $C_{40}H_{62}O_{14}$ -766.9Da).

https://doi.org/10.1371/journal.pone.0200053.g001



sub-domains A and B, which are connected via random coils. It has two important drug binding sites known as Sudlow's site II and I [9,10] which are domain IIIA, IIA and also domain IB noticed as one of drug binding site [11]. It is well established that HSA has 35 residues of Cys and forms 17 disulfide bonds that contributes to the stability of the protein. The single  $34^{th}$  residue of Cys imparts the protein its anti-oxidant property [12]. This negatively acute phase protein exerts pharmacological property because of its long half-life of 19 days, and its ability to bind with several exogenous as well as endogenous compounds [13]. The interaction between the drugs and plasma protein influences the absorption, bio-distribution, metabolism and excretion of the drug. Our group has earlier reported various therapeutic phytochemicals like lupeol, trimethoxyflavone, asiatic acid, lupeol and  $\beta$ -sitosterol its derivative binds strongly to serum albumin [14–17].

Since with anolide is having several kind of biological importance and we presume that other four derivatives of with anolide A ( $C_{28}H_{38}O_6$ ), with anolide B ( $C_{28}H_{38}O_5$ ), with anoside IV ( $C_{40}H_{62}O_{15}$ ) and with anoside V ( $C_{40}H_{62}O_{14}$ ) also may have good the rapeutic role. So far the role of these molecules in biological samples including *in vitro* or *in vivo* have not been explored. Since, human serum albumin is an important transport protein, we have chosen this protein to study the pharmocokinetics and pharmakodynamics of the phytocompounds.

### Materials and methods

### Preparation of stock solutions

Fat free HSA was procured from Sigma Aldrich and working concentration of  $100\mu M$  was made by dissolving in 100mM PBS of pH 7.4 to maintain the physiological condition. Withanolides A (CAS No. 32911-62-9), B (CAS No. 56973-41-2) and withanosides IV (CAS No. 362472-81-9), V (CAS No. 256520-90-8) which are extracts of extracts of Indian Ginseng plant which were procured from Natural Remedies Pvt.Ltd, Bengaluru, India with purity of ~99%. These compounds were first dissolved in dimethyl sulphoxide (DMSO) at 20 mM. This stock solution was further diluted to a concentration of  $100\mu M$  working stock in PBS (pH 7.4) similar to our previously reported studies [18,19]. All other chemicals used were of analytical grade from Sigma Aldrich.

### Room temperature fluorescence spectra

Fluorescence spectroscopy is an astounding technique used to study the interaction between protein and ligands and calculation of binding constant and free energy. Concentration of HSA was kept constant at  $1\mu M$  and Withanolides A&B and withanosides IV & V were titrated in an increasing concentration from  $1\mu M$  to  $9\mu M$  in 0.1mM PBS of pH 7.4. Perkin Elmer LS55 fluorescence spectrometer was used to record the spectra and incubation time for all the derivatives were kept constant for 5 mins. Emission spectra was recorded in the range of 300-500nm, with parameters set around like our previous studies [20]. Excitation wavelength of HSA was kept at 285 nm and slit width 5 nm for excitation and emission spectra. Three independent experiments were carried out and each time spectra recorded was almost identical.

### Molecular displacement

For determining the exact binding site of the withanolides A&B and withanosides IV&V derivatives to HSA, we have studied the interaction of these derivatives with HSA in the presence of certain site specific markers (Lidocaine for domain I, Phenylbutazone for domainII, and Ibuprofen for domain III [21–23]. The choices for the site specific individual markers were based upon previous studies, it has been proved that these markers were specific to the site I–III, and



extensive binding site studies of different ligands with HSA were given in the literature. In view of those studies, we have purchased these markers from Sigma alridch with catalogue No. for our studies (Lidocaine (CAS No. 137-58-7), Phenylbutazone (CAS No. 137-58-7) and Ibuprofen for domain III (CAS No. 15687-27-1). The concentration of HSA and the markers were kept constant at 1  $\mu$ M, and remaining all parameters were same as fluorescence spectroscopy. Experiments were done in triplicates and based upon the binding energy values, the binding sites were determined.

### Circular dichroism measurements

For exploring the conformational change of the protein upon addition of a ligand, circular dichroism is referred to as the 'Gold Standard'technique. Circular dichroism (CD) spectropolarimeter, Jasco-815 was used for the study and the temperature was kept constant at 25 °C. Spectra were recorded in a quartz cell with path length of 0.02cm. Data was recorded from 190-260nm with scan speed of 50nm/sec. The concentration of HSA was persistent at 1 $\mu$ M and the concentation of drugs 2, 4, 6  $\mu$ M were added gradually similar to the previous studies [24]. CDNN 2.1 web based software was used to calculate the change in percentage of  $\alpha$ -helix,  $\beta$ -sheet and random coils from its native conformation upon addition of withanolides and withanosides with increasing concentrations.

### Atomic force microscopy

Atomic Force Microscopy was used to visually detect any change in the topography of the protein molecule surface upon addition of the ligand. AFM experiments were done by NT-MDT solver scanning probe microscopy in semi contact mode using cantilever (0.3mm) with a force constant (5.5–22.5N/m) and the typical imaging resonance frequency was 140 kHz. 3.6x 1.6x0.4mm was the size of the gold-coated silicon probes used; tip height was 14–16µm and radius of curvature 10 nm [25]. For sample preparation, 20 µL of 2 µM free HSA was spread on a glass slide and incubated for 10 minutes and then it was washed with 1ml de-ionized water to remove loosely bound molecules from the surface; and for HSA-ligand complexes, 20 µL of a 10 µM with anolides and with anosides were first incubated with HSA and similarly spread on a glass slide, washed and dried under for 5 min. The dried samples were then imaged by AFM in non-contact mode.

### Transmission electron microscopy (TEM)

FE1 Tecnai  $G^2S$ -Twin-200kv instrument was used to observe the change in the morphology of the protein upon addition of the ligand, in high resolution.  $1\mu M$  HSA was used as the control and for HSA-ligand complexes,  $1\mu M$  HSA was incubated with  $2\mu M$  of withanolides (A and B) and withanosides (IV and V) individually. A drop of these samples was added on the carbon coated copper grids and excess sample was removed by absorption with filter paper. Before drying of the samples 2% uranyl acetate negative stain was added and final observation was made as described[19].

### Molecular docking

Molecular docking is a computation tool used to predict the predominant binding mode of the ligand to a protein and to locate geometrically and energetically the most stable conformer complex. Here, we have used Autodock 4.2.3 (http://autodock.scripps.edu) to generate the 50 docked conformers of the protein ligand complexes by using genetic lamarckian algorithm. The crystal structure of HSA (PDB ID: 1AO6) was downloaded from the Brookhaven Protein



Data Bank. Three-dimensional structure of with anolides and withanosides was built from 2D structure and geometry, and optimized using Discovery studio 3.5 software. Water molecules were removed, Kollmann charges and polar hydrogen atoms were added to the PDB structure of HSA before analysis. Grid size of  $126 \times 126 \times 126$  along X, Y and Z axis with 0.586 Å grid spacing was generated to carry out blind docking of withanolides and withanosides with HSA. The docking parameters used were: maximum number of energy evolutions: 250,000; GA population size: 150; and the number of GA runs; 30 [26]. The conformer with the lowest binding energy was used for further studies and it was in sync with the experimental results obtained by Fluorescence spectroscopy.

### Molecular dynamics

Molecular dynamics (MD) Simulation for 10 ns was performed at 300K and 1 bar pressure for the energetically most stable conformer by using GROMACS V 4.6.3 software (http://www.gromacs.org). The free energy obtained from fluorescence and the best conformer from docking results was used for the MD simulations. The topology parameters of HSA were created by using Dundee PRODRG2.5 server (http://davapc1.bioch.dundee.ac.uk/cgi-bin/prodrg). The complex structure was immersed in a box of  $7.335 \times 6.135 \times 8.119 \text{ nm}^3$  dimension with extended simple point charge (SPC) water molecules. Sodium counter ions were added to maintain electro-neutrality. All the parameters were same as our previously reported work [27]. Simulation and analysis were performed on Linux cluster with 36 nodes (dual Xeon processor) at the Bioinformatics facility, University of Hyderabad.

### Results

### Fluorescence spectroscopy

The active principles of these phytochemicals withanolide A, withanolide B, withanoside IV and withanoside V were not well understood related to food supplements but ashwagandha has been used as a ayurvedic remedy for various ailments. Since, HSA is an important protein to transport the small molecules to the target places, thus, we have focused our study to understand the binding mechanism of these isolated molecules with HSA. The intrinsic fluorescence in HSA is because of the presence of a single tryptophan residue at the position 214, also there are 18 tyrosine and 33 phenylalanine residues. By continuous titration of phytochemicals withanolide A, withanolide B, withanoside IV and withanoside V to HSA, the fluorescence of protein was quenched. These results inferthat the intrinsic fluorescence of HSA is quenched gradually with increasing concentrations of withanolides and withanosides derivatives because of the change in microenvironment around Trp214 residue. Its inner filter affect can be corrected by using the following equation,

$$F_{cor} = F_{obs} 10(A_{exc} + A_{emi})/2 \tag{1}$$

Where  $F_{cor}$  and  $F_{obs}$  are corrected and observed fluorescence intensity respectively.  $A_{ext}$  and  $A_{emi}$  are absorbance at fluorescence excitation (285 nm) and emission (360 nm) wavelengths [28]. To validate whether the complex is undergoing dynamic or static quenching, bimolecular quenching constant was calculated from the slope of  $F_O/F$  vs Q and it was found to be linear, which indicates that it is undergoing static quenching. The fluorescence data was analyzed using the stern-volmer equation

$$Fo/F = 1 + k_a t_0[Q] = 1 + K_D[Q]$$
 (2)

where F<sub>0</sub> and F are fluorescence intensities, in the absence and presence of the quencher. Q is

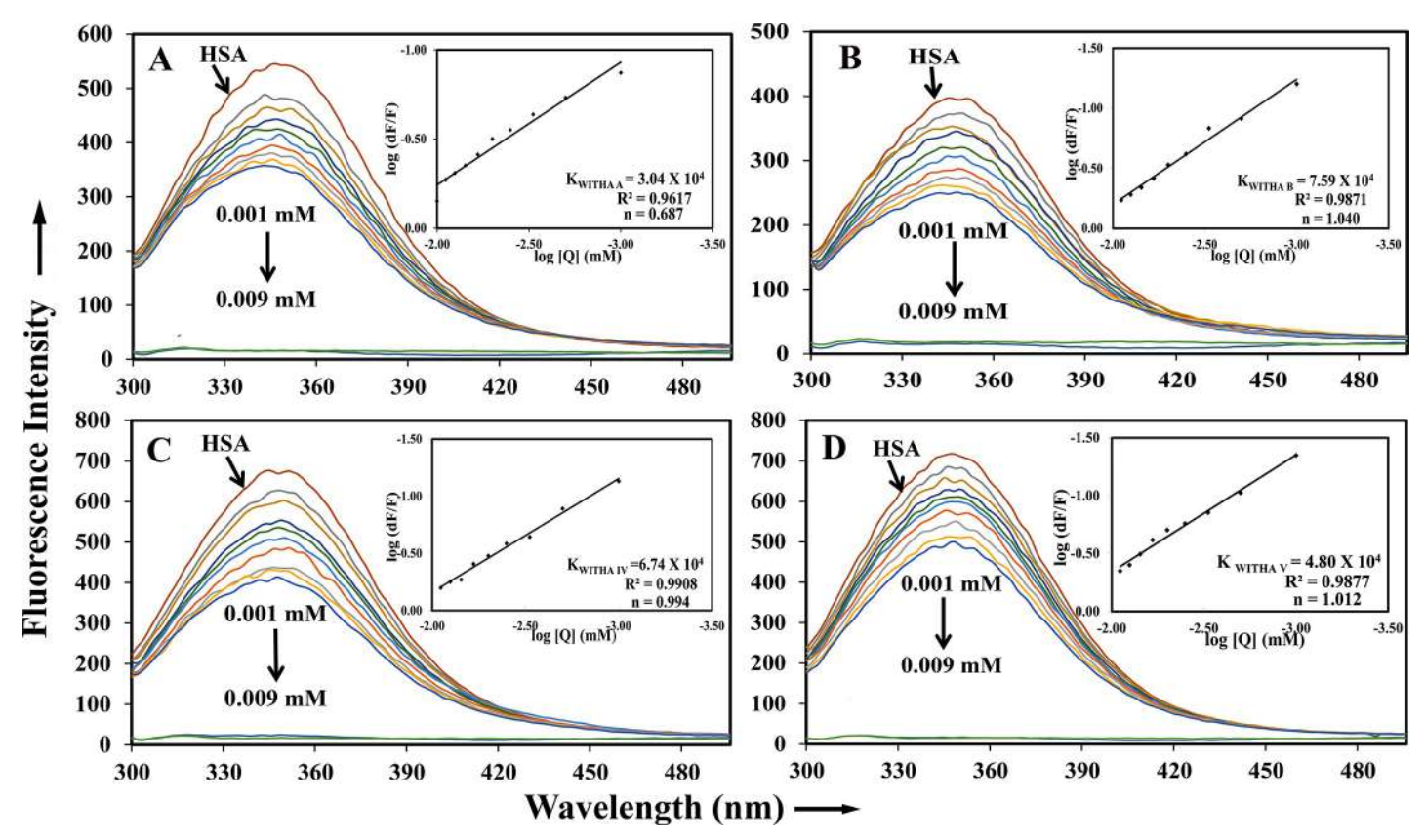


Fig 2. Fluorescence spectroscopic studies of HSA with withanolide and withanoside molecules, indicating the interaction of the drug with plasma protein. The association constant ( $K_S$ ) and free energy change along with stern-volmer plots showing fluorescence quenching constant ( $K_S$ ) and plot of Fo/F against [Q] at  $K_S$  and  $K_S$  nm and  $K_S$  nm for (A) withanolide A, (B) withanolide B, (C) withanoside IV and (D) withanoside V.

quencher concentration and  $K_D$  is the stern-volmer quenching constant which can be written as  $K_D = Kqt_0$ ;  $t_0$  is the lifetime of the fluorophore for HSA (5.6ns). Since the interaction between withanolides and withanosides, and HSA is by static mode of binding, the modified stern-volmer regression curve is used to determine the binding constant (Ks) and the number of binding sites (n), where n is the slope and Ks is the binding constant.

$$\log[(Fo - F)/F] = \log K_c + n\log[Q] \tag{3}$$

The binding constants were calculated to be  $K_{Withanolide\ A} = 3.04\pm0.05\ X\ 10^4\ M^{-1}$ ,  $K_{Withanolide\ B} = 7.59\pm0.05\ X\ 10^4\ M^{-1}$ ,  $K_{Withanoside\ IV} = 6.74\pm0.03\ X\ 10^4\ M^{-1}$  and  $K_{Withanoside\ V} = 5.33\pm0.05\ X\ 10^4\ M^{-1}$  respectively as shown in (Fig 2A–2D). This data indicates that withnolide and withanoside derivatives are strongly binding to the HSA. Hence, our results are in agreement with previously published phytochemicals were strongly associated with HSA [29,30]. Also, the obtained binding constants are in concurrence with the food and drug administration (FDA) which indicates that phytochemicals used here withanolide A, withanolide B, withanoside IV and withanoside V could be potential therapeutic molecules.

The standard free energy change is calculated by using the following equation.

$$\Delta G^{\circ} = -RT \ln K \tag{4}$$

Where  $\Delta G$  is the free energy change, R is the gas constant at room temp and K is binding constant calculated from fluorescence data. The free energy changes upon binding of



with anolides and withanosides with HSA was -5.61 Kcal  $\mathrm{M}^{-1}$ , -6.63 Kcal  $\mathrm{M}^{-1}$ , -6.56 Kcal  $\mathrm{M}^{-1}$ and -6.36 Kcal  $\mathrm{M}^{-1}$  respectively at 25  $^{0}$  C. This indicates that the interaction between the drugswith serum albumin is mainly hydrophobic interactions. The computationally derived free energy change was found to be totally in sync with the experimental data.

### Displacement studies

Using site specific markers we can understand the exact binding of ligand molecules to the specific domains of HSA. Hence, there are different site specific markers like lidocaine for domain I, phenylbutazone for domain II and ibuprofen for domain III [22] and using these markers the fluorescence was performed to analyze the specific binding domain of HSA on interaction with withanoside and withanolide derivatives [28,31]. Because of the structural and molecular similarity of four derivatives, all of them showed fluorescence emission quenching by displacing phenylbutazone, i.e. they are binding on domain II of HSA with a binding constant were  $K_{\text{WithanolideA+pb}} = 2.57 \pm 0.05 \text{ X } 10^4 \text{ M}^{-1}$ ,  $K_{\text{WithanolideB+pb}} = 6.84 \pm 0.05 \text{ X } 10^4 \text{ M}^{-1}$ ,  $K_{\text{WithanosideIV+pb}} = 1.89 \pm 0.05 \text{ X } 10^4 \text{ M}^{-1}$  and  $K_{\text{WithanosideV+pb}} = 4.80 \pm 0.03 \text{ X } 10^4 \text{ M}^{-1}$ . The free energy changes for different were -6.09 Kcal  $M^{-1}$ , -6.56 Kcal  $M^{-1}$ , -7.17 Kcal  $M^{-1}$  and -6.42 Kcal  $M^{-1}$  respectively(Fig 3A–3D). We also performed with other site specific markers (i.e lidocaine, ibuprofen), however, they were not displaced by the withnolide compounds. These results indicate that the drug molecules are specifically binding to Sudlow's drug binding site I. Our

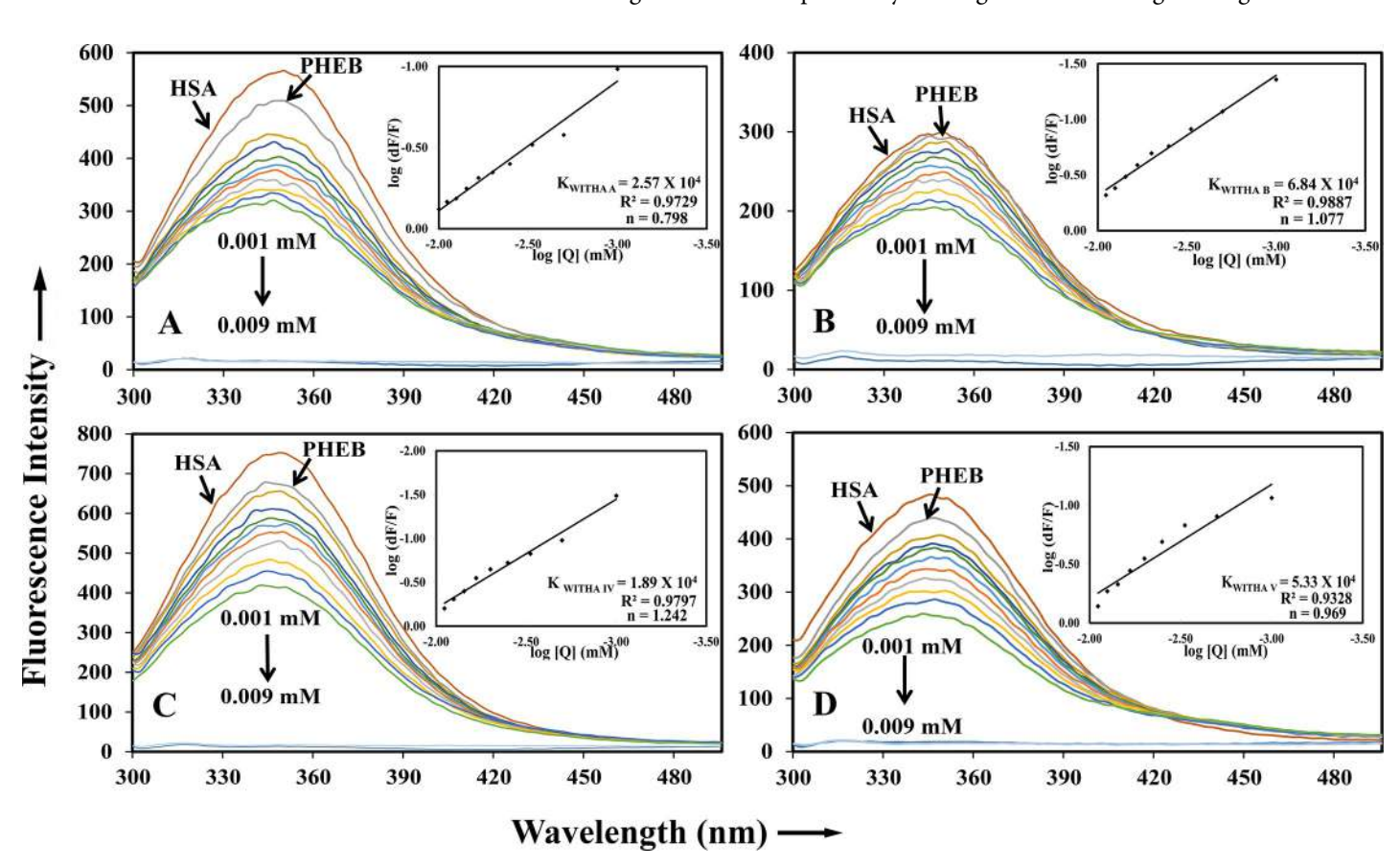


Fig 3. Site displacement studies using site-specific markers; Phenylbutazone (PHEB) was used as marker for HSA domain IIA (Sudlow site I). Fluorescence spectroscopic studies performed using HSA and Phenylbutazone at equal concentrations ( $1\mu$ M) and drugs with increasing concentrations ( $1\mu$ M ~  $9\mu$ M) (A) HSA-PHEB-withanolide A (B) HSA-PHEB-withanolide B (C) HSA-PHEB-withanoside IV and (D) HSA-PHEB-withanoside V.

https://doi.org/10.1371/journal.pone.0200053.g003



Experimental results are in congruence with the computational data as also illustrated in our previous reports [32].

### Circular dichroism

Circular dichroism is a fundamental technique to study any secondary structural change upon interaction of protein and ligand. HSA showed a dip at 208 and 222nm in the far UV region which are mainly originated from helical structure [20]. The secondary structure of HSA comprises of 58%  $\alpha$ -helix, 20%  $\beta$ -sheet (parallel and anti-parallel) and 22% random coils, but upon titration with withanolide and withanoside molecules there was partial unfolding of HSA protein and change in the dip in 208 and 222nm as shown in (Fig 4A–4D).

Conformational analysis was done using CDNN software, shows the percentage of  $\alpha$ -helix increasing up to 69.30±2.5, 70.54±2.5, 66.8±2.5 and 61.5±2.3 upon binding with withanolide A, withanolide B, withanoside IV and withanoside V respectively, and simultaneously there is decrease in the percentage of  $\beta$ -sheet and random coil (S1 Table). In general most of the ligand molecules binding to HSA [33,34]. Similar studies were done for various molecules and revealed that upon binding of ligands, there is change in the secondary structure of HSA[35].

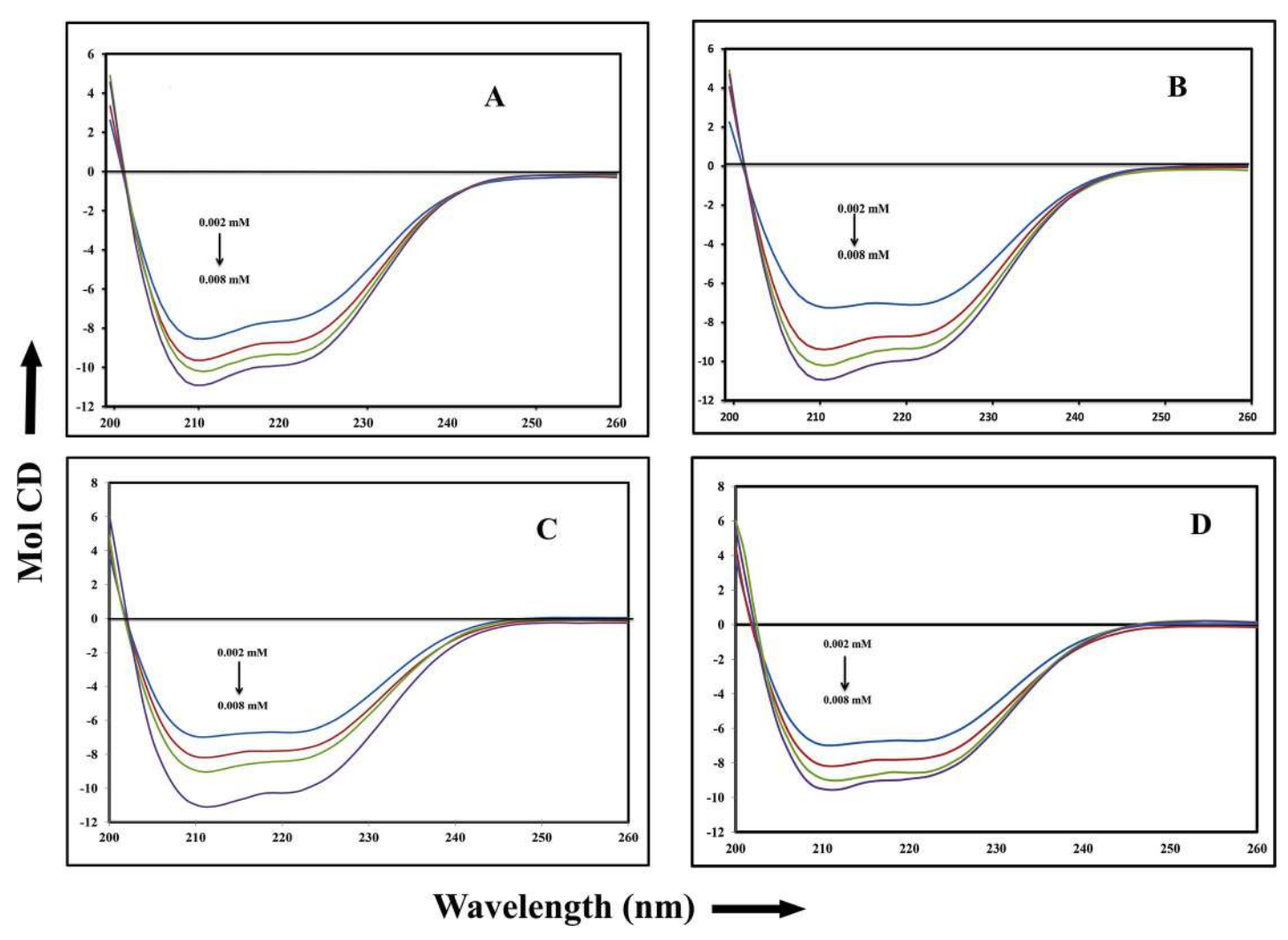


Fig 4. Circular Dichroism studies of the free HSA and HSA-drug complexes. The free HSA and HSA-drug complexes in aqueous solution with a protein concentration fixed at  $1\mu M$  and with increasing drug concentrations at 2,4, and 6  $\mu M$ . (A) with anolide A (B) with anolide B (C) with anoside IV and (D) with anoside V.

https://doi.org/10.1371/journal.pone.0200053.g004



### Topological observations from atomic force microscopy

To corroborate topological changes in surface of free HSA and HSA upon addition of drug derivatives, atomic force microscopy (AFM) was used. The results explain that upon incubation with drug molecules, there is a significant increase in the size of the complex as shown in (Fig 5A–5J). But as the molecular weight of withanoside IV and withanoside V is larger than that of withanolide A and withanolide B, the complex formed by interaction with withanoside IV and withanoside V are larger. The unliganded HSA is showing a small size comparatively with bound HSA with withanaloides, and the results corroborate with the previous studies [36]. The complex in the presence of withanolide (A, B), and withanoside (IV, V) were showing remarkable increase in size i.e. growing around to become 70nm, 130nm, 190 nm and 300 nm (S1 Fig). These results indicate that the above molecules are formed complexes with HSA. Our results deciphered that it could be the hydrophobic contacts play a major role while binding of withanolides and withanosides compounds with HSA complexation [37] which is in an agreement with the free energy calculations. These experiments were performed in triplicates and similar results were reproduced always.

### Transmission emission microscopy

TEM was used to visualize the structural and topographical change in HSA and ligated HSA upon incubation with various drug derivatives [38]. At resolution of  $0.2\mu M$  the size of unligated HSA molecule were found to be of size  $0.04\pm10\mu M$ , whereas in the presence of withanolide A and B, and withanoside IV and V, it increased to  $0.06\pm10\mu M$ ,  $0.06\pm10\mu M$ , and  $0.07\pm10\mu M$ ,  $0.08\pm10\mu M$  respectively (Fig 6A–6E), which can interprets the complexes formed by the interaction of HSA with these derivatives. Thus, it can be derived that interaction among the protein and withanolide A, withanolide B, withanoside IV and withanoside V are taking place and these results are in harmony with the results obtained from other techniques.

### Molecular docking

The displacement studies by the use of site specific markers indicated that the withanolide and with anoside derivatives were binding at Sudlow's drug binding site I of HSA. Autodock 4.2.3 software was used further to confirm the precise binding site and residues on HSA upon binding of these derivatives. Since the binding location of the protein is of utmost importance to study the biological activity of the drug and it also plays a major role in pharmacokinetics and pharmacodynamics of the drug. Crystal structure of HSA was procured from Protein Data Bank (PDB Code: 1A06). Withanolide A is binding to HSA by hydrogen bond formation by interacting with Glu208 in the hydrophobic cavity of subdomain IIA, and withanolide B is interacting with His338, withanoside IV is forming a hydrogen bond at Arg197 and Lys205, and withanoside V is interacting with residues of Tyr341 and Tyr334 and Leu305; with binding constants of K<sub>Withanolide A</sub> = 4.93 X  $10^4 \,\mathrm{M}^{-1}$ ,  $K_{\text{Withanolide B}} = 7.42 \,\mathrm{X} \, 10^4 \,\mathrm{M}^{-1}$ ,  $K_{\text{Withanoside IV}} = 2.50 \,\mathrm{X} \, 10^4 \,\mathrm{M}^{-1}$  and  $K_{\text{Withanoside V}} = 2.49 \,\mathrm{X}$  $10^4 \,\mathrm{M}^{-1}$  and free energy were be -6.40 Kcal  $\mathrm{M}^{-1}$ , -6.64 Kcal  $\mathrm{M}^{-1}$ , -3.27 Kcal  $\mathrm{M}^{-1}$  and -3.26 Kcal  $\mathrm{M}^{-1}$ respectively at 25 °C respectively. The results were shown in (Fig 7A–7L), and are generated by using the Pymol software (https://pymol.org), and Ligplot (www.ebi.ac.uk/thornton-srv/software/ LIGPLOT) is used to illustrate the two-dimensional interaction by hydrogen bond formation and hydrophobic interactions. The Binding constant values calculated computationally were in accordance with the values obtained experimentally [31,39].

### Molecular dynamics

Molecular simulation studies compute the behaviour of a system as a function of time. It has emerged as a powerful tool for understanding the interaction between protein and ligands to



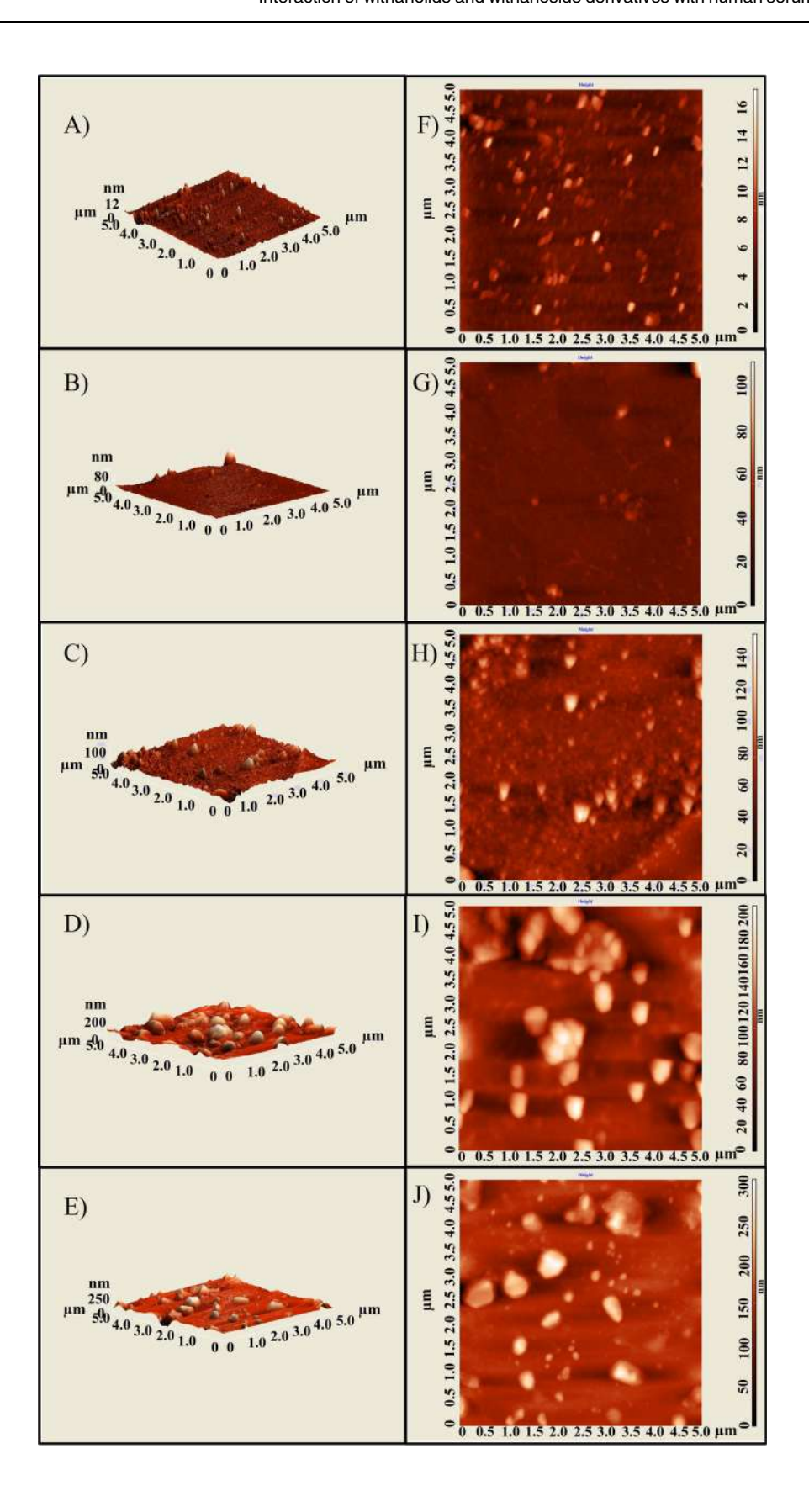




Fig 5. Atomic Force Microscopic (AFM) studies to visualize alteration in HSA molecule topology in presence of with anolide and with anoside derivatives at 10  $\mu$ M resolution. (A) Only HSA (B) HSA+with anolide A (C) HSA +with anolide B (D) HSA+with anolide IV and (E) HSA+with anolide V.

predict how conformational changes occur to achieve the lowest free energy conformer. Usually, RMSD (root mean square deviation), RMSF (Root mean square fluctuation) and Rg (radius of gyration) are used to know the change in the microenvironment, atomic fluctuation, rigidity and stability of the HSA-ligand complexes in comparison to HSA alone [40,41]. Hence, in our study we have measured the same parameters for HSA with withanolide and

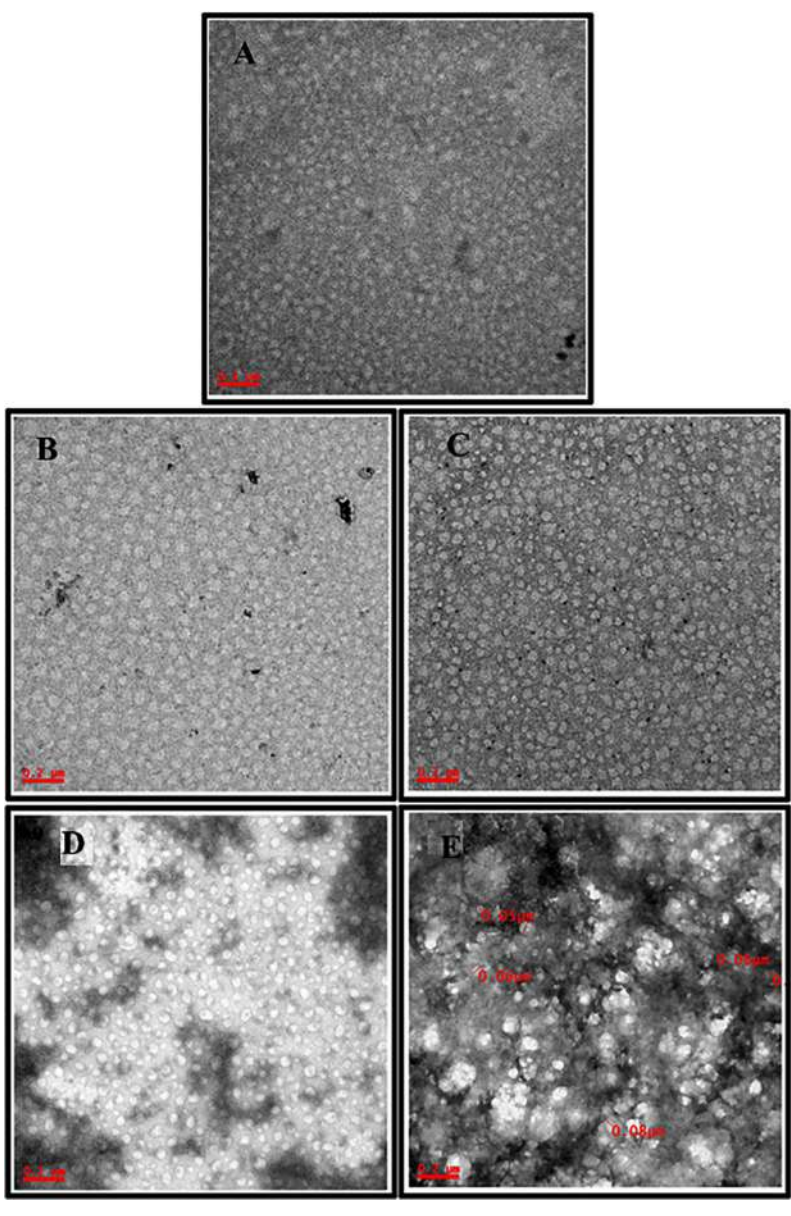


Fig 6. Transmission Electron Microscopic (TEM) studies to visualize alteration in HSA molecule topology in presence of with anolide and withanoside derivatives at 200 nM resolution. (A) Only HSA (B) HSA+ withanolide A, (C) HSA+ withanolide B, (D) HSA+ withanolide IV and (E) HSA+ withanolide V.

https://doi.org/10.1371/journal.pone.0200053.g006



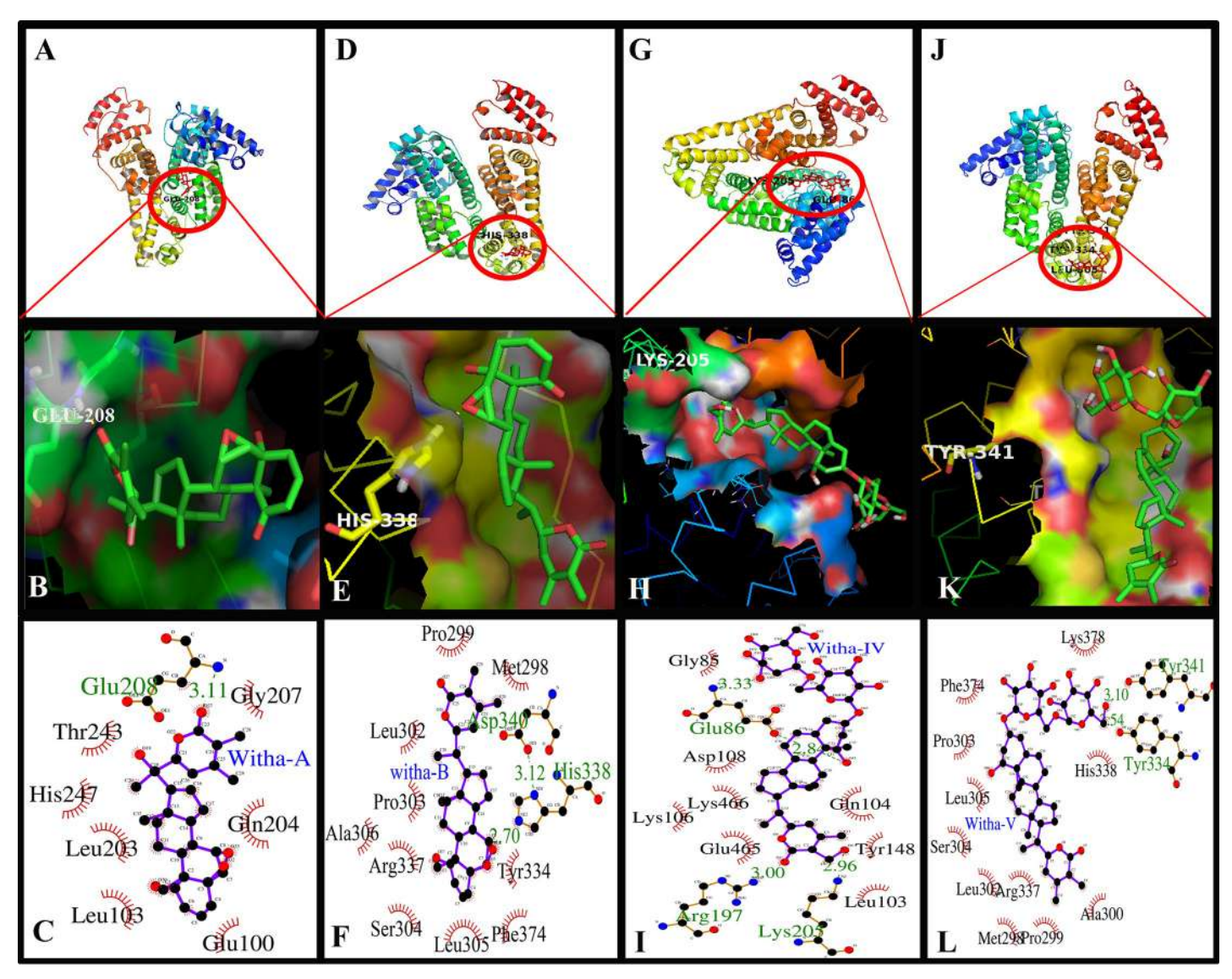


Fig 7. Molecular docking studies between HSA and withanolide A, withanolide B, withanoside IV and withanoside V showed that the minimum binding energy conformer is very close to the experimentally determined values. (A, D, G, J) Cartoon model of HSA showing withanolide derivatives A, B, IV and V docked in the binding pocket using Autodock 4.2. (B, E, H, K) Pymol generated images showing withanolide A, withanolide B, withanoside IV and withanoside V binding in their specific binding site of HSA. The cavity of hydrophobic and hydrophilic amino acid residues surrounding the probe. (C, F, I, L) Ligplot showing the hydrophobic interactions of HSA with withanolide derivatives.

with anoside complexes to understand the interaction mechanism. Energetically the most stable complex of docking was taken and dynamics was studied for 10ns.

Generally, Rg is used for measuring the compactness of structure, hence Rg of with anolides and withanosides complexes showed stability throughout the 10ns after initial rigidity at 2ns. The Rg value of unliganded HSA is,  $2.65\pm0.35$ nm, the complex HSA-withanolide A, HSA-withanolide B, HSA-withanoside IV and HSA-withanoside V showed fluctuations in between  $2.63\pm0.05$ nm,  $2.61\pm0.02$ nm,  $2.65\pm0.03$ nm, and  $2.65\pm0.02$ nm, respectively showing the stability of the complexes. These results indicate the conformational and stability changes in the secondary structure of HSA, which is totally in congruence with the results obtained from circular dichroism.



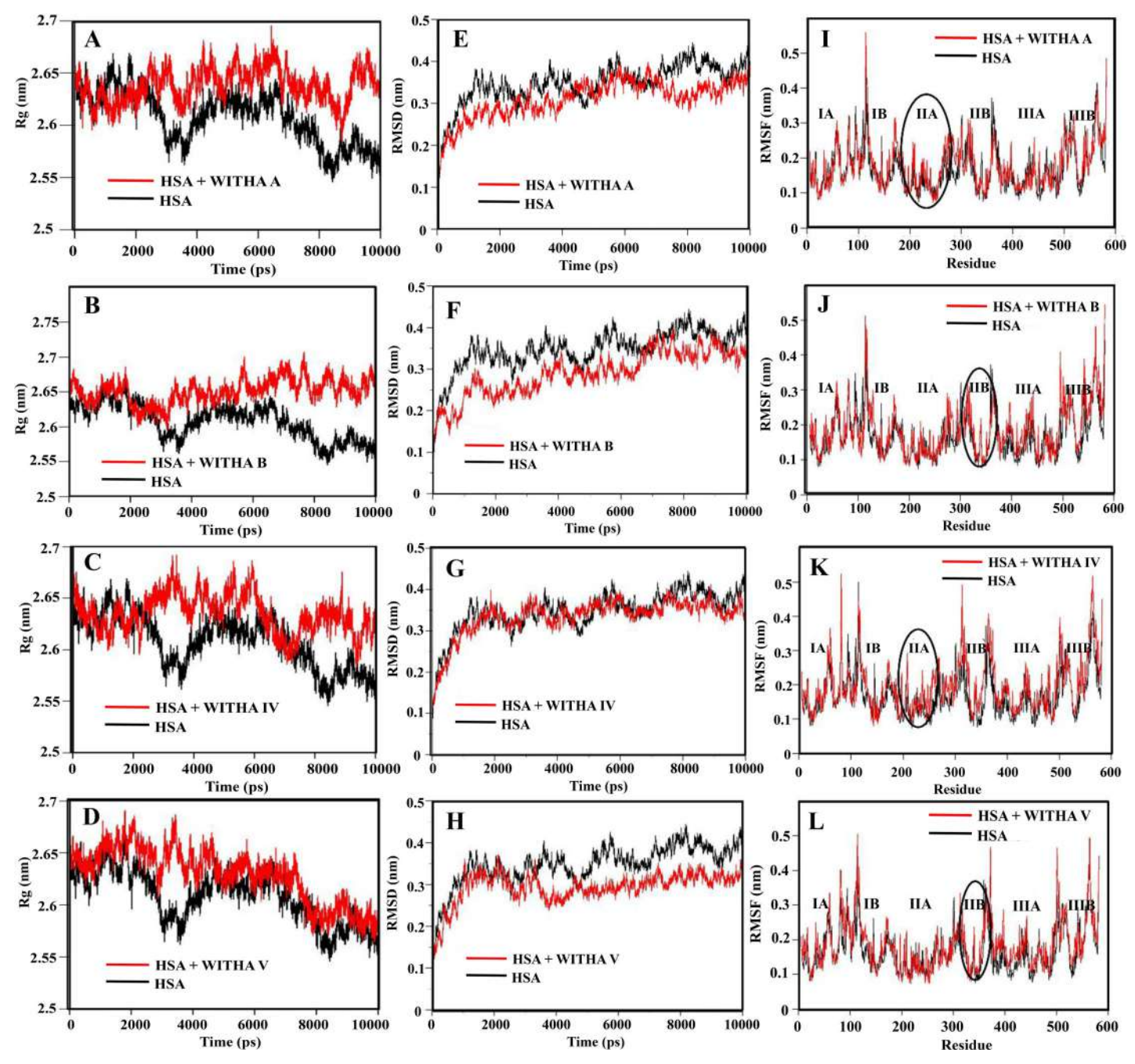


Fig 8. (A-D)-Time evolution of the radius of gyration (Rg) during 10 ns of MD simulation of unliganded HSA and HSA-drug derivatives complexes. (E-H)-Plot of RMSD values for unliganded HSA and HSA-drug derivatives complexes. (I-L)- Comparison of the RMSF of Calcium atoms along the sequence derived from the 10 ns simulations.

To access the stability of the system RMSD of the complex atoms was analysed as a function of time for MD trajectory. The RMSD values of atoms of protein backbone (C-C $\alpha$ -N) were calculated for only HSA and HSA-ligand complex. RMSD of HSA-withanolide A, HSA-withanolide B, HSA-withanoside IV, and HSA-withanoside V showed stability at 3ns and remained constant throughout 10ns. From 0-10ns trajectory data the RMSD value of unliganded HSA is 0.4 $\pm$ 0.03nm while for HSA-ligand complexes fluctuations were in between 0.3 $\pm$ 0.03nm, while



with anolide B had initial fluctuations which later stabilized at 6.5 ns from 0.35±0.03nm as shown in (Fig 8A-8L). It can be concluded that the complexes remain stable with no major change from the initial docked conformer owing to the stability of the ligated HSA.

Rigidity of peptide structure and thermal vibrations were measured by RMSF values. Local protein mobility was seen by analysing the time averaged RMSF values of only HSA and the HSA-drug complexes. As these derivates of withanolide A, withanolide B, withanoside IV and withanoside V binds to HSA, there is increased rigidity and flexibility in different sub domains of HSA which is plotted against the residue number. The microenvironment around the binding site showed strong overlapping of binding region of the HSA-withanolide A, HSA-withanolide B, HSA-withanoside IV and HSA-withanoside V and are in between 200–250 residues which are a part of hydrophobic cavity of HSA and there is more rigidity around those amino acids indicating strong interaction at binding site 1(S2 Fig). Hence, MD data is an indication that the withanolide A, withanolide B, withanoside IV and withanoside V derivatives are binding with HSA with stable conformations and hence this study can be extend to study the therapeutic role in biological samples.

### **Conclusions**

The goal of this study was to elucidate the effect of interaction of phytocompounds, i.e. derivatives of Withania somnifera (Ashwagandha) namely withanolide A, withanolide B, with anoside IV and with anoside V, with carrier plasma protein HSA. Quenching of fluorescence emission of HSA showed the formation of HSA-ligand complex formation with binding constant of  $K_{Withanolide\ A} = 3.04\pm0.05\ X\ 10^4\ M^{-1}$ ,  $K_{Withanolide\ B} = 7.59\pm0.05\ X\ 10^4\ M^{-1}$ ,  $K_{\text{Withanoside IV}} = 6.74 \pm 0.03 \text{ X } 10^4 \text{ M}^{-1}$  and  $K_{\text{Withanoside V}} = 5.33 \pm 0.05 \text{ X } 10^4 \text{ M}^{-1}$ . These binding constants fall under the range of 103–10<sup>6</sup> M<sup>-1</sup>, which is in the range of known FDA approved drugs. Circular Dichroism also shows partial unfolding of the protein upon interaction of these molecules with HSA and further it was confirmed by AFM and TEM on basis of morphological and topological changes in the protein-ligand complexes. Our experimental results illustrated strong binding between these derivatives with HSA and isin corroboration with the in silico data of molecular docking and MD simulations. Owing to similar molecular and structural formula all the derivatives of Withania somnifera, were seen to displace phenylbutazone and bind on Sudlow's site I. Using MD simulation the stability of only HSA and HSA-drug complexes were qualitatively compared for 10 ns. The study undertaken in our lab will be helpful in further understanding the pharmacokinetics and pharmacodynamics of these compounds and it provides a base to further exploit the far-reaching pharmaceutical potential of these steroidal derivatives.

### Supporting information

**S1 Fig. The profile of atomic fluctuations.** Atomic fluctuations of unliganded HSA and HSA-Withanolide and Withanoside complexes to the active site amino acid residues present in the site I of HSA.

(DOCX)

S2 Fig. The HSA-withanoside derivative complexes at 10 ns simulations showed rigidity of residues in their respective domains.

(DOCX)

S1 Table. This table shows percentage change in the secondary structure upon addition of different concentration of withanolide and withanoside drugs.

(DOCX)



### **Acknowledgments**

We thank Bioinformatics facility, School of Life Sciences, University of Hyderabad for computer facility. SD and MK acknowledges CSIR and UGC-Kothari for fellowship.

### **Author Contributions**

Conceptualization: Rajagopal Subramanyam.

Data curation: Shreya Dubey, Monika Kallubai, Arijit Sarkar.

Formal analysis: Shreya Dubey.

Funding acquisition: Rajagopal Subramanyam.

Investigation: Shreya Dubey, Monika Kallubai, Rajagopal Subramanyam.

Methodology: Shreya Dubey, Monika Kallubai, Arijit Sarkar.

**Project administration:** Rajagopal Subramanyam.

Resources: Rajagopal Subramanyam.

Software: Monika Kallubai.

Validation: Shreya Dubey, Monika Kallubai, Arijit Sarkar.

Visualization: Monika Kallubai.

Writing - original draft: Shreya Dubey, Rajagopal Subramanyam.

Writing – review & editing: Rajagopal Subramanyam.

### References

- Glotter E. Withanolides and related ergostane-type steroids. Nat Prod Rep. 1991; 8(4):415–40. https://doi.org/10.1039/NP9910800415 PMID: 1787922.
- Dhar N, Razdan S, Rana S, Bhat WW, Vishwakarma R, Surrinder K. A Decade of Molecular Understanding of Withanolide Biosynthesis and In vitro Studies in Withania somnifera (L.) Dunal: Prospects and Perspectives for Pathway Engineering. Front Plant Sci. 2015; 6(1031)1–20. https://doi.org/10.3389/fpls.2015.01031 PMID: 26640469.
- Mirjalili MH, Moyano E, Bonfill M, Cusido RM, Palazon J. Steroidal lactones from Withania somnifera, an ancient plant for novel medicine. Molecules. 2009; 14(7):2373–93. <a href="https://doi.org/10.3390/molecules14072373">https://doi.org/10.3390/molecules14072373</a> PMID: 19633611.
- 4. Verma SK, Kumar K. Therapeutic uses of Withania somnifera (Ashwagandha) with a note on withanolides and its pharmacological actions. Asian J Pharm Clin Res. 2011; 4(1):1–4.
- Mishra LC, Singh BB, Dagenais S. Scientific basis for the therapeutic use of Withania somnifera (ashwagandha): a review. Altern Med Rev. 2000; 5(4):334–46. PMID: 10956379.
- Chuang VT, Otagiri M Stereoselective binding of human serum albumin. Chirality. 2006; 18(3):159–66. https://doi.org/10.1002/chir.20237 PMID: 16432913.
- 7. Peters T Jr. Serum albumin. Adv Protein Chem. 1985; 37:161–245. PMID: 3904348.
- 8. Carter DC, He XM, Munson SH, Twigg PD, Gernert KM, et al. Three-dimensional structure of human serum albumin. Science. 1989; 244(4909):1195–8. PMID: 2727704.
- 9. Peters TJ. All About Albumin. Academic Press. 1995; 1–432 ISBN: 9780080527048.
- Sudlow G, Birkett DJ, Wade DN Further characterization of specific drug binding sites on human serum albumin. Mol Pharmacol. 1976; 12(6):1052–61. PMID: 1004490.
- Zsila F Subdomain IB Is the Third Major Drug Binding Region of Human Serum Albumin: Toward the Three-Sites Model. Mol Pharm. 2013; 10(5):1668–82. https://doi.org/10.1021/mp400027q PMID: 23473402.
- Curry S, Brick P, Franks NP. Fatty acid binding to human serum albumin: new insights from crystallographic studies. Biochim Biophys Acta. 1999; 1441(2–3):131–40. PMID: 10570241.



- Varshney A, Sen P, Ahmad E, Rehan M, Subbarao N, Khan RH. Ligand binding strategies of human serum albumin: how can the cargo be utilized? Chirality. 2010; 22(1):77–87. <a href="https://doi.org/10.1002/chir.20709">https://doi.org/10.1002/chir.20709</a> PMID: 19319989.
- Gokara M, Sudhamalla B, Amooru DG, Subramanyam R.) Molecular interaction studies of trimethoxy flavone with human serum albumin. PLoS One. 2010; 5(1):e8834. https://doi.org/10.1371/journal. pone.0008834 PMID: 20098677.
- Gokara M, Malavath T, Kalangi SK, Reddana P, Subramanyam R Unraveling the binding mechanism of asiatic acid with human serum albumin and its biological implications. J Biomol Struct Dyn. 2014; 32 (8):1290–302. https://doi.org/10.1080/07391102.2013.817953 PMID: 23844909.
- Kallubai M, Rachamallu A, Yeggoni DP, Subramanyam R Comparative binding mechanism of lupeol compounds with plasma proteins and its pharmacological importance. Mol Biosyst. 2015; 11(4):1172– 83. https://doi.org/10.1039/c4mb00635f PMID: 25710711.
- Sudhamalla B, Gokara M, Ahalawat N, Amooru DG, Subramanyam R Molecular dynamics simulation and binding studies of beta-sitosterol with human serum albumin and its biological relevance. J Phys Chem B. 2010; 114(27):9054–62. https://doi.org/10.1021/jp102730p PMID: 20565066.
- 18. Gokara M, Narayana VV, Sadarangani V, Chowdhury SR, Varkala S, Ramachary DB, Subramanyam R. Unravelling the binding mechanism and protein stability of human serum albumin while interacting with nefopam analogues: a biophysical and insilico approach. J Biomol Struct Dyn. 2017; 35(10):2280–2292. https://doi.org/10.1080/07391102.2016.1216895 PMID: 27453381.
- Yeggoni DP, Rachamallu A, Subramanyam R Protein stability, conformational change and binding mechanism of human serum albumin upon binding of embelin and its role in disease control. J Photochem Photobiol B. 2016; 160:248–59. <a href="https://doi.org/10.1016/j.jphotobiol.2016.04.012">https://doi.org/10.1016/j.jphotobiol.2016.04.012</a> PMID: 27130964.
- Subramanyam R, Gollapudi A, Bonigala P, Chinnaboina M, Amooru DG Betulinic acid binding to human serum albumin: a study of protein conformation and binding affinity. J Photochem Photobiol B. 2009; 94(1):8–12. https://doi.org/10.1016/j.jphotobiol.2008.09.002 PMID: 18945624.
- Yamasaki K, Rahman MH, Tsutsumi Y, Maruyama T, Ahmed S, Kragh-Hansen U, et al. Circular dichroism simulation shows a site-II-to-site-I displacement of human serum albumin-bound diclofenac by ibuprofen. AAPS PharmSciTech. 2000; 1(2):E12. https://doi.org/10.1208/pt010212 PMID: 14727845
- Ghuman J, Zunszain PA, Petitpas I, Bhattacharya AA, Otagiri M, Curry S. Structural basis of the drugbinding specificity of human serum albumin. J Mol Biol. 2005; 353(1):38–52. <a href="https://doi.org/10.1016/j.jmb.2005.07.075">https://doi.org/10.1016/j.jmb.2005.07.075</a> PMID: 16169013.
- Hein KL, Kragh-Hansen U, Morth JP, Jeppesen MD, Otzen D, Moller JV, et al. Crystallographic analysis reveals a unique lidocaine binding site on human serum albumin. J Struct Biol. 2010; 171(3):353–60. https://doi.org/10.1016/j.jsb.2010.03.014 PMID: 20347991.
- Yeggoni DP, Manidhar DM, Suresh Reddy C, Subramanyam R Investigation of binding mechanism of novel 8-substituted coumarin derivatives with human serum albumin and alpha-1-glycoprotein. J Biomol Struct Dyn. 2016; 34(9):2023–36. https://doi.org/10.1080/07391102.2015.1104264 PMID: 26440860.
- Yeggoni DP, Rachamallu A, Subramanyam R. A comparative binding mechanism between human serum albumin and [small alpha]-1-acid glycoprotein with corilagin: biophysical and computational approach. RSC Adv. 2016; 40225–40237. https://doi.org/10.1039/C6RA06837E.
- Yeggoni DP, Rachamallu A, Kallubai M, Subramanyam R Cytotoxicity and comparative binding mechanism of piperine with human serum albumin and alpha-1-acid glycoprotein. J Biomol Struct Dyn. 2015; 33(6):1336–51. https://doi.org/10.1080/07391102.2014.947326 PMID: 25054206.
- Yeggoni DP, Subramanyam R Binding studies of L-3,4-dihydroxyphenylalanine with human serum albumin. Mol Biosyst. 2014; 10(12):3101–10. https://doi.org/10.1039/c4mb00408f PMID: 25209359.
- Yadav SA, Yeggoni DP, Devadasu E, Subramanyam R Molecular binding mechanism of 5-hydroxy-1-methylpiperidin-2-one with human serum albumin. J Biomol Struct Dyn. 2018; 36(3):810–817. <a href="https://doi.org/10.1080/07391102.2017.1300106">https://doi.org/10.1080/07391102.2017.1300106</a> PMID: 28278025.
- 29. Sun Y-e, Wang W-d. Study on the interaction of bioactive compound S-allyl cysteine from garlic with serum albumin. J Food Drug Anal. 2017; 25:385–390. https://doi.org/10.1016/j.jfda.2016.08.013 PMID: 28911681.
- Gokara M, Kimavath GB, Podile AR, Subramanyam R Differential interactions and structural stability of chitosan oligomers with human serum albumin and alpha-1-glycoprotein. J Biomol Struct Dyn. 2015; 33(1):196–210. https://doi.org/10.1080/07391102.2013.868321 PMID: 24359035.
- Yeggoni DP, Kuehne C, Rachamallu A, Subramanyam R. Elucidating the binding interaction of andrographolide with the plasma proteins: biophysical and computational approach. RSC Adv. 2017; 7:5002–5012. https://doi.org/10.1039/C6RA25671F.



- Nerusu A, Srinivasa Reddy P, Ramachary D, Subramanyam R Unraveling the Stability of Plasma Proteins upon Interaction of Synthesized Androstenedione and Its Derivatives—A Biophysical and Computational Approach. ACS Omega. 2017; 2(10):6514–6524. https://doi.org/10.1021/acsomega.7b00577 PMID: 30023521.
- Yuan L, Liu M, Liu G, Li D, Wang Z, et al. Competitive binding of (-)-epigallocatechin-3-gallate and 5-fluorouracil to human serum albumin: A fluorescence and circular dichroism study. Spectrochim Acta A Mol Biomol Spectrosc. 2017; 173:584–592. <a href="https://doi.org/10.1016/j.saa.2016.10.023">https://doi.org/10.1016/j.saa.2016.10.023</a> PMID: 27776313.
- **34.** Subramanyam R, Goud M, Sudhamalla B, Reddeem E, Gollapudi A, Nallaepalli S, et al. Novel binding studies of human serum albumin with trans-feruloyl maslinic acid. J Photochem Photobiol B. 2009; 95 (2):81–8. https://doi.org/10.1016/j.jphotobiol.2009.01.002 PMID: 19230701.
- Neelam S, Gokara M, Sudhamalla B, Amooru DG, Subramanyam R Interaction studies of coumaroyltyramine with human serum albumin and its biological importance. J Phys Chem B. 2010; 114(8):3005

  12. https://doi.org/10.1021/jp910156k PMID: 20136105.
- Kallubai M, Reddy SP, Dubey S, Ramachary DB, Subramanyam R Spectroscopic evaluation of synthesized 5β-dihydrocortisol and 5β-dihydrocortisol acetate binding mechanism with human serum albumin and their role in anticancer activity. J Biomol Struct Dyn. 2018; 1–18. <a href="https://doi.org/10.1080/07391102.2018.1433554">https://doi.org/10.1080/07391102.2018.1433554</a> PMID: 29375009.
- Chanphai P, Froehlich E, Mandeville JS, Tajmir-Riahi HA Protein conjugation with PAMAM nanoparticles: Microscopic and thermodynamic analysis. Colloids Surf B Biointerfaces. 2017; 150:168–174. https://doi.org/10.1016/j.colsurfb.2016.11.037 PMID: 27914253.
- Huang J, Xie J, Chen K, Bu L, Lee S, Cheng Z, et al. HSA coated MnO nanoparticles with prominent MRI contrast for tumor imaging. Chem Commun (Camb). 2010; 46(36):6684–6. https://doi.org/10. 1039/c0cc01041c PMID: 20730157.
- Li S, He J, Huang Y, Wang Q, Yang H, Xu K, et al. Interactions of cucurbit[6,7]urils with human serum albumin and their effects on zaltoprofen transportation. RSC Adv. 2016; 6:85811–85819. <a href="https://doi.org/10.1039/C6RA17508B">https://doi.org/10.1039/C6RA17508B</a>.
- Rapaport DC, Blumberg RL, McKay SR, Christian W. The Art of Molecular Dynamics Simulation. Computers in Physics. 1998; 1–456 https://doi.org/10.1063/1.4822471.
- Radibratovic M, Minic S, Stanic-Vucinic D, Nikolic M, Milcic M, et al. Stabilization of Human Serum Albumin by the Binding of Phycocyanobilin, a Bioactive Chromophore of Blue-Green Alga Spirulina: Molecular Dynamics and Experimental Study. PLoS One. 2016; 11(12):e0167973. https://doi.org/10.1371/journal.pone.0167973 PMID: 27959940.



#### Journal of Biomolecular Structure and Dynamics



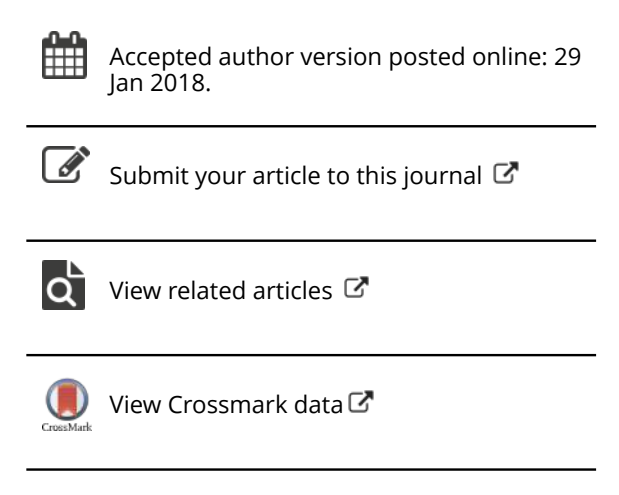
ISSN: 0739-1102 (Print) 1538-0254 (Online) Journal homepage: http://www.tandfonline.com/loi/tbsd20

# Spectroscopic evaluation of synthesized $5\beta$ -dihydrocortisol and $5\beta$ -dihydrocortisol acetate binding mechanism with human serum albumin and their role in anticancer activity

Monika Kallubai, Srinivasa P Reddy, Shreya Dubey, Dhevalapally B Ramachary & Rajagopal Subramanyam

To cite this article: Monika Kallubai, Srinivasa P Reddy, Shreya Dubey, Dhevalapally B Ramachary & Rajagopal Subramanyam (2018): Spectroscopic evaluation of synthesized  $5\beta$ -dihydrocortisol acetate binding mechanism with human serum albumin and their role in anticancer activity, Journal of Biomolecular Structure and Dynamics, DOI: 10.1080/07391102.2018.1433554

To link to this article: <a href="https://doi.org/10.1080/07391102.2018.1433554">https://doi.org/10.1080/07391102.2018.1433554</a>





#### Journal of Biomolecular Structure and Dynamics



ISSN: 0739-1102 (Print) 1538-0254 (Online) Journal homepage: http://www.tandfonline.com/loi/tbsd20

## Probing the interaction mechanism of menthol with blood plasma proteins and its cytotoxicity activities

Daniel Pushparaju Yeggoni, Aparna Rachamallu, Shreya Dubey, Argha Mitra & Rajagopal Subramanyam

**To cite this article:** Daniel Pushparaju Yeggoni, Aparna Rachamallu, Shreya Dubey, Argha Mitra & Rajagopal Subramanyam (2017): Probing the interaction mechanism of menthol with blood plasma proteins and its cytotoxicity activities, Journal of Biomolecular Structure and Dynamics, DOI: 10.1080/07391102.2017.1286264

To link to this article: <a href="http://dx.doi.org/10.1080/07391102.2017.1286264">http://dx.doi.org/10.1080/07391102.2017.1286264</a>

+	View supplementary material 🗗
	Accepted author version posted online: 16 Feb 2017. Published online: 08 Mar 2017.
	Submit your article to this journal 🗹
dil	Article views: 5
α	View related articles 🗹

Full Terms & Conditions of access and use can be found at http://www.tandfonline.com/action/journalInformation?journalCode=tbsd20

Binding of phytochemicals derived from Withania somnifera to human serum albumin and its derivative peptides retard amyloid fibrillation

by Shreya Dubey

Submission date: 25-Jan-2021 10:39AM (UTC+0530)

Submission ID: 1493779141 File name: shreya.docx (125.32K)

Word count: 22289

Character count: 119989

Prof. S. RAJAGOPAL

Dept. of Plant Sciences
School of Life Sciences
University of Hyderabad

Hyderabad-500 046.

Binding of phytochemicals derived from Withania somnifera to human serum albumin and its derivative peptides retard amyloid fibrillation

ORIGINALITY REPORT

27%

SIMILARITY INDEX

INTERNET SOURCES

**PUBLICATIONS** 

Hyderabad-500 046.

Hyderabad-500 046.

PRIMARY SOURCES



Shreya Dubey, Monika Kallubai, Rajagopal Subramanyam. "Improving the inhibition of βamyloid aggregation by withanolide and withanoside derivatives", International Journal of s. RAJAGOPAL School of Life Sciences University of Hyderabad Biological Macromolecules, 2021

Publication



journals.plos.org

Internet Source



Shreya Dubey, Monika Kallubai, Arijit Sarkar, Rajagopal Subramanyam. "Elucidating the active interaction mechanism of phytochemicals. Prof. S. RAJAGOPAL withanolide and withanoside derivatives with Dept. of Plant Sciences School of Life Sciences Laboratory, 2018 to bring to your kind notice that Alliversity of Hyderabad Publication plagianism Report (45%) of mur DL D Hadain Angles and 1966. human serum albumin", Cold Spring Harbor

reviewed international

www.science.gov

Prof. S. RAJAGOPAL Dept. of Plant Sciences School of Life Sciences, University of Hyderabad Hyderabad-500 046.

14 US.WOW.COM
Internet Source

Internet Source

<1%

15	Gokara, Mahesh, Tirupathi Malavath, Suresh Kumar Kalangi, Pallu Reddana, and Rajagopal Subramanyam. "Unraveling the binding mechanism of asiatic acid with human serum albumin and its biological implications", Journal of Biomolecular Structure and Dynamics, 2014. Publication	<1%
16	Neil J. Bruce, Deliang Chen, Shubhra G. Dastidar, Gabriel E. Marks, Catherine H. Schein, Richard A. Bryce. "Molecular dynamics simulations of A $\beta$ fibril interactions with $\beta$ -sheet breaker peptides", Peptides, 2010 Publication	<1%
17	www.randox-lifesciences.com Internet Source	<1%
18	Veerababu Nagati, Sailaja Nakkka, Daniel Pushparaju Yeggoni, Rajagopal Subramanyam. "Forskolin-loaded human serum albumin nanoparticles and its biological importance", Journal of Biomolecular Structure and Dynamics, 2019 Publication	<1%
19	www.tandfonline.com Internet Source	<1%
20	ir.amu.ac.in Internet Source	<1%

Fabio Sterpone, Olivia Berthoumieu et al.

"Amyloid β Protein and Alzheimer's Disease:

When Computer Simulations Complement

Experimental Studies", Chemical Reviews, 2015

Publication

Hanie Mahaki, Hamid Tanzadehpanah, Osama K. Abou-Zied, Neda Hosseinpour Moghadam et al. "Cytotoxicity and antioxidant activity of Kamolonol acetate from Ferula pseudalliacea, and studying its interactions with calf thymus DNA (ct-DNA) and human serum albumin (HSA) by spectroscopic and molecular docking techniques", Process Biochemistry, 2019

Publication

Renu Wadhwa, Arpita Konar, Sunil C. Kaul.
"Nootropic potential of Ashwagandha leaves:
Beyond traditional root extracts",
Neurochemistry International, 2016

<1%

Publication

25

Shreya Dubey, Suneel Kumar Madana, Monika Kallubai, Arijit Sarkar, Rajagopal Subramanyam. "Unraveling the stability of plasma proteins upon interaction of synthesized uridine products: biophysical and molecular dynamics approach",

<1%

of. S. RAJAGOPAL
Dept. of Plant Sciences
School of Life Sciences
School of Hyderabad
University of Hyderabad
Hyderabad-500 046.

### Journal of Biomolecular Structure and Dynamics, 2019

Publication

Sławomir Wójcik, Melissa Birol, Elizabeth Rhoades, Andrew D. Miranker, Zachary A. Levine. "Targeting the Intrinsically Disordered Proteome Using Small-Molecule Ligands", Elsevier BV, 2018

<1%

- Publication
- Weiying Liu, Fengxian Sun, Moxin Wan, Fang Jiang, Xiangyu Bo, Laixiang Lin, Hua Tang, Shumei Xu. "β-Sheet Breaker Peptide-HPYD for the Treatment of Alzheimer's Disease: Primary Studies on Behavioral Test and Transcriptional Profiling", Frontiers in Pharmacology, 2018

<1%

Eun Jeong Cho, Seung In Um, Jeong Hoon Han, Byeonghee Kim et al. "The cytoprotective effect of Rumex Aquaticus Herba extract against hydrogen peroxide-induced oxidative stress in AGS cells", Archives of Pharmacal Research, 2016

<1%

- Publication
- answersdrive.com

<1%

Internet Source

30

Daniel Pushparaju Yeggoni, Mahesh Gokara, Darla Mark Manidhar, Aparna Rachamallu et al.

<1%

"Binding and Molecular Dynamics Studies of 7-Hydroxycoumarin Derivatives with Human Serum Albumin and Its Pharmacological Importance", Molecular Pharmaceutics, 2014 Publication

31	Sirirat Klongpanichapak. "Melatonin protects SK-N-SH neuroblastoma cells from amphetamine-induced neurotoxicity", Journal of Pineal Research, 8/2007 Publication	<1%
32	"Taurine 11", Springer Science and Business Media LLC, 2019 Publication	<1%
33	www.medicalnewstoday.com Internet Source	<1%
34	"Science of Ashwagandha: Preventive and Therapeutic Potentials", Springer Science and Business Media LLC, 2017 Publication	<1%
35	www.interimhealthcare.com Internet Source	<1%
36	"Albumin in Medicine", Springer Science and Business Media LLC, 2016 Publication	<1%
37	Mohd Aamir, Vinay Kumar Singh, Manish Kumar	<1%

Dubey, Mukesh Meena et al. "In silico

Prediction, Characterization, Molecular Docking, and Dynamic Studies on Fungal SDRs as Novel Targets for Searching Potential Fungicides Against Fusarium Wilt in Tomato", Frontiers in Pharmacology, 2018

Publication

Veerababu Nagati, Monika Kallubai, Dinesh Kumar Chinthapalli, Rajagopal Subramanyam. "Exploration of binding studies of β-oxalyldiamino propionic acid (β-ODAP), a non-protein amino acid with human serum albumin-biophysical and computational approach", Journal of Biomolecular Structure and Dynamics, 2018

<1%

Publication

Submitted to The Hong Kong Polytechnic University

<1%

Student Paper

Satyabala Neelam, Mahesh Gokara, Babu Sudhamalla, Damu G. Amooru, Rajagopal Subramanyam. "Interaction Studies of Coumaroyltyramine with Human Serum Albumin and Its Biological Importance", The Journal of Physical Chemistry B, 2010

<1%

Publication

41

Qin Nie, Xiao-guang Du, Mei-yu Geng. "Small molecule inhibitors of amyloid β peptide

<1%

aggregation as a potential therapeutic strategy for Alzheimer's disease", Acta Pharmacologica Sinica, 2011

Publication

42	Ji, Jun, Li Zhang, Yuan-Yuan Wu, Xiao-Yu Zhu, Su-Qing Lv, and Xi-Zuo Sun. "Induction of apoptosis by d-limonene is mediated by a caspase-dependent mitochondrial death pathway in human leukemia cells", Leukemia & Lymphoma, 2006.  Publication	<1%
43	www.nature.com Internet Source	<1%
44	mdpi.com Internet Source	<1%
45	worldwidescience.org Internet Source	<1%
46	Tabish Qidwai. "QSAR modeling, docking and ADMET studies for exploration of potential antimalarial compounds against Plasmodium falciparum", In Silico Pharmacology, 2017 Publication	<1%
47	Daniel Pushparaju Yeggoni, Aparna Rachamallu, Rajagopal Subramanyam. "Protein stability, conformational change and binding	<1%

mechanism of human serum albumin upon

binding of embelin and its role in disease control", Journal of Photochemistry and Photobiology B: Biology, 2016

Publication

48

Kazuya Nomura, Akisumi Okamoto, Atsushi Yano, Shin'ichi Higai, Takashi Kondo, Seiji Kamba, Noriyuki Kurita. "Ab initio molecular simulations on specific interactions between amyloid beta and monosaccharides", Chemical Physics Letters, 2012

<1%

Publication

49

Mercè Boada, Oscar López, Laura Núñez, Zbigniew M. Szczepiorkowski, Mireia Torres, Carlota Grifols, Antonio Páez. "Plasma exchange for Alzheimer's disease Management by Albumin Replacement (AMBAR) trial: Study design and progress", Alzheimer's & Dementia: Translational Research & Clinical Interventions, 2019

<1%

Publication

50

amb-express.springeropen.com

Internet Source

<1<sub>%</sub>

51

Venturini, Diego, Bruna Pastrello, Maria Luiza Zeraik, Ivani Pauli, Adriano Defini Andricopulo, Luiz Carlos Silva-Filho, V. S. Bolzani, Nelson Henrique Morgon, A. R. da Souza, and Valdecir Farias Ximenes. "Experimental, DFT and

docking simulations of the binding of diapocynin to human serum albumin: induced circular dichroism", RSC Advances, 2015.

Publication

52	nib.gov.in Internet Source	<1%
53	www.frontiersin.org Internet Source	<1%
54	Samari, Fayezeh, Mojtaba Shamsipur, Bahram Hemmateenejad, Taghi Khayamian, and Sajjad Gharaghani. "Investigation of the interaction between amodiaquine and human serum albumin by fluorescence spectroscopy and molecular modeling", European Journal of Medicinal Chemistry, 2012.  Publication	<1%
55	www.oneblood.org Internet Source	<1%
56	www.researchgate.net Internet Source	<1%
57	www.deepdyve.com Internet Source	<1%
58	Uttam Anand, Saptarshi Mukherjee. "Binding, unfolding and refolding dynamics of serum albumins", Biochimica et Biophysica Acta (BBA) - General Subjects, 2013	<1%

59	Submitted to University of Liverpool Student Paper	<1%
60	Ascenzi, P "Allostery in a monomeric protein: The case of human serum albumin", Biophysical Chemistry, 201005 Publication	<1%
61	pubs.rsc.org Internet Source	<1%
62	Archit Garg, Darla Mark Manidhar, Mahesh Gokara, Chandramouli Malleda, Cirandur Suresh Reddy, Rajagopal Subramanyam. "Elucidation of the Binding Mechanism of Coumarin Derivatives with Human Serum Albumin", PLoS ONE, 2013 Publication	<1%
63	Submitted to University of West London Student Paper	<1%
64	Submitted to Central Queensland University Student Paper	<1%
65	Kragh-Hansen, Ulrich. "Molecular and practical aspects of the enzymatic properties of human serum albumin and of albumin–ligand complexes", Biochimica et Biophysica Acta (BBA) - General Subjects, 2013.  Publication	<1%

Craig, Nancy. "Molecular Biology- Principles of Genome Function", Oxford University Press, 2020

<1%

Publication

67

Daniel Pushparaju Yeggoni, Aparna Rachamallu, Shreya Dubey, Argha Mitra, Rajagopal Subramanyam. "Probing the interaction mechanism of menthol with blood plasma proteins and its cytotoxicity activities", Journal of Biomolecular Structure and Dynamics, 2017

< 1 %

Publication

68

Shreya Dubey, Monika Kallubai, Rajagopal Subramanyam. "Comparative binding of Swertiamarin with human serum albumin and α-1 glycoprotein and its cytotoxicity against neuroblastoma cells", Journal of Biomolecular Structure and Dynamics, 2019

rof. S. RAJAGOPAL

rof. S. RAJAGOPAL

Dept. of Plant Sciences
School of Life Sciences
School of Life Sciences
University of Hyderabad

Hyderabad-500 046.

Hyderabad-500 046.

Publication

Exclude quotes

On

Exclude matches

< 14 words

Exclude bibliography

n